Title	Type 1 ryanodine receptor interactions
Authors	English, Kathleen Kelly
Publication date	2015
Original Citation	English, K. K. 2015. Type 1 ryanodine receptor interactions. PhD Thesis, University College Cork.
Type of publication	Doctoral thesis
Rights	© 2015, Kathleen K. English - http://creativecommons.org/licenses/by-nc-nd/3.0/
Download date	2024-04-27 01:16:06
Item downloaded from	https://hdl.handle.net/10468/2238

Type 1 Ryanodine receptor Interactions

Kathleen Kelly English BSc.

Thesis presented for examination for the degree of PhD. in Medicine (Physiology) to National University of Ireland, Cork.

Department of Physiology,

Head of Department: Prof. Ken O'Halloran

Supervisor: Dr John Mackrill

September 2015

Table of Contents

Contents

Declaration:

I declare that all work in this thesis is my own (except where stated) and has not been presented for examination for any other degree.

Signed:

Kathleen K. English

_____

Papers:

Closing a small gap in our understanding of excitation-contraction coupling: JSR90/JFP90 is Junctophilin 1

Kathleen K. English, Vincenzo Sorrentino, Anna Carla Aiello,Maeve Kiely, Patrick A. Kiely, Brian Mcdonagh, John J. Mackrill. (2014) *Calcium Signaling* VOL.1 NO.1 2373-1168

Abstracts:

Characterisation of Junctophilin 1 (JPH1) expression in rabbit skeletal muscle. **Kathleen K. English,** John J. Mackrill. Presented in poster form at the European Muscle Conference, September 2014.

Closing a Gap in skeletal muscle Excitation-Contraction coupling: the 90 kDa Junctional foot protein is Junctophilin 1. **K.K English,** A. Carla, V. Sorrentino, J.J. Mackrill.Oral communication presented at Royal Academy of Medicine Biosciences meeting, June 2013.

Characterisation of a putative SRC Homology 3 domain binding region in the Type 1 Ryanodine receptor. **K.K. English,** W. Hu, D. Sheehan, J.J.Mackrill. Poster presentation and oral communication at RAMI Biosciences meeting, June 2011.

Acknowledgements

I cant write an acknowledgement section without mentioning the amazing staff of the Mercy hospital, without whom I definitely wouldn't have managed, thanks for keeping me alive guys!

As always (she did put manners on me after all), I'd like to thank my lovely supportive family: Mom for minding me and always being in my corner; she takes full responsibility for my being a physiologist, after all, she bought me a how your body works book when I was 5, followed by years of watching ER and looking up the diseases. Thanks also to Dad, who always encourages me to bet on myself, and is never too busy to dole out sound advice or help jumpstart my car! Thank you Dr Tom English, for the many understanding chats and pep-talks. Thanks to Barry (and Aoife and Violet) for lightening the mood and all the support, and an extra big thank you to the best big little sister in the world, for her undying support, the many care packages and always having my back; thanks Gracie!

Finally, last but not least, to John Catchpole, my favourite human on the planet. Thank you for being kind, rational and amazingly understanding. I'm not sure how you put up with papers and wool all over the apartment, as well as my ranting about blotchey blots and cheeky undergrads, but you did, and frankly you deserve some sort of medal. I'm very excited about this new post-college part of our life, and I couldn't wish for a more perfect better half!

I would like to dedicate this thesis to my wonderful family, to John Catchpole, and to anyone who "just needs this last replicate to work!"

List of figures

List of tables:

Abbreviations

αα: Amino acid.

Ab: antibody

AHX: Aminohexanoic acid

ALL-N: N-acetyl-Leu-Leu-norleucinal, Ac-LLnL-CHO. Calpain inhibitor I.

APS: Ammonium Persulfate.

ARVD2: Arrymthogenic right ventricle Dysplasia

ATP: Adeonsine Triphosphate.

BSA: Bovine Serum Albumin.

CaM: Calmodulin

CaMKII: Calmodulin Kinase II.

CASQ: Calsequestrin

$Ca_v1.1$ channel:voltage sensitive calcium channel type one, also known as L-type voltage operated calcium channels or Dihydropyridine receptor.

CAV3: Caveolin 3.

CBC: Cross Bridge Cycling.

CCD: Central Core Disease.

CICR: Calcium Induced Calcium release.

CIH: Chronic Intermittent Hypoxia.

CHAPS: (3-((cholamidopropyl)dimethylammonio)-1-propane-sulfonate), 2

CHERP: Calcium homeostasis endoplasmic reticulum protein.

CLFS: Chronic Low Frequency Stimulation.

CMC: Chloro-Meta-Creosol.

CPVT: Catecholaminergic polymorphic ventricular tachycardia.

CRU: Calcium release unit.

DHPR: Dihydropyridine receptor (also known as L-type Voltage operated Calcium channels or $Ca_v 1.1$)

DMD: Duchenne Muscular Dystrophy.

DTT: Dithiothreitol.

EC Coupling: Excitation Contraction Coupling.

EDL: Extensor Digitorum Longus.

EDTA: Ethylenediaminetetraacetic acid.

EGCG: Epigallocatechin gallate

ER: Endoplasmic Reticulum.

EtOH: Ethanol.

FBS: Fetal Bovine Serum.

FKBP12, 12.6: FK 506 binding protein (12 or 12.6)

FMOC: Fluorenylmethyloxycarbonyl chloride.

GRB2: Growth factor receptor Bound protein 2.

GST: Glutathione-S-Transferase.

IEF: Isoelectric Focussing.

IPTG: Isopropyl β-D-1-thiogalactopyranoside.

JPH 1,2,3 or 4: Junctophilin 1,2,3 or 4.

JP-45: Junctional protein 45

JSR-90: Junctional Sarcoplasmic Reticulum protein 90.

KO: Knock out.

Leup: Leupeptin.

mAb: Monoclonal antibody.

MALDI ToF: Matrix-assisted laser desorption/ionization Time of Flight analysis.

mAKAP: Muscle A Kinase anchoring protein.

MAPK: Mitogen activated Protein Kinase

mdx mouse: Mouse model of Duchenne Musclar dystrophy.

MeOH: Methanol.

MG-29: Mitsugumin 29.

MH: Malignant Hyperthermia.

MmD: Multi-minicore disease.

MORN motif: Membrane opposition and Recognition Nexus.

MW: Molecular weight.

N-terminal: NH_2 terminal end of a protein.

NCK1: Non-catalytic region of tyrosine kinase adaptor protein 1.

NCX: Sodium-calcium exchanger protein.

NFAT: Nuclear factor of activated T-cells.

NP-40: Nonidet P-40 detergent (octylphenoxypolyethoxyethanol).

pAb: Polyclonal Antibody

PATS assay: peptide array target screening assay..

Pep A: Pepstatin A.

PBS: Phosphate Buffered Saline.

pI: Isoelectric point.

PKA: Protein Kinase A.

PKC: Protein Kinase C.

PLCγ1: Phospholipase C γ 1.

PM: plasma membrane.

PMCA: Plasma membrane Calcium ATPase Pump.

PMSF: phenylmethanesulfonylfluoride.

PTN1: Pleiotrophin 1.

PVDF: polyvinylidene difluoride.

R_f: Retardation factor.

RIPA Buffer: Radio immunoprecipitation Assay buffer.

ROS: reactive oxygen species.

RyR 1,2 or 3: Ryanodine receptor (type 1,2 or 3).

S100a: S100 calcium-binding protein A1.

SCRAM: scrambled (peptide)

SDS: Sodium Dodecyl Sulfate

SDS-PAGE: Sodium Dodecyl Sulfate Polyacyrlamide electrophoresis.

SEPN1: Selenoprotein N 1.

SERCA: Sarcoplasmic/Endoplasmic reticulum Calcium ATPase pump.

siRNA: small interfering RNA.

SH2: SRC-Homology 2 domain

SH3: SRC-Homology 3 Domain.

SH3B: SH3 domain binding region.

shRNA: small hairpin RNA.

SOCE: Store-operated Calcium entry.

SR: Sarcoplasmic reticulum.

TBS: Tris Buffered Saline.

WT: Wild type.

Abstract:

Excitation-contraction coupling is an essential part of skeletal muscle contraction. It encompasses the sensing of depolarisation of the plasma membrane coupled with the release of Ca^{2+} from intracellular stores. The channel responsible for this release is called the Ryanodine receptor (RyR), and forms a hub of interacting proteins which work in concert to regulate the release of Ca^{2+} through this channel. The aim of this work was to characterise possible novel interactions with a proline-rich region of the RyR1, to characterise a monoclonal antibody (mAb VF1c) raised against a junctional sarcoplasmic reticulum protein postulated to interact with RyR1, and to characterise the protein recognised by this antibody in models of skeletal muscle disease such as Duchenne Muscular dystrophy (DMD) and sarcopenia. These experiments were performed using cell culture, protein purification via immunoprecipitation, affinity purification, low pressure chromatography and western blotting techniques. It was found that the RyR1 complex isolated from rat skeletal muscle co-purifies with the Growth factor receptor bound protein 2 (GRB2), very possibly via an interaction between the proline rich region of RyR1 and one of the SH3 domains located on the GRB2 protein. It was also found that Pleiotrophin and Phospholipase Cγ1, suggested interactors of the proline rich region of RyR1, did not co-purify with the RyR1 complex.

Characterisation of mAb VF1c determined that this monoclonal antibody interacts with junctophilin 1, and binds to this protein between the region of 369-460, as determined by western blotting of JPH1 fragments expressed in yeast. It was also found that JPH1 and

JPH2 are differentially regulated in different muscles of rabbit, where the highest amount of both proteins was found in the extensor digitorum longus (EDL) muscle.

JPH1 and 2 levels were also examined in three rodent models of disease: the *mdx* mouse (a model of DMD), chronic intermittent hypoxia (CIH)-treated rat, and aged and adult mice, a model of sarcopenia. In the EDL and soleus muscle of CIH treated rats, no difference in either JPH1 or JPH2 abundance was detected in either muscle. An examination of JPH1 and 2 expression in *mdx* and wild type controls diaphragm, vastus lateralis, soleus and gastrocnemius muscle found no major differences in JPH1 abundance, while JPH2 was decreased in *mdx* gastrocnemius compared to wild type. In a mouse model of sarcopenia, JPH1 abundance was found to be increased in aged soleus but not in aged quadriceps, while in exercised quadriceps, JPH2 abundance was decreased compared to unexercised controls. Taken together, these results have implications for the regulation of RyR1 and JPH1 and 2 in skeletal muscle in both physiological and pathological states, and provide a newly characterised antibody to expand the field of JPH1 research.

Chapter 1: Introduction

1.1: Ca²⁺ signalling in skeletal muscle

As in any tissue, maintaining Ca^{2+} homeostasis is crucial to the health of the cell, and consequently the entire tissue. Ca^{2+} is sequestered in discrete regions of the sarcoplasmic reticulum (SR), ready for release upon activation of contraction (see section 1.1.). Untimely or unwarranted entrance of Ca^{2+} can have serious implications for the cell, including apoptosis, necrosis or cellular dysfunction. Calcium ions are utilised as a second messenger in a huge variety of cellular processes, including neurotransmitter release, gene expression and muscle contraction. Calcium regulated cellular processes involve changes in calcium concentration in both the cytoplasm and other cellular compartments (Cheng, Lederer, 2008).

Calcium release in the cell is tightly regulated. Calcium signalling can have long ranging (such as changes in gene expression) or short ranging effects, like brief contractions seen in skeletal muscle twitches. Internal calcium ion concentrations are modulated by many proteins, which together are termed the Ca^{2+} toolkit, described by Berridge, Bootman and Lipp. The Ca^{2+} toolkit is a tissue specific set of proteins involved in the regulation of calcium inside the cell according to its needs. As dysregulated Ca^{2+} can be catastrophic for cellular fate; influx and efflux of this ion are tightly controlled. Calcium enters the cytosol from the extracellular milieu, and in muscle cells, from the SR and other cellular organelles. Calcium ions are in constant flux throughout all the organelles of the cell, particularly in muscle cells. The resting Ca^{2+} concentration of skeletal muscle is approximately 100 nM, while the replete

Ca^{2+} concentration in SR is approximately 0.5 to 1mM. (Baylor and Hollingworth, 2003; Calderón *et al,* 2014). Ca^{2+} release events from a single Calcium release unit (CRU) (discussed in section 1.1.c onwards) in muscle are known as sparks, and these localised Ca^{2+} release events contribute to the formation of micro-signalling domains within cells. Skeletal muscle contraction cannot occur without Ca^{2+} release from intracellular stores (Berridge, 2000; Berridge, Lipp and Bootman, 2000; Cheng and Lederer, 2008).

1.2: Skeletal muscle structure

Skeletal muscle is responsible for diverse processes such as locomotion, posture maintenance, respiration and vocalization. At the cellular level, muscle is made up of long chains of multinucleated cells called myofibres. These are organised into rods called muscle fibres and include the nerves and blood vessels supplying them. Groups of muscle fibres are bundled together to form fascicles, which themselves are assembled together to form muscle tissue. Skeletal muscle is usually attached at least one end to bone via a tendon (Lieber *et al,* 2011).

1.2.a: Neural supply to skeletal muscle:

Most skeletal muscles are under both voluntary and involuntary control. Neural input to skeletal muscles arrives from the spinal cord via motor neurons. The main effectors of skeletal muscle contraction are α-motor neurons, most of which are monosynaptic. Each α-motor neuron innervates a specific number of muscle cells (ranging from few to several hundred). An α-motor neuron and the muscle fibres it stimulates are together termed a motor

unit. Motor units have varying numbers of muscle fibres; typically the lower the number of motor units, the finer the control of that muscle. Action potentials travel through these α-motor neurons to their motor units to elicit contractions. α- motor neurons terminate at neuromuscular junctions (NMJ).

1.2.b: Skeletal Muscle Cell Structure

Skeletal muscle cells are multinucleated, and contain mitochondria, a well developed endoplasmic reticulum (termed sarcoplasmic reticulum or SR in muscle), as well as other cellular components. Muscle fibres contain rows of sarcomeres, (comprised of thin filaments of actin, tropomyosin, troponin C, I and T, and thick filaments composed of myosin), which are attached to each other via the Z-line. The sarcomeres appear striated, due to the repeating nature of the contractile proteins, and are surrounded by a well-developed network of the SR, which contains the main calcium store in skeletal muscle. The plasma membrane of muscle cells folds inward into what are known as TTubules, which abut the SR at specific junctions known as triads. A diagram of skeletal muscle structure can be seen in figure 1.2.b.i. Skeletal muscle cells have specialised infoldings of plasma membrane called transverse- tubules (T-tubules), crucial to the spreading of the wave of depolarisation throughout the muscle cell. These T-Tubules interface with specialised, swollen regions of the SR called terminal cisternae. This enlarged SR interfaces with T Tubules at specific junctions called triads. T-tubules and triads are crucial to muscle contraction (Stromer *et al* 1974). A schematic of this structure can be seen in Figure 1.2.b.i.
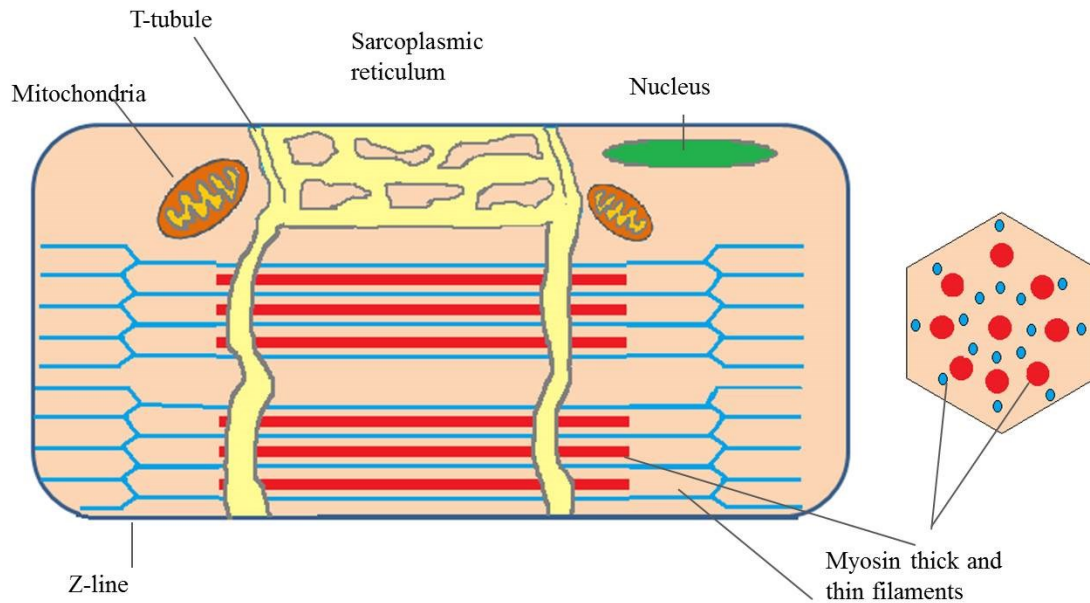
Figure 1.2.b.i: Schematic of a skeletal muscle cell. The diagram shows that the SR forms a well developed net around the contractile apparatus of the cell. Several nuclei and mitochondria are visible. The T-tubules are shown in yellow. This diagram also shows the interdigitation of thin (actin) and thick filaments (myosin ATPase seen here in red), which participate in cross bridge cycling (right hand side).

1.2.c: Sarcomere structure.

Sarcomeres are the contractile unit of skeletal muscle, and are made up of thin actin filaments and thick myosin filaments. The thin actin filaments are surrounded by a troponin C, troponin I and troponin T proteins, which occupy myosin binding sites in resting skeletal muscle. Myosin thick filaments have numerous heads, which in contracting muscle interact with the actin thin filaments to contract the sarcomere, and thus the muscle. A schematic of the sarcomere structure can be seen in figure 1.2.c. Myosin can be seen as thick black lines,

while F actin is depicted in yellow. The A-band comprises F actin filaments (thin filaments) and the thick filaments (assembled myosin) in a lattice arrangement, which are packed slightly differently depending on the species: a haexagonal arrangement exists in insects flight muscle, but in vertebrates a tetragonal "super-lattice" of actin and myosin is more common. The A band also contains troponins T, I and C as well as tropomyosin, which play an essential role in regulating the thin-thick filament interaction crucial to muscle contraction (Squire, 1977; Craig and Woodhead, 2006). The I-band contains both the thin filaments and Z-line proteins. The Z line forms discs at the end of each sarcomere, attaching them linearly to each other, and is made up of primarily titin, nebulin and nebulette proteins. Z-line discs vary in size depending on the muscle fibre type: they are smaller in faster muscle types, about 30-50 nm, while in cardiac and slower muscle fibres, Z line width can be 100 nm wide (Epstein and Davis, 2003). As well as providing a structural scaffold for actin and α-actinin to bind to, Z-lines have important roles in passive force transmission and in stretch sensing in muscle cells (Luther *et al*, 2003; Luther, 2009; Lieber *et al*, 2011). Titin also participates in forming the M-line (the centre of the M-band, the region of thick myosin filaments without heads), and here provides a scaffold for myosin rod assembly in conjunction with obscurin. Obscurin also links other parts of the cyoskeleton such as the T-Tubule to the sarcomere, allowing quick communication between regions of muscle cells (Obermann *et al*, 1996; Kontrogianni-Konstantopoulos *et al*, 2003; Caldwell *et al*, 2015; Hu *et al*, 2015).
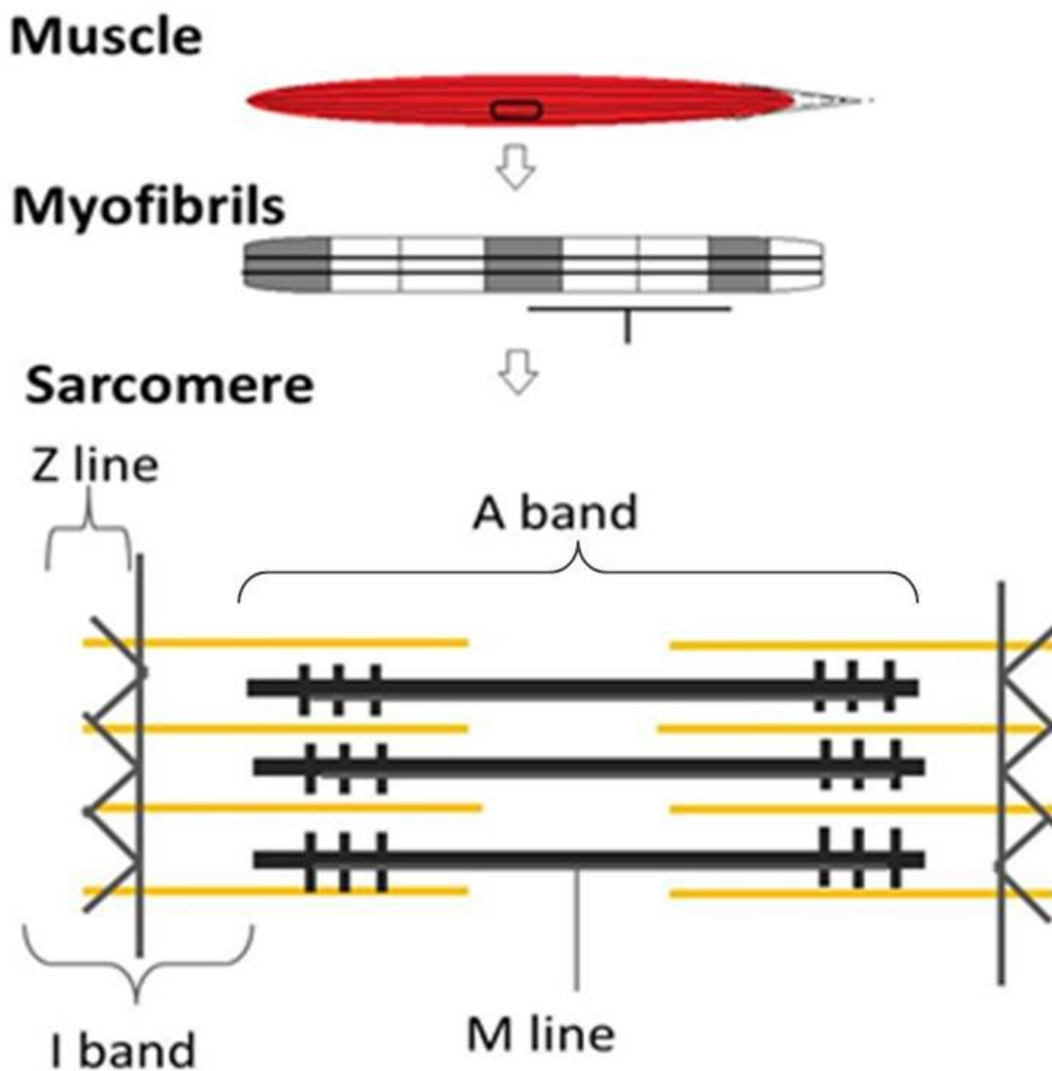
Figure 1.2.c: Schematic showing the structure of myofibrils is made up of sarcomeres.
The A band (dark staining region) is made up of thick myosin filaments, and this contains the
myosin ATPase heads necessary for interaction with the actin thin filaments (orange) in cross
bridge cycling. The I band is comprised of these filaments and the Z disc, which link the
sarcomeres together, end to end. The dark staining myosin and light staining actin thin
filaments *en masse* give skeletal muscle its striated appearance.

1.3 : Muscle fibre Types

In humans, muscle fibres are of three main types, type I, type IIa and type IIb. These were first classified as red and white muscles by Ranvier in 1874, based on the colour of the muscle, but it has since been discovered that muscle fibre types can be classified on the basis of contraction speed and protein expression. There are three main methods of classifying muscle: by histochemical staining of myosin ATPase, analysis of myosin heavy chain (part of the myosin ATPase molecule which interacts with the actin thin filament) expression in individual fibre types by immunohistochemistry or single fibre SDS-PAGE, or by enzymatic analysis of the oxidative state of muscle fibres being examined. There are four main fibre types in mammals, type I, type IIA, type IIX, and type IIB, as determined by ATPase- based histochemical staining. While all are expressed in varying proportions in smaller mammals such as mice and rats, humans do not express the type IIb fibre subtype (Scott *et al,* 2001; Westerblad *et al,* 2010). Confusion can persist in fibre type nomenclature based on fibre types determined by *immuno*histochemical staining, which uses antibodies to determine the exact myosin heavy stain isoform expressed in a muscle fibre. Multiple or a gradient of myosin heavy cahin isoforms can be expressed in some skeletal fibres, these are known as mixed fibres (Schiaffino, Reggiani, 2011).

Type I fibres are the slowest isoform, meaning that they express type I myosin ATPase, giving them the slowest rate of cross bridge cycling, but they are highly fatigue resistant. Muscle comprised primarily of type I fibres (e.g. the soleus, an anti-gravity muscle

in the leg) are red because of their high capillary density and increased myoglobin concentration (compared to other muscle fibre types). Type I muscle needs high capillary density to provide oxygen to an increased number of mitochondria present within the muscle fibres, as the main energy source in these muscle is oxidative phosphorylation. It is for this reason that slow muscle fibres are also known as slow oxidative fibres. Slow fibre types have a less well developed SR, while fast fibre types have a highly structured SR. Slow fibre types have a lower power output than faster fibre types, and peak Ca^{2+} release is also lower in the former. Structurally, slow fibre types have a thicker Z line, which may be linked to stability under conditions of prolonged contractions. Crucially, slower muscle fibre types are more fatigue resistant, due to their increased capacity for oxidative metabolism, whereas faster fibre types are progressively less fatigue resistant from IIa-IIx to IIb, of which the latter almost totally reliant on glycolytic as opposed to oxidative metabolism. The speed of calcium release from the SR in slow fibres is approximately three-fold slower than in fast twitch muscle fibres, and they typically express differing levels or isoforms of proteins such as DHPR, RyR, SERCA2a, and parvalbumin, an intracellular calcium buffer (Pette and Staron, 1997; Pette and Staron, 2000: Baylor and Hollingworth, 2003). A list of comparisons between fast and slow muscle types can be seen in table 1.3.a.

Protein/ cell component	Slow muscle type	Fast
Mitochondria	++++	++
Myosin ATPase	Type I	Types IIA/ IIX/ IIB
parvalbumin	---	+++
Phopholamban	++	---
RyR1	++	++++
RyR3	++	+
DHPR	++	+++
SERCA	isoform 2A	isoform 1A
Calsequestrin	fast, cardiac isotype	fast isoform
NCX	isoform 1	isoforms 1 and 3
Troponin C,I, T	slow isoform	fast isoform
Myosin ATPase	Type I	Types IIA/ IIX/ IIB

Table 1.3.a: Differing cell components in slow and fast muscle types.

Although fibre types can be readily distinguished on those criteria outlined above, it is not always clear cut which fibre type a motor-unit will contain. As fibre type composition is affected by activity level, it is possible for muscle fibres to express a range of fibre types, and under certain conditions to switch between them. Typically, fibre types blend with their next closest type, along the axis of Type I→I/IIa →IIa→IIa/IIx→IIx→IIx/IIb→IIb. Muscle fibres expressing a few types of myosin ATPase are known as hybrid or mixed fibres, and exist to provide shaped responses to the demand put on that particular muscle (Schiaffino and Reggiani, 2011). Type I to type II fibre shifts are common after spinal injury and a reduction of motor-neuron input to the muscle, under the effect of microgravity or in simple detraining. Shifts from type IIa to type IIb phenotypes are common, whereas a shift from type II to type I is less common, and has only experimentally been achieved using denervation and chronic low frequency stimulation (CLFS). Often, endurance training will induce a more oxidative phenotype (e.g. a hybrid fibre of type I/IIa) but total type II to I transitions are very rare (Aigner and Pette, 1992; Pette and Staron, 2001; Scott *et al,* 2001). Endurance training exerts

this effect on skeletal muscle in a number of different ways: it increases mitochondrial biogenesis, thus increasing oxidative capacity and enhancing resistance to fatigue, and also causes an increase in protein synthesis. This in turn increases Ca^{2+} release, production of reactive oxygen species (ROS), and by way of mild hypoxia, angiogenesis. These changes culminate in a shift towards a more oxidative, fatigue resistant phenotype.

1.3.b: Muscle Fibre type determination

Muscle fibre type is determined by several mechanisms. The first is the satellite cells from which the muscle fibre originates, as this will partially determine the type of myosin ATPase produced by the cell (Kalhovde *et al,* 2005). Muscle fibre type is also shaped by the input each motor unit receives from its corresponding alpha motor neuron: constant low frequency stimulation will encourage the production of slow fibre type components (e.g. as seen in muscle used for maintaining posture), while high frequency input for short periods of time will encourage the production of fast fibre type proteins (such as that found in muscle used for sprinting). As motor neuron input determines the amount and frequency of Ca^{2+} release in skeletal muscle cells, it follows that calcium signalling can affect gene expression and so affect fibre type. As such, moderate but longer lasting Ca^{2+} release will induce the activation of the calcineurin phosphatase enzyme, which when interacting with calmodulin kinase (CaMKII) has been implicated in the maintenance of slow fibre type components (Parsons *et al,* 2003). Conversely, during high frequency stimulation, increases in Ca^{2+} release facilitate the interaction of CaMKII with other effectors, and induce the expression of fast fibre type proteins (Crabtree, 1999, Tavi and Westerblad, 2011). These mechanisms demonstrate how

spatial and temporal aspects of Ca^{2+} release in skeletal muscle can affect gene expression (Gundersun, 2001).

1.3.a: Skeletal muscle contraction

First, a stimulating action potential is propagated along the α-motor neuron unil it reaches the neuromuscular junction (NMJ). Here, the neurotransmitter acetylcholine (ACh) is released at the synapse between the motor neuron and the muscle cell, where it binds to nicotinic ACh receptors on the muscle cell membrane. This induces opening of the ACh receptors which allow an influx of sodium ions (as well as other ions) into the cell, causing depolarisation of the cell membrane (Almers, Stanfiel and Stühmer, 1983; Yarov-Yarovoy *et al,* 2012). This wave of depolarisation spreads down the T-Tubule, and causes the opening of voltage sensitive Ca^{2+} ion channels, dihydropyridine receptors (DHPRs, also known as $Ca_V1.1$). DHPRs allow a small influx of Ca^{2+}ions, and also cause the allosteric opening of the type 1 ryanodine receptor (RyR1), a Ca^{2+} channel located on the SR membrane. The opening of this channel increases the Ca^{2+} concentration of the cytoplasm, which allows the initiation of cross bridge cycling (Franzini-Armstrong *et al,* 1991; Takehura *et al*, 1995).
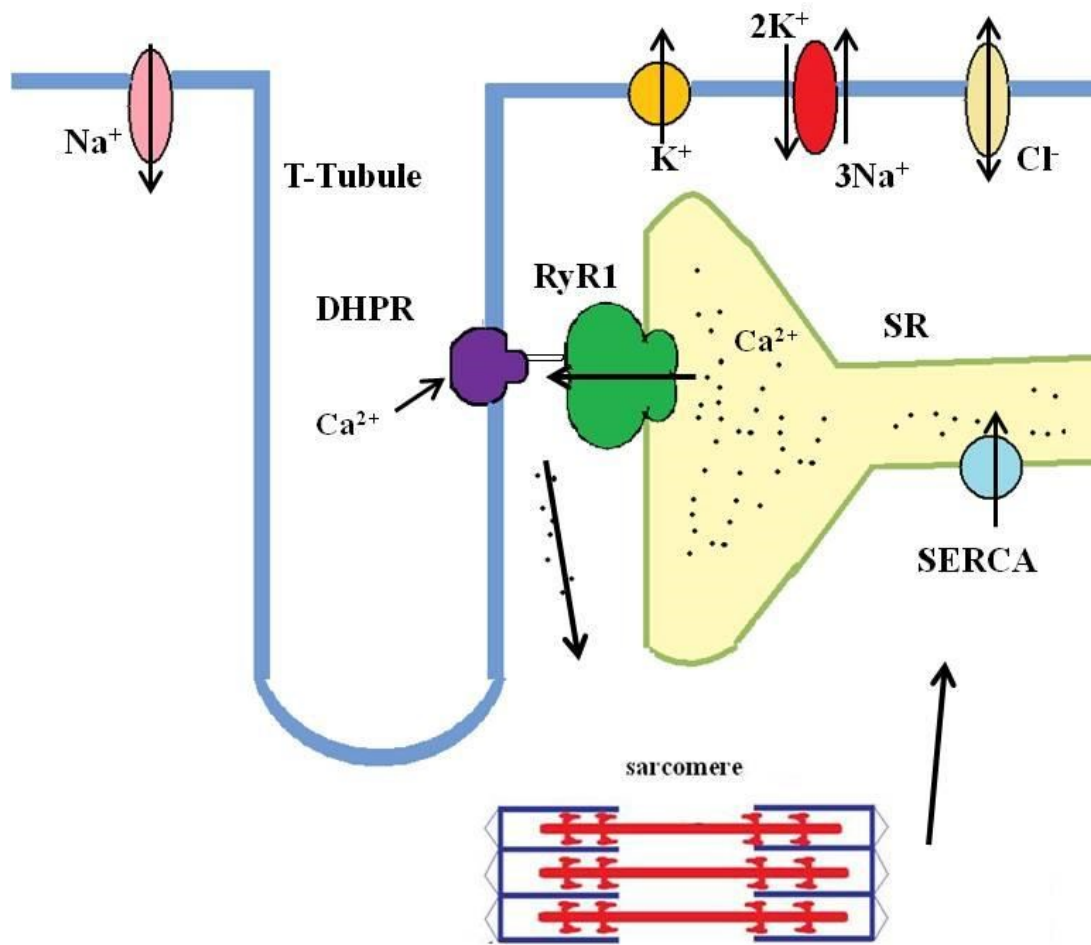
Figure 1.3.a: Schematic of the T-tubule and SR in the process of muscle contraction. Depolarising waves travel down the T-Tubule, gating DHPRs. These allosterically open the RyR1 channel, allowing the release of Ca^{2+} ions from the SR through RyR1. The increased Ca^{2+} concentration in the cyoplasm activates cross bridge cycling by removing the inhibitory troponin complex from myosin binding sites on thin filaments. Relaxation occurs by re-uptake of Ca^{2+} into the SR via SERCA and by extrusion through NCX.

1.3.b: EC coupling: role of the Ryanodine Receptor

Excitation contraction coupling (EC coupling) is the name given to the process of depolarisation induced calcium release from SR stores, which provides an intermediate step between membrane depolarisation and cross-bridge cycling in skeletal and cardiac muscles. EC coupling in skeletal muscle occurs at the triad, a specialised structure found in skeletal muscles, described in section 1.2.b. The dihydropyridine receptors (DHPRs) are L-type calcium channels which reside in the T Tubule membrane, and are made up of 5 subunits: α1S, the pore-forming unit, 1βa, a cytoplasmic subunit, and two transmembrane subunits α2δ and γ1 (Flucher *et al,* 2005). DHPRs provide the signal for RyR opening, by way of a physical interaction between the II-III cytoplasmic loop found in the α1S subunit and RyR1. In essence, DHPR in the skeletal muscle acts as a voltage sensor for RyR1. Movement of DHPR's II-III loop (and possibly junctophilin 1) causes the allosteric opening of RyR1. This allows calcium ions to flow from the SR, at a rate of approximately 200 μM/ms via the RyR and possibly other SR membrane channels, and these Ca^{2+} ions go on to participate in cross-bridge cycling and the generation of force by skeletal muscle as described in section 1.3.c (Calderon *et al,* 2014). EC coupling cannot occur without these two proteins, as shown by the *dysgenic* (DHPR knock out) or *dyspedic* ("footless"- RyR knock out) animals or myotubes (Takehura *et al,* 1995; Buck *et al,* 1997). Removal (by knockout or naturally arising variant) of either protein proved to be lethal, thus myotubes and cell lines from these animals have been used for characterisation of their interactions and calcium transients (Buck *et al,* 1997). Using these experimental tools, Franzini-Armstrong *et al* found that DHPR proteins were necessary for correct triad formation, while Avila *et al* found that RyR1-mediated Ca^{2+} release was necessary for DHPR expression in dyspedic myotubes (Franzini-

Armstrong *et al,* 1991; Avila *et al,* 2001). In skeletal muscle, special arrangements of four DHPR channels arranged around one RyR channel exist, and are known as tetrads. Tetrads are abolished in the absence of RyR1, and are incorrectly formed when only RyR3 (another isoform of RyR) is expressed instead (Protasi *et al* 1998; Protasi *et al,* 2000). The minimum specific regions for within RyR1 required for tetrad formation are residues 1272-1455, which were elucidated to be essential for this in studies using RyR1/3 chimeras expressed in dyspedic myotubes (Sheridan *et al,* 2006). It is plausible that this region of RyR1 interacts with the α1S subunit (specifically the II-III loop) and the 1βa subunit of DHPR, both of which have been shown to be important for tetrad formation and for orthograde and retrograde signalling between the two channels in EC coupling (Franzini-Armstrong *et al,* 2009). A diagram of EC coupling is shown in figure 1.3.a, and a diagram of tetrad formation is shown in Fig 1.3.b. As discussed, cross bridge cycling cannot occur without release of Ca^{2+} from the SR, and this process can be damaged by process that affect gating of any of the proteins involved or by EC-uncoupling, where the DHHPR and RyR proteins are uncoupled for a myriad of reasons. EC uncoupling is postulated to have a role in the pathology of sarcopenia and in muscle damage after strenuous exercise (Reganathan *et al,* 1997; Corona *et al,* 2010).
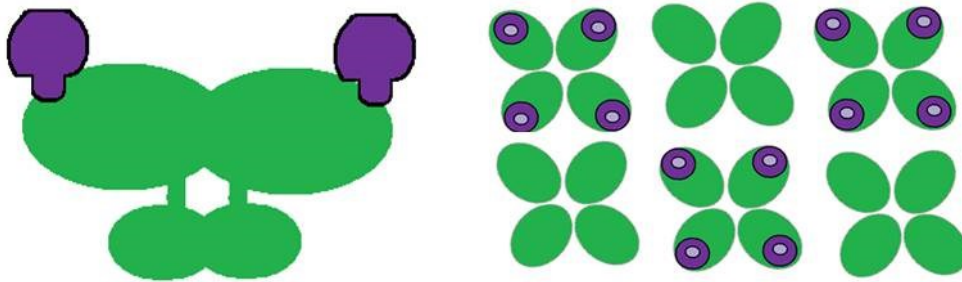
Figure 1.3.b: Diagram of the location of RyRs and DHPRs in the triad. The left panel shows RyR1 (green) and DPHRs (purple) as seen from the plane of the SR membrane One DHPR channel binds to each monomer of RyR, forming a tetrad. Every second RyR protein has a tetrad which interacts with it, and this forms a checkerboard-like pattern (right hand panel), as seen from the plasma membrane.

1.3.c: Cross Bridge cycling:

Increased myoplasmic Ca^{2+} causes the formation of a troponin C-Ca^{2+} complex, which moves the troponin away from myosin binding sites on the actin thin filament. The four main steps of cross bridge cycling are as follows: myosin heads (with bound ADP and Pi) bind to the actin thin filaments, with the heads perpendicular to the binding region (steps 1 and 2, fig. 1.3.c.i). ADP and Pi are then released from the myosin heads, and this causes the myosin head to flex and to bind to the actin closer to the centre of the sarcomere. This pulls the ends of the sarcomere (the Z discs) closer together, and forms the "power stroke" of sarcomere

contraction (step 3 in figure 1.3.c.i). The myosin ATPase heads can now bind a fresh molecule of ATP, which is rapidly hydrolysed (step 4 in fig 1.3.c.i), setting up the myosin and actin filaments to go through the cycle again. The cross bridges of myosin and actin filaments will keep cycling as long as cytoplasmic Ca^{2+} remains high. This model of cross bridge cycling is known as the Sliding Filament model (Huxley, Niedergerke, 1954; Gordon *et al*, 1966, Huxley, Simmons, 1971, Weber and Franzini-Armstrong, 1994; Cooke, 2004). The speed of ATP hydrolysis determines the rate of muscle contraction, and is in turn determined by the abundance and isoform of myosin ATPase expressed in each subtype of skeletal muscle.
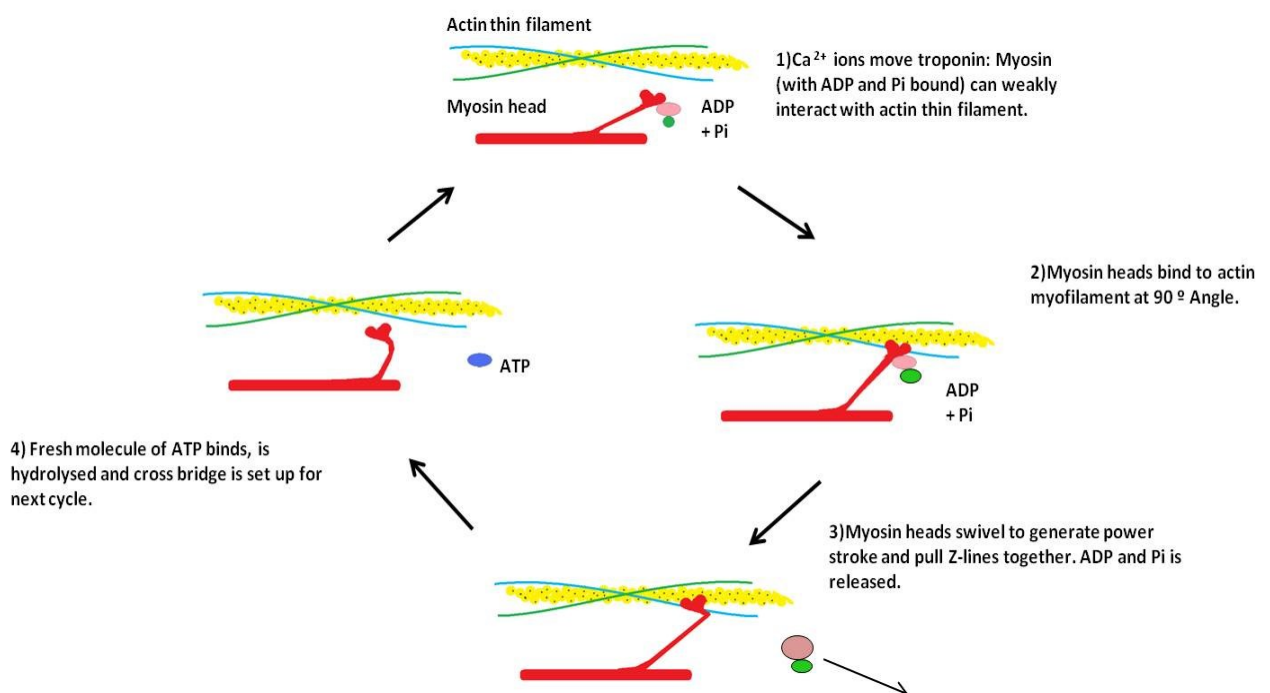
Figure 1.3.c.i: Schematic of Cross bridge cycling in skeletal muscle. Step 1 shows the hydrolysis of ATP into ADP and Pi (after the release of Ca^{2+} from the SR), which allows the

myosin head (red) to prepare for binding to the actin thin filament (yellow). Step 2 shows the myosin heads interacting with the actin thin filament at a 90º angle. Step 3 shows the swivelling of the myosin head to a 45º angle, which generates the force for sarcomere shortening, combined with the release of ADP. Step four shows the binding of a fresh molecule of ATP, allowing the cycle to begin again.
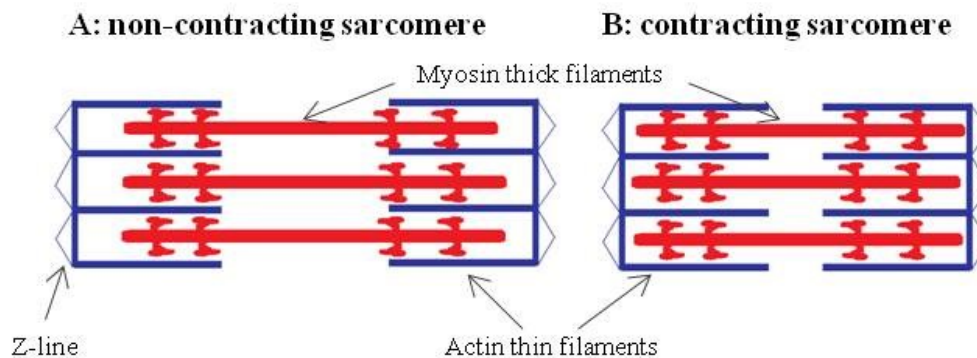
Figure 1.3.c.ii: Diagram of sarcomere shortening in cross bridge cycling. Panel A shows a non-contracting sarcomere, where myosin heads are ready to interact with the actin thin filaments. Panel B shows a contracted sarcomere, where the power stroke of myosin heads swivelling has pulled the two z lines closer together, shortening the sarcomere. This is the basis of muscle contraction.

1.3.d: Relaxation of skeletal muscle

Removal of cytoplasmic Ca^{2+} is necessary for the relaxation of skeletal muscle. This is accomplished primarily by re-sequestering Ca^{2+} ions into the SR by the SERCA (Sarcoplasmic/ Endoplasmic reticulum Ca^{2+} pumps), which reside in the SR membrane. Some Ca^{2+} is extruded through plasma membrane pumps such as the sodium-calcium exchanger

(NCX) or the plasma membrane Ca^{2+} pump, PMCA, although this is much less significant than that resequestered by SERCA (Brini and Carafoli, 2010).

1.3.e: Skeletal Muscle Fatigue

Fatigue is a major factor in skeletal muscle performance, and is mediated by several factors. These include decreased myofibrillar sensitivity to Ca^{2+}, increasing Pi content in the myoplasm, and the SR, where it decreases the pool of Ca^{2+} available for release, since it can buffer this cation. Fatigue due to high stimulation can also increase ROS production, which has knock on effects for signalling protein such as RyRs, and may act as an off-switch to prevent damage (see section 1.1.c.iv). Force generation and conduction speed are decreased, and relaxation speed is also affected (mediated by ATP via Ca^{2+} ion removal by SERCA pump). There is evidence the EC-uncoupling may also play a role in the decline in force production, especially after eccentric (muscle-lengthening) contractions (Evans and Lambert, 2007; Westerblad *et al,* 2010; Corona *et al,* 2010).

1.4.a: Structure and function of RyRs

Three isoforms of RyR exist, each encoded by a separate gene. RyR1 is found at highest levels in skeletal muscle, RyR2 is expressed predominantly in cardiac and smooth muscle, while RyR3 has a rather more diffuse expression pattern, and are found at their highest in brain and diaphragm muscle (Mackrill *et al,* 1997; Conti, Gorza and Sorrentino, 1996). RyRs have also been found in non-excitable cells, where they may have crucial roles in maintaining membrane potential and calcium homeostasis (Xue *et al,* 2000; Davis *et al,* 2013).

RyRs are usually homotetrameric, forming complexes of molecular weight of 2.3 MDa, rendering them the largest known ion channels. Each monomer is made up of approximately 5000 amino acids, with monomeric molecular weights of approximately 565 kDa. Topologically, the RyRs are comprised of an N-terminal domain extending from amino acids 1-4500 which resides in the cytoplasm (the "foot structure"), a transmembrane region with 6 transmembrane segments and a cytosolic C-terminal domain (Zalk *et al,* 2014). The large N-terminal domain makes up about 80% of the proteins mass, and its large "square-prism" surface of roughly 120Å serves as a massive interface with which many proteins and pharmacological agents interact, allowing them to exert effects on Ca^{2+} release from intracellular stores (Wagenknecht, Samso, 2002). The N-terminal region has been divided into 15 domains based on appearance in cryoelectron microscopy (numbered 1-15) (Shersysheva *et al* 2008, Wagenknecht, Samsó, 2002). Domain 1 appears to form the link between the cytoplasmic and ER/SR luminal regions and may resemble columns, while

domain 2 may make up the Ca^{2+}-traversing pore region. Domain 3 is of special interest, as it is not only the largest domain but also makes up the "handle", which may allow inter-RyR interactions and thus are important for the arrays of ryanodine receptors (the "checkerboard" pattern of RyRs, see Fig.1.3.b) seen in tissues like skeletal muscle and regulation by calcium ions (Yin *et al,* 2008: Zalk *et al,* 2014; Efremov *et al,* 2014).

Domains 5-10 comprise the "clamp region" and facilitate many inter- and intramolecular interactions, and structural changes occur here which are associated with opening and closing of the channel (Samso *et al* 2009, Sherysheva *et al* 2008). Inter- and intramolecular interactions are crucial for correct functioning of RyRs, and can be altered by pharmacological agents, such as dantrolene, and accessory proteins such as FKBP12 and FKBP12.6, which are discussed in sections 1.4.b and 1.5. The transmembrane assembly of the RyR is roughly 70Å in length, and is predicted to start at or near $\alpha\alpha$ 4500, or more specifically, the stretch of amino acids extending from 4554-4575 are extremely hydrophobic, and are likely to be embedded in the SR membrane (Takeshima *et al*., 1989; Zorzato *et al*., 1990; Grunwald and Meissner, 1995). Between Wagenknecht *et al* and Efremov *et al,* the structure of the transmembrane region has been resolved using electron cyromicroscopy to a resolution of 6Å and this resolution has revealed the presence of 24 transmembrane helices with two sets of four branch-like regions of high density, which extend from the cytoplasmic face toward the SR lumen (Samsó *et al,* 2005: Efremov *et al,* 2015). These branches converge in two points to form negatively charged rings which make up the ion selectivity filter on the luminal side, and a gate structure near the cytoplasmic vestibule. This gives the transmembrane region an "inverted-tepee" structure, which is

comparable to the bacterial KscA K$^+$ channel. It is postulated that these branches can rotate based on open or closed state of the channel, because of the changes in angle of the luminal portion of the RyR relative to the cytoplasmic region upon opening and closing, in agreement with the "zipping and unzipping" model proposed by Ikemoto and Yamamoto (Ikemoto, Yamamoto, 2002). Selectivity is maintained by a well conserved –GVRAGGID- sequence (in RyR1, amino acid 4891-4900) as determined by comparison to K$^+$ channel selectivity filters (Gao *et al* 2000). Mutations in highly conserved transmembrane and luminal portion of RyR1 have been shown to cause slow Ca^{2+} leak form the SR associated with symptoms of hypotonia seen in central core disease (CCD) (Tilgen *et al,* 2001). The luminal portion of the RyR makes up of the remaining 10-20 % of the molecule. Although the very tail end of the C-terminus is located in the cytoplasm, the luminal face also has many interacting partners important for regulation of calcium release, and assessment of Ca^{2+} stores, such as calsequestrin, junctin and triadin (Mackrill *et al,* 1999)
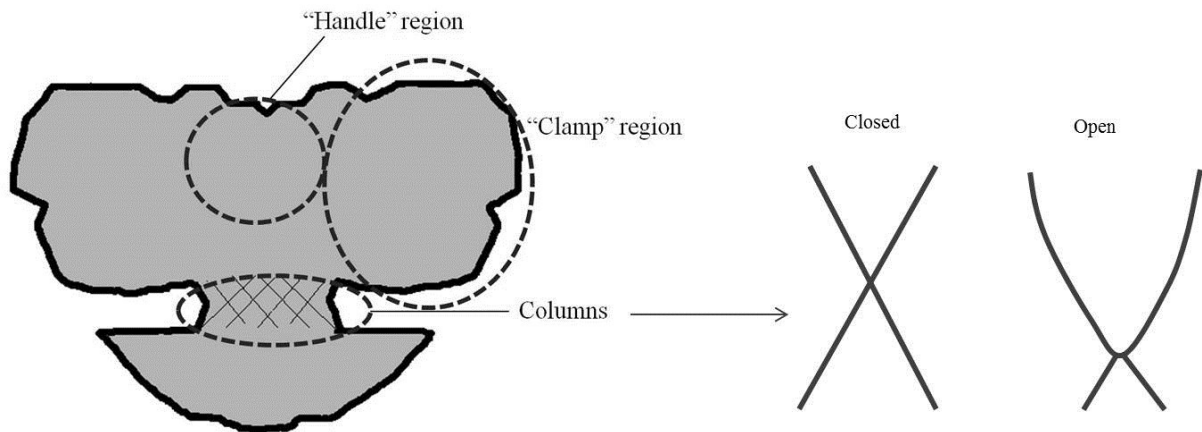
Figure 1.4.a: Diagram of RyR1 structure: locations of handle, column and clamp regions are denoted by dashed lines. The large N-terminal region (located in the cytoplasm) is connected to the luminal region via the "columns". A schematic of the column location when the channel is open and closed can be seen on the right hand side. When opening, the columns swivel out and downwards to allow ion flux (adapted from Samsó *et al,* 2005: Efremov *et al,* 2015).

1.4.b: RyR interactions

RyR calcium channel function relies on the ability of these proteins to interact and be affected by endogenous and exogenous effectors, including natural ligands such as FKBP (FK506-binding proteins), calmodulin, junctin, CHERP (Calcium Homeostasis Endoplasmic Reticulum Protein), and triadin, as well as pharmacological agents such as ruthenium red, 4-chloro-m-creosol, dantrolene, caffeine and natrin toxin (Mackrill, 1999, Mackrill 2010, Ryan et al, 2011). These interactions are vitally important for the elucidation of disease mechanisms (eg. RyR2-FKBP12.6 interaction in heart failure) and are also useful in studying the RyR. Protein ligands which interact with the RyR can fall into three broad categories: those that interact at the cytoplasmic, membrane, or SR/ER luminal face.

Cytoplasmic and plasmalemmal interacting proteins include FKBPs, DHPR, CaM, protein kinases, sorcin, homer proteins and S100s. The dihydropyridine receptor (DHPR) forms the voltage sensor for Ca^{2+} release in skeletal muscle. It is a plasmalemmal voltage sensitive calcium channel, located in T-tubules, directly opposed to the SR. This is described in section 1.3.b.

FK506- binding proteins 12 and 12.6 (FKBP, also known as calstabins), named for their ability to bind the immunosuppressant macrolides FK506 and rapamycin and for their apparent molecular weights of 12 and 12.6 kDa, interact with RyR subtypes 1 and 3 or 2 respectively (Mackrill, 2010). They are understood to stabilize the closed and open state of the channel, and may help mediate RyR-RyR interactions in array formation in skeletal

muscle (Gaburjakova *et al,* 2001; Samso *et al*, 2006; Efremov *et al* 2015; Zalk *et al,* 2014). One FKBP-molecule binds per monomer of RyR, i.e. four per receptor complex, and this interaction can be disrupted by addition of either of the macrolide drugs mentioned (Wagenknecht, Samsó, 2002). FKBP12 proteins are reported to bind at residue 2461-2462, and as well as stabilising the channel in the open or closed conformation, are said to be involved in coupling neighbouring RyRs to each other (Marx *et al* 1998). Although traditionally, FKBP12 was thought to bind only to RyR1, it has recently been found that FKBP12 can interact with RyR2, and that FKBP12.6 can interact with RyR1 and encourages channel opening, however there is little FKBP12.6 expressed in skeletal muscle. Further work is necessary to elucidate the wider effects of these interactions (Efremov *et al,*2014;Venturi *et al,* 2014).

Calmodulin (CaM), like the FKBPs also binds one monomer of RyR per molecule CaM, and can exert two different effects on ryanodine receptors depending whether or not it is bound to calcium. In the presence of millimolar Ca^{2+} concentrations, Ca^{2+}-CaM can behave as an inhibitor of RyR function, serving as an important "stop sign" for calcium release. At submicromolar Ca^{2+} concentrations, apo-CaM acts as an activator of various RyR isoforms. The binding site of CaM and apo-CaM are slightly different, but are located near each other, within the crevice formed at the junction of domain 3 and domain 5 for Ca^{2+}-CaM and at domain 3 for apo-CaM, perhaps to allow quick movement and calcium status reporting during Ca^{2+} release cycling (Seiler *et al,* 1984; Ikemoto, Yamamoto, 2002; Wright *et al,* 2008; Cornea *et al,* 2009; Huang *et al,* 2012).

Junctophilins are a group of four proteins expressed in various types of excitable cells. First described by Takeshima *et al* in 2000, there are four different isoforms (JPH1, 2, 3 and 4), expressed at their highest levels in skeletal muscle, cardiac muscle and neuronal tissues respectively. The main function of JPHs is to bring the t-tubule (in muscle) and endoplasmic reticulum together, and thus they are crucial to maintaining essential membrane structures (Takeshima *et al,* 2000). This is facilitated by the three regions of JPH1. The most C-terminal part of the protein has a conserved SR/ER membrane insertion sequence, which effectively tethers the end of the protein. Following this is an α-helical segment, which acts like a spring, and at the N-terminal end, is a hook shaped area which contains up to eight MORN (Membrane Occupation and Recognition Nexus) motifs, which have an affinity for sphingocholine and other lipids, and thus allow binding of the proteins to the plasma membrane (Nishi *et al,* 2000). In this way the junctophilin family behave as scaffolding which effectively link the SR/ER and plasma membrane. In skeletal muscles, this especially important, as triads need to be tethered to the plasma membrane for effective calcium release from the SR. JPH2 is also expressed in skeletal muscle, but there is no evidence that it interacts with RyR1; however knock down of both JPH1 and 2 in myotubes does have an effect on SOCE and altered caffeine mediated Ca^{2+} release (Hirata *et al,* 2011). JPH1 knock out animals die perinatally due to a suckling deficiency, while JPH2 knock out was embryonically lethal. JPH1 knock out animals displayed deformed triads and impaired Ca^{2+} signalling and force generation in skeletal muscle myotubes (Ito *et al,* 2001). Since then, it has been shown that as well as interacting with the plasma membrane of cells via their MORN motifs, JPH1 also interacts with DHPR and RyR1, and that it interacts with RyR1 in a redox-sensitive and conformationally dependent manner (Phimister *et al,* 2007; Golini *et al,*

2011). While JPH1 is confirmed to co-localise with RyR1 and DHPR in skeletal muscle, the subcellular location of JPH2 has been shown to be in discrete and separate areas of the SR membrane, indicating that in skeletal muscle, JPH2 may have more of a structural role (Jayasinghe *et al,* 2014).

As well as those listed, protein kinases and glycolytic enzymes also bind to the cytosolic face of the RyR, and perform various different post-translational modifications which can have effects on ligand binding and calcium release. Integral membrane proteins such as triadin and junctin may help anchor the RyR complex in the SR membrane, and may also provide nearby binding sites for potential effectors. One of these effectors is likely to be calsequestrin, (CASQ) which binds to the tail of triadin and junctin, or directly to the RyR. CASQ is an acidic Ca^{2+} storage molecule which has intermediate capacity for Ca^{2+} binding. Depending on whether it is bound directly or indirectly to the RyR (via triadin or junctin, depending on isoforms), or its phosphorylation state, it can activate or inhibit Ca^{2+} release (Szegedi *et al,* 1999). CASQ is the main Ca^{2+} buffer in the SR, and can "sense" SR $[Ca^{2+}]$ because it polymerises with increasing $[Ca^{2+}]$, and its state of polymerisization and phosphorylation status can also affect Ca^{2+} binding (Beard et al, 2009). Two isoforms of CASQ are expressed in fast or slow muscle fibre types, CASQ1 is found in fast twitch muscle and can bind up to 80 mol/mol Ca^{2+}; while the slow isoform, CASQ2 can bind up to 60 mol/mol Ca^{2+}, and is expressed in slow twitch and cardiac muscle cells. CASQ1 expression is found to increase in muscles that have been subjected to chronic low frequency stimulation (Froemming *et al,* 2000; Park *et al,* 2004). CASQ1 knock out animals have been generated, and have decreased SR Ca^{2+} content, as well as decreased Ca^{2+} release via RyR1 in fast fibres

(Olojo *et al,* 2011). CASQ1 knock out animals have also been reported to have an MH like phenotype (Paolini *et al,* 2007; Protasi *et al,* 2009).

Junctin is a 33 kDa non-catalytic splice variant of the aspartate β-hydroxylase protein. It has a short N-terminal cytoplasmic region, a transmembrane domain and a long C-terminal tail found within the SR lumen. Its main function is to anchor CASQ to RyR with triadin, although it binds to a separate region of RyR1. When added to the luminal face of bilayers containing RyR1 proteins, it can increase the opening activity of the channel, but when bound to CASQ it will decrease the open probability of RyR1 channels (Goonasekera *et al,* 2007; Dulhunty *et al,* 2009). Knock down of this protein indicates that it has a role in maintaining the calcium store of the SR (Wang *et al,* 2008).

Triadin is a 95 kDa protein found in skeletal muscle. Like junctin, it helps to anchor CASQ to the lumenal face of RyR1. It has been shown to bind to the C-terminal end of RyR1, around the regions containing residues 4907, 4908 and 4878 (Kobayashi *et al,* 2000; Rezgui *et al,* 2005; Goonasekera *et al,* 2007). Knock out models have been created, and have shown a decrease in Ca^{2+} content in the SR, as well as a decrease in muscle strength, but no other major phenotype was observed (Oddoux *et al,* 2009). Shen *et al* (2007) also found that knock out of triadin caused a decrease in junctophilin 1, junctin and CASQ expression in muscle cells. Triadin is also expressed in cardiac muscle, but here it is found at different molecular weights to that in skeletal muscle (Chopra *et al,* 2009).

JP-45 (junctional protein 45) is an integral membrane protein of 45 kDa which interacts with the calcium release unit (CRU-described in section 1.3.b). Although at times

confused with JPH1 or 2, it is not the same protein. JP-45 interacts with CASQ and DHPR, and alters the sensitivity of the DHPR based on the SR store calcium content. It is found to be decreased in aged muscle compared to younger controls (Andersson *et al,* 2003; Yasuda *et al* 2013).

S100a is a calcium binding protein located in the cytoplasm of skeletal muscle cells. It has a molecular weight of 10-12 kDa, and contains an N-terminal EF hand, middle hinge region and a C-terminal EF hand. This middle hinge region becomes more hydrophobic when Ca^{2+} ions are bound to the surrounding EF hand motifs, and this facilitates interaction with other proteins (Prosser *et al,* 2001). This hinge region interacts with the CaM binding region of RyR1, where it exerts an effect of increasing the open probability of the channel. It may also assist in the formation of the RyR1 tetramers. S100a knock out muscle fibres have decreased SR Ca^{2+} release in response to changes in voltage, indicating that S100a has an important role in EC coupling (Wright *et al,* 2009).

Mitsugumin 29 (MG-29) is a 29 kDa protein located in the SR membrane of skeletal muscle cells. It contains 4 transmembrane domains, and forms hexamers to exert its effect on RyR gating. Experimentally, MG-29 increases the open probability of RyR1, but has no effect on unitary conductance. Knock out models have shown that ablation of MG-29 causes swollen T-Tubular membranes and misaligned triads, as well as rapid SR Ca^{2+} content depletion and rapid fatigue. These results show MG-29 has a role in triad organisation, crucial for correct EC coupling (Nagaraj *et al,* 2000; Treves *et al,* 2009).

Selenoprotein N1 (SEPN1) is a 60 kDa protein that has been shown to be associated with RyR1, where it is necessary for full channel activity. It has a role in redox sensing and modulation of Ca^{2+} release via RyR1 (Jurynec *et al*, 2008). SEPN1 mutants have been implicated in the pathogenesis of multi minicore disease (MmD, discussed is section 1.1.c.v) and this protein is essential to the process of muscle regeneration and satellite cell maintenance (Jungbluth *et al*, 2007; Castets *et al*, 2012).
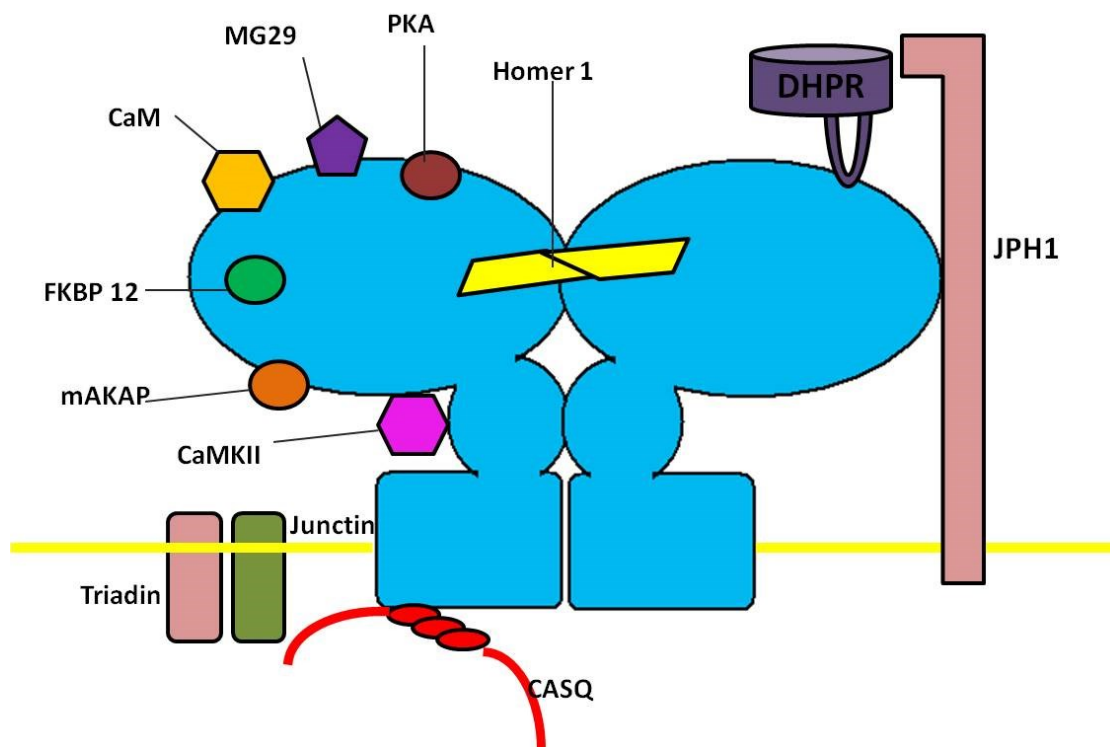
Fig 1.3.c: Schematic of some of the known RyR1 interacting proteins. Many proteins are known to interact with RyR1, and assist in modulating calcium release from the SR.

Homer is an adapter protein expressed in brain, heart and skeletal muscle. Homer 1 has been shown to modulate the response of RyR1 to Ca^{2+} ions and to affect the response of RyR1 to voltage changes (via DHPR). Investigation of Homer 1 knock out has been performed in myotubes and in a mouse model, and Homer 1 KO results in a skeletal muscle myopathy with decreased myofibre cross-sectional area and decreased force generation. Homer 1 proteins have an N terminal EVH1 (Ena/vasodilator-stimulated phosphoprotein homology 1) domain which facilitates their interaction with many proteins. Homer 1 interacts with RyR1 via the EVH1 domain, which binds to a proline rich region located in the cytoplasmic region of RyR1 (Feng *et al,* 2002; Stiber *et al,* 2008). Homer 1 has a coiled-coiled C-terminal domain, which facilitates dimerization, and interacts with other intracellular channels such as $InsP_3Rs$ and TRPC channels (Salanova *et al,* 2013).

Other proteins that have been implicated in RyR1 regulation include caveolin 3 (CAV3) which has been found to co-localise and interact with RyR1 in skeletal muscle. CAV3 is responsible for the formation of caveolae in many cell types, and interacts with several proteins. CAV3 is also associated with the dystrophin complex at the plasma membrane of muscle cells, which is responsible for the correct transduction of force across muscle cells (see chapter 6). CAV3 KO animals have no perceptible caveolae, show T-Tubule deformation and altered dystrophin localisation. Mutations in the CAV3 gene have been associated with limb girdle muscular dystrophy (Galbiati *et al,* 2001; Whiteley *et al,* 2012).

Recently, Ryan *et al* have detailed a novel interaction between RyR1 and CHERP (calcium homeostasis endoplasmic reticulum protein), identified using a histidine-tagged fragment of

RyR1 as bait expressed in HEK293 cells combined with mass spectroscopy. This protein is thought to participate in EC-coupling, and co-immunoprecipitation experiments show it is expressed in mouse soleus muscle fibres (Ryan *et al*, 2011). Taken together, one can surmise that a vast (and ever-growing) list of protein interact with the RyR1 protein, which are necessary to shape the release of Ca^{2+} ions in response to the specific needs of the muscle being contracted. A diagram of some interactions that occur at the calcium release unit can be seen in figure 1.1.c.iii, while a table summarising the role of RyR1 interactors and the consequence of their ablation can be seen in table 1.1.c.iv. Protein-protein interactions are not the only means of RyR regulation, as post translational modifications also aide the shaping of Ca^{2+} release from intracellular stores, as discussed in the next section.

Protein	Cellular component	Action	Knock out?	Reference
Calmodulin	Cytoplasm	Bind Ca^{2+}, interacts with RyR, inhibits channel opening.	--	Rodney *et al*, 2000
Calsequestrin	SR terminal Cisternae	Binds Ca^{2+} in SR lumen, avaliable for release. Signal low SR Ca^{2+} stock	MHs phenotype, decreased SR calium stores, decreased calium release in fast fibres (CASQ1 KO)	Beard *et al*, 2009: Protasi *et al*, 2009: Olojo *et al*, 2011.
Caveolin 3	PM	Caveolae formation	No Caveolae, T-Tubule deformation	Whiteley *et al*, 2012
FKBP12	Cytoplasm	Stabilises RyR in open and closed state	Improved recovery after exercise	Carmody *et al*, 2001; Ondrias *et al*, 1998; Corona *et al*, 2008.
Homer	Cytoplasm	Biphasic effect on RyR.	Myopathy, decreasde force and cross sectional area of muscle fibres. Perturbed TRP cation channle localisation	Feng *et al*, 2008.: Stiber *et al*, 2008; Pouliquinand Dulhunty, 2009.
Junctin	SR lumen	Binds Triadin/ CSQ/RyR1	Knock down: negative effect on calcium store	Beard *et al*, 2008
Junctophilin 1	SR-PM interface. C-terminal embedded in SR membrane	Role in signalling between DHPR an RyR, may have redox sensing function	Abberations in SOCE. Defective triad formation and EC coupling	Golini *et al*, 2011, Phimister *et al*, 2011.
Triadin	SR lumen	Anchors CSQ	Decreased exp of other EC proteins, decreased calcium in SR, decreased strength	Shen *et al*, 2007: Oddoux *et al*, 2009:
SEPN 1	Cytoplasm	Redox function	Required for channel activity, redox sensing	Jurynec *et al*, 2008
S100A	Cytoplasm	calcium binding	Can decrease calcium ion release, KO have increased fatigue and decreased force generation and contraction	Prosser *et al*, 2008

Table 1.4.d: well-known RyR1 interacting proteins and the effect of their ablation.

1.5: Regulation of RyR by small molecules and ions

RyR1 is acted upon by a wide variety of pharmacological agents, most notably ryanodine, the plant alkaloid after which they are named. Other pharmacological agents which exert an effect on RyRs include dantrolene, ruthenium red, 4-chloro-*meta*-cresol (CMC) and caffeine.

Ryanodine exerts a biphasic effect on RyR channels, whereby concentrations in the submicromolar range activate a small Ca^{2+} flux through the channel, via a subconductance state, while millimolar concentrations cause the irreversible closure and inactivation of RyRs (Rousseau *et al,* 1987; Zimanyi *et al,* 1992; Ogawa *et al,* 1994). Labelled ryanodine ([^{3}H]ryanodine) is widely used in single channel and Ca^{2+}ion flux studies (Hamilton *et al,* 1989; Mackrill, 2010). Caffeine is also widely used in Ca^{2+} release studies. It alters the sensitivity of RyR to Ca^{2+}, on the luminal side, causing an increase in Ca^{2+}release through the channel. Caffeine is thought to bind RyR1 near the D1 (divergent region 1) (Sitsapesan *et al,* 1995: Du *et al,* 2000:Kong *et al,* 2008).

CMC is a potent agonist of RyRs, and it interacts with type 1 and 2 but not type 3 RyRs. CMC may also have a role in shaping the store operated calcium entry response in skeletal muscle (Zeng *et al,* 2014). Ruthenium red is a cationic chemical stain used in histological preparations. It is a potent inhibitor of RyR-mediated Ca^{2+} release at nM to μM concentrations (Lukyaenenko *et al,* 2000). Another inhibitor of RyRs is dantrolene, which has a clinical application during episodes of malignant hyperthermia, (see section 1.1.c.v.). Dantrolene inhibits Ca^{2+} release from RyRs, and some evidence exist to show that it may alter DHPR-RyR communication as well (Szentesi *et al,* 2001; Paul-Peltzer *et al,* 2002; Bannister 2013). Many other pharmacological agents have agonist or antagonistic effects on RyR gating, including procaine, Polychlorinated Biphenol and epigallocatechin gallate, (a compound found in green tea) (Feng *et al,* 2008; Mackrill, 2010).

Calcium ions have a bi-phasic effect on RyR gating. At low concentrations (1-10µM), calcium ions have an activating effect on RyR. Concentrations in the range of 1-10mM have been found to inhibit RyR1 (Fill and Coppello, 2002). Recently, Efermov *et al* described a mechanism for Ca^{2+}-mediated modulation of RyR1, whereby an EF hand motif located on the cytoplasmic side of RyR1 binds to Ca^{2+} and induces an allosteric regulation of the gating region of RyR1 (Efermov *et al*, 2014).

Magnesium ions also modulate RyRs in two ways: at intracellular concentrations of 600-1000 µM, Mg^{2+} can displace Ca^{2+} from the regulatory domain of RyR and when in complex with ATP, can enhance RyR activity by promoting channel opening. RyR1 appears to be more sensitive to Mg^{2+} concentration fluxes than RyR2 or RyR3, and Mg^{2+} has been shown to be necessary for coupled gating of RyRs (Jóna *et al*, 2001; Porta *et al*, 2012).

RyRs are known to be phosphorylated by many kinases, including Protein Kinase A (PKA), cGMP (cyclic guanosine monophosphate), Calmodulin Kinase and Protein Kinase C Phosphorylation by PKA results in the activation of RyR1, inducing Ca^{2+} release from the SR (Coronado *et al*, 1994). Ruehr *et al* found that PKA was localised to RyR1 via the MKAP tether (Ruehr *et al*, 2003). Marx *et al* have stated that "hyperphosphorylation" of the RyR1 channels shifted its Ca^{2+} sensitivity and resulted in "leaky" channels (Marx *et al*, 2000). Phosphorylation of RyR channels has been implicated in the effect of ionotropic factors during skeletal muscle contraction. In response to isoproterenol and muscle stimulation, the PKA mediated phosphorylation of serine-2844 of RyR1 was found to be increased. This phosphorylation event led to increased Ca^{2+} release and increased force generation in treated

muscles, while an S2844A mutation abolished this effect (Andersson *et al*, 2012). A serine residue at 2843 has also been implicated in increasing RyR1 channel "leakiness" in human vastus lateralis biopsies performed after a single bout of resistance exercise. Interstingly, the leaky RyRs were only found in type I fibres in the biopsies, indicating that fibre type specific regulation of RyRs may occur (Gehlert *et al*, 2012). Phosphorylation events at the clamp region of RyR1 have also been found to be important. Yuchi *et al* (2012) found that phosphorylation of residues involved with the clamp region of RyR had tangible effects on interdomain allosteric interactions (Yuchi *et al,* 2012).

Redox modulation of RyRs is hugely important in skeletal muscle. Redox modification of RyRs is accomplished by oxidation or nitrosylation of free thiol groups found within the RyR subunits, and is mediated by nitric oxide (NO) via nNOS (neuronal nitric oxide synthase) or glutathione S transferase (GST) proteins among other mediators such as H_2O_2 and ROS. Increasing the oxidation status of RyR decreases calcium release from intracellular stores, primarily by altering its sensitivity to activation and inhibition to Ca^{2+} and Mg^{2+} -ATP respectively. An increase in reduced thiols on the RyR1 protein increases Ca^{2+} release, as determined in purified SR vesicles and single channel recordings (Sun *et al,* 2001). In this way RyRs can function as redox sensors in skeletal muscle, and may aid in the process of coupling SR Ca $^{2+}$release with mitochondrial output. Oxidation and S-nitrosylation of RyR1 have been linked to the pO_2 levels in muscle tissue, and may represent a matching of perfusion with contraction level (Sun *et al,* 2013). Redox modification of RyRs can also indirectly affect gating, as modification of free thiol content can alter both inter-subunit interactions within RyR1 and the interactions with FKBP12, JPH1, triadin and CaM, and may

have a role in shaping proteasomal degradation of RyRs, by affecting protease-RyR1 interaction (Zissimopoulos and Lai, 2006). In pathological states such as sarcopenia, increased reactive oxygen metabolites can contribute to RyR modulation, and increased neuronal nNOS has been found to be associated with RyR1 in muscle from patients affected by rheumatoid arthritis, and these RyRs were also found to have increased peroxynitrate mediated damage as well as increased Ca^{2+} transients (Andersson *et al,* 2011; Yamada *et al,* 2014). Interacting proteins such as JPH1 are also affected by thiol content, and this in turn can regulate the interaction of JPH1 with RyR1 (Zissimopoulos and Lai, 2006: Phimister *et al*, 2011).
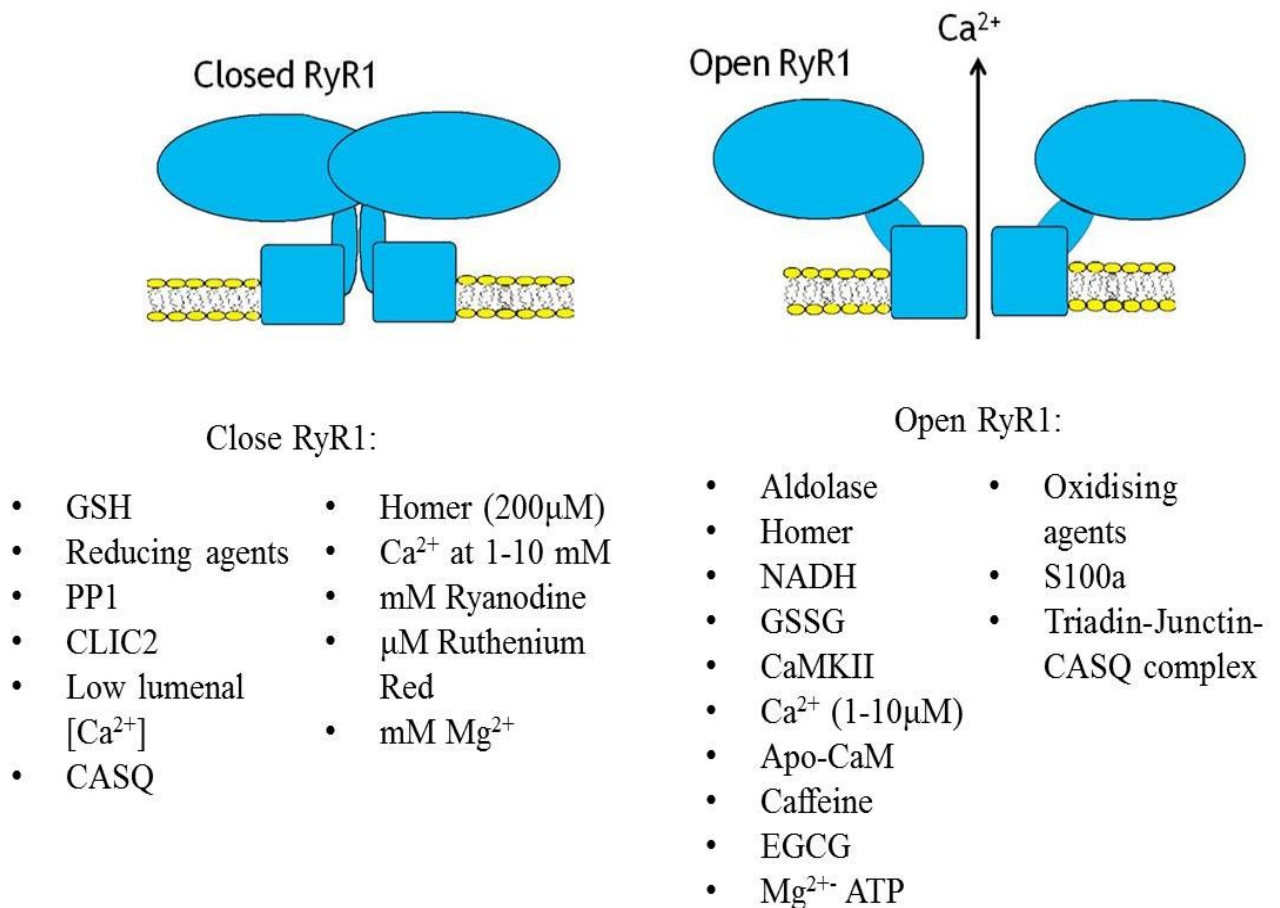
Figure 1.5.a: Diagram of RyR in open and closed state. The central columns which contain the selectivity filter splay outwards during channel opening, allowing Ca^{2+} ions to be released from the SR. A list of modulators are presented underneath the channel diagrams.

1.6: RyRs in disease

Since RyR complexes are so large and are crucial to proper Ca^{2+} homeostasis, perturbations of the macro- and micro-molecular interactions within and around the calcium release unit invariably cause some degree of channel dysfunction and disease.

1.6.a: Malignant Hyperthermia

Malignant hyperthermia is a pharmacogenetic disorder, where a patient has an unwarranted reaction to volatile anaesthetics or depolarising muscle relaxants, such as succinylcholine. An MH episode is characterised by a hypermetabolic crisis, and causes hyperthermia, muscle rigidity, acidosis, tachycardia, and rhabdomyolysis. First described by Denborough in 1962, MH is a low penetrance disease i.e. it may not occur with every anaesthetic administration, and is diagnosed using an *in vitro* contracture test, which exposes a biopsied muscle sample to volatile anaesthetics or caffeine and monitors the contractile response (Denborough *et al*, 1962). Episodes can also be induced by high body temperatures (>37ºC). Malignant hyperthermia can be caused by over 200 point mutations in the RyR1 gene (MacLennan, Zvaritch, 2010), located on chromosome 19q13.2, which cause aberrant Ca^{2+} release from the SR in response to depolarising anaesthetics.

Epidemiological studies suggest that 1:60,000 adults or 1:15,000 children are affected by MH. Up to 70 % of cases are caused by autosomal dominant mutations in the *RYR1* gene, many of which are clustered in three "hotspots" near the N-terminal end, the mid-region and C-terminal pore region of the protein (M[c] Carthy, Mackrill, 2004). Some of these mutations

have been shown to cause domain unzipping or faulty interdomain interactions, resulting in aberrant Ca^{2+} release and the metabolic disaster that ensues. Dantrolene, the only available therapy for an MH episode (along with rapid cooling) reportedly re-stabilizes the faulty domain interactions (Kobayashi *et al*, 2005). The various mutations have been categorised as having four differing effects on RyR function causing either hypersensitivity, a leaky channel with depleted SR stores, the inability to release calcium at all or reduced expression of RyR (Treves *et al*, 2008, Canato *et al*, 2014). Many mutations found in RyR that are linked to MH are also linked to central core disease, thus the hot-spot regions 1-3 are also known as MH/CCD regions 1,2 and 3 (Monnier *et al*, 1997)

1.6.b: Central Core Disease

Central core disease (CCD) is a disease of skeletal muscle where delayed motor milestones, hypotonia and atrophy are accompanied by the appearance of centrally located, amorphous cores in the musculature, which disrupt myofibrillar organisation and perturb both the mitochondria and the SR network (Jungbluth, 2007). It presents with varying degrees of severity, with some patients completely unaware that they have it, while others have severe pathologies including proximal muscle weakness and or skeletal muscle deformities. Often it presents with type I fibre predominance, and diagnosis is made on the basis of biopsy and weakness, (Quinlivan *et al*, 2003). Causative mutations have been found in the C-terminal portion of RyR1 (Wu *et al*, 2006). It is thought that mutations here either cause leaky RyRs or EC uncoupling, leading to the pathological state seen in this disease (Treves *et al*, 2008). In a mouse model of one form of CCD, (with a heterozygous expression of RyR1 I4898T mutation) Boncompagnani *et al* found that type 1 fibres (predominant in the soleus) display

66

Z-line streaming, and that type IIa, x and b fibres were relatively spared of this abnormality. In contrast, the faster type II a b and x fibres were found to have apparently swollen SR compartment compared to their WT counterparts. This mouse model also displayed reduced Ca^{2+} transients in response to electrical stimulation, and the authors suggest that the effects seen in this model are reminiscent of those found in aged muscle (Boncompagnani *et al*, 2010).

1.6.c: Multi-mini Core Disease

Multi-minicore disease (MmD) is an autosomal recessive disorder which can be caused by mutations in RyR1 or the associated protein SEPN1, resulting in many small cores of non-oxidative material found along the length of muscle fibres (Jurynec *et al*, 2008). The pathological effects of the disease are varied, but spinal rigidity, hip girdle dislocation, opthalmoplegia, and respiratory insufficiency(which can cause secondary right ventricular heart failure) have been documented (Jungbluth, 2007). Mutations in the RyR1 gene linked to this disease have been found in the N-, C-terminal fragments and middle portion of the RyR1 protein (Zhou *et al*, 2010). Decreased RyR1 expression has also been cited as a causative factor (Monnier *et al*, 2003). The SEPN1 protein associates with RyR1, and is mutated in certain forms of MmD, especially those causing scoliosis and respiratory impairment. SEPN1 is postulated to participate in redox modulation of RyR1 (Ferrerio *et al*, 2002, Jurynec *et al*, 2008). Hirata *et al* suggest that "relatively relaxed" zebrafish, which carry a nonsense mutation in RyR1b, are a good model of MmD, and that they display decreased Ca^{2+} transients in affected skeletal muscle compared to controls (Hirata *et al*, 2007).

It is possible that as yet undiscovered interacting proteins or perhaps that fact that RyRs can form heteroteramers in some tissues could provide further information on diseases of skeletal muscle, and may explain the diverse pathological features seen in similar diseases (Murayama *et al,* 1997). Mutations of RyR2, or its associated proteins, expressed in heart are analogous to those which cause MH and CCD in RyR1 (i.e., occur in the same "hot-spot regions") and have been linked with arrhythmogenic right ventricular dysplasia type 2 (ARVD2) and catecholeminergic polymorphic ventricular tachycardia (CPVT) (Leenhardt *et al,* 1995; Priori *et al,* 2001;Tiso *et al,* 2001; Kobayashi *et al*, 2009, MacLennan, Zvaritch, 2010). ARVD2 results in cardiomyocytes being replaced by fatty and fibrotic tissue, and ARVD2-associated mutations in RyR2 cause a persistent Ca^{2+} leak via the channel, elevating cytoplasmic $[Ca^{2+}]$, which can result in ventricular arrhythmia (Corrado *et al*, 2000: Tiso *et al,* 2001). CPVT has many forms but may involve hyperphosphorylation of RyR2 by either PKA or CaMKII after β-adrenergic stimulation, leading to stress-induced ventricular tachycardia. Another mechanism involves a mutation of Arg-4496-Cys in the C terminal region of RyR2, resulting in a lower affinity binding site for the RyR-associated protein, FKBP12.6 (discussed in section 1.5) which stabilizes RyR2 in the open conformation (Kobayashi *et al*, 2009).

2.1: Aims and objectives:

As the information presented in this literature review demonstrate, a considerable amount of knowledge has been generated regarding the Type 1 RyR in the past few decades, particularly with regard to its role in health and disease. However, further work is necessary to elucidate the nature of novel interactions with the RyR1 complex, such as those suggested by *in silico* analysis. To rectify this, we sought to confirm or refute some of these interactions *in vitro* using a biotinylated peptide mimetic of the proline rich region of RyR1 coupled with chromatography and SDS-PAGE based detection to identify any interacting proteins. The results of this analysis can be found in chapter 4.

Attempts were made to clarify and expand upon a suggested interaction between RyR1 and an unknown protein termed JSR-90, which was reported using the VF1c mAb. To do this we characterised mAb VF1c using western blotting based experiments. The results can be seen in chapter 5.

We also sought to clarify the role of Junctophilin 1, (a protein known to interact with RyR1 in skeletal muscle) in different types of skeletal muscle and in models of disease whose pathology extends to skeletal muscle tissue, such as Duchenne muscular dystrophy, chronic intermittent hypoxia and sarcopenia. The results of this study can be found in chapter 6.

Chapter 3:Materials and methods

3.1. Cell culture

3.1.a: General Culture

Materials:

Unless otherwise stated, all cell culture plasticware, was purchased from Sarstedt (Sarstedt Ltd., Drinagh, Wexford, Ireland), Sigma-Aldrich (Sigma-Aldrich Ireland Limited, Vale road, Arklow, Wicklow, Ireland), MyBio Ltd.(MyBio Ltd., Hebron Business Park, Kilkenny) or GIBCO ® (C/O:Bio-Sciences,3 Charlemont Terrace ,Crofton Road, Dun Laoghaire, Dublin).

Reagents used include Dulbeccos modified Eagles medium (DMEM, Cat. No. D5796, Sigma-Aldrich), supplemented with penicillin/streptomycin (cat no. 15070-063, GIBCO®, and Fetal bovine serum (FBS) (Sigma, cat no: 12003C). For subculture, 0.25% (w/v) Trypsin-EDTA (GIBCO®) and Trypan blue (0.4%(w/v), from Sigma, Cat no T6146) was used.

Equipment: Thermo CL10 Centrifuge (Thermo-Fischer Scientific Incorporated, Basingstoke, Hampshire RG21 6YH). Haemocytometer (AC1000 Improved Neubauer, Hawksley Medical and Lab Equipment, Lancing, Sussex, BN15 8TN)

3.1. b: General methods: Cell culture.

Cells were typically grown in Dulbecco's Modified Eagles Medium (DMEM, Sigma-Aldrich) supplemented with 10% heat-inactivated fetal bovine serum and 1% penicillin and streptomycin solution, and were maintained at 95% O_2 with 5% CO_2 in a humidified Thermo Scientific Water-Jacketed incubator.

3.1. c: Subculture.

Subculture of cells was performed as needed or weekly, based on cell confluency. Culture medium was aspirated from the cell monolayer, which was then washed with 2 ml of 0.01% trypsin/EDTA solution. This was removed by aspiration and cells were incubated at 37˚C for 3-5 minutes in 4 ml trypsin solution to detach adherent cells. This cell suspension was centrifuged in a Thermo scientific CL10 swing bucket rotor at 500 g_{max} for 5 minutes, and the supernatant was removed. Fresh media, warmed to 37˚C was added and the pellet dispersed with gentle trituration through a 10 ml pipette. Cells were then either counted using a haemocytometer for plating or diluted (1 volume of cell suspension: 10 volumes of media for A7r5 myocytes or 1:20 for A549 or C2C12 cells, depending on cell doubling time). Cells were transferred to a new vessel and the growth media replenished as needed.

The A549 adenocarcinoma cell line was maintained in DMEM, supplemented with 10% foetal bovine serum and 1% penicillin and streptomycin (Sigma). Cells were grown to 80% confluency or above, and removed from flasks using two washes of cold 10 mM EDTA in PBS and a cell scraper. The cell suspension was centrifuged in a Thermo scientific

centrifuge CL10 at 500 g_{max} for 5 min, and cell pellets were either snap frozen in liquid nitrogen or used immediately (see homogenate preparation, section 3.3).

3.1.d: C2C12 cells and Differentiation assay.

Materials: DMEM with 10% FBS, differentiation medium (DMEM with 0.5% FBS), 10 mM EDTA in PBS (EDTA from Sigma, cat no E6758). Cell scrapers and 100mm cell culture plates from Sarstedt.

C2C12 cells were subcultured in 100 mm dishes and maintained in 10% FCS-DMEM. Upon reaching 80% confluency, the media was changed to DMEM containing 0.5% FCS to encourage myotube formation. Media was replaced daily and cells/myotubes were harvested from between 24 h and 8 days after addition of differentiation media. Cells and myotubes were detached by washing twice in room temperature 10 mM EDTA in PBS and scraping with a cell scraper. Samples were then flash frozen or used immediately, and were processed as described in section 3.3.

3.1.e: siRNA Knock-Down of JPH1.

Reagents: N-ter™ Nanoparticle siRNA Transfection reagent, (Sigma: N2913) JPH1 silencer RNA (Sigma, EHU078801).RNAse Zap decontamination solution (Sigma R2020). RNAse-free water, DMEM (with and without 10% FBS), 6 well plates, C2C12 cell line.

C2C12 cells were seeded at a concentration of 5x 10^4 cells per well in 6 well plates. The cells were differentiated until myotubes were seen on visual inspection (day four). All

tubes used were autoclaved at 121º C for 15 min and the working area of the bench liberally sprayed with RNAse Zap decontamination solution. NTer nanoparticles were diluted into a 16% working solution and (using RNAse free water) and incubated with 10 or 20 nM of JPH1 silencer esiRNA or Flourescein esiRNA (negative control) for 30 minutes at 37°C to allow complexes to form. N-TER nanoparticles interact non-covalently with the siRNA particles, and then, by interacting with lipids in the plasma membrane, allow the whole complex to enter cells (Sigma Aldrich Technical Bulletin N0788). After the complex formation step, siRNA-N-TER nanoparticle complexes were added to C2C12 cell layers and covered in 1.5ml of serum-free or 0.5% serum content DMEM, and replaced in the incubator for 24 hours. Experiments were performed in duplicate. After a 24 hour incubation, the cells were scraped in 50 μl of ice cold RIPA buffer (with protease inhibitors, see sample preparation section3.3) and flash frozen using liquid nitrogen. Samples were stored in a -80°C freezer until analysed for JPH1 protein content via western blotting (see section 3.5).

3.1.f: A7r5 rat smooth muscle aortic cell line and calpian inhibition assay.

Materials: ALL-N calpain 1 inhibitor (N-acetyl-Leu-Leu-norleucinal, Ac-LLnL-CHO) Cat. No. A6185, Sigma. A23187, (calcium ionophore, Cat. No. C7522, Sigma) BAPTA-AM, (1,2-bis(2-aminophenoxy)ethane-*N,N,N',N'*-tetraacetic acid, A4926, Sigma) DMSO (Dimethylsulfoxide, (Cat. No. D2650, Sigma)).SDS-PAGE sample Buffer: (250 mM Tris HCL pH 6.8, 10% SDS, 30% glycerol, 0.4% bromophenol blue.)

A7r5 cell lines were maintained and subcultured as described in section 3.1.1. For calpain inhibition assays, cells were seeded in 6 well plates and allowed to grow until 70-80% confluency. Cells were incubated with a range of concentrations of ALL-N, A23187, the esterified calcium buffer BAPTA-AM, 0.1% DMSO in final volume of 2 ml and control DMEM solutions with 2 ml of media per well. The cells were incubated for 1, 3, 6 and 24 h, after which they were incubated on ice in 50 µl of 2X reducing SDS-PAGE sample buffer per well and scraped into 1.5ml tubes. Samples were either snap frozen or boiled at 100˚C for 7 min and loaded onto 7.5% SDS-PAGE gels

Chemical	Concentration	Role
DMSO	0.1% total vol(2 ml)	vehicle
ALL-N	20 µM in 2mls	calpain inhibitor
A23187	20 µM	Calcium ionophore
BAPTA -AM	20 µM	Calcium chelator

.

Table 3.1.f: Chemicals and concentrations used in calapin cleavage assays. A7r5 cells were incubated with the outlined chemicals in 6 well plates (in triplicate) in 2 mls of DMEM for 3 or 6 hours.

3.2: Animal tissue studies :

All named researchers possessed the required animal licenses and the protocols were approved by the University College Cork Animal experimentation ethics committee or the corresponding regulatory body for their respective instituitions. For FKBP12-Glutathione S-

Transferase affinity purification and rabbit muscle western blot experiments, male Wistar rats and ex-breeder male white New Zealand rabbits were housed on 12 hourly day and night cycles in the Biological Services Unit, UCC with *ad libitum* access to food and water. Rats were anesthetised by either CO_2 inhalation or euthetal administration (performed by and under care of Dr Maria Buckley, or Ms. Elaine Barry (Department of Physiology, UCC) and Dr Cliona O Mahoney (Department of Parmacology, UCC). Rabbits were sacrificed by cervical dislocation. Muscle tissue (see table 3.3.1) was excised and flash frozen in liquid nitrogen.

3.2.a: CIH and Sham rat treatment:

Under the supervision of Prof Ken O Halloran at the Department of Physiology, University College Dublin, male Wistar rats were housed in 12 hr light and dark cycles with free access to food and water. Chronic intermittent hypoxia was achieved by placing the rats in chambers with alternating room air/5% O_2 (CIH animals, n= 6) or alternating room air-room air every 90 seconds (Sham animals, n=5) for 8 hrs per day for two weeks(essentially as described in Shortt *et al* 2013). Animals were sacrificed (By K O'Halloran) via administration of 5% isoflurane followed by cervical dislocation, after which muscles were excised and flash frozen. Extensor Digitorum Longus (EDL) and Soleus muscles were analysed for JPH1 and 2 expression via western blot.

3.2.b: Adult versus Aged animals:

In the laboratory of Dr. Brian McDonagh (University of Liverpool, Department of Musculoskeletal Biology, Institute of Aging and Chronic Disease), male C57BL/6 mice were

housed in 12 hr light/dark cycles with free access to food and water. At 12 and 25 months of age, mice were anesthetised using 0.15 mg/ml Dormitor and 20mg/ml Ketaset, followed by cervical dislocation. Soleus and a portion of quadriceps were excised and either underwent an isometric contraction protocol (*in vivo* isometric contraction) or were snap-frozen and sent to this laboratory, where the experiment was blinded by JJM. The muscle samples were homogenised as described in section 3.3.

The isometric contraction protocol performed by Dr. McDonagh was as follows: mice were anesthetised and surface electrodes were placed on the ankle and around the upper leg of both hindlimbs. Contractions were elicited for 15 minutes duration using a square wave pulse 0.1 ms in duration at 100 Hz and 70 V for 0.5 s every 5 seconds as described in (McArdle *et al*, 2001). Following the isometric contraction protocol the mice were sacrificed and the muscles were excised and snap frozen in liquid nitrogen.

3.3: Sample Preparation.

3.3.a:Materials:

Protease inhibitors: aprotinin (Cat. No. A1153, Sigma), leupeptin (Cat. No. L2884, Sigma). Pepstatin A (Cat. No. P5318, Sigma). Phenylmethanesulfonyl Fluoride, (PMSF, Cat. No. P7626, Sigma).Trizma HCL (T5941, Sigma) Sodium Deoxycholate (D6750, Sigma) Sodium dodecyl sulphate (SDS, L4390, Sigma). Sodium chloride (NaCl, S7653, Sigma). Sucrose (S903, Sigma). Homogenisation Buffer I: 25mM Tris-HCl pH7.4 and 0.5M $MgCl_2$. Homogenisation Buffer II: 25mM Tris-HCl pH 7.4, 0.5M sucrose, and 0.3M KCl. Radio

Immunoprecipitation assay (RIPA) Lysis buffer: 150 mM NaCl, 1% NP-40, 0.5% sodium deoxycholate, 1% SDS, 50mM Tris-HCl pH 8.8 plus freshly added protease inhibitors Ultra Turrax Homogeniser with 10 mm probe (Model Z722464GB, Sigma), Omni Prep GLH homogeniser (Model GLH 115, Omni International) with 5 mm probe (Model B5-075, Omni International), Spectramax Multimode Spectrophotometer (Molecular Devices), Sanyo MSE Soniprep 150 (Model B-052, Sanyo), Eppendorf 5810 centrifuge, (Model 5810. 000.327, Eppendorf).

3.3.b: Homogenisation

Homogenisation of cell pellets was performed using pre-chilled buffers I and II, with freshly added protease inhibitors leupeptin, pepstatin A, aprotinin and PMSF (for concentration used, see table 3.5.b). Briefly, cell pellets were homogenised by 50 strokes in a loose-fitting glass Teflon homogeniser in 1.25 ml of buffer I, followed by the same volume of buffer II and underwent another 10 strokes (adapted from Chen *et al,* 1993). This crude homogenate was aliquoted and used immediately or snap-frozen and stored at -80°C.

3.3.c: RIPA lysis

Cell pellets were incubated in ice-cold RIPA buffer and kept on ice for 30 min. Lysates were sonicated using a Soniprep 150 (Sanyo MSE) for ten s at a probe amplitude of 5μm and centrifuged at 10,000 $_g$ for 30 min in a pre-cooled (4°C) Eppendorf 5810 centrifuge. The supernatant was retained, separated into aliquots, labelled and assayed for protein concentration according to the method of Bradford (Bradford, 1976). Bradford reagent was

used as it was the most cost-effective way to accommodate the varying buffer needs of the lab.

3.3.d: Muscle preparation:

The muscle tissue samples listed in Table. 3.3.d.i were obtained in the following manner: animals were sacrificed either by sodium pentobarbital administration and/or cervical dislocation (see section 3.2). Skeletal muscle and heart samples were excised and snap frozen in liquid nitrogen. Muscle samples were weighed and placed in five to ten volumes of modified RIPA buffer (15mM NaCl, 0.1% NP-40, 0.05% sodium deoxycholate, 0.1% SDS, 5mM Tris-HCl pH 8.8 plus freshly added protease inhibitors (table 3.3.d.ii)), and were then homogenised by three thirty second bursts of an OMNI Probe ($\geq$ 200 µl per sample) or Ultra Turrex homogeniser ($\leq$ 1 ml sample volume). Total lysate/homogenate samples were then centrifuged at 13000 g_{max} for thirty minutes to pellet any debris. The resulting supernatant was divided into 0.5ml aliquots, a separate sample was taken for determination of protein content by the Bradford assay and the remaining aliquots were snap-frozen in liquid nitrogen and stored at -80°C until use.

.

	Rabbit	Rat	Guinea pig	Mouse
Heart	√	√	√	√
Diaphragm	√	√	√	√
Sterno hyoid	√	√	√	√
Sterno mastoid	√			
Gastrocnemius	√	√	√	√
Soleus	√	√	√	√
Vastus Lateralis	√	√	√	√
Latissimus Dorsi	√			

Table 3.3.d.i: Muscles excised from rodents.

Protease Inhibitors	Inhibits	Stock	Used at
Aprotinin	Trypsin, Chymotrypsin and plasmin	2mg/ ml	2μg/ml
Leupeptin	Lysosomal proteases	2mg/ ml	2μg/ml
Pepstatin A	Aspartic Proteases	2mg/ ml	2μg/ml
Sodium Fluoride	Serine and Threonine Phosphatases	500mM	200mM
PMSF (phenylmethylsulfonyl fluoride)	Serine and cysteine Porteases	50mM	5mM/ml

Table 3.3.d.ii: Protease Inhibitors and Phosphatase Inhibitor used in Homogenisation and RIPA based sample preparation.

3.3.e: Bradford assay

Bradford assays were performed in 96 well plate format using a 1:100 dilution of samples prepared with deionised water and vortexed for thirty seconds. Samples, or standards and deionised water (made up to 100μl) were pipetted into wells of 96 polystyrene clear plate in duplicate and mixed with Bradford reagent (100 μl) (Sigma, Cat. No. B6916) in the manner described in tables 3.3.c and d. The Bradford method of protein quantification is a colorimetric reaction which works on the premise of Coomassie brillliant blue interaction with proteins (Bradford, 1976). In an acidic solution, Bradford reagent (in its unbound state a reddish brown colour) binds to arginine and aromatic amino acids within proteins and causes the absorbance of the solution to shift from 470nm to 595 nm peak absorbance, giving a blue colour, which can be read using a spectrophotometer. The Bradford assay was used as it is a quick and simple method for determination of the protein content of samples. Detergent-containing samples must be diluted before protein quantification can occur using the Bradford method, as SDS and other detergents can interfere with detection. Samples are compared and their protein content intrapolated using a standard curve of known protein concentrations, frequently albumin. Plates were read using a Spectramax photometer at a wavelength of 595 nm, and compared to bovine serum albumin standard curve (BSA, Sigma, A7906).

BSA concentration (1μg/μL stock)	Distilled water (μL)	Bradford reagent (μL)
0	100	100
0.5	99.5	100
1	99	100
1.5	98.5	100
2	98	100
2.5	97.5	100
3	97	100
3.5	96.5	100

Table 3.3.e.i: BSA, distilled water and Bradford reagent concentrations and layout for Bradford assay.

Sample dilutions	Sample volume from 1 in 100 stock)	Distilled water (μL)	Bradford (μL)
1 in 1000	10	90	100
1 in 1000	10	90	100
1 in 500	20	80	100
1 in 500	20	80	100
1 in 250	40	60	100
1 in 250	40	60	100
1 in 100	100	0	100
1 in 100	100	0	100

Table 3.3.e.ii: Typical Sample dilutions, distilled water content and Bradford reagent volumes used in protein determination using the Bradford assay.

3.3.f: Over expression of FKBP12-GST protein for affinity purification assays

Generation of a PGEX-2TK plasmid containing a GST tagged FKBP12 sequence was performed by JJM and is described by Carmody et al. (Carmody *et al, 2001*).This plasmid or a GST only plasmid was transfected into competent DH5α' *E. coli* cells, stocks of which were and maintained at -20°C. Cultures of FKBP12-GST or GST only transfected bacteria were used to inoculate 5 ml of LB broth (containing 100 μg/ml ampicillin) overnight (New Brunswick Scientific Excella E24 incubator). These cultures were then expanded by addition of 1 ml of overnight culture to 50 mls of LB broth and grown at 37°C until an Optical density of 0.6 was obtained at 600nm (using an Eppendorf Biophotometer). Bacteria were then induced to synthesize GST or FKBP12-GST protein by addition of 1 mM isopropyl β-D-thiogalactoside (IPTG) followed by incubation for approximately 2 hours at 27 °C. The bacterial suspension was collected by centrifugation at $3000 \times g_{max}$ for 10 min at 4°C in Eppendorf Centrifuge 5810 rotor. The bacterial pellet was then lysed in lysis solution containing 0.1% Triton X-100 and 100 μg/ml lysozyme in ice-cold PBS and sonicated in three 10 s bursts (on ice). The lysate were then cleared by centrifugation at 20,000 g_{max} in a pre-cooled Jouan MR 1822 centrifuge for 60 min at 4°C.

The resulting supernatant was then incubated glutathione Sepharose 4B beads (GE healthcare) in FKBP wash buffer (300 mM sucrose,170 mM NaCl, 0.1% CHAPS (3(cholamidopropyl)dimethylammonio)-1-propane-sulfonate), 2 mM dithiothreitol, 20 mM Tris–HCl pH 7.4 and protease inhibitors) in 15 ml tubes fixed onto a shaker overnight at 4°C. After incubation, the beads were pelleted using a Labnet bench top microfuge for 1 minute at 16,600 g_{max} and washed using ice cold FKBP WB with added protease inhibitors (as used in

sample homogenisation). This was repeated three times. GST or FKBP-GST bound beads were either used immediately or stored at 4°C.

For use in affinity purification experiments, rat brain or quadriceps muscle was homogenised as described in section 3.3. The total membranes fraction was solubilised for 1 hour at room temperature in 2% CHAPS, 500mM NaCl, with 20 mM Tris HCl pH 7.4 with added protease inhibitors, and then centrifuged at 20,000 g for 1 hour at 4°C (Jouan MR 1822 refrigerated centrifuge). The resulting supernatant was aliquoted, diluted to five times its volume (to dilute NaCl to 100 mM) with Tris HCl pH 7.4 and 10 ml of this solution was incubated with glutathione Sepharose 4B beads, GST-bound beads or FKBP12-GST bound beads overnight with rotation at 4°C. Following incubation, the samples were cleared by centrifugation in 1.5 ml Eppendorf tubes at 16,600 g_{max} and samples of supernatant and pelleted bead-protein complexes were taken for subsequent analysis by SDS PAGE and Western blot.

3.4: Peptide array and Chromatography.

3.4.a: Materials:

Hydroxyapatite matrix (Calbiochem, now distributed by Sigma, cat no 55497)Heparin agarose matrix(H6508, Sigma) reactive red matrix(R0503, Sigma) Phenyl Sepharose Matrix(P7892, Sigma) Concanavalin agarose (C7555, Sigma). Wash and elution buffers, as described in table 3.4.a. Solubilisation buffer (1% Triton-X 100, 0.5M NaCl, 20mM Tris-HCl pH 7). Hyd Ap column buffer (10mM NaH_2PO_4, 100µM $CaCl_2$, 0.1%

Triton-X100, 20% glycerol, and 100mM NaCl).Triton-x-100 detergent (T8787, Sigma). CHAPS (3-((cholamidopropyl)dimethylammonio)-1-propane-sulfonate), 2) C5070, Sigma). Phosphate buffered saline (137.5 mM NaCl, 2.68 mM KCl, 10.14 mM Na_2HPO_4 , 1.76mM $KH_2 PO_4$.) Tris Buffered saline (140 mM NaCl, 20 mM Tris-HCL pH 7.4). Methanol (179957, Sigma). Bovine serum albumin, fraction V (Sigma, O5479). Streptavidin peroxidase, ultrasensitive (S23438, Sigma). Isoelectric focussing equipment (Amersham Biosciences) and IPG strips were from GE healthcare life sciences, Amersham Place, Little Chalfont, Buckinghamshire, HP7 9NA UK). Biotinylated peptides as described in section 4.1. SDS-PAGE reagents as described in section 3.5.

3.4.b: Batch Chromatography

A549 homogenate (2 mg protein/ml, prepared as described in section 3.3.b) was solubilised for 1 hour at room temperature in 1% Triton-X 100, 0.5M NaCl, 20mM Tris-HCl pH 7.4 and freshly added protease inhibitors. The solubilised samples were then cleared in a Beckman Avanti JA 25-50 rotor for 1 h at 75,600 g_{max} at 4°C and the resulting supernatant and pellet were diluted with Tris-HCl pH 7.4 to 100 mM NaCl concentration and incubated overnight at 4°C with 40 μl of resuspended concanavalin A, heparin agarose, hydroxyapatite, phenyl sepharose and reactive red matrices. These were collected by centrifugation using a tabletop microcentrifuge (Labnet microfuge) and washed repeatedly with ice-cold wash buffer (see Table 3.4.a for wash/elution buffers below) between clearing via centrifugation for 5 min at 14500 g_{max}. After washing, proteins were eluted using various elution buffers (see table 3.4.a). Pellet and supernatant samples were dissolved in 1X SDS-PAGE sample buffer, heated to 100°C for 7 min and loaded onto 7.5% polyacrylamide gels with 4%

stacking gel as described in Section 3.5 (see table 3.5a and b). Samples were either transferred to PVDF membranes for Western blotting or stained in Coomassie brilliant blue.

Matrix used	Binding Mode	Wash Buffer	Elution Buffer
Concanavalin A	Affinity chromatography: Lethcin binding	20 mM Tris HCl pH7.4, 0.2% CHAPS	0.5 M NaCl, 20 mM Tris HCl pH 7.4, 0.2% CHAPS
Heparin Agarose	Ion exchange or affinity chromatography	20 mM Tris HCl pH 7.4, 0.2% CHAPS	0.5 M NaCl, 20 mM Tris HCl pH 7.4, 0.2% CHAPS
Hydroxy Apatite	Mixed mode: Ion exchange (NaCl buffer) or interaction with P and C sites (phosphate or calcium gradient)	20 mM Tris HCl pH 7.4, 0.2% CHAPS	0.5 M NaCl, 20 mM Tris HCl pH 7.4, 0.2% CHAPS
Phenyl Sepharose	Hydrophobic interaction chromatography	0.5M NaCl, 20 mM Tris HCl pH7.4, 0.2% CHAPS	20 mM Tris HCl pH 7.4, 0.2% CHAPS
Reactive Red	Affintiy Chromatography: binds -NH2 groups	0.5 mM DTT, 20mM Tris pH8.8, 0.2% CHAPS	1M KCl, 20mM Tris pH8.0, 0.5mM DTT,0.2% CHAPS

Table 3.4.a: matrices used in batch chromatography and corresponding wash and elution buffers.

3.4.c: Hydroxyapatite chromatography:

One gram of Hydroxyapatite matrix was prepared by re-suspension followed by at least three washes of PBS to remove any fine particulate matter. The slurry was then loaded into 25 ml columns, to a depth of 1-2cm bed height, and tapped to remove air bubbles. The column was equilibrated with 3 rinses of wash buffer containing 10mM NaH_2PO_4, 100μM $CaCl_2$, 0.1% Triton-X100, 20% glycerol, and 100mM NaCl. Solubilised A549 sample (1-2 mg protein/ml) was diluted with 5 volumes of Tris pH 7.4 to lower NaCl concentration to

100mM, and the pre-cooled solute was loaded onto the column. Samples of all flow-through and eluents were collected, and the column was kept at approximately 4°C using ice-packs. Proteins were eluted from the column using a stepwise NaCl gradient from 100mM to 2M concentration, and the column was washed between elution steps with 2 column volumes of wash buffer. Elution Buffer contained 50mM NaH_2PO_4, 100µM $CaCl_2$, 0.1% Triton-X100, 20% glycerol and 100mM-2M NaCl. After sample collection, 200µl of each fraction was incubated overnight at -20°C in 1ml acetone to concentrate any proteins present, after which samples were centrifuged at 16,600 g_{max} for 10-30 min at 4 °C, the acetone removed and pellet dried briefly. Twenty microlitres of 2X reducing SDS-PAGE sample buffer was added to each sample, which were then boiled at 95°C and centrifuged before loading onto 10% polyacrylamide gels for SDS-PAGE and subsequent staining or transfer as described in section 3.3.

3.4.d: Peptide Overlay

Peptide assay was performed to determine optimum signal to noise ratio for the biotinylated peptides. Three hundred micrograms of protein from crude A549 homogenate was subjected to 10% polyacrylamide SDS-PAGE with a 4% stacking gel. Gels were transferred and blocked as described previously, except 5% BSA in TBS was used as blocking and incubation buffer. The blots were incubated in varying amounts of either SH3B, SCRAM peptides or 5% BSA in TBS using a multiscreen system from Biorad. Peptide concentrations used for both SH3B and SCRAM peptides were 10, 5, 2, 1, 0.1, 0.05, 0.02, 0.01 µM, diluted in 5% BSA in TBS, and were incubated overnight at 4°C with rotation (SH3B and SCRAM peptides were custom ordered from Genscript and are described in

section 4.1). The membranes were washed using TBS with 0.1% CHAPS (3 x 10 minute washes). Blots were incubated in 1:10,000 Streptavidin peroxidase HRP in 5% BSA in TBS with 01% CHAPS for 1 hour at room temperature. They were then developed as described in section 3.5.c. Subsequent peptide overlays were performed in the same manner using the optimised amount of SH3B peptide, as described in section 4.1.

3.4.e: Biotin Blocking of spurious reactions

Materials: as for peptide overlay, Streptavidin (unlabbelled-Sigma Cat no S4762), Biotin (Sigma, Cat no B4501).

After peptide overlay blots were transferred to PVDF membranes and blocked as normal, a second blocking step was performed to occupy any natural biotin-containing proteins. This was performed by incubating the blot using 0.5-1 mg/ml streptavidin in TBS at room temperature for 30 minutes to 1 hour, followed by washing twice in plain TBS. To prevent biotinylated peptides binding to the streptavidin, the blots were then incubated in a four-fold amount of Biotin (e.g.: if 1 mg/ml of streptavidin was used, a concentration of 4 mg/ml of biotin was employed) in TBS for 1 hour, rinsed with standard wash buffer twice and the peptide assay was continued as described in section 3.4.d.

3.4.f: Isoelectric focusing:

Isoelectric focusing was performed in the Biochemistry Department of University College Cork, in collaboration with and under the supervision of Prof. David Sheehan and Dr. Wentao Hu. Pooled 2M NaCl-eluents from hydroxylapatite chromatography were concentrated using acetone to 300μg/μl and dissolved 125μl of IEF rehydration buffer, containing 2μl destreak solution and 5μl carrier ampholytes from Sigma and Amersham, respectively. Samples were vortexed and centrifuged briefly to ensure they were thoroughly mixed, and 125μl of the sample was used to rehydrate iso-electric focusing strips of either 7 or 18cm length, with a pH gradient from 3-10 or 4-7, overnight. During focusing, strips in the rehydration tray were covered in mineral oil to prevent dehydration and sample loss. After rehydration the strips were focused at 500 V (1 h), 1000 V (8 h) and held at 5000V (8 hours. Strips were flash-frozen using liquid nitrogen for storage or used immediately.

3.4.g: Press-Blotting of IEF Strips:

Defrosted 18cm IEF strips with a pH gradient of 4-7 were transferred directly to PVDF membranes. The PVDF was pre-soaked in methanol and equilibrated in press-blot solution (500mM NaCl, 200mM Tris HCl pH7.4) for 5 minutes. The membranes were then laid onto the IEF strips and weighed down with filter papers soaked in press-blot solution. Dry filter papers were stacked on top of the IEF strip-PVDF sandwich, which was then covered and weighed down for 15-30 min. After transfer the blots were washed TBS with 0.1% CHAPS for 5 minutes and blocked as described previously.

3.5 : SDS-PAGE and Immunoblotting

3.5.a: Materials:

Biorad Tetra electrophoresis apparatus and transfer system. Sample buffer: 250 mM Tris HCL pH 6.8, 10% SDS, 30% glycerol, 0.4% bromophenol blue. 10X SDS PAGE running Buffer (1L): 10 g SDS, 30.3g Tris Base, 144g Glycine.10X Transfer Buffer (1L): 3.7g SDS, 25.22g Tris Base, 112.6 g Glycine. Precision Plus Protein™ All Blue Standards, Bio-Rad, (Cat. No. 161-0373), Pierce prestained Molecular weight marker, Thermo-Scientific, (Cat. No. 26612) or "Colorburst" electrophoresis marker, (Sigma Cat. No. C1992), Methanol, Sigma (Cat. No. 322415). Thermo Scientific Enhanced chemiluminesence substrate (catalog no: PL-32106), homemade ECL substrate (H_2O_2 (cat no.216763), p-Coumaric acid(cat no. C9008) and luminol (cat no. 123072) from Sigma) (ECL component 1: 0.5mM luminol 0.4mM p-Coumaric acid, 10 ml 0.5M Tris HCL pH 8.5, made up to 50 ml. ECL component 2: 0.02% H_2O_2,10ml 0.5M Tris pH 8.5, made up to 50 ml total volume with deionised water.) Kodak Carestream film, 5 x 7', (Sigma, Z30428). AGFA developer (CP1000) Licor C-Digit blot scanner, (Cat. No. 980-13723, LICOR Biosciences UK Ltd, St. Johns Innovation Centre, Cowley Road, Cambridge, CB4 0WS, United Kingdom). Coomassie brilliant blue R250 (Sigma Cat. No.B8522). Immobilon-P PVDF membrane (IPVH00010, Merck Millipore, Tullagreen, Carrigtwohill, Cork, Ireland).

3.5.b: SDS-PAGE

All samples were subjected to electrophoresis on either 7.5% or 10% resolving gels with a 4% stacking gel, with the exception of RyR blots (3% stacking gel with a 5 or 6% resolving gel, see tables 3.5a and b below). The polyacrylamide gels were fixed into the electrophoresis rig and the wells were washed with 1X running buffer. The chambers of the electrophoresis rig were filled with the same buffer. DTT (50 mM) was added to 2X sample buffer (250 mM Tris HCL pH 6.8, 10% SDS, 30% glycerol, 0.4% bromophenol blue) and added to samples containing 30-60μg of protein Samples were then boiled for 7 min at 100°C in 1.5ml Eppendorf tubes and centrifuged for 1 min in a benchtop Labnet microcentrifuge at $16,600_{gmax}$ at room temperature. Samples were immediately placed on ice and 20-30 μl of supernatant were loaded slowly into wells of 1.5 mm gels.

SDS-PAGE gels were run at 20 mA per gel for approximately 90 min, or until the dye-front was within 5 mm of the bottom of the gel. After electrophoresis gels were either briefly rinsed in deionised water and stained for 1-4 hours in Coomassie brilliant blue R250 in a scrupulously clean staining tray, or transferred to Immobilon-P Polyvinylidene Flouride (PVDF) membranes.

Stacking Gel	3% Acrylamide	4% Acrylamide
30% acrylamide/ Bis acrylamide (29:1)	0.4 ml	0.533 ml
Tris-HCl pH 6.8	1 ml	1 ml
distilled water	2.14 ml	2.5 ml
10% SDS	40 µl	40 µl
10% Ammonium persulfate (APS)	16 µl	16 µl
TEMED (N,N,N',N'-tetramethylethane-1,2-diamine)	4 µl	4 µl
Glycerol	0.4 ml	

Table 3.5.a: Components of stacking gels (4 ml total volume) use in SDS-PAGE experiments. The stacking gel uses a lower pH and larger pores (due to lower acylamide percentage) to evenly stack the proteins before they are electrophoresed into the resolving gel. The 3% gels have glycerol added to stabilise them due to low acrylamide content.

Resolving Gel	5%	6%	7.50%	10%	12%	15%
30% acrylamide/ Bis acrylamide (29:1)	1.33 ml	1.6 ml	2 ml	2.6 ml	3.2 ml	4 ml
Tris-HCl pH 8.8	1 ml	1 ml	1 ml	2 ml	2 ml	2 ml
distilled water	5.55 ml	5.2 ml	4.88 ml	3.38 ml	2.68 ml	1.8 ml
10% SDS	80 µl	80 µl	80 µl	80 µl	80 µl	80 µl
10% Ammonium persulfate (APS)	32 µl	32 µl	32 µl	32 µl	32 µl	32 µl
TEMED (N,N,N',N'-tetramethylethane-1,2-diamine)	8 µl	8 µl	8 µl	8 µl	8 µl	8 µl
Overlay with Isopropanol	(200 µl)	(200 µl)	(200 µl)	(200 µl)	(200 µl)	(200 µl)

Table 3.5.b: Components of resolving gels (8ml total volume) used in SDS-PAGE experiments. Gels were overlaid with 200 µl of 70% isopropanol to smooth the top of the

gel. This was washed off with distilled water prior to pouring the stacking gel. Higher percentages of acrylamide were used to separate lower molecular weight proteins.

3.5.c: Immunoblotting

Transfer of proteins from SDS-PAGE gels to PVDF membranes was performed for 70 min at 70 V in a pre-cooled Biorad wet transfer apparatus. Upon removal from transfer apparatus, membranes were rinsed in dH_2O, stained in 0.1% Ponceau S solution in acetic acid (Cat. No. 78736, Sigma) to ensure transfer of proteins to the membrane was successful, washed with PBS and blocked for two hours at room temperature in 5% milk in PBS on a shaking platform at approximately 30 rpm. Blots were then incubated in different antibodies (Table 3.2.e) in blocking buffer overnight at 4°C in plastic sheets sealed with a heat sealer. As many bubbles as possible were removed prior to sealing in the membranes. Following primary antibody incubation, blots were separately washed thrice (ten min per wash) in PBS or PBS with 0.1% Tween-20, and incubated with secondary antibody/peroxidase conjugates (anti-rabbit, Sigma Aldrich catalog number O545) anti-mouse (A9917) or anti-goat IgG (A8919), 1:1000 dilution) in blocking buffer for 1 h at room temperature (18-22°C). Blots were then re-washed as described and developed via incubation with 0.5 ml each of ECL reagent 1 and 2 for 1 min followed by exposure to X-ray film (Kodak) in a developing cassette, followed by development on an AGFA developer, or by scanning with a Licor Blot scanner.

Enhanced chemiluminsecence has widely replaced colourimetric detection of protein on western blots. ECL buffers typically involve two buffers, one which contains H_2O_2 and the

other which contains luminol, a substrate for horse radish peroxidase (HRP) HRP-linked antibodies react with H_2O_2 in buffer A and luminol in buffer B to facilitate the production of light. In this laboratory, ECL reagents were either from Thermo Scientific or homemade using (H_2O_2 (cat no.216763), p-Coumaric acid (cat no. C9008) and luminol (cat no. 123072) from Sigma) (ECl component 1: luminol (0.5mM), 0.4mM p-Coumaric acid, 10 ml 0.5M Tris HCL pH 8.5, made up to 50 ml. ECL component 2: 0.02% H_2O_2, 10ml 0.5M Tris pH 8.5, made up to 50 ml total volume with deionised water and stored in the dark at 4ºC. Blots were rinsed briefly in PBS or TBS containing no detergent after third wash following secondary antibody incubation. Meanwhile, 1 ml of buffers A and B (per blot) or components 1 and 2 were pipetted on to an acetate sheet fixed to an X-ray blot cassette. Blots were placed protein-side down and gently moved from side to side to properly mix buffers A and B using a plastic tweezers. After a 1 min incubation period, excess buffer was removed using paper towel placed at the edge of the blot and lifting the cassette at a 45° angle. The blot was flipped to display the protein-side up, an acetate sheet was quickly placed on top and bubbles were removed from the sandwich using a roller or heavy bottle. The cassettes were then brought to the dark room and exposed to Kodak X-ray film. X-ray films are covered with an emulsion of silver halide crystals which react with light producing a latent image which when developed is reduced to a black image on the film.

After development, films were marked with locations of molecular weight markers (Thermo scientific, Biorad All Blue precision plus or Sigma Colorburst) and washed with PBS. X-ray films were then imaged by use of a Vilbur Lourmat light box and UVIPro transilluminator box and camera, and images were taken and recorded as JPEG files using

UVI Photo MW software (UVI Tech, UVItec Limited, Unit 36, St John's Innovation Centre, Cowley Street, Cambridge CB4 0WS, United Kingdom). For many blots, reprobing with a second or third antibody was performed as follows: blots were washed in either PBS or TBS thrice for 10 minutes. To strip off the bound antibodies, blots were incubated in either stripping buffer (0.75g Glycine, 0.05g SDS, 500 μl Tween 20; made up to 50 ml with distilled water and brought to a pH of 2.2) at 50°C for thirty minutes in a sealed bag, or incubated in a clean tray with approximately 30 ml of 0.2M NaOH for 3 minutes at room temperature. After stripping blots were re-blocked in 5% milk in PBS/TBS (as appropriate) for 1 hour and re-probed overnight at 4°C in a new primary antibody solution.

3.5.d: Coomassie staining of blots

Upon completion of western blotting procedures, PVDF membranes were stained with a solution containing 0.1% Coomassie Brilliant blue R250 (Sigma Cat. No.B8522) in methanol and distilled water (50:50 ratio) for 3 minutes in a tray cleaned with ethanol, as described in (Welinder and Ekblad, 2011). Destaining was completed using a solution of ethanol, acetic acid and water (Acetic Acid: EtOH: dH_2O ratio of 1:5:4). Destaining solution was changed after thirty minutes or until protein bands were clearly visible. Membranes were then air dried and imaged using a UVIPro transilluminator box and camera, as described in the western blotting section.

3.5.e: Peptide synthesis

Spot synthesis of peptides onto nitrocellulose membranes was completed in the laboratory of Dr. P.A Kiely at the University of Limerick, Ireland. 18-mer fragments of rabbit JPH1 were synthesised by Ms. Maeve Kiely with FMOC (9-Fluorenylmethyloxycarbonyl) chemistry using an automatic spot synthesis program and an Autospot Robot ASS 222 (from Intavis Bioanalytical Instruments). Peptides were synthesised on a continuous nitrocellulose support and were detected under UV light. Upon receipt of the peptide arrays in UCC, they were treated essentially as described for Western blot experiments using mAb VF1c, except that all buffers employed Tris buffered saline, and washes were increased to 15 minutes per wash. Peptide arrays were developed using both fluorescent secondary antibodies (Cy2 ^{TM} and Cy3 conjugated AffiniPure Donkey Anti-rabbit and anti mouse IgG Secondary antibody, Cat. No.711225-152 and 715225-150, Jackson ImmunoResearch Europe Ltd. 1:10,000 dilution in 1% milk in TBS) and HRP-tagged secondary antibodies (1;2000 dilution, in 1% milk in TBS) using thermo ECL reagents and film from Sigma.

3.5.f: Over- expression of Junctophilin fragments in Yeast.

In the laboratory of Prof V. Sorrentino in Sienna, fragments of human JPH1 were expressed in *Saccharomyces cerevisiae* strain Y153 by Ms. Anna Carla, as described in (Bagnato *et al,* 2002) except using cDNA fragments corresponding to amino acids 1-233(a) 232-369 (b), 141-278(c), 141-278 (d), 229-460(e), 154-278 (f), 229-550(g, 154-635 (h) of human JPH1.These were cloned into a pGBKT7 vector and expressed under the control of a

GAL4-BD promoter using a Matchmaker III system from Clontech. Positive clones were selected by β-galactosidase assays. The positive yeast clones were expanded, lysed and run on 10% SDS PAGE followed by transfer to PVDF membranes which were dried and sent to our laboratory. Upon receipt of the membranes, they were rehydrated using a 15 s immersion in methanol and were blocked as described in section 3.5.b in 5% milk in PBS.

Clone name	A	B	C	D	E	F	G	H
JPH1 fragment	1-233	232-369	369-571	141-278	229-460	154-278	229-550	154-635

Table 3.5.c: Table describing the fragments of JPH1 expressed in yeast. These were generated by Ms. Anna Carla of the University of Sienna, Italy, these were synthesised to confirm or deny the interaction of mAb VF1c with JPH1 protein.

Antibody	Target	Dilution	Buffer	Company
VF1c	SR protein of 90 kDa	1 in 1500	5% milk/ PBS	Novus biological
JP1	Junctophilin 1	1 in 1500	5% milk/ PBS	Invitrogen
JP2	Junctophilin 2	1 in 1500	5% milk/ PBS	Santa Cruz biotech
Xa7	RyR1	1 in 1000	5% milk/ PBS	Santa Cruz biotech
Spectrin	Spectrin/ Fodrin II	1 in 1000	5% milk/ PBS	Antibody Verify
H300	RyR	1 in 1000	5% milk/ PBS	Santa Cruz biotech
RS4	RyR	1 in 1000	5% milk/ PBS	
SERCA 2	SERCA 2 protein	1 in 1000	5% milk/ PBS	Santa Cruz biotech
α-Tubulin	α Tubulin	1:50 000	5 milk/ in PBST (0.01% Tween-20)	Abcam
β-Actin	β Actin	1:20,000	5% BSA in TBST (0.01% Tween-20)	Calbiochem
PLC γ1	Phopholipase C γ1	1 in 1000	5% milk/ PBS	Sigma
PTN	Pleiotrophin 1	1 in 1000	5% milk/ PBS	OWL labs

Table 3.5.d.: Primary Antibodies used in western blot experiments.

3.5.g: Western blot quantification

After development, blot films were marked with location of molecular weight markers, and photographed using a Ulight box and UVItec CCD camera and acquisition software. The images were saved on to a removable disc in JPEG format. Images were analysed using Image J software (http://imagej.nih.gov/ij/). Bands of interest were located and sealed off using the straight line tool, and the area under the curve was measured for each band. For coomassie stained blots, the entire lane was measured and the sum of all peaks measured to give a reading for total protein per lane. For normalising to tubulin or total protein per lane, the intensity for each band of interest was divided by the intensity of the corresponding actin, tubulin or Coomassie stained lane. These manoeuvres were performed using Microsoft excel.

3.6: Statistical analysis

All statistical calculations were performed using Microsoft Excel or GraphPad Prism software with the exception of power calculations, which were performed using an online calculator (http://statpages.org/proppowr.html see appendices). Data from densitometry of blots was prepared in Excel, and then Prism was used to generate graphs and compare means in statistical tests. Unless otherwise stated, means of protein abundance as detected via western blot in test group were normalised to the control group (e.g. *mdx* JPH1 abundance in diaphragm was normalised to JPH1 abundance in wild type diaphragm etc.), and compared using a Students' T-Test (two-tailed). Significant differences were acknowledged when the p

value was found to be less than 0.05. For comparisons of multiple parameters, a one way analysis of variance was completed, again taking significance as a p value of less than 0.05.

3.7: Bioinformatic analysis:

Materials: Uniprot protein database (http://www.uniprot.org/), Protein Blast local Alignment tool (http://blast.ncbi.nlm.nih.gov/Blast.cgi). Online human predicted interaction database (OPHID - http://ophid.utoronto.ca/ophidv2.204/), Expasy Proteomic tools server (http://www.expasy.org/proteomics). TagIdent (http://web.expasy.org/tagident/). Clustal Omega protein alignment software (http://www.clustal.org/omega/) (Sievers *et al,* 2011)

Bioinformatic analysis were performed as described in sections 4.3, and 4.4. In most cases, FASTA sequences or accession numbers of desired proteins were obtained from the Uniprot website and used as input where necessary in Clustal Omega alignments. For identification of potential RyR1 interactors, the RyR1 protein was screened using the OPHID database, and potential interactors were tested experimentally (Chapter 4, section 4.4.1). To assemble a list of potential interaction partners based on experimental data (chapter 4, section 4.3), molecular weight, cellular location and isoelectric point and selected species were entered into the TagIdent database, which then generated a list of possible proteins of interest, or in this case a list of potential interactors. The results can be seen in Appendix I.

3.7.b: Calpain cleavage site approximation in JPH1 and JPH2:

Materials: Uniprot protein database, Site Predictor calpain cleavage prediction software (http://www.dmbr.ugent.be/prx/bioit2-public/SitePrediction/) (Verspurten *et al*, 2009).

 FASTA sequence of JPH1 and 2 from rat, rabbit, mouse and human were obtained from from the Uniprot database. The sequences were separately inputted into the site predictor engine and analysed for calpain I or calpain II cleavage sites. Results were compared across the defined species, and calpain cleavage sites common to all were compiled into the tables seen in chapter 5.

3.7.c: R_f measurement

Materials: ruler, molecular weight standards (ThermoPierce molecular weight markers, cat no: 26612, Colourburst® Molecular weight markers, Sigma, cat no:C1992 or All-Blue Prestained protein plus,: Biorad cat no 1610373), Light box, CCD camera, SDS PAGE Coomassie or silver- stained gel or Blot (as in section 3.5 and 3.6), Microsoft Excel software (Microsoft, 2007).

Blots and gels were measured on the lightbox by placing te ruler as close as possible and in a straight line next to the molecular weight standards. The distance between the top of the gel (the beginning of the resolving gel) and the bottom of the gel (the dye-front) were noted. The distance travelled by each molecular weight marker was then measured, and the ratio of the distance travelled over length of gels or blots were used to generate a curve using Excel software. Bands of unknown or undetermined molecular weight were also measured and

their molecular weight was extrapolated from the curve generated by the standards. An example is shown in Figure 3.5.a

Molecular weight (Da)	Dist. Travelled (mm)	dist. travelled / gel length	Log of MW	R_f
250000	4	0.07	5.397940009	0.067797
150000	6.5	0.11	5.176091259	0.110169
100000	13	0.22	5	0.220339
75000	18.5	0.31	4.875061263	0.313559
50000	27.5	0.47	4.698970004	0.466102
37000	36.5	0.62	4.568201724	0.618644
25000	48	0.81	4.397940009	0.813559
15000	54	0.92	4.176091259	0.915254
10000	59	1.00	4	1

SH3B	Dist. Travelled (mm)	dist. travelled / gel length	$R_f - c$	R_f / x	MW (kDa)
Band 1: 120kDa	9	0.15	-3.88	5.17	146.365
Band 2: 75 kDa	19	0.32	-3.71	4.94	87.03

Figure 3.5.a: Example of R_f measurement. The distances travelled by molecular weight markers are treated as standards and used to extrapolate the apparent molecular weight of proteins of interest.

Chapter 4: Characterisation of potential RyR1-SH3 Binding domain interaction partners

4.1:Introduction

The type 1 Ryanodine receptor (RyR1) is a large homotetrameric protein with many different regions, as described in section 1.4.a, one of which is a proline rich region between the amino acids of 4254 to 4631. This proline rich region is has so far been poorly characterised, but due to its position in divergent region 1 of RyR1, has the potential to be important to protein-protein interactions and may be the site of regulation of Ca^{2+} inactivation in this channel (Benacquista *et al*, 2000).

Based on the *in silico* analyses of Wu *et al* in 2007, peptide array target screens identified a region of RyR1within the proline rich area which interacts with a candidate Src Homology 3 (SH3) binding domain. Wu *et al* used modular expression of SH3 domains from 8 proteins as "prey" and screened them with over 1000 potential interacting peptides (used as bait) in what was termed a peptide array target screening (PATS) assay. It was found that the proline rich region near the C terminal end of RyR1 (amino acids 4521-4533) could interact with the modular SH3 domains from PLCγ1 (amino acids 791-851), NCK1 and GRB2 in the array. To further characterise this interactions, and identify any other interacting protein(s), biotinylated peptides were designed by JJM to mimic the RyR1 proline-rich region, and were used in s series of over lay experiments (see results section 4.3.a to 4.3.f).

SH3 domains are non-catalytic domains, first identified by Mayer in 1988 (Mayer *et al*, 1988). They are small protein modules of approximately 50-70 amino acids, with the average SH3 domain being 60 αα residues in length (Sudol, 1998). While they are non-catalytic, they are crucial in cell signalling pathways as they mediate protein-protein interactions, and can thus increase local concentrations of effector molecules and enzymes with their relative binding partners.

Roughly 400 SH3 domains are encoded within the human genome, and are known to be expressed in at least 350 proteins (Larson et al, 2000, Jia et al, 2005). SH3 domains are typically comprised of 5 β-pleated sheets, termed βa-βe, which are linked by the RT-Src loop between βa-βb, the n-Src loop between βb-βc and the distal loop separating the βc and βd helices. The β-pleated sheets and loops fold into two perpendicular sheets, which have been named sheet 1 and 2 for clarity. Sheet 1 is comprised of βa, βe and the first half of βb. At a 90º angle to this, sheet 2 is formed from βc, βd and the second half of βb, which has a conserved kink in the middle of it, allowing it to participate in the two sheets via hydrogen bonding, known as the "β-bulge" (Larson, Davidson, 2000). The overall structure is important for creating "binding pockets", three of which exist in SH3 domains, and they form an indented space into which ligands can fit, and helps maintain the structural integrity of the interaction. The conserved RT and N-Src loops contribute to the specificity of binding with ligands. It should be noted that SH3 domains are able to fold and unfold within a biologically relevant timescale, which is to say that the folding and unfolding of SH3 domains have been measured at 1 second up to 1 hour, and this unfolding can be important for structure maintenance and allowing access to other domains within the protein (Wales and Engen,

2006). SH3 domains are known to bind Class I, II or II ligands, of which Class I and II both have the canonical –PxxP motif but with N- or C-terminal positive amino acids flanking them, which determines their binding orientation with respect to the RT-Src Loop. Class III ligands also exist, and are less specific. The location of the proteins themselves also contributes specificity upon the binding region (Mongiovi *et al,* 1999; Bartelt *et al*, 2015). The RyR1 proline rich region lies between amino acids 4462-4532, an area close to the ER membrane, and any interaction here could have important effects on gating, and thus on disease associated with calcium channel dysregulation. This area is also contained within the divergent region 1, a large, poorly conserved region of RyR1 (compared to RyR2 and 3) which has been implicated in the regulation of Ca^{2+} - inactivation of the channel, and thus it is imperative to confirm and validate any interactions which occur in this region (Benacquista *et al,* 2000).

To ascertain if any protein binds to this region of RyR1, two synthetic peptides were designed. The SH3B peptide mimics a class I (-AxPxxP-) SH3B binding region, corresponding to the sequence -PPKKQAPPSPPK- (amino acids 4520-4532 of RyR1, see Fig 4.1.a, which shows a species comparison of RyR1 proline rich regions and the fit of each orientation of the peptide as an SH3 binding region) with a biotin moiety at the N-terminal region and a linker region to allow flexibility; while the SCRAM control peptide has the same amino acids in a randomly scrambled order. Scrambling of the control peptide was done by assigning each amino acid in the SH3B peptide a number from 1-12, and an online random number generator was used to pick these out and so generate a peptide sequence without bias. The peptides also have an Aminohexanoic acid group (AHX) which allows

flexibility of the peptides and maintains distance between the streptavidin-biotin interface. This means the two peptide probes have the same amino acid composition and molecular weight, but different sequences. The biotin moiety facilitates detection using streptavidin peroxidase, as the biotin-streptavidin has been shown to have a dissociation constant of 4 x 10^{-14} M, and requires temperatures of 70°C to break the interaction (Holmberg *et al,* 2005). A cartoon of these peptides can be seen in Fig. 4.1.a. For these reasons, SH3B and SCRAM peptides were used to attempt to identify potential novel binding partners for RyR1.

4.2: Aims:

The aim of this research was to characterise the protein-protein interactions of the proline rich region of RyR1 using biotinylated mimic peptides SH3B and a scrambled version, SCRAM in overlay and pull down experiments. Cell culture screens were used to identify a suitable RyR1-expressing raw material, followed by overlay experiments using SH3B and SCRAM peptides to determine optimum working concentrations for these peptides. Chromatography matrices (reactive red, phenyl sepharose, heparin agarose, hydroxyapatite and concanavalin a, described in detail in the material and methods section) were used to further isolate potential interaction partners, and finally RyR1 complexes were isolated using bacterial overexpression of FKBP12 in immuoaffinity experiments followed by western blot analysis to test the validity of RyR1-protein interactions suggested by Wu *et al* (2007) and the Online Human Protein Interaction database (OPHID).
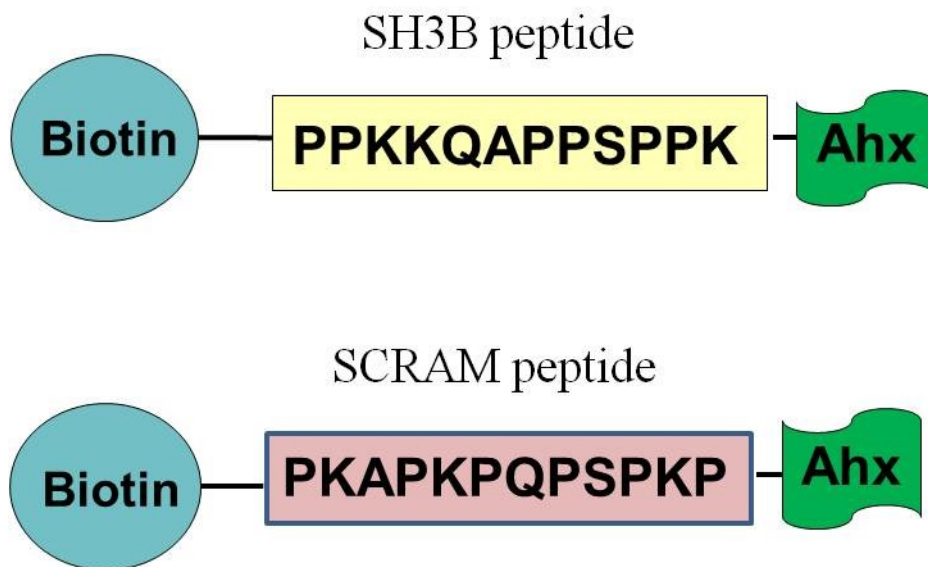
Figure 4.1: Cartoon of biotinylated peptides used in overlay and pull down experiments.
The peptides have a C terminal Biotin moiety and an N-terminal amidation group to help stabilize the peptide.

Figure 4.2: Clustal Omega alignment of the Proline rich region (αα4462-4532) of Human, rabbit, pig, mouse, rat and chimpanzee RyR1.

The Clustal Omega suite of EMBL was used to generate an alignment of the proline rich region believed to be involved in interactions with an SH3 domain-containing protein. (http://www.ebi.ac.uk/Tools/msa/clustalo/). SH3 domain ligands usually have either a class I (R/KxxPxxP), Class II (PxxPxR/K) or Class III structure (P-rich segments without the surrounding charged amino acids), but RyR1 has a proline rich region which could contain all three classes (Tonikan *et al*, 2009). RyR1 from *Homo sapiens* has both class I and II ligands, which are highlighted (yellow and blue boxes). It is possible that these putative SH3 domain ligands could interact with one or more SH3 domain containing proteins (Kang *et al,* 2000).

4.3: Results

4.3.a: Cell line screening for SH3B binding peptides

To determine if any proteins which could interact with SH3B peptide were detectable in a range of human and rodent cell types, homogenates from A549, JEG3, rat A7r5, SH-SY-5Y, Jurkat, U937, HL-60 and mouse C2C12 cell lines were subjected to peptide overlay as described in section 3.4. A summary of these is provided in table 4.3.a. Cell types were chosen based on their availability and expression of RyR1.

The resulting peptide overlay shows two bands at 150 kDa and 90 kDa (calculated molecular weight using R_f ,see section 3.6.c) are detectable in A549, JEG-3, A7r5, SH-SY-5Y and C2C12 cell lines. Molecular weights were estimated based on retardation factor (R_f) using the molecular weight markers as standards (graphs of R_f can be found in the appendix). Bands of 80kDa apparent molecular weight were detected in U937 and HL60 cell lines, with a possible band at 75 kDa in the Jurkat cell line. While C2C12 and A7r5 cell lines are from mouse and rat respectively, and do not have the same SH3 binding region on RyR1 as that found in humans,(see figure 4.3.a), they do display bands at 90 and 150 kDa.

Based on band intensity, A549 lung adenocarcinoma cell line was chosen for further study. A549 cell lines also had the advantage of growing quickly, thus enabling up-scaling of purification. Optimisation experiments were performed using A549 homogenate to determine the best signal to noise ratio for biotinylated peptide overlay.

	Organism	Tissue Type	Express RyR1?	Reference
A549	Human	Lung epithelial adenocarinoma	√	Xue et al 2000
A7r5	Rat	embryonic aorta smooth muscle	√	Hammoud et al, 2013
C2C12	Mouse	myoblast from CH3 mice	√	Bultynck et al, 2001
HL-60	Human	promyelocytic, from peripheral blood	RyR2	Girard *et al*, 2001
Jeg-3	Human	Placental epithelia, choriocarcinoma	√	Choudoury et al 2010
Jurkat	Human	T lymphocyte, peripheral blood	√	Hosoi et al, 2001
SH-SY5Y	Human	metastatic neuroblastoma, from bone marrow	√	Oules et al, 2012.
U-937	Human	leukemic monocyte lymphoma	√	Hosoi et al, 2001

Table 4.3.a: List of cell lines used in pilot overlay experiment. Cell lines (A549, A7r5, C2C12, HL-60, JEG-3, JURKAT, SH-SY-5Y, and U-937) which all express at least one isoform of RyR were subjected to peptide overlay using the biotinylated SH3B peptide. All cell lines express RyR1, except for HL-60, which express RyR2.
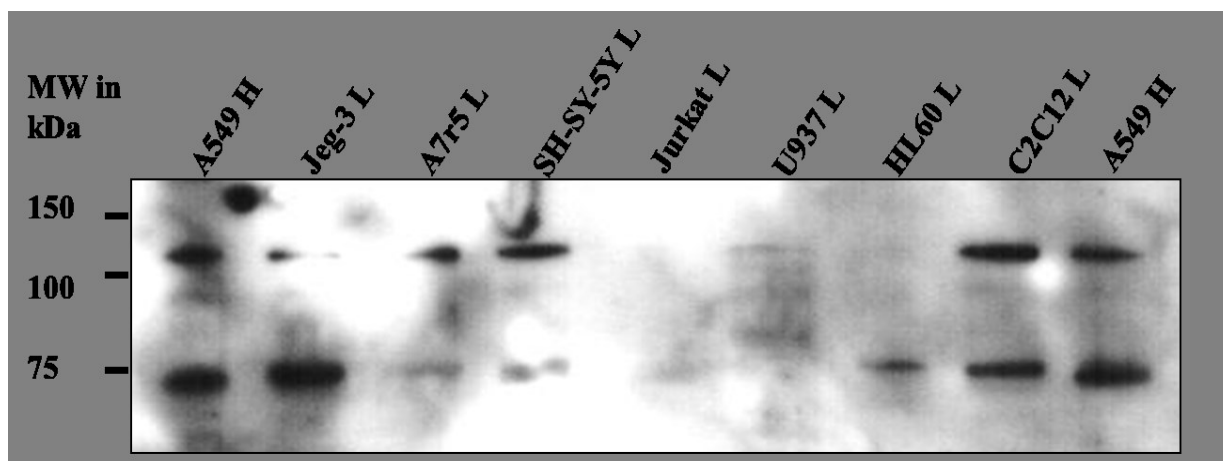
Figure 4.3.a: Investigation of SH3B-interacting proteins in cell lines. Cell lines were homogenised, or were used to prepare lysates, and were subjected to SDS-PAGE and transfer to PVDF membranes, followed by peptide overlay with the SH3B biotinylated peptide. Using this technique, a band was detected at 150 kDa in A549, JEG-3, A7r5, SH-SY-5Y, and C2C12 cells. A band at 90kDa in molecular weight was detected in all cell lines except Jurkat and U937 cells.

4.3.b: Peptide Assay

To determine the optimum working concentration of SH3B peptide for use in overlay experiments, multiscreen experiments were performed with a range of concentrations of SH3B peptides. This was performed to find the optimum signal to noise ratio. A549 homogenate was screened via peptide overlay with 5-0.1 µM of SH3B peptide, and the lowest signal to noise ratio was found using a concentration 0.1 µM. At this concentration,

two clear bands were visualised at approximately 120 and 75 kDa, as seen in figures 4.3.b,
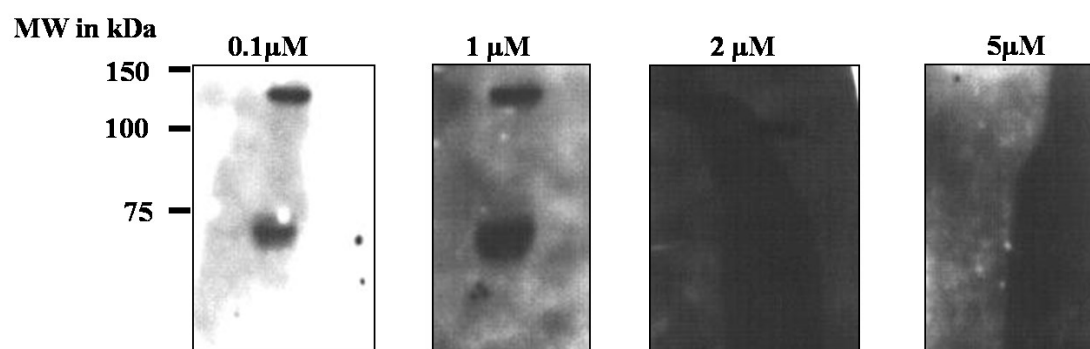
however the 2 and 5 µM panels are difficult to make out due to high background.

Figure 4.3.b: SH3B peptide overlay optimisation: Varying concentrations of SH3B peptide used in overlay experiments to probe A549 homogenate for interacting proteins. Bands are seen at approximately 125 and 75 kDa with the greatest clarity at 0.1µM SH3B.

4.3.c: Batch Chromatography

To further characterise the 125 and 75 kDa proteins, a selection of matrices were used in chromatography assays to remove contaminants. Solubilised A549 homogenate was incubated with various matrices on a small scale format as described in section 3.4.b, in an attempt to purify any novel interacting proteins for further analysis, e.g. by mass spectroscopy. While all matrices seemed to enrich the protein, hydroxyapatite and heparin agarose were found by visual inspection to have the greatest amount of 125 and 75 kDa

proteins, thus these matrices were chosen for larger scale purification of the proteins of interest.
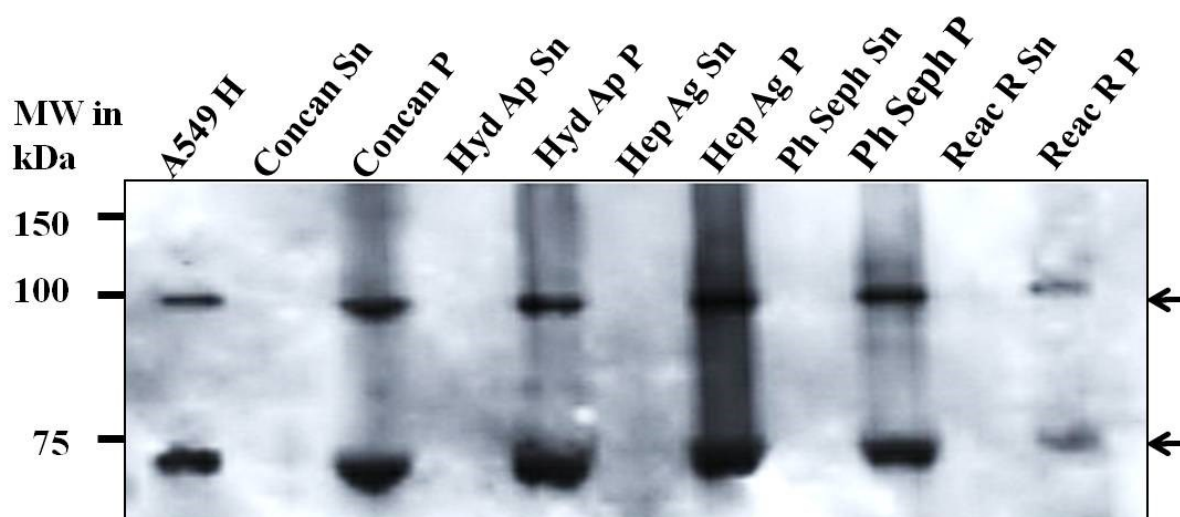
Figure 4.3.c: Batch chromatography of solubilised A549 homogenate. Matrices loaded were concanavolin A (Con), hydroxyapatite (Hyd A), heparin agarose (Hep A), phenyl sepharose (Pen) and reactive red (Reac R) matrices. The highest amount of protein detected from equal amounts of A549 homogenate with 0.1μM of SH3B peptide was in heparin agarose and hydroxyl apatite samples.

4.3.d Hydroxyapatite Chromatography

Hydroxyapatite chromatography was chosen as it provided a good yield of protein as detected using SH3B overlay (Heparin agarose also also tried, however the perotein could not be eluted at specific times using our buffer system, (data not shown) thus Hyproxyapatite was chosen for further analysis) Low-pressure column chromatography was performed using a

rehydrated hydroxyapatite matrix from Sigma, in the manner described in section 3.4. Hydroxyapatite was chosen for further study as this matrix yielded the highest amount of protein in the batch purification. Proteins were eluted from the column using a 100mM-2M NaCl gradient, and in the case of hydroxyapatite, the 75 kDa protein was eluted at 2M NaCl concentration (Figure 4.3.d.i). The proteins present in each fraction were compared using SDS PAGE and silver staining, and at 2M NaCl, several proteins were eluted, as seen in Fig 4.3.e, however only one of these proteins was detected at 75 kDa using an overlay experiment with the SH3B peptide. This protein was also found, along with another protein at 120kDa in the "Flow-through" sample. Hydroxyapatite was thus used for further isolation of these interaction proteins.

For convenient execution of SH3B, SCRAM and BLANK (Steptavidin-HRP-only controls), and to increase protein concentration, fractions were pooled into four samples. A549 homogenate (control sample), flow-through, 0.1-1M NaCl wash and 2M samples were subjected to peptide overlay, shown in Fig. 4.3.d.iii. In the 0.1-1M and 2M fractions, a band of 75 kDa apparent molecular weight was detected in all three blots (SCRAM, BLANK and SH3B), indicating that this protein was revealed to be a non-specific interaction. The SH3B panel also depicts a band at 125 kDa in all four fractions. If this protein does indeed bind to the SH3 binding domain of RyR1, further studies would have to be performed to confirm this
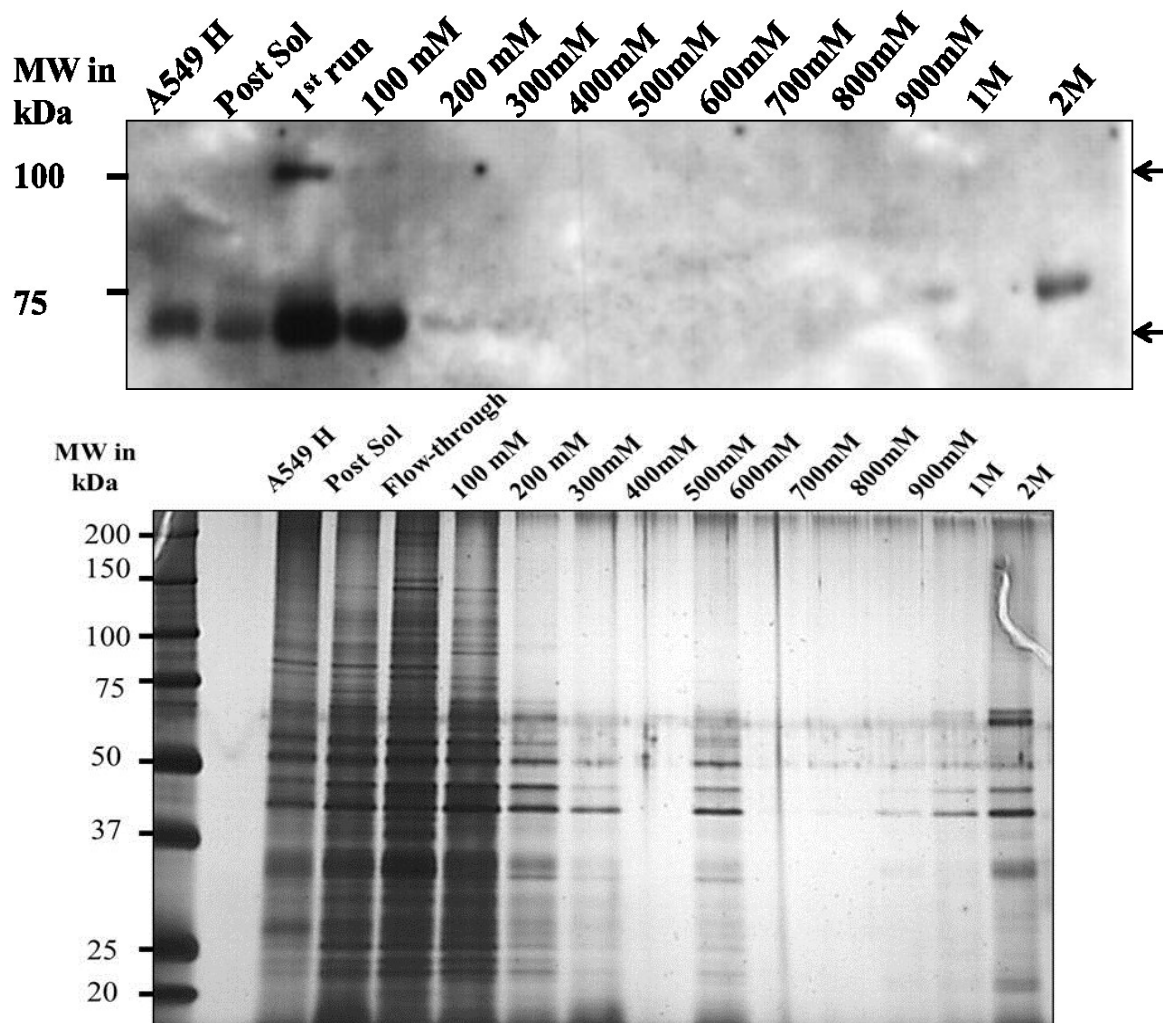
Figure 4.3.d.i : (top) A549 homogenate subjected to hydroxyapatite chromatograpy and peptide overlay using SH3B peptide or Silver stained(bottom). Solubilised and diluted A549 homogenate (1.5mg/ml A549 homogenate per solubilisation, 30 μg protein loaded per lane) was subjected to hydroxyapatite chromatography followed by peptide overlay with SH3B peptide. Equal volumes (10 mL) of each sample were concentrated using acetone

preciptitation at -20 °C overnight, then resolved by SDS-PAGE, transferred by western blotting and probed with the SH3B peptide in an overlay assay. A protein of 75 kDa apparent molecular weight was detected in the homogenate, solubilised material, flow-through, and in the 100 mM, 200 mM, 300 mM and 2M NaCl elution steps. The flow-through and 100mM fractions also contain a band at approximately 100 kDa (upper arrow). The 100 kDa protein is not seen in the 2M fraction. The bottom image shows Silver stained gel showing the A459 homogenates, post sol, flow-through, 0.1, 0.2, 0.3, 0.4, 0.5, 0.6, 0.7, 0.8, 0.9, 1M, and 2M fractions in lanes 3-15 respectively. There is a strong band in the 2M fraction at 75 kDa

4.3.e: Isoelectric focusing

Isoelectric focusing is the process of separating a protein or set of proteins according to their differing isoelectric points (pI). As each protein has a different isoelectric point based on its amino acid composition and post-translational modifications, this technique can theoretically be used to identify or narrow the identity of an unknown protein, as long as there are adequate detection methods. For this reason concentrated samples eluting at 2M NaCl from pooled hydroxyl apatite chromatography experiments were subjected to isoelectric focussing using strips with a pH gradient of 4-10. These strips were then press-blotted on to PVDF membranes and probed using the SCRAM and SH3B peptide. The results (Figure 4.3.e.i) show that the SH3B peptide detected a protein with an isoelectric point in the region of 5-6, with another band visible at an approximate pH between 6-7 pH units. These are likely to correspond to the two bands found using peptide overlay experiments (based on comparisons with stained gels, which show that many contaminants have been removed) and thus narrow the identity of these proteins to those within the given pI ranges. Using this

information, combined with knowledge of the molecular weight and the fact that this protein is more likely to only be expressed in humans, a "TagIdent" search was performed using these parameter to generate a pool of possible identities for this novel RyR1-interactor, the results of which can be seen in appendix I, Table 8.1.c.

In the SCRAM probed strip, multiple bands were detected, indicating that the SCRAM peptide or biotin moiety attached to it has interacted with several proteins, resulting in a "smeared" appearance. This demonstrates a non-specific interaction of this peptide with many proteins in the "2M" fraction, or it could be due to incomplete blocking of free sites on the membrane resulting in non-specific interactions.

In an attempt to gain more information about these potential RyR1 interactors, isoelectric focussing was performed using concentrated 2M fractions from the same experimental setup. The concentrated fractions were focussed on 7 and 18 cm strips with a pH gradient of 4-10, and were transferred to PVDF membranes by capillary transfer method. This allowed the direct imaging of protein locations along the length of the IEF strip, and thus gives an approximate indication of the isoelectric point (pI) of these peptide binding proteins. In this case, the SCRAM peptide gave many results along the length of the IEF strip, while the SH3B peptide gave a more specific result, with one major band at the positive end of the strip, which is closer to a pI of 4. This is interesting, as elution from a hydroxyl apatite

column at 2M NaCl would imply that the protein was basic in nature.

SH3B

＋ SCRAM **▬**

pH: 4   10
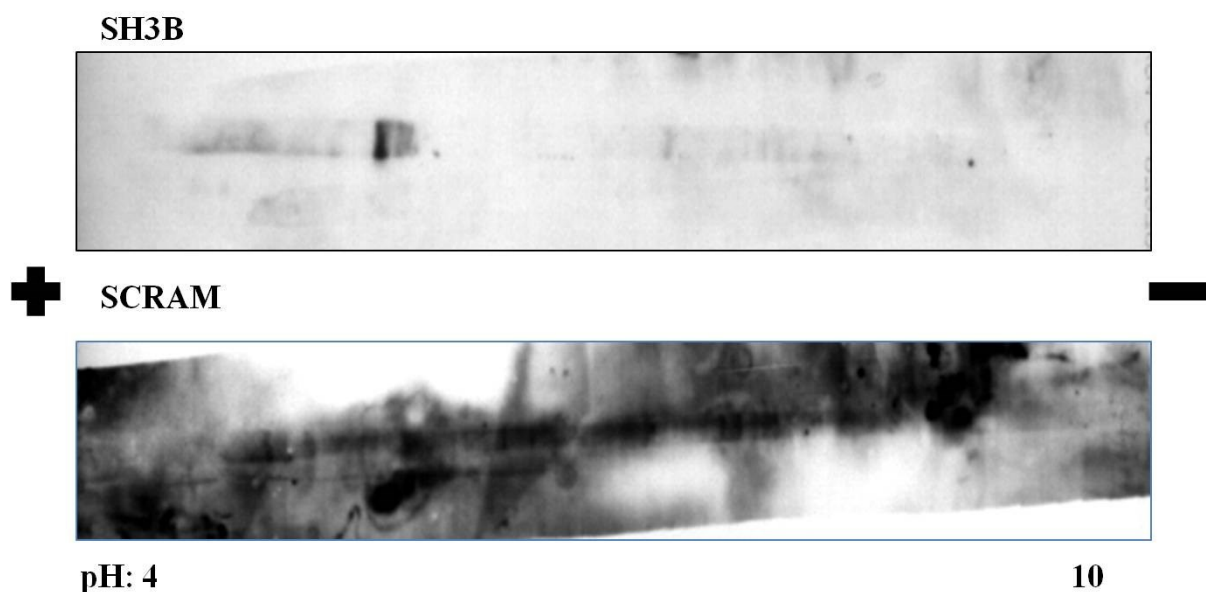
Figure 4.3.e: IEF and peptide overlay using SH3B and SCRAM peptides. Peptide overlay probe of 2M fractions (1.5 to 2 mg.ml total protein concentration) for hydroxyl apatite chromatography subjected to IEF along a pH gradient of 4-10. Three bands can be seen in the SH3B panel (top), while the SCRAM panel has many indistinct bands.

4.3.f: Biotin block of spurious reactions

When increasing the concentration of protein loaded on gels for peptide overlay from 40 to 60 μg per well, the "BLANK" and SCRAM panels had very similar bands to those seen previously only in the SH3B labelled panels. This implied that streptavidin peroxidase was binding to a biotin-containing or biotin like protein, and could thus be competed away from the (possibly very weak) interaction of SH3B and SCRAM peptides with potential targets. To mitigate this, and to resolve the problem of false positives, peptide overlay blots were

118

performed as described previously, but including an additional step in which blots, were incubated with streptavidin to occupy any biotin or biotin-like proteins. Because streptavidin has four biotin binding regions (Sano and Cantor, 1995), biotin was then incubated with the PVDF membrane to fill these sites and prevent the peptide from interacting here (described in section 3.4.e). The membranes were then treated as for a standard peptide overlay using SH3B, SCRAM and BLANK (Streptavidin-HRP only control). This method partially blocked the bands seen at 120 kDa in homogenate and cytosolic samples (lanes 1 and 2), indicating that these bands are due to spurious interactions with streptavidin-HRP, however biotin block treatment does not alleviate the spurious band seen at 75 kDa. This indicates that another method of detection may be more suitable to identifying proteins using these peptides.
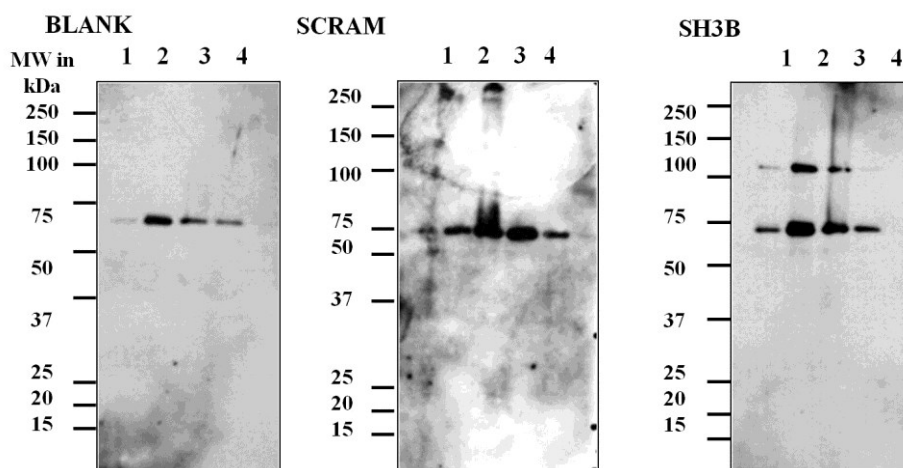
Figure 4.3.d.iii: **Peptide overlay of hydroxyapatite fractions from A549 cell line.** To increase detectable protein levels, pooled Hydroxyapatite fractions from solubilised A549 cell homogenate with A549 homogenate, flow through, 0.1-1M and 2M fractions (lanes 1-4 respectively) incubated with 50 nM Peptides or 5% BSA in TBS (BLANK, secondary only control).
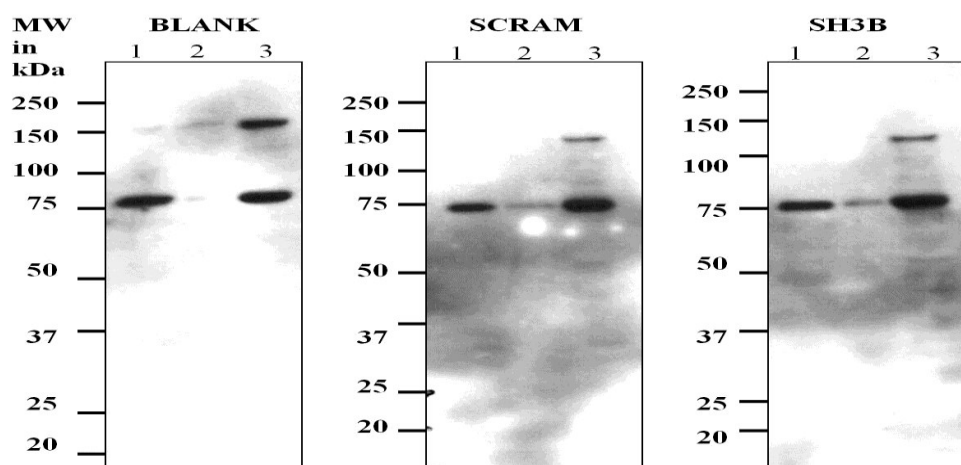
Figure 4.3.f.i: Biotin-block of spurious reactions. A549 samples (60µg of protein per well of homogenate, cytosol and total membranes, lanes 1, 2 and 3 respectively) were subjected to

peptide overlay as described, except after blocking, blots were incubated in 0.1mg/ml Streptavidin in TBST, followed by three 10 min washes to remove any unbound streptavidin. This was followed by the addition of 0.5mg/ml biotin in TBST for 60 minutes at room temperature, after which the peptide overlay was performed as described previously.

Taken together, the blots and gels shown in figures 4.3.b-f show that hydroxyapatite matrix could be used to isolate two proteins from A549 homogenate in the SH3B-probed blot. The proteins were detected at approximately 100-120 kDa and 75 kDa and at an isoelectric point of roughly 5-7. Both proteins appears in SH3B, SCRAM and BLANK control blots, thuis are most likely spurious reactions with the streptavidin-HRP.Attempts to block this reaction were undertaken using a niotin block protocol, however these were not successful. Although attempting to purify novel interactors of RyR1, Hydroxyapatite chromagtraphy inadvertently purified contaminants. Other methods were thus employed to characterise novel interaction partners for this region of RyR1.

4.3.g: Novel RyR1 accessory proteins from Protein Interaction Databases.

In an attempt to further characterise the interactions suggested in Wu *et al* (2007), experiments were performed to confirm or deny the interaction of RyR1 with PLCγ1 and Pleiotrophin1 (PTN-1) as suggested by as OPHID (Online Human Interaction database, http://ophid.utoronto.ca/ophidv2.204/: Brown and Jurisica, 2005). The use of *in silico* analysis of protein-protein interactions has proven invaluable to the understanding of cellular physiology as a whole, but care must be taken to validate any putative interactions. Many RyR1 interactions described in online databases such as OPHID are from *in silico* data only,

or a combination of predicted and high-throughput experimental results, so it would be useful to purify these proteins in complex with RyR1 to validate these *in silico* interactions.(A table of interactions described using RyR1 as the input protein in OPHID can be seen in appendix 1, Fig 8.1.f). This in turn could determine the functional effect they have, if any, on RyR1 function, and also any other cellular pathways that they may interact with. Two such interactions were that with phospholipase C gamma 1 subunit, (PLCγ1), a widely expressed signalling protein with varied roles in MAPK and Ca^{2+} signalling, and pleiotrophin (PTN), a ubiquitous cytokine with phosphatase inhibitor implicated in bone growth, muscle regeneration and angiogenesis (Camarino *et al*, 2013). Interactions between these proteins and RyR1 would be very interesting, based on their role in the cell. PLCγ1 is a 147kDa member of the phospholipase C enzyme family whose function is to hydrolyse phosphatidylinositol-4,5 bisphosphate ($PI(4,5)P_2$) into the widely utilized second messengers inositol 1,4,5 triphosphate and diacylglycerol (Ins $(1,4,5)$ P_3 and DAG respectively). These second messengers go on to mediate Ca^{2+} release from internal stores and PKC activation. PLCγ1 is thus known to have roles in diverse processes like signal transduction and gene expression regulation (Fukami *et al*, 2010). Pleiotrophin is an 18 kDa heparin binding protein which is involved bone formation, angiogenesis and neurite outgrowth, and is highly expressed in developing animals or tumors. Usually a secreted protein, it has recently shown to be translocated to the nucleus upon interaction with the protein nucleolin (Koutsioumpa *et al*, 2012). Due to its widely diverse roles in signalling cascades, and its implication as a tumor promoter, an interaction with RyR1 could be very important.

To study these interactions, isolation of the RyR1 complex was performed via an affinity purification 'pull down' experiment, followed by western blot analysis with antibodies of potential interacting proteins. To this end, GST tagged FKBP12 fusion protein was used to isolate the RyR1 complex from rabbit skeletal muscle microsomes. As described in section 1.4.b, FKBP12 is a 12 kDa protein which interacts with RyR1. FKBP12 (and its cardiac homolog FKBP12.6) have been successfully expressed in bacterial cells with an added GST tag and used in affinity based isolation of RyR complexes (Mackrill *et al, 2001*). Skeletal muscle (leg muscle from rat) was used as RyR1 is expressed in at its highest levels in this tissue (Mackrill *et al, 1997*). Pilot experiments revealed that very low levels of PLCγ1 were expressed in skeletal muscle, but was detectable in brain homogenates from rat, so solubilised brain and muscle samples were used in the FKBP12 pull down assay. Although the main isoform expressed in neural tissue is RyR3, RyR1 is also expressed, although in much lower levels (Mackrill *et al, 1997*). A Coomassie stained gel showing these fractions with the appropriate controls (GST only brain, GST only muscle) is shown in Fig. 4.3.g.i. These complexes were probed with anti-RyR antibodies to confirm presence of RyR protein followed by αPLCγ 1, αPTN, αGRB2 and αJPH1 antibodies, as outlined in Chapter 3. Results can be seen in Fig. 4.3.g.ii-v. The αPLCγ 1, αPTN and αGRB2 antibodies were used as Wu *et al* (2007) suggest that these proteins (as well as NCK1) interact with RyR1 via the proline rich region located between amino acid 4520-4532. The FKBP12 pull down experiments were used to validate these interactions in vitro.
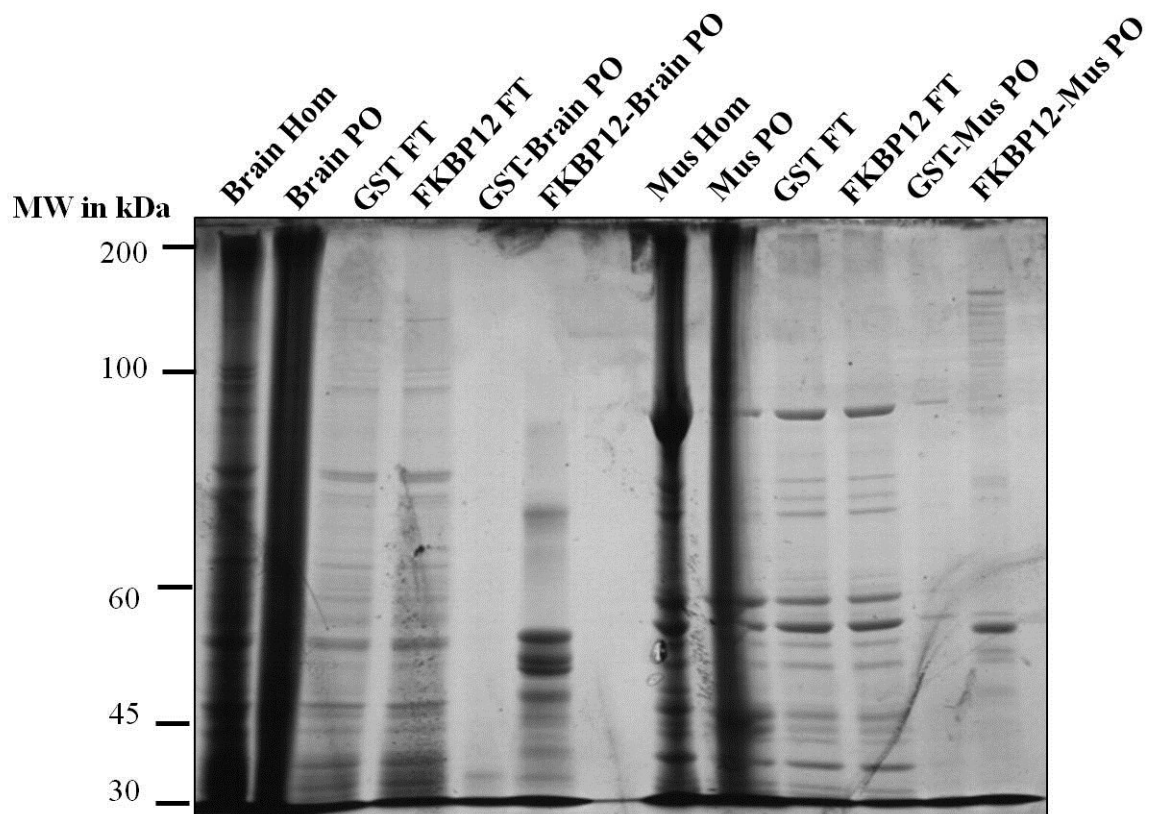
Figure 4.3.g.i: Coomassie stained rat brain and muscle samples subjected to solubilisation and pull down using FKBP12 –GST beads run on a 6% SDS PAGE gel. Rat brain and muscle (VL) samples (40 µg total protein per lane, 3.5 mg/ml protein per solubilisation experiment) were solubilised and incubated with either GST bound beads or FKBP12-GST beads generated using bacterial fusion proteins. (Hom: Homogenate, PO: post solubilisation, FT: Flow through)
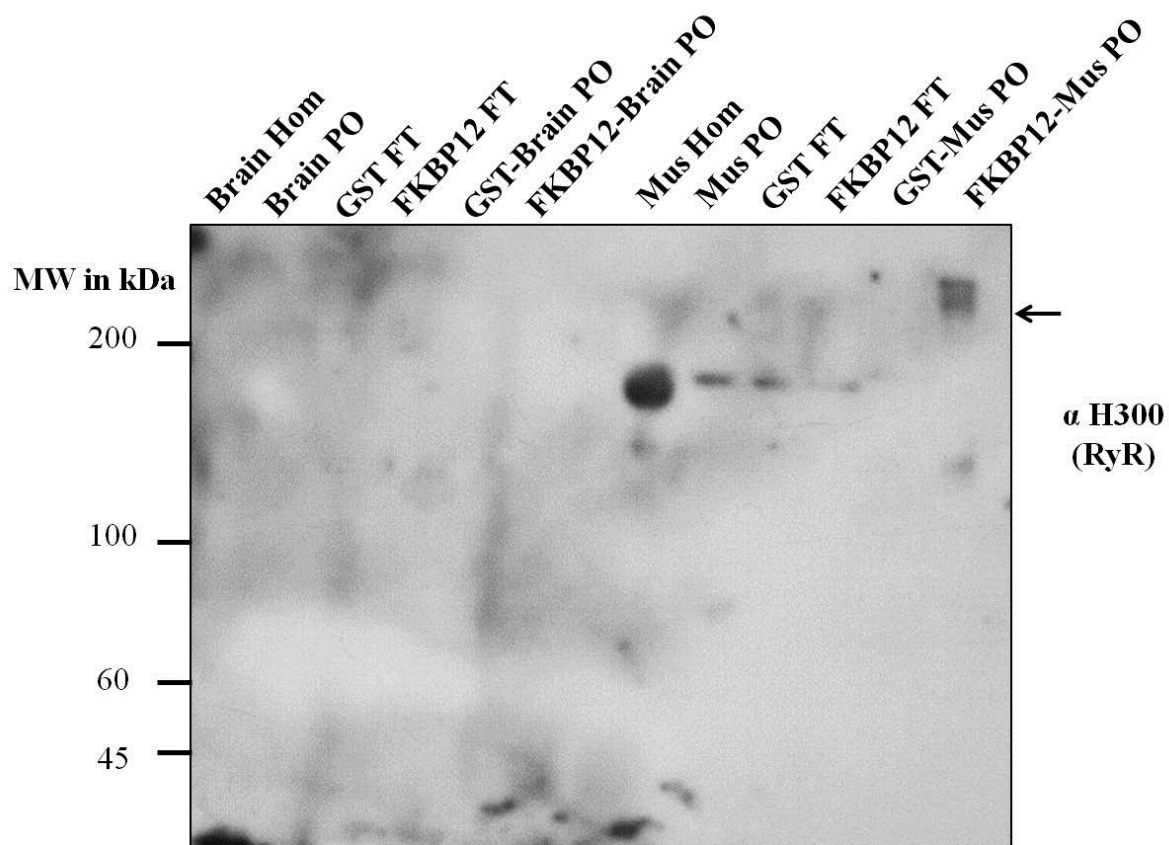
Figure 4.3.ii: Rat brain and muscle samples subjected to solubilisation and pull down using FKBP12 –GST followed by western blot with H300 anti-RyR antibody. Rat brain and muscle were subjected to FKBP12 pull down as described above and transferred to PVDF followed by staining with H300 anti-RyR antibody. Little if any RyR is detectable in any of the brain samples, however an enriched band can be seen in the FKBP12-Muscle pull down lane, at (approximately 350 kDa- above range of MW markers) as well as a degraded band in the muscle homogenate and post solubilised fraction. This demonstrates that the RyR complex is isolated using this assay, and is enriched compared to muscle homogenate or post solubilised samples.
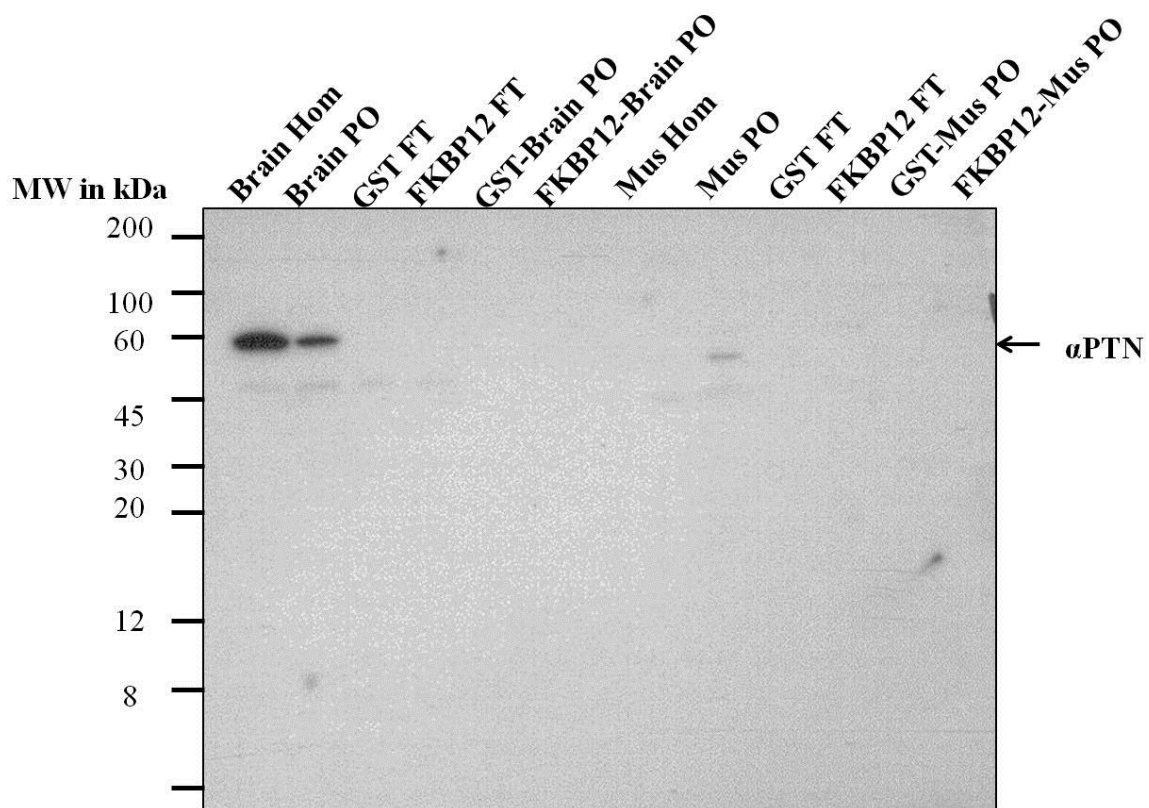
Figure 4.3.g.iii: FKBP12 pull down using rat brain and muscle, probed with α Pleiotrophin (PTN) antibody. Bands can be seen in rat brain homogenate and post solubilised fractions at approximately 60 kDa and 50 kDa. 50 kDa bands can be seen in the GST and FKBP12 flow through (GST, FKBP12 FT) lanes, indicating that PTN has not bound to the RyR1- FKBP12 complex in this instance. A different banding pattern is seen in muscle, where PTN is undetectable in muscle homogenate but appears enriched in the post solubilised sample (muscle PO). This could be due to nuclear translocation of PTN. No PTN is seen in

the GST-Muscle or FKBP12-Muscle samples, indicating that PTN has not been isolated by the control or FKBP12 binding complex.
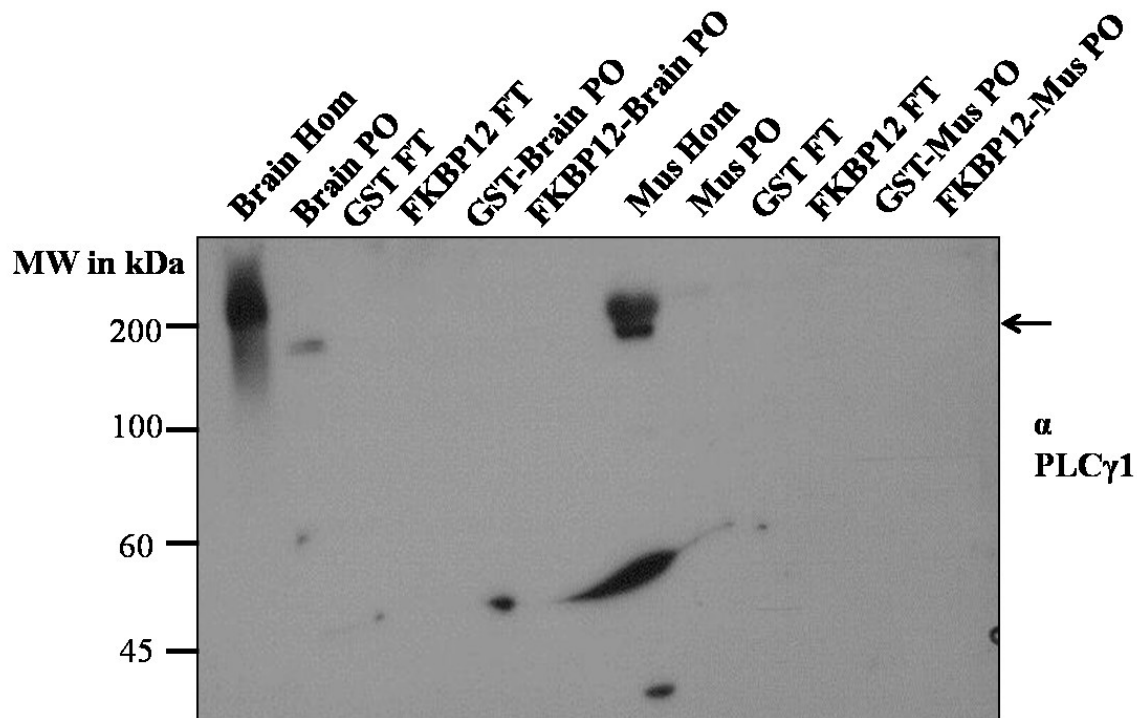
Figure 4.3.g.iv: FKBP12 pull down probed with αPLCγ 1 antibody. Rat and brain samples incubated with FKBP12 as described above were run on 10% SDS PAGE gels followed by transfer to PVDF and probing with αPLCγ 1 antibody. Bands are detectable in brain homogenate, brain post sol, muscle homogenate and post sol at an apparent molecular weight of 180-200 kDa. As the predicted molecular weight of PLCγ1 is 150 kDa, this is likely to be the correct band. No PLCγ1 was detected in either brain or muscle FKBP12 pull down fractions, indicating that under these conditions, PLCγ1 cannot be isolated in complex with RyR1.
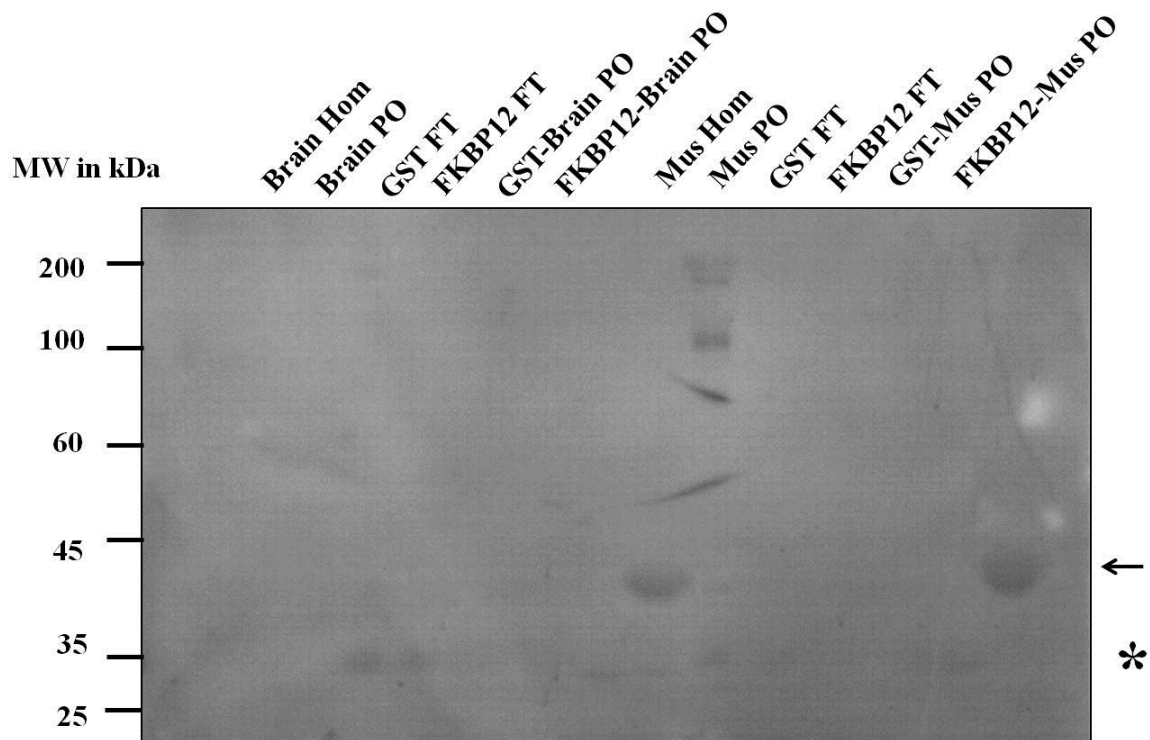
Figure 4.3.g.v: Western blot of Brain and muscle samples from rat incubated with FKBP12 fusion proteins and probed with αGRB2 antibody. Rat brain and muscle samples were treated as described above and incubated with FKBP12 fusion proteins expressed in bacteria or GST only controls. Little if any GRB2 is detected in brain samples, but is detected at 40 kDa in muscle homogenate and at 160 kDa in muscle post-sol samples. An enriched band is visible at 40 kDa in the FKBP12 –muscle pull down lane, showing that GRB2 can be isolated with the RyR1 complex under these conditions.

These results indicate that under these conditions, PTN 1 and PLC γ1 do not interact with RyR1, or that the interaction is not strong enough to allow isolation using recombinant FKBP12. These two results highlight the need to thoroughly validate *in silico* or high

throughput experiments. Fig 4.3.g.v shows the same FKBP 12 pull down experiment probed with αGRB2 antibody. The results show a visible, enriched band at approximately 30 kDa, the correct weight for GRB2 (marked with an arrow). (McPherson *et al*, 1994) There is a lower background band at 25 kDa (marked with an asterisk), which is a result of non specific interaction with the secondary antibody (controls can be seen in appendix I, Fig 8.1.e). This interaction is interesting, as GRB2 is an adapter protein, it is likely to be allowing the interaction of RyR1 and other proteins, and due to its role as a tyrosine kinase activator, this interaction could have huge implications for the regulation of calcium signalling in muscle. Further studies will have to be performed to confirm this, and should include immunoprecipitation of either RyR1 and or GRB2 with cross probing with antibodies to confirm the interaction, and perhaps siRNA knock down of GRB2 followed by functional studies of Ca^{2+} release from the RyR1 to monitor effect.

4.4: Discussion:

It remains important to investigate this region of the type 1 RyR. As it is close to the transmembrane domain, allosteric or posttranslational modifications here could have vast implications for cellular Ca^{2+} homoeostasis. In 1993, Treves *et al* found that a polyclonal antibody targeted to the amino acids 4425-4621 of RyR1 could have an effect on the regulation of the channel by Ca^{2+} ions. This region of RyR1 also encompasses the "divergent region 1", which may confer a very specific function to any proteins interacting in this area. (Treves *et al,* 1993, Benaquista *et al,* 2000)

Although the SH3B peptides did not give visible results that were not apparent contaminants, it would have been really useful to study this interaction. As the SH3 domain can have less than stringent binding partners, the -PxxP- motif may not be strong enough to interact on its own, without the rest of the protein. The –PxxP- motif may also be only a portion of the binding region, or not involved at all. It has been found that SH3 require the cooperation of residues outside the –PXXP- motif for binding to occur (Bartelt *et al,* 2015). Along the same lines, the peptide probe may not be long enough to confer specificity, leaving all available streptavidin molecules to bind to contaminants.

The results outlined above demonstrate that biotinylated peptide overlay is an unreliable method for protein interaction discovery. Although faint bands in the SH3B overlay panels existed outside the main contaminants at 120 and 75 kDa, they were not consistent and some of them were visible in the SCRAM and blank panels. Bands of a similar molecular weight were found in Yeow-Fong *et al,* who expressed SH3 domains from SNX9 as GST fusion proteins and used them as "prey" in an overlay experiment to screen rat brain and testis tissue for interactors of the SNX9 protein (Sorting nexin 9, involved in mitosis). This indicates that the non -specific interactions are not exclusive to cell culture, and that very careful raw material choice and experimental design are necessary to gain meaningful information from overlay experiments. Stringent controls must also be employed (Yeow-Fong *et al,* 2005, Kim *et al* 2010). A more reliable method must be used to investigate any binding partners which interact with this region of RyR.1 Kim *et al* suggest removal of contaminants via passing solubilised material through a streptavidin-sepharaose column before proceeding with biochemical detection with biotinylated peptides, however this adds

another step to sample preparation which could significantly increase cost, sample loss and degradation. Confounding results also appeared with the IEF purification experiments, which based on the estimation of isoelectric point gave a result at a pI of 4-6. This contradicts the estimated pI of proteins eluted using increased NaCl gradients from hydroxyl apatite columns, which are usually basic under the conditions used (Cummings *et al*, 2009), although this is disputed by Hou *et al* (2011) who state that there was no correlation between protein retention and isoelectric point of that protein with elution using increasing NaCl gradients and constant phosphate concentration (Cummings *et al*, 2009; Hou *et al*, 2011). Taken together, these results demonstrate that either contamination of samples has occurred or more likely, that several contaminants are detected from the streptavidin peroxidase-HRP alone. Although intended as a purification step, in this instance Hydroxyapatite chromatography acted as an enriching step for contaminants, and thus could be used to remove this from future analyates.

Further attempts to characterise interactions with RyR1 and proteins suggested in the OPHID database were carried out using the FKBP12 fusion protein pull down of RyR1 complexes followed by probing with αPLCγ1, αPTN, and αGRB2 antibodies. RyR complex isolation was achieved, as demonstrated by the αRS4 western blot, however neither the αPLCγ1 and α-PTN antibodies showed any bands in the pull down sections. This does not exclude the possibility of either of these proteins interacting with RyR1, however, it has not worked in this experimental set up. It is possible that the αPLCγ1 antibody (generated against rabbit) does not have the required specificity (although BLAST searches of the human and rabbit PLCγ1 show little variation in the immunogenic peptide as described on the suppliers

website). Pleiotrophin may have not have been detected in the 6 or 7.5% SDS PAGE gel, but subsequent experiments showed that both PLCγ1 and PTN1 were detected in the brain homogenate using 10 and 15% gels respectively, indicating that their absence in the pull down fractions is not due to poor antibodies. However, a band was visible at 60kDa, indicating that it may have been in complex with a larger protein (despite rigorous sample boiling and addition of DTT, this is not unheard of, and may not have been amenable to other interactions.   It is also possible that the starting material was degraded, leaving very little to be detected, or that the PTN antibody actually detercts some other protein. Future efforts to validate these interactions could be improved by using the most recent muscle samples available and the use of varied complex purification techniques, as well as a gradient gel to maximise protein resolution and detection.

The GRB2-RyR1 complex interaction, seen in Fig. 4.3.g.v is a potentially novel result, and has interesting ramifications for calcium signalling in muscle cells. GRB2 has an SH2 domain in the middle region of the protein, flanked by a SH3 domain on either side (Maignan *et al,* 1995). As these data are essentially preliminary results, careful validation must be performed to validate this interaction, and determine the effect this interaction has on the cell. The first step would be to confirm that the GRB2 antibody does in fact bind to GRB2, perhaps by use of an inhibitory peptide mimetic of the antigen used to generate the antibody and then to confirm GRB2–RyR complex interaction, by co-immunoprecipitation and incubation with RyR and GRB2 antibodies. Regrettably, such experiments were outside the time constraints of this study. Current theory states that not only does GRB2 have a role in Ras –MAPK signalling, but also as an adapter for receptor Tyrosine kinases. As an adaptor

protein, GRB2 uses its SH2 and 3 domains to bring other proteins closer together. In the case of the Ryanodine receptor, this may mean that the GRB2-RyR1 interaction is facilitating the close apposition of another molecule which may exert some sort of regulation on RyR gating. In permeabilised T lymphocytes, GST-GRB2 incubation had no effect on RyR mediated Ca^{2+} release, however a known associate of GRB2, p59[fyn], a non-receptor tyrosine kinase associated with T-cell receptors, did cause transient phosphorylation of RyRs and an increase in Ca^{2+} ion release from cADPR and ryanodine sensitive stores in permeabilised Jurkat T cells . (Guse *et al,* 2001).This could mean that GRB2 could link p59[fyn] and RyR for quick regulation of calcium signalling based on signal transduction through T-Cell receptors in immune cells. In muscle, as RyR1-mediated Ca^{2+} release is so specialized and tightly regulated, it is feasible that tissue-specific-tailoring (the specialisation of the Ca^{2+}signalling toolkit) of this interaction could occur (Berridge, 2000: Bootman *et al,*2001). A functional GRB2 knock out has been generated by Maina *et al,* and it showed drastic reductions in muscle development, particularly in limb buds (Maina *et al,* 1996). Taken together with its potential interaction with RyR1, this hints that GRB2 may have a role in the regulation of calcium release and possibly in the regulation of skeletal muscle growth. GRB2 knock out animals are not viable, but GRB2 knockdown in C2C12 cells display increased insulin uptake (Maina *et al*, 1996; Liu *et al,* 2009) and in B cells, GRB2 knock down was seen to lead to "hyperreactive" receptor signalling, and these cells showed abnormal congregation behaviour in the spleen. (Liu *et al,* 2009; Jang *et al,* 2011) Thus, in muscle cells, the GRB2-RyR1 interaction could have vast implications for muscle cell growth and differentiation as well as insulin related signalling. As GRB2 is also implicated in the formation of artherosclerotic lesions (Proctor *et al,* 2007) and is a potential target for anti-proliferative drugs (Zhang *et al,*

2003), further study of this interaction is necessary to understand the many signalling pathways which could be affected by aberrations in this interaction, and the potential for these are discussed in section 4.5.

4.5: Future Studies:

The biotinylated peptides were used as a way of mitigating the time and labour intensive purification of intact RyRs, however overexpression of the SH3-binding region with one or more tags to facilitate purification of any complexes formed in a suitable cell line model might be a more effective strategy. This strategy was employed by Kobayashi *et al* , who engineered a "multifunctional GFP" (mfGFP) protein with built-in streptavidin binding peptide, c Myc and an 8x Histidine tag for visualisation and tandem affinity purification of both clathrin and RyR1 from HeLa cell lines with minimal contamination products. The mfGFP tagged RyR1 was also easily visualised via confocal microscopy, and no mis-localisation was observed (Kobayashi *et al*, 2008). Ryan *et al* used a similar experimental design where a large fragment of RyR1 (amino acids 1-4243) was expressed in HEK-293 cells with a 6x-Histidine tag attached. This fusion protein and associated interacting proteins were then purified by Ni-NTA metal affinity chromatography, and the resulting proteins characterised by liquid chromatography mass spectrometry (LC-MS). Interacting proteins were validated by western blotting and Calcium homeostasis endoplasmic reticulum protein (CHERP) was found to be a novel component of the RyR1 complex (Ryan *et al,* 2011). This experimental set up demonstrates that novel interactors of RyR1 can be found, but using a combined approach of purification followed by proteomic applications will yield the most

accurate results. A caveat of this study is the choice of raw material, as HEK-293 cells may not actually express all the proteins capable of interacting with RyR1. In the same manner, future studies could focus on the SH3 binding region or RyR1 using both a muscle and non-muscle cell type/ tissue as a raw material, as this could provide more meaningful data on the role of any specific interactors.

In terms of the GRB2-RyR1 interaction, further analysis needs to be performed to fully characterise this partnership. Such studies should include a comprehensive study of the areas of each protein which interact with each other, and could be done by mutating the putative binding regions (e.g. changing key proline residues in the PRR of RyR1 etc) or by deleting fragments of either of the SH3 domains found in GRB2. This could be followed by functional effects of blocking this interaction either by mutational studies or by knock down of the GRB2 protein and looking at the effect this has on calcium signalling and growth of the cell. Recently, Simister *et al* discovered a novel small molecule inhibitor of GRB2, and this could prove really usefull in altering GRB2 interactions *in vitro* and monitoring the effects, thus giving a quick and non-cytotoxic method of studying GRB2-RyR complex interactions (Simister *et al,* 2013).

Chapter 5: mAb VF1c Characterisation

5.1.: Introduction

In 1987, Campbell *et al* performed a series of experiments designed to characterise the proteins involved in EC coupling (Campbell *et al*, 1987). This study led to the generation of several widely used antibodies targeted against several proteins involved in the EC coupling proteins, including XA7, a monoclonal antibody which interacts with RyR1. One of the antibodies generated, VF1c, was shown to interact with a 90 kDa protein, found in the terminal cisternae of muscle (determined by differential centrifugation of rabbit muscle homogenate followed by western blotting), which was termed " Junctional sarcoplasmic reticulum protein-90" or JSR-90. This protein was shown to interact with RyR1, and was known to be phosphorylated by an unknown endogenous kinase protein. Subsequent analysis of this protein revealed that it was found at higher abundance in fast twitch muscle (ATPase and immunostaining experiments) of rabbit, and that its expression was higher in the vastus lateralis muscle of aged men compared to their younger counterparts (Olhendieck, 1990, Campbell *et al,* 1987). Despite the generation of a large amount of data about this JSR-90 protein, it was never identified nor was the antibody fully characterised. To address this, studies in the laboratory of JJM were undertaken to characterise this antibody and identify its target. Immunoprecipitation experiments followed by MALDI-ToF analysis revealed the 75 and 90 kDa bands identified by the VF1c antibody to be two fragments of the Junctophilin 1 (JPH1) protein, separated by a calpain cleavage site (a PEST motif, as delineated by ePESTfinder software). A diagram of the results obtained are shown in Fig. 5.1.3.a.

Junctophilins are a family of four proteins (JPH1, 2, 3 and 4), encoded by four separate genes. They span the gap between the endo-or sarcoplasmic reticulum and plasma membrane of excitable cells, at subplasmalemmal junctions. JPHs are also expressed in some non-excitable tissue such as mammary and prostate epithelia, as shown by gene array studies (Pawłowski *et al,* 2011; Marin-Aguilera *et al,* 2012). Discovered in 2000 by Takeshima *et al,* (2000), JPHs are especially important in skeletal and cardiac muscles, where JPH1 and 2 are the predominant isoforms respectively, and where failure of interaction between the PM and SR can lead to failure of EC coupling. As implications of diseases such as MH show, the misfiring of Ca^{2+} ions can be catastrophic in excitable tissues. JPH subtypes 3 and 4 are mostly found in neuronal tissue, and JPH3 is implicated in Huntingtons-like syndrome and motor discoordination (Nishi *et al,*2002).

5.1.a:Junctophilin structure and function:

Junctophilins share approximately 38% amino acids identity (JPH1, 2, and 3 only, Nishi *et al*, 2001), but all have essentially the same predicted structure: an N-terminal region, containing between 5 and 8 MORN (Membrane Occupation Recognition Nexus) motifs which facilitate interaction with lipids on the inner leaflet of the plasma membrane. (Takeshima *et al* 2000;Nishi *et al,* 2000). Distal to these motifs, a spring-like, highly conserved alpha helix region permits a gap between the plasma membrane and the SR, and allows for a 12 nm space. The COOH terminal contains the transmembrane domain which inserts into the SR membrane. (Takeshima *et al* 2000: Garbino *et al,* 2009)

Various knock-out and knock-down animals have been generated to analyse the function of JPH. JPH4 KO mouse appears to have no deficit, whereas a JPH1 knock out died shortly after birth due to feeding and breathing irregularities. (Ito *et al*, 2003). As the JPH1 knock out animals were unviable, inducible knock down via virally delivered shRNA against JPH1 and 2 were utilised in skeletal muscle fibres from mice, and reducing the expression of these proteins lead to decreased store operated Ca^{2+} entry (SOCE), disrupted triad structure, defective Ca^{2+} release from SR and a decreased Ca^{2+} pool within the SR. This implicates JPH1 not only in RyR1 regulation but also in the maintenance of correct cellular Ca^{2+} concentrations, crucial to proper muscle function (Hirata *et al,* 2006). JPH1 negative myotubes were also found to have decreased expression of STIM and ORAI proteins, which play an important role in SOCE, and to have decreased TRPC3 and 1, but not TRPC 4 or 6 expression. (Li *et al,* 2010). As well as mediating contact between the DHPR and RyR1, JPH1 has also been found to interact with caveolin 3, (CAV3) a scaffolding protein located at caveoli of the plasma membrane (Golini *et al,* 2011). JPH2 knock-out mice are embryo-lethal, but analysis of cardiac muscle found irregular dyad formation and impaired Ca^{2+} release (Takeshima *et al*, 2000), and mutations in JPH2 have been linked to hypertrophic cardiomyopathy in both humans and mice (Landstrom *et al,*2007).
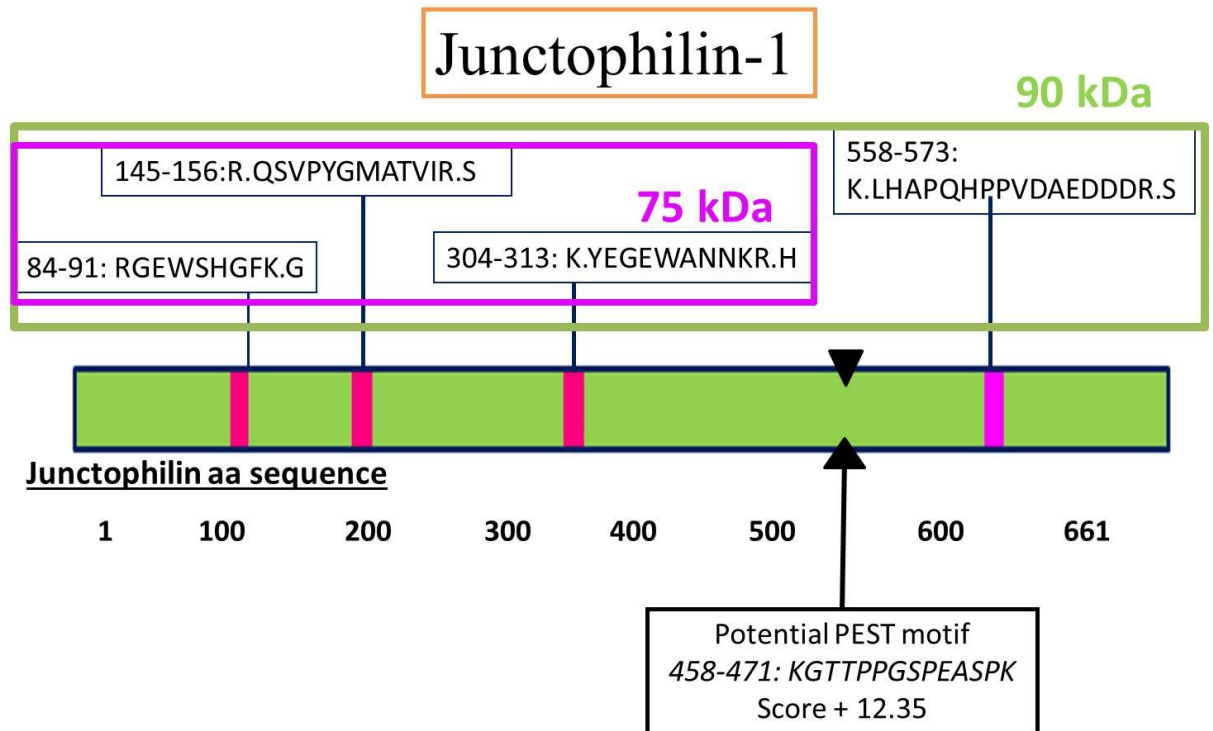
Figure 5.1.a: diagram of JPH1 protein amino acid sequence: with the amino acid sequences found by MADLI-ToF analyses of bands immunoprecipitated from rabbit skeletal muscle using the mAb VF1c. The sequences obtained from the 90 kDa band appear in green box, while the sequences from the lower 75 kDa band appear in the pink box. A potential PEST motif, a consensus site of calpain cleavage, lies between the two, and may explain why there are two bands (original data generated by JJM: English *et al,* 2014).

5.2: Aims: VF1c Characterisation

The aims of this work were to confirm the interaction of mAb VF1c with JPH1 and to characterise this interaction. To this end, yeast-expressed fragments of JPH1 were probed with mAb VF1c and an antibody known to target the C-terminal end of JPH1. This

determined the region of JPH1 that mAb VF1c interacts with. Further experiments were performed to assess the amount of JPH1 in rabbit and rat tissue of muscle and non-muscle origin. As it was suggested by Murphy *et al* suggest that both JPH1 and JPH2 undergo calpain mediated proteolytic cleavage, experiments were carried out to determine if this could be prevented by the chelation of calcium or using a calpain inhibitor in a cell culture model (A7r5 cells, known to express JPH1, Hammoud *et al*, 2013) (Murphy *et al,* 2013).

5.3: Results

5.3.a: VF1c antibody characterisation

In a collaborative effort with the laboratory of Prof. Vincenzo Sorrentino in Sienna Italy, fragments of rabbit JPH1 were expressed in yeast, resolved by SDS-PAGE, transferred to PVDF membrane and sent to this lab, where the blots were screened with the VF1c and JPH1 (targeted to the C-terminal region) antibodies. The JPH1 fragments expressed in yeast contained amino acids 1-233, 232-369, 369-571,141-278, 229-460, 154-278, 229-550 and 154-635. The VF1c mAb bound to four fragments: 229-460, 369-571, 229-550 and 154-635. This confirms that VF1c binds to JPH1, and indicates that the epitope for this antibody is between residues 369- 460. To confirm the validity of this approach, another antibody, raised against the C-terminal portion of the protein was used to probe a duplicate experiment. This pAb JP1 antibody bound only to the fragment expressing the most C-terminal amino acids, or fragments 154-635. These results can be seen in Fig. 5.1.3 a and b, which also show how mAb VF1c and pAb JP1 antibodies interact along the length of the protein. In an effort to narrow down the binding region of mAb VF1c even further, peptide arrays expressing

gradually decreasing fragments of the 369-460 region of JPH1 were synthesised on nitrocellulose membranes by the laboratory of Dr. Patrick Kiely, at the University of Limerick. These peptides arrays were then probed with the VF1c antibody, and these results (Figure 8.2.a, appendix) show multiple peptide spots interacting with this antibody. Thus, the secondary antibody could be binding to the peptides, giving false positive signals, or VF1c could bind a conformational epitope of the JPH1 protein, which would not be represented on a peptide array.
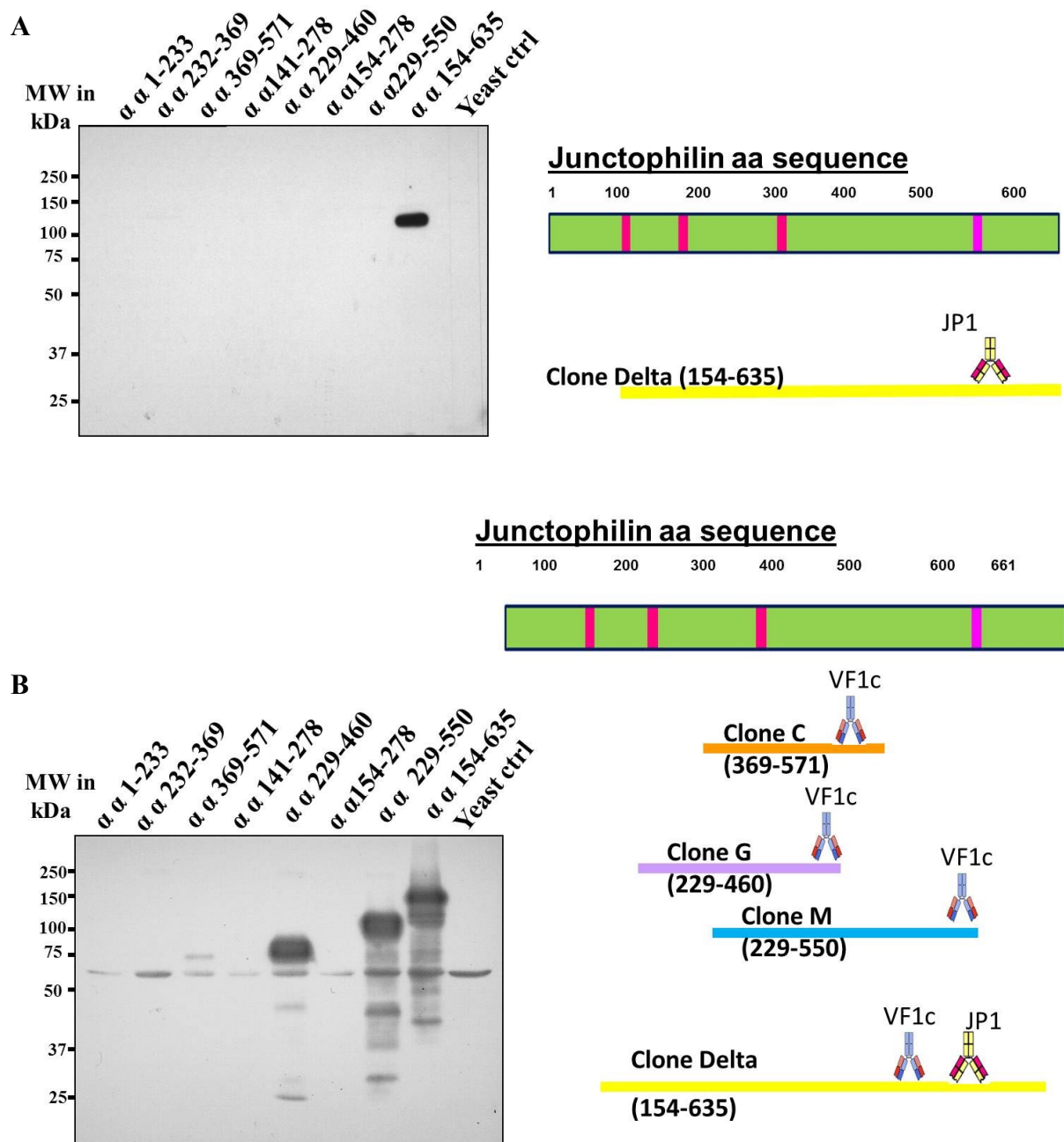
Figure 5.3.a: Yeast expressed fragments of GST-tagged JPH1 probed with A) a poly clonal C-terminal JP1 antibody. or B) mAb VF1c Fragments of JPH1 protein (amino acids 1-233, 232-369, 369-571, 141-278, 229-460, 229-550 and 154-635 of JPH1) were expressed in yeast , resolved by SDS PAGE , transferred to PVDF membranes and probed with pAb JP1 (panel a) and mAb VF1c (panel b). The JP1 antibody bound only to the most C-terminal

fragment(amino acids 154-635 of JPH1), while mAb VF1c bound to fragments expressing amino acids 369-460. A 60 kDa band is present in all lanes of panel b, including the yeast only control lane, indicating that this is an artefact (n=1, two technical replicates).

5.3.b: JP1 and VF1c mAb comparison in mouse muscle .

To further confirm that mAb VF1c interacts with JPH1 protein, mouse muscle samples (intercostal, soleus, sternocleidomastoid, tibilias anterior, and vastus lateralis (termed Sterno Mast, TA and VL respectively) were excised, homogenised, subjected to western blot using these antibodies. Rabbit skeletal muscle (latissimus dorsi) was utilised as a control. The results show that mAb VF1c detects two bands in mouse skeletal muscle, at 100 and 85 kDa in all tissues except intercostal muscle, where mAb VF1c detects two bands at a slightly higher molecular weight of 120 and 90 kDa, and soleus, which shows no detectable JPH1 in these experiments (see R_f measurement, appendix II). The bands have a similar appearance to that seen in rabbit muscle control. The pAb JP1 panel shows a strong interaction with a protein at 60 kDa and a fainter interaction at 85 kDa in rabbit tissue. This band aligns with that detected by mAb VF1c. Taken together with the antibody characterisation experiments (section 5.1.1.b), this implies that in mouse and rabbit skeletal muscle, JPH1 is cleaved somewhere in the region of 369-460, and that as mAb VF1c interacts with this region of JPH1, two bands are detected. As pAb JP1 antibody interacts with the C-terminal end of the protein, this detects a faint amount of full length JPH1 and a cleaved portion at 60 kDa in rabbit skeletal muscle. Possibly due to poor transfer, pAb JP1 did not interact with any proteins in mouse skeletal muscle, even though mAb VF1c did, showing that JPH1 is detectable in these samples.
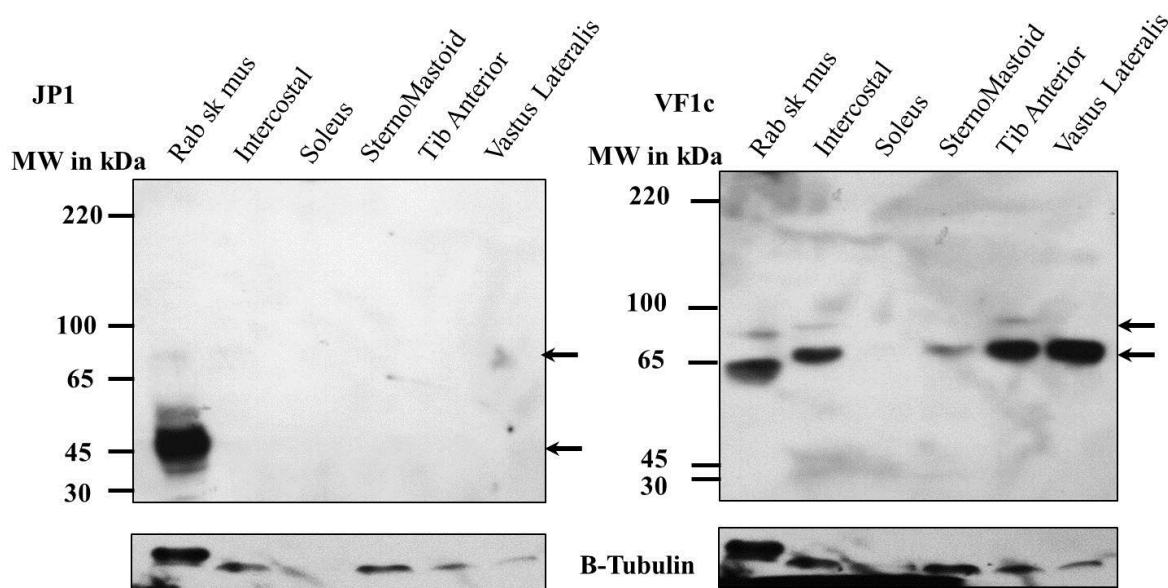
Figure 5.3.b: Western blot experiment of Mouse muscle samples probed with pAb JP1 and mAb VF1c. Mouse intercostal, soleus sternomastoid, tibilis anterior and vastus lateralis (with rabbit skeletal muscle as positive control) muscle were probed with pAb JP1 and mAb VF1c. No bands were detected in the mouse samples using the pAb antibody, however two bands at 120 and 90 kDa were detected using mAb VF1c. The blots were both probed with anti-tubulin antibodies as a control.

5.3.c: Investigation of JPH1 and 2 expression in organs from rat.

Detection of JPH1 in Rat Muscle and organs using VF1c mAb.:

Several muscle groups and organs from rat were excised, frozen in liquid nitrogen and subsequently homogenised and probed with mAb VF1c and pAb JP2 antibodies by western blot, and the results are shown in Fig. 5.1.3.c. The VF1c antibody detects proteins at 91 and 80 kDa (marked with arrows) in vastus lateralis, soleus, diaphragm, sternohyoid, and

intercostal muscle samples, while no JPH1 is detected in brain, heart, lung, liver, pancreas, spleen or adrenal gland. The asterisks mark bands indistinguishable from those seen in secondary only controls. Although not shown in this data, VF1c does detect JPH1 in the A7r5 cell line, and it has been shown to express JPH1 (Hammoud *et al,* 2013).The pAb JP2 antibody interacts with two bands, at 96 and 70 kDa in all skeletal muscle types as well as heart. This indicates that JPH2 is also cleaved by some form of cellular protease (likely a calpain, (Murphy *et al,* 2013)). As JPH2 is visible at 90 kDa in heart samples, this intimates that JPH2 is less susceptible to proteolytic cleavage in this tissue.
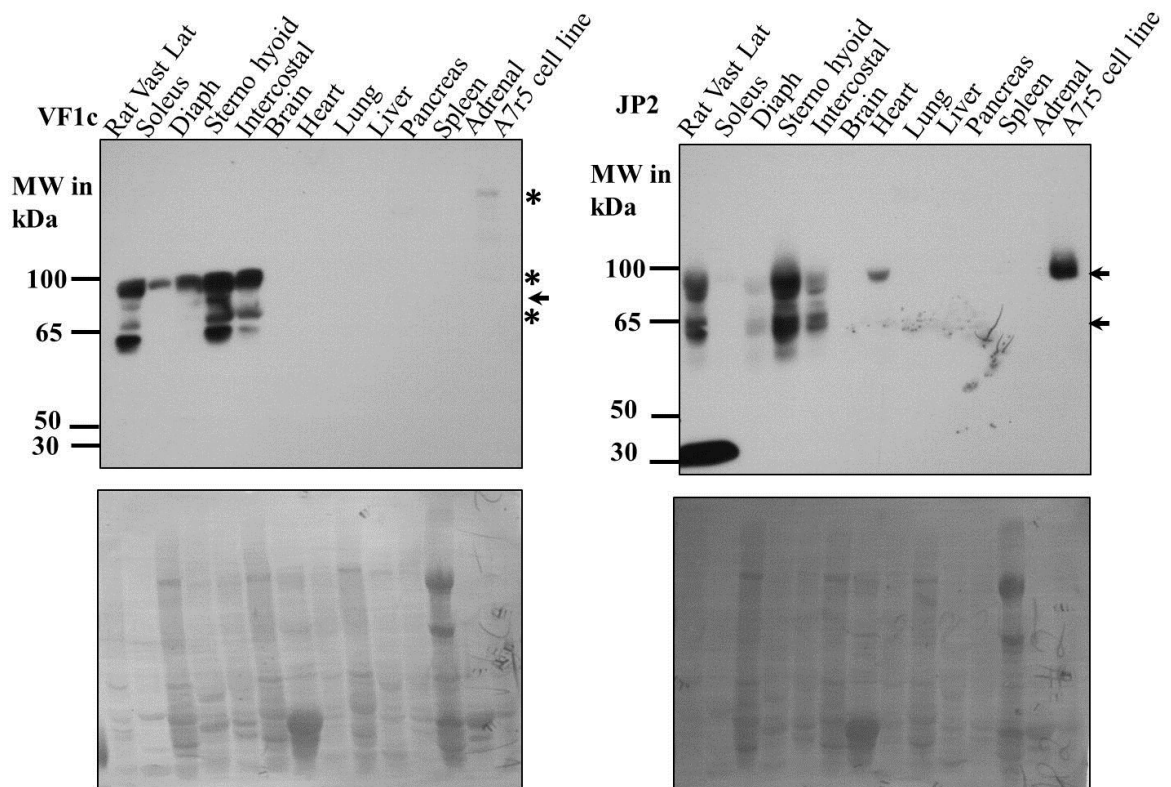
Figure 5.3.c: Expression pattern of JPH1 and JPH2 protein in rat tissues Rat VL, soleus, diaphragm, sternohyoid (SH), intercostal, brain, heart, lung, liver, pancreas, spleen, adrenal

gland and A7r5 cell line lysates (35µg protein /well)were subjected to SDS PAGE and western blotting using VF1c and JP2 antibodies. Asterisks mark bands seen in secondary antibody only controls, while arrow mark those found only in mAb VF1c or pAb JP2 blots. These results show that JPH1 (VF1c blot) is not detectable in the organs tested, but JPH1 is present in rat skeletal muscle at an apparent molecular weight of 90 and 80 kDa (arrows) (for R_fs and secondary-only controls see appendix III) JPH2 was detected in all muscle samples (extremely low levels of JP2 in soleus in this instance) as well as heart and A7r5 (rat embryonic smooth muscle cell line) at an apparent molecular weight of 96 and 70 kDa. Coomassie stains of PVDF membrane are shown as loading control (n=2)

JPH2 is the main isoform in the heart and possibly smooth muscle, as the A7r5 cell line also expresses JPH2 as a 90 kDa band, which implies that it may be less susceptible to proteolytic cleavage. Although a faint band is visible in VF1c at 220 kDa in the A7r5 lysate sample, it was not different to that seen in secondary only controls (figure 8.3.a, Appendices). Interestingly, varying levels of both JPH1 and 2 were detected in the skeletal muscle samples, and this result was further analysed using rabbit muscle.

5.3.d: Comparison of JPH1 and 2 in various skeletal muscle from rabbit.

Fig 5.3.d shows a screen of different muscle types from rabbit, which were analysed via western blot using mAb VF1c. The purpose of this blot was to confirm whether or not JPH1 is expressed in higher amounts in in type II muscle fibres, as suggested by Guo *et al* (Guo *et al,* 1994). As shown in Fig 5.1.3.c, EDL muscle (a predominantly type II muscle) has the highest amount of VF1c immunoreactivity, followed by latissimus dorsi and TA muscles. Remarkably, the diaphragm muscle (a mixed fibre type muscle that is in constant use) and soleus muscle (which in humans perform as anti-gravity muscles) have the lowest amount of JPH1 abundance, and in these muscles JPH1 migrates at a lower molecular weight. This could be the result of different specialised post translational modification or indeed cleavage of these proteins, which may be necessary in long-acting muscles. There is also a disparity in the amount and the molecular weight of JPH1 and 2 seen in intercostals muscle, another set of muscle which undergoes frequent use. Here, JPH1 was found at a molecular weight 90 and 100 kDa, while JPH2 was found at a molecular weight of 95 kDa. To determine the relative amounts of JPH1 compared to JPH2 in different muscle types, the same tissues were probed with an antibody against JPH2. These blots show a similar trend to that seen with JPH1, but the differences in expression between muscle types were less marked and were not significant.
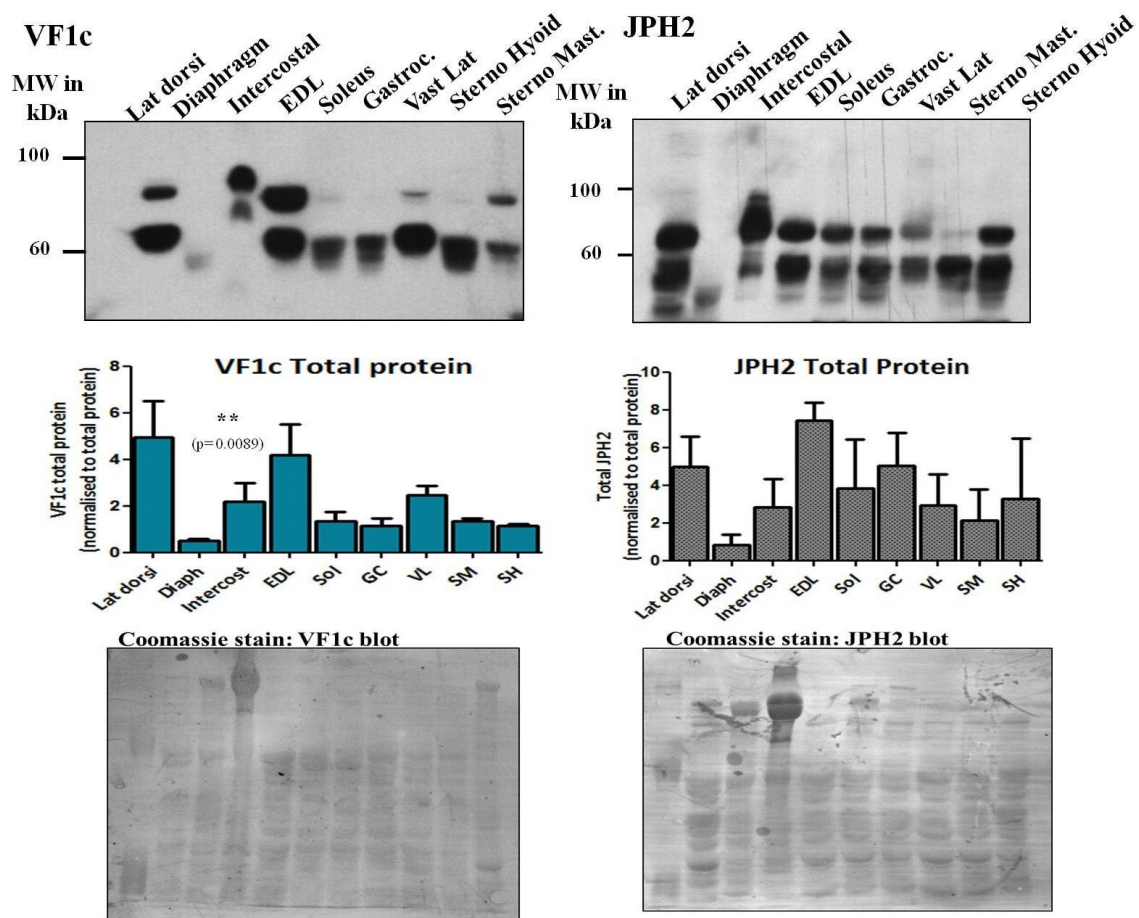
Figure 5.3.d: VF1c and JPH2 screen of Rabbit muscle types. Muscles from male rabbits (lat. Doris, diaphragm, Intercostal, EDL, Soleus, Gastrocnemius, Vastus lateralis, Sternomastoid and sternohyoid, 45µg/protein per lane) were screened for JPH1 and JPH2 expression using VF1c and JP2 antibodies. Intercostal muscles show a higher molecular weight form of JPH1 and 2, while diaphragm and soleus show decreased amounts of JPH1. The highest amount of JPH1 was seen in EDL muscle.Diaphragm has significantly less JPH1 abundance compared to Intercostal muscle (p=0.0089,one way analysis of variance, n =3)

5.3.e and f: Characterisation of JPH1 protein expression and siRNA knock-down in C2C12 myotubes.

C2C12 mouse myotubes were grown and differentiated using 0.5% FCS-containing DMEM for up to 7 days, and JPH1 protein levels were compared to undifferentiated controls by western blot. JPH1 shows a biphasic expression pattern , whereby it peaks between day 2 and 4 of differentiation and decreases again by day 7 (Fig 5.3.e). The JPH1 blot shows increased cleavage at day 2 (band visible at 60 kDa, in contrast to the 100 kDa bands seen in other lanes , figure 5.1.3.f). This diffuse banding pattern vould be due to the JPH1 antibodies binding site occuring distal to the predicted calpain cleavage site within the JPH1 protein. However, it should be noted that consistent results were difficult to obtain, and it seems likely that there is either no peak in JPH1 expression in C2C12 myotubes or that it is highly sensitive to cell passage number and condition.

Attempts to down regulate JPH1 were performed using siRNA knock down of the protein, (Fig 5.3.f) Apparent down regulation was achieved, particularly under serum free conditions, however, JPH1 exression was raised in NFS (Vehicle, N-TER peptides transfection reagent) only and fluorescent siRNA negative controls. Results were also obfuscated by differences in antibody binding. Fig.5.3.f shows attempted knock down of JPH1 protein using N-TER peptides and siRNA mixes from Sigma. These results show that although a small decrease was achieved (particularly using the serum free set-up) , the knock down of JPH1 was inconsistent, and actually increased in fluorescent-only controls and in cells incubated with 20 nM of siRNA mix. These blots do show the difference in binding capabilities between the

JPH1 and VF1c antibodies, and show that mAb VF1c has an apparent higher affinity for JPH1 protein
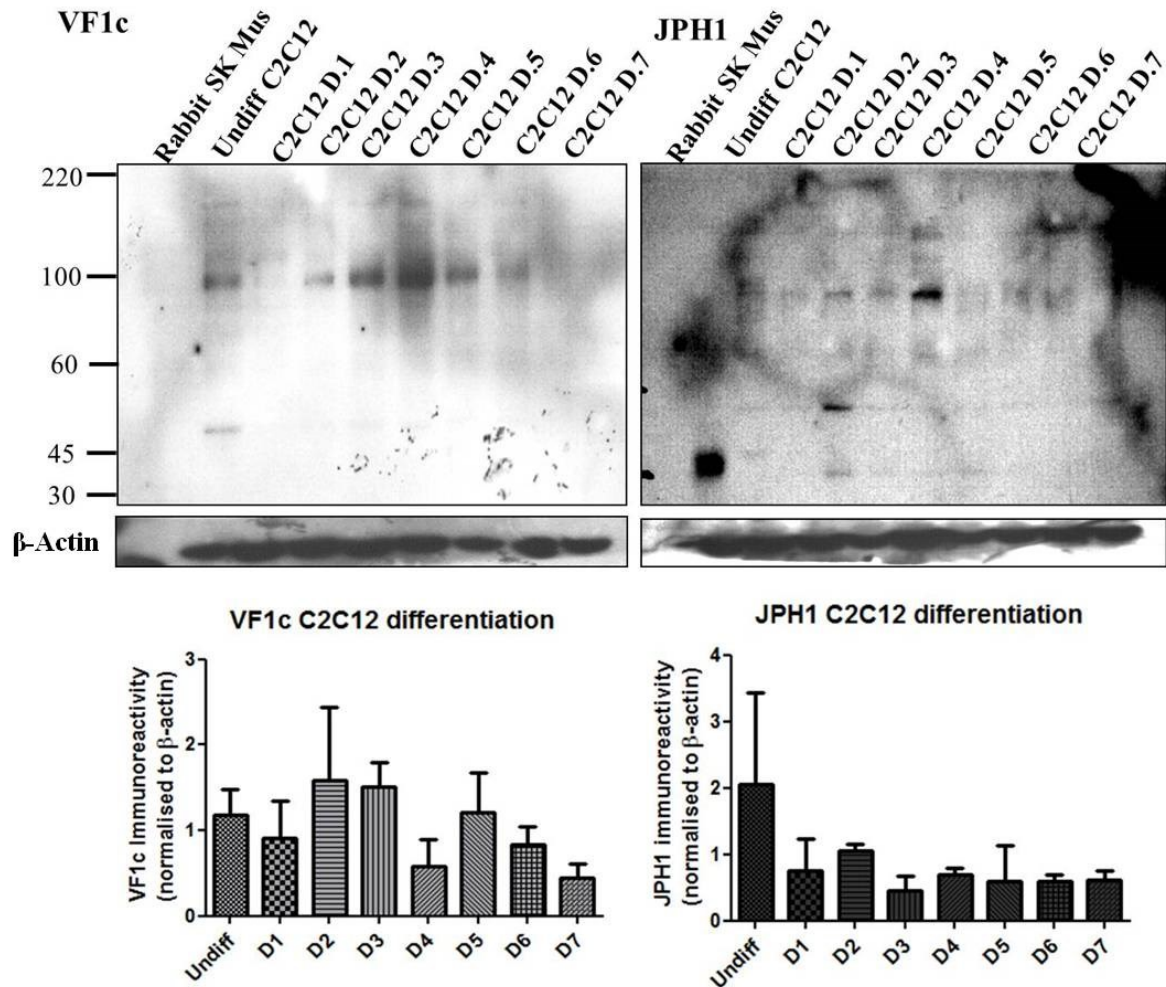
Figure 5.3.e: JPH1 abundance in differentiating C2C12 myotubes: C2C12 mouse myotubes (30μg protein/lane) were analysed for JPH1 abundance via western blot. The highest abundance was found between day 3-4, although results were highly variable.(3 replicates).
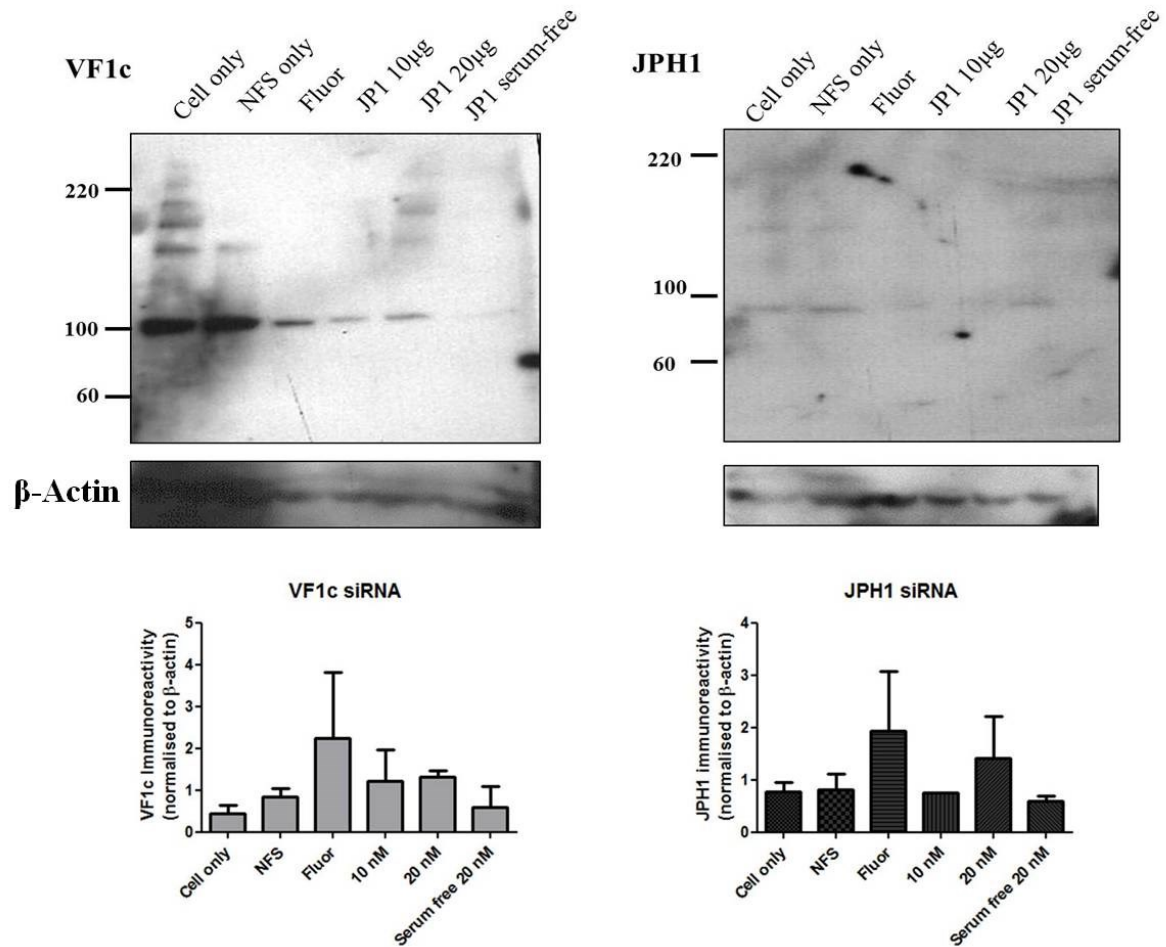
Figure 5.3.f: siRNA knock down of JPH1 protein. N-TER peptides were used as transfection reagents with siRNA targeting the JPH1 mRNA, theoretically causing a down-regulation in the protein (25 µg/protein lane). Fluorescent and non siRNA (NFS only) controls were used to monitor effects (n=3).

5.3.g: Calpain Cleavage study using A7r5 cell lines and *in silico* analysis of likely calpain targets in JPH1 and 2.

Aim: to characterise the proteolytic cleavage of JP1 and 2 by calpain proteins in the A7r5 rat smooth muscle cell line and to use *in silico* analysis of JPH1 and 2 sequences to pin-point potential calpain cleavage regions. These experiments were performed to ascertain whether calpain inhibition or exacerbation (via treatment with ALL-N, a calpain I and II inhibitor, BAPTA-AM, a calcium chelator or A23187, a calcium ionophore), would have an effect on the abundance of total JPH1 and 2 levels as detected by western blot using pAbs JP1, JP2 and mAb VF1c

Murphy *et al*, (2012) performed calpain activation experiments on JPH1 and 2 by incubating muscle homogenate and skinned muscle fibres in high concentrations of calcium, to activate calpains I and II. They found that both JPH1 and 2 were cleaved by proteases after incubation in high calcium concentrations, but this does not exclude the effect of other proteases nor does it confirm the action of calpains on JPH1 and 2. To expand on this and to see if a timeframe of calpain cleavage on JPH proteins could be determined, calpain cleavage experiments were performed using the A7r5 cell line (the mouse muscle cells line C2C12 was tried for this assay but due to uneven growth, A7r5 rat aorta cell lines were used instead) Although a smooth muscle cell line, A7r5s express calpains I and II, similar to skeletal muscle and both Junctophilin 1 and 2 (Jiang, *et al*, 2008: Hoummod *et al*, 2013)

A7r5 cell lines were grown in 6 well flasks and treated with BAPTA-AM, ALL-N, A23187 and DMSO as vehicle control. BAPTA-AM is a cell permeable calcium ion-chelator, and in

this instance was used to decrease the cytoplasmic calcium ion concentration and thus inhibit calpain activation (Mandic *et al,* 2002). ALL-N (N-Acetyl-L-leucyl-L-leucyl-L-norleucinal, also known as calpain inhibitor I) is a pharmacological inhibitor of calpain I and calpain II (Wang and Yuen, 1994: Waters *et al,* 1997). A23187 is a calcium ionophore which facilitates the entrance of calcium ions into the cell as it traverses them membrane, thus it increases the intracellular calcium concentration (Watson, 1978: Katusic *et al,* 1988). It was used to encourage the activation of calpains in A7r5 cells. Using this experimental set up, It was hypothesised that cleavage of JPH1 and 2 could be inhibited by incubation with BAPTA AM or ALL-N, while cleavage of these proteins could be induced by incubation with A23187, which would raise the intracellular calcium concentration. Experiments were carried out as described in materials and methods section 3.1.1.f. An *in silico* study was also undertaken to try and identify likely calpain targets on JPH1 and JPH2 proteins using online databases. The results can be seen in figures 5.1.3.g and h.
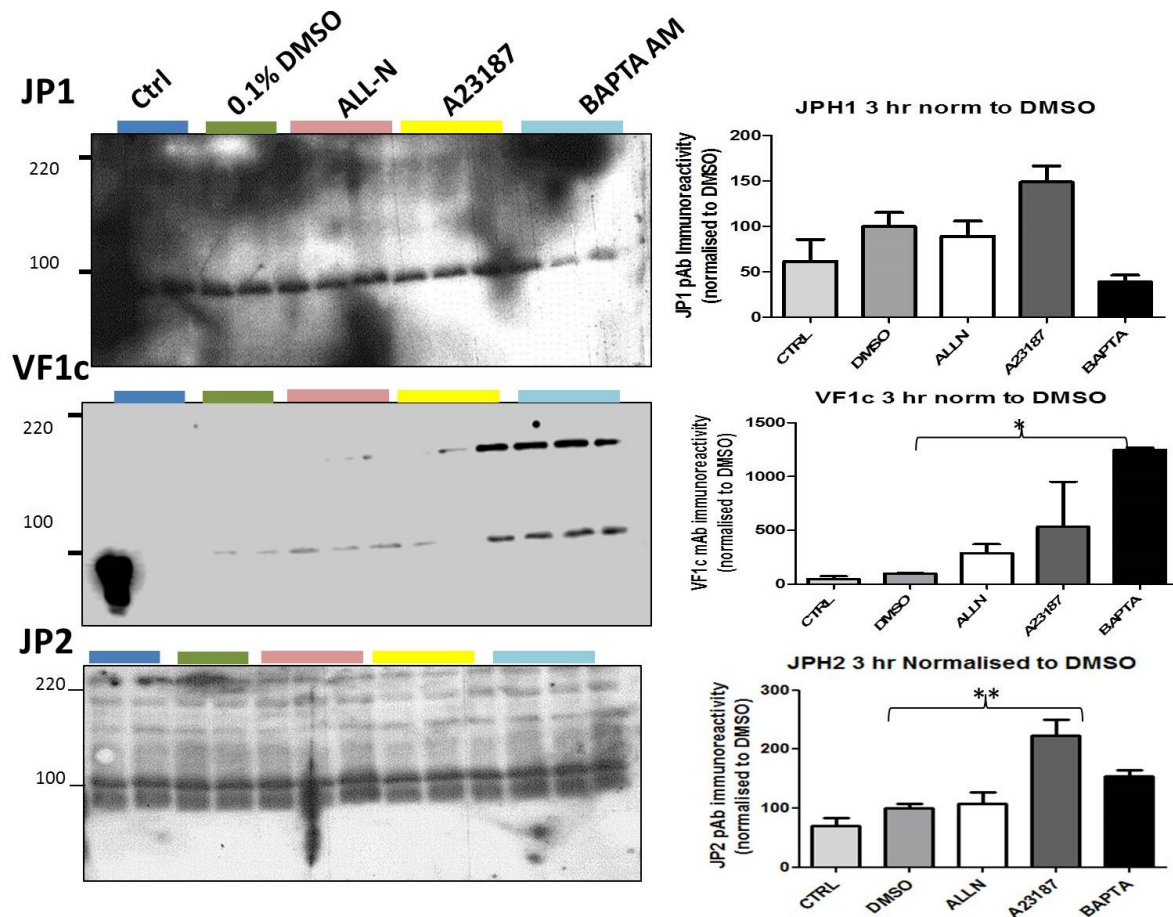
Figure 5.3.g.i: 3 hour incubation of A7r5 cells with calpain inhibitors. Western blot of A7r5 cells incubated with 0.1% (total concentration) of DMSO (vehicle), 20 μM ALL-N, A23187 and BAPTA –AM for 3 hours, analysed for JPH1 and 2 expression.JPH2 abundance is significantly increased in A23187-treated cells, which may imply that increased Ca^{2+} concentration may increase JPH2 abundance. Conversely, an increase in JPH1 abundance (detected with mAb VF1c) is found after incubation with a calcium ion chelator BAPTA-AM. This could imply that JPH1 and 2 are differentially regulated (n=3, one-way analysis of variance with Dunnetts multiple comparison post test: all values were compared to DMSO)

At 3 hours, no significant results were seen with the pAb JP1, however using the VF1c mAb, western blot detection of JP1 protein abundance showed a significant increase in total abundance after treatment with 20μM BAPTA –AM, a calcium chelator, compared to vehicle

treated controls (p=0.0312). This means that removal of calcium ions from the cytosol of A7r5 muscle cells may lessen the amount of calpain cleavage undergone by JPH1. One would have expected an increase in JPH1 abundance in cells treated with ALL-N, a calpain I inhibitor, however this increase was non-significant (as determined by One-way ANOVA followed by Dunnetts multiple comparison tests). It is likely that ALL-N inhibition was ineffectual in these experiments. Surprisingly, A23187 (a calcium ionophore) treatment caused an increase in both JP1 and JP2 detection after three hours, and in JP2-probed blots this increase was significantly higher (p= 0.036) than in vehicle-treated controls. JP1 probed blots showed increased abundance in A23187 treated samples, but a decrease in BAPTA-AM treated samples, in stark contrast to the results seen using the VF1c antibody. It should be noted that there was stubborn background on JP1 pAb treated blots, and this is likely to have interfered with analysis.

Due to the confounding results obtained after three hours, it was postulated that 3 hours was too short a treatment time, thus treatment with ALL-N, A23187 and BAPTA-AM and DMSO only and media-only controls were extended to 6 hours in the same cell line. In 6 hour treated samples, again, pAb JP1 treated blots were swamped in persistent high background, which is likely to have partially obscured the analysis using this antibody. The panel probed with JP1 pAb shows the highest abundance of JPH1 protein in media only control lanes, with steadily decreasing abundance in DMSO-, ALL-N, A23187- and BAPTA-AM-treated cells. Detection of JPH1 protein using the VF1c mAb showed a significant increase in JPH1 abundance in DMSO (vehicle) treated samples compared to media only controls, which is interesting as DMSO should not have any effect. ALL-N treatment (Calpain I/ μ-Calpain inhibitor) caused

a significant decrease in JPH1 abundance compared to DMSO treated controls (p= 0.005), hash mark on graph), while A23187 and BAPTA-AM treated JPH1 levels were not significantly different from vehicle treated controls. It should also be noted that when JP1 blots and VF1c blots were run in tandem, the corresponding films could be perfectly aligned when overlaid, further corroborating the fact that JPH1 is detected by the VF1c antibody. In pAb JP2-probed blots, again, there was a significant difference in vehicle and media only controls, so all data was normalised to the vehicle, DMSO, by way of Dunnets multiople comparison tests. JPH2 was detected as a doublet at 100 kDa in molecular weight, with background bands visible at higher molecular weights. ALL-N incubation showed no difference in JPH2 abundance, while A23187 incubation caused a significant decrease in JPH2 abundance (p=0.02, hash mark on graph), as expected. BAPTA-AM treatment for 6 hours caused a massive decrease in JPH2 abundance compared to vehicle only controls, (p=0.003, black diamond on graph).
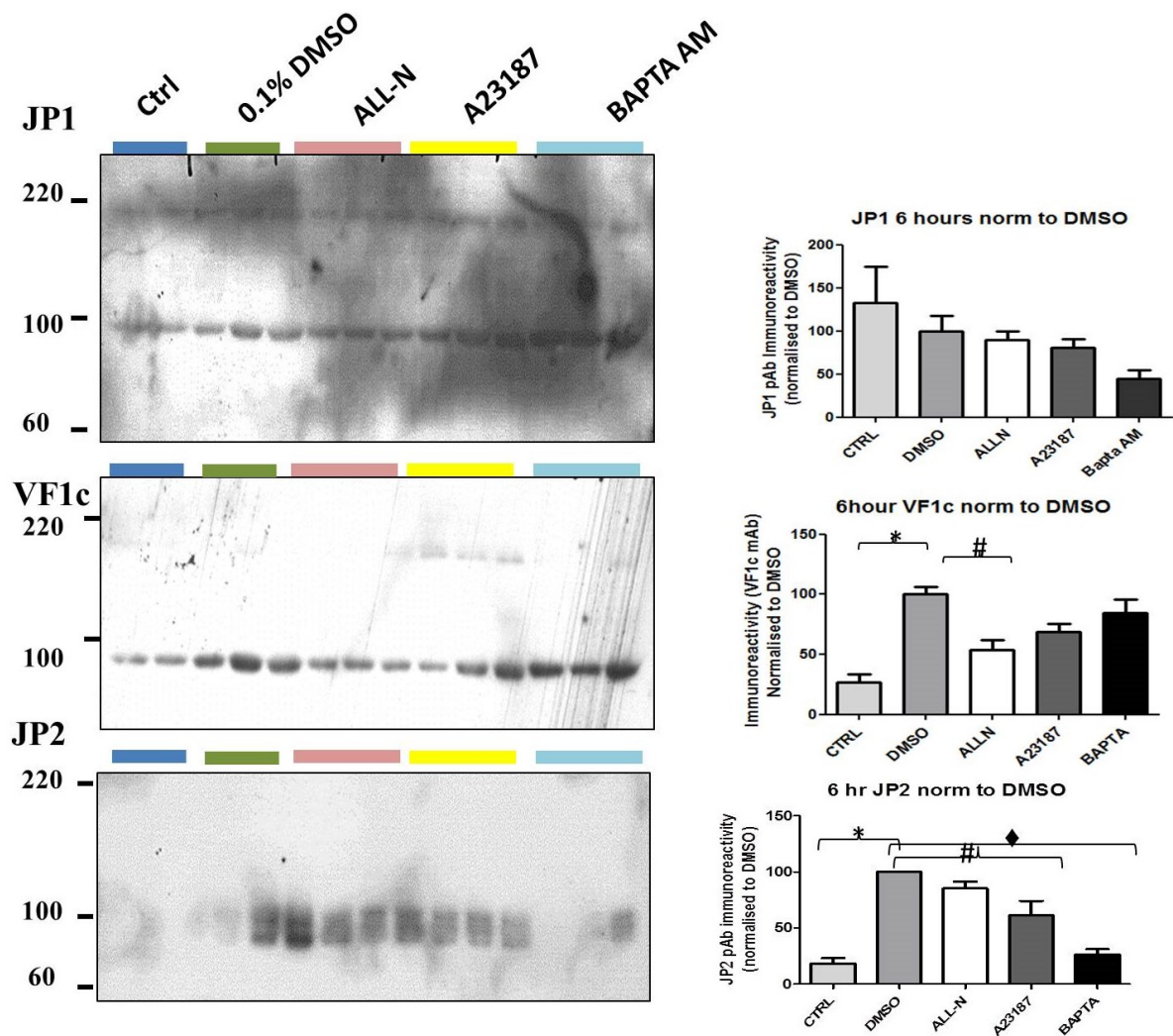
Figure 5.3.g.ii: 6 hour incubation of A7r5 cells with calpain inhibitors. JPH1 and JPH2 abundance were measured in A7r5 cells incubated with media only, vehicle (0.01% DMSO), ALL-N, A23187, BAPTA-AM for 6 hours via western blotting with pAb JP1, JP2 and mAb VF1c. JP1 abundance was decreased in ALL-N incubated samples compared to vehicle incubated controls, in mAb treated blots, however this was not found in pAb JP1 treated samples. JPH2 abundance was decreased in A23187 and BAPTA-AM treated samples compared to controls.

Score	JPH1 calpain 1 cleavage sites	N terminal	C terminal
>99.99%	226 to 231	24.6 kDa	47.1 kDa
>99%	224 to 229	24.4 kDa	47.3 kDa
>99%	394 to 399	43.0 kDa	28.7 kDa
>99%	390 to 395	42.7 kDa	29.0 kDa
>95%	465 to 470	51.1 kDa	20.6 kDa
>99%	544 to 549	59.5 kDa	12.2 kDa
>95%	572 to 577	62.6 kDa	9.1 kDa
>95%	575 to 580	62.8 kDa	8.8 kDa
>95%	601 to 606	65.6 kDa	6.0 kDa
>95%	610 to 615	66.6 kDa	5.1 kDa

Score	JPH1 calpain II cleavage site	N-Terminal	C-Terminal
>99.99%	161 to 166	17.9 kDa	53.8 kDa
>99.99%	157 to 162	17.5 kDa	54.2 kDa
99%	201 to 206	21.8 kDa	49.8 kDa
99%	226 to 231	24.6 kDa	47.1 kDa
99%	465 to 470	51.1 kDa	20.6 kDa
99%	544 to 549	59.5 kDa	12.2 kDa
>95%	555 to 560	60.9 kDa	10.8 kDa
>95%	518 to 523	56.7 kDa	14.9 kDa
>95%	597 to 602	65.2 kDa	6.5 kDa

Score	JPH2 Calpain I cleavage sites	N-terminal(kDa)	C-terminal (kDa)
>99%	230-235	24.9 kDa	49.7 kDa
>99%	237-244	26.6 kDa	48.1 kDa
99%	161-166	17.8 kDa	56.9 kDa
99%	157-162	17.4 kDa	57.2 kDa
99%	600-605	64.4 kDa	10.3 kDa
95%	98-105	11.0 kDa	63.2kDa

Score	JPH2 Calpain II cleavage sites	N-terminal (kDa)	C-terminal (kDa)
99%	152-162	17.4 kDa	56.8 kDa
99%	161-172	17.8 kDa	56.4 kDa
99%	232-240	23.9 kDa	50.4 kDa
99%	260-272	27.3 kDa	47.0 kDa
95-99%	218-230	23.5 kDa	50.8 kDa
95%	365-385	41.0 kDa	33.3 kDa
95%	221-230	23.9 kDa	50.4 kDa

Table 5.3.i: *In silico* **analysis of Rabbit, mouse, rat and human JPH1 and 2 sequences using online Calpain-cleavage predictors.** Online and freely available programs (Site predictor) were used to calculate the potential calpain cleavage sites on JPH1 and JPH2 proteins.

JPH1 and 2 protein sequences were also analysed using online software (Site Predictor-http://www.dmbr.ugent.be/prx/bioit2-public/SitePrediction/) (Verspurten *et al*, 2009) and a species comparison was performed between rabbit, rat, mouse and Human isoforms. The results, seen in table 5.1.3.j, show that both JPH1 and 2 have the potential to be cleaved by calpains I and II. Looking at cleavage events mediated by Calpain I, JPH1 has one very likely calpain cleavage site across all four species (indicated by the score of 99.99% or higher, dark

grey box), while JPH2 has two very likely sites, between 230-235 and 237-244 (purple boxes, table 5.3.j). The highest scoring calpain II cleavage sites on both JPH1 and JPH2 occur in a similar region, (amino acids 161-166 and 157-162 for JPH1, and 152-162 and 161-172 for JPH2). It is very possible that these regions are conserved across junctophilins, which lead to a Blast alignment of JPH1 and 2 sequences from rabbit, rat, mouse and human (see appendix II, Figure 8.2.g). In agreement with (Garbino *et al,* 2009) the alignments show that the region of JPH1 and 2 which are most likely to be cleaved by calpains I and II are in fact conserved across the four species analysed here. It is important to note that although the FASTA sequences for JPH 1 and 2 (which were analysed here) give computed molecular weights of 75 kDa total, in SDS PAGE JPH1 or 2 are rarely if ever found at that apparent molecular weight (this is discussed in detail in chapter 6, section 6.4). It should also be noted that the fragment readouts given here assume one cleavage event per protein, and that this many more cleavage events may occur *in vivo.*

5.4: Discussion

Fig. 5.1.3a and b show that mAb VF1c interacts with JPH1, and that it interacts at within the region of 369-460 amino acids, near the mid-section of the protein. As this antibody has previously been used to detect a protein termed JSR-90, current knowledge on JPH1 can now be coalesced with previous studies of JSR-90. This reveals that JPH1 is

phosphorylated by an endogenous kinase (Guo *et al,* 1994), is preferentially stained in fast fibres and under non-reducing conditions migrates at 170 kDa, indicating potential dimer formation or, its participation in a protein complex. Froemming's study in 1999 show that JSR-90 is sharply down-regulated after chronic low frequency stimulation, (a model of fast to slow fibre type transition) of rabbit muscle, and was most abundant in EDL muscle (Froemming *et al,* 2000). These results are supported by the work presented here. Although the peptide array experiments failed to provide definitive data, cumulatively they hint that mAb VF1c may bind to JPH1 in a conformational manner. It is noteworthy that the mAb VF1c interacts with JPH1 in an area very close to its DHPR binding region (residues 232-369, with a faint interaction seen in pull down experiments using residues 369-571(Golini *et al,* 2011)). Knowing that the mAb VF1c can detect JPH1 will provide novel avenues of study for the interaction of JPH1 with RyR and DHPR, as well as novel interactors which together shape the release and regulation of Ca^{2+} ions in the cell.

Rat and mouse tissue were analysed for expression of JPH1 and JPH2 via western blot. Using pAb JP1, only 1 band, a positive control band in rabbit skeletal muscle lane was detected, and it had an apparent molecular weight of 45-50 kDa. This is different to the staining pattern observed using mAb VF1c, which detected two bands at 85 and 60 kDa. Consideration must be given to the binding regions of the antibodies used, as it has been shown that mAb VF1c interacts with the middle region of JPH1, while pAb JP1 interacts only with the C-teminal region. It is likely that the C-terminal of the protein has been cleaved off and may have run off the gel, and thus could not be detected by pAb JP1. Future analysis

could employ higher percentage gels or ideally a gradient gel would optimally resolve the fragments of JPH1 and 2.

The analysis of JPH1 and 2 in rabbit muscle gives further weight to the experiments performed by Guo *et al* (1994), where they observed increased staining in type II fibre-rich muscles using the VF1c antibody. These results confirm this finding, and go further by showing that of the muscles tested, the highest amount of JPH1 is detected in EDL muscle, followed by latissimus dorsi. This is important to the field, as JPH1 expression corresponds loosely with RyR1 expression, which several studies have found to be highest in fast type skeletal muscle (Froemming *et al* 2000, Conti *et al,* 1996, Protasi *et al*, 2000). Knowing relative levels of JPH 1 and 2 could prove very useful to any future scientist trying to purify said proteins. An interesting further study would be the analysis of type 1 RyRs in the same samples, and to compare the ratios of JPH1 to RyR1 and DHPRs, or any other interactors, such as Caveolin 3 (White *et al,* 2012). For this analysis to be completed, highly specific antibodies targeted to RyR1 and DHPR would be necessary. An important point is that prior to homogenisation, the tissue excision, protease addition, homogenisation and freezing should be as swift as possible, as EC coupling proteins such as Junctophilins and RyRs are readily degraded by proteases (Brule *et al,* 2010, Murphy *et al,* 2013).

As well as the potential for further cleavage of JPH1, differences exist in expression levels and molecular weight between the various muscle types. In rabbit diaphragm (and to a lesser extent, soleus) had significantly lower JPH1 expression than found in EDL muscle, while the intercostal muscles express JPH1 which migrates with a calculated MW of 129 kDa

and 88 kDa, while the EDL, GC, SH ,SM muscles have calculated molecular weights of 85 and 67-70 kDa. Diaphragm muscle expresses JPH1 with an apparent molecular weight of 60 kDa. Regarding JPH1 levels in diaphragm and soleus tissue, it is known that muscles with a slower phenotype express higher levels of calpain proteolytic enzymes compared to their fast fibre type counterparts, and that that μ-calpain (also known as calpain I) is localised to the microsomes, as opposed to freely diffusible in the cytoplasm in fast muscle types such as the EDL (Sultan *et al,* 2000). This could account for both the lower molecular weight and decreased abundance found in these tissues. As these muscles undergo constant (diaphragm) or extended contraction times (soleus, an anti-gravity muscle), it is possible that JPH1 is constantly being synthesized and broken down. It should be noted that other proteolytic enzymes could also play a factor, if indeed degradation is the cause of the decreased molecular weight, and not a muscle-specific splice variant. A splice variant could be the case for intercostal muscles, which undergo constant or near constant use. A specific feature of intercostal muscles is that they undergo frequent eccentric contractions, and as showed by Corona *et al* (2010), these lengthening contractions of muscle can activate calpain-mediated cleavage of JPHs. A possibility is that to prevent continuous damage and repair, a splice variant of JPH1 could exist without some of the postulated cleavage areas (see fig 5.1.a), thus migrating at a greater molecular weight. Another possibility is that JPH interacting with another protein, cellular component or itself could render it less susceptible to proteolytic cleavage in this muscle type. Intercostal muscles have also been shown to have altered transcription-intiating mechanisms to limb muscle. In field-stimulated FDB and soleus muscles, NFAT translocation to the nucleus was increased as expected, but in intercostals fibres NFAT translocation was decreased after 90 minutes of stimulation, implying

163

differential regulation of this transcription factor in intercostals muscle tissue (Robison *et al*, 2014). The authors postulate that altered regulation of NFAT will have concomitant effect on protein expression in this muscle, and thus it is possible that JPH1 and 2 fall under NFATs remit. Either way, analysis of various muscle types in rabbit has shown that JPH1 is likely to be specifically regulated depending on the function of the muscle, and highlights the importance of JPHs in muscle physiology.

In Fig.5.3.e and f it appears that mAb VF1c and pAb JP1 are interacting with the same protein. Despite attempts to characterise JPH1 expression in maturing C2C12 myotubes, confounding results were obtained. Junctophilin 1 expression seems to have a biphasic expression pattern, peaking 2 or 3 days after differentiation flowed by a decrease to undifferentiated levels. As these cells are a widely used tool in EC coupling research and especially in analysis of junctophilins, it is important to characterise the expression of JPHs in these models (Golini *et al,* 2011, Hirata *et al,* 2006). However, an important caveat of these experiments is that the state and passage number of these cells can be a confounding variable. Another option for studying this protein could be isolated muscle fibres, which can also be used for calcium signalling studies, however these are significantlly more expensive to get and maintain, as they require whole animals to be sacrificed. Interestingly, in C2C12 cells the JPH1 protein is a full 90 kDa, as opposed to in skeletal muscle controls where it migrates at 75 and 65 kDa. This indicates that a difference in protein processing or cleavage exists between these two tissues, and is likely to do with the activity of the cells. As seen in chapter 6, exercise can have solubilising effects on the junctophilins, thus a contraction protocol followed by JPH analysis in C2C12 cells could be rally interesting (Corona *et al,*

2010; Murphy *et al*, 2013). It is likely that JPH1 would be detected at a lower molecular weight, in its cleaved form after such a protocol. Importantly, C2C12 cells need to be at optimum condition and passage, as their expression profile and ability to differentiate properly into myotubes decreases at high passage numbers. Further attempts to knock down JPH1 expression in C2C12 cell lines proved unsuccessful, due to effects caused by the siRNA delivery system (Fig 5.1.3.g). Other researchers have had more reliable results using virally delivered siRNA particles and found that knocking down both JPH1 and JPH2 caused deformed triads, reduced capacity for SOCE and altered caffeine induced Ca^{2+} release from the SR (Hirata *et al,* 2006). These results should be interpreted with caution though, as they are results of a double knock down. That said, the rabbit muscle expression profile presented here describes a more constant role for JPH2, in that its levels are not as variable as JPH1, indicating that JPH1 has more of a role in the "fine tuning" of Ca^{2+} signalling in muscle cells, while JPH2 has a largely structural role. A "Fine-tuning" role for JPH1 is logical for several reasons. As it is a known contact for DHPR and RyR and participates in orthograde and retrograde signalling, JPH1 is well placed to manage Ca^{2+} and be an active participant in calcium ion relese events (Golini *et al,* 2011). Phimister *et al* found that JPH1 interacted with RyR1 protein in a conformationally dependent manner, and that it may have redox sensing abilities (Phimister *et al,* 2007). This proves that JPH1 can be thought of as "scaffolding that talks" instead of a simple, non-reactive structural protein. It is highly likely that JPH1s role in retrograde and orthograde Ca^{2+} signalling will become clearer in the next few years. It will be interesting to see if any natural mutations in JPH1 give rise to disease, as they could prove invaluable to fully understanding its function. One mutation (R213P) in JPH1 has been linked to Charcot-Marie-Tooth disease (CMT), a heritable and progressive neuropathy which affects

motor and sensory nerves, and in muscle, can cause varying degress of weakness and or atrophy. In CMT one patient with the R213P, mutated JPH1 is unable to rescue SOCE in affected tissue, and JPH1 was found lodged in miotchondria which could hint that JPH1 has a role in linking RyR-associated and mitochondrial associated complexes (Pla-Martin *et al,* 2014).

As the C2C12 model has proven unreliable, the A7r5 cell line was selected for study with a calpain cleavage inhibitor, ALL-N. Future studies using the C2C12 model could delete the PEST sequence (the likely area of calpain cleavage of JPH1, see Fig 5.1.3a) and assess functional consequences. It is quite likely that decreasing the length of the JPH1 protein would have a massive functional effect within muscle, perhaps via orthograde signalling. Removal of the PEST sequence could also have very interesting consequences for RyR1 and DHPR expression and function. The results presented here show that although skeletal and smooth muscle cell lines are similar (in calpain expression at any rate, as smooth muscles express calpain I and II as well (Zhang and Johnson, 1992), the A7r5 cell line is not the best match for skeletal muscle proteins. However, they do imply that JPH regulation is important in smooth muscle contraction, as it can be regulated within hours of addition of relevant substance (e.g. BAPTA AM), and this has implications for smooth muscle biology. That JPH levels could be altered by calcium ionophore/chelator addition implies that in resting smooth muscle (apart from basal contractions which may be present in cell culture samples), an ideal Ca^{2+} concentration exists for maximum full length JPH1 and 2: a "goldilocks" Ca^{2+} concentration, where full length JPH 1 and 2 out weigh calpain-cleaved JPHs. It is difficult to say whether JPHs are being constantly cleaved and regenerated, or if calpain cleavage is an

event tied to cell requirements and functions, such as a bout of contractile activity. Recent studies in heart and skeletal muscle tissue imply that calpain cleavage of JPH1 and 2 are contraction induced, but this may not be the case in smooth muscle (Wehrens *et al,* 2015 Murphy *et al,* 2012). Some flaws exist in these confounding results, and it may be that experimental pitfalls need to be negotiated. These pitfalls include DMSO causing an increase in JPH1 and 2 abundance after 3 and 6 hours incubation. This could be due to DMSO passing through membranes, and perhaps causing damage. In yeast, DMSO incubation has been shown to increase the biosynthesis of membrane components such as phospholipids and to thus increase membrane proliferation, and it is possible that this also occurs in the smooth muscle cells used in this study (Murata *et al,* 2003). As JPH proteins interact with plasma membranes of cells via their MORN motifs, and that this interaction is crucial to the shape and correct functioning of this protein, it is feasible that changes in memebrane structure or composition could cause a change in JPH protein levels. High levels of DMSO have also been found to allow increased Ca^{2+}ions to enter the cell, which could also have affected the abundance levels of JPH proteins (Murata *et al,*2003: de Menovial *et al,* 2012: Bennett *et al,* 2013). DMSO concentration in these experiments did not exceed 0.1% of total volume of media added to 6 well plates, but the possibility of incomplete plate closure and thus media evaporation or concentration cannot be excluded, however it is very unlikely. Thus it is more likely that DMSO has effects on JPH abundance via alterations in Ca^{2+}concentration or membrane based effects. This could have massive implications for future study of JPH proteins in cell culture models, particularly as A7r5s are a popular model for vascular injury. It is very interesting that the field of Junctophilin research has focused strongly on cardiac and skeletal muscle, while JPH research in smooth muscle is relatively new. In the future,

JPHs may be shown to be intrinsic to correct functioning of vascular tissue as well as skeletal and cardiac muscle. Interestingly, the N-ter peptides used to introduce siRNA moieties into the C2C12 cell lines also caused slight increases in JPH1 expression, despite attempting to do the exact opposite (section 5.3.c). It could be that membrane disruption (especially any which affect the lipid compostion or integrity of cell membranes) of any sort has an impact on JPH expression. This makes sense as removal of JPH1 as seen in KO animals has deleterious effects on calcium flux in the cell via RyR and thus on cellular fate, so if the membrane were damaged, it would make sense to upregulate JPH proteins which could steady RyR-mediated Ca^{2+} release. This bears similarities to what occurs after repetitive eccentric contractions, which when performed in mouse cause the upregulation of JPH1 three days after the bout of muscle-lengthening exercises (Hirata *et al,* 2006: Phimister *et al,* 2007: Corona *et al,* 2010). .

An *in silico* analysis of potential calpain I and II cleavage sites on JPH1 and 2 was undertaken, and several sites were found. The most likely cleavage sites for JPH1 and 2 were both found in the N terminal region of JPH1 and 2. It is important to note that although the FASTA sequences for JPH 1 and 2 (which were analysed here) give computed molecular weights of 75 kDa total, in SDS PAGE JPH1 or 2 are rarely if ever found at that apparent molecular weight (this is discussed in detail in chapter 6, section 6.4). It should also be noted that the fragment readouts given here assume one cleavage event per protein, and that this many more cleavage events may occur *in vivo.* In concordance with *in silico* efforts performed in this work, Gou *et al* recently found that JP2 protein is indeed cleaved by calpain I, and is split into four smaller peptides, at 100, 75, 37 25 and 20 kDa, which supports the

work presented in chapter 5 and 6. They confirmed this using fusion proteins of JP2 fragments, and found that three calpain cleavage sites are N terminal, while one was found in the C terminal region, which mutagenesis studies defined as the main calpain cleavage site. Similar experiments have not been performed for JP1, however, based on the similarity between the results presented here and that from *in silico* analysis, we can assume that at least three calpain cleavage sites exist in JP1 protein.The results shown in fig 5.3.i show that although not a perfect model of caplain cleavage sites, many residues were similar to those found in Gou *et al* (2015), so it can be assumed that this *in silico* analysis is a good starting point for further study of calpain interactions of these proteins. As Guo *et al* found that cleavage of JPH2 hindered cardiac contractility (an observation backed up by Murphy *et al* and by the known hypertrophy causing mutations in JPH2), it has been shown that JP1 cleavage is also detrimental to signalling in skeletal muscle (Corona, *et al,* 2010, Murphy *et al,* 2013, Guo *et al,* 2015). Using Biogrid cuckoo calpain hunter and CaMBPD, Guo *et al* predicted calpain cleavage site to be in the region of R565T, consistent with predictions made in fig.5.3.i. This is significant for JPH2, as it shows several key facts: i) JPH2 is cleaved as part of muscle function and ii) JPH2 cleavage has a role in cardiac dysfunction (a fact supported by Wu *et al*, 2014 and Beavers *et al,* 2013) who showed that RyR2 binds to JP2 and that a mutation (E169K) causes decreased interaction of these two proteins and increased calcium ion leak from the SR) and iii) that extrapolating these results and expanding the calpain cleavage knowledge on JPH1 will aid in understanding several muscle disorders including those in smooth muscle. Various evidences exist for this: (Murphy *et al*, 2013: Corona *et al,* 2010). This also supports the work presented in chapter 6, where a burst of exercise appeared to cause an increase in JP1 and JP2 cleavage, as determined by western

blot. This implies that calpain cleavage has a big role in maintaining EC coupling in skeletal muscle cells and Junctophilin levels must be regulated quickly and in response to the activity or contraction level of the muscle it is expressed in. Evidence of muscle specific regulation can be seen in figures 5.3c, while the changes in JPH total abundance in age and exercise can be seen in section 6.3.b..

It has been observed that ANGII can affect not only JP2 expression (causing upregulation) but the expression of RyR2 also (Gul *et al,* 2007: Cai *et al,* 2015). This has implications for cardiac disease and hugely, the regulation of RyRs, which is highly complex and has not been fully elucidated yet (Cai *et al,* 2015; Wu *et al*, 2014). Puerarin, found in a traditional Chinese herbal remedy used in cardiovascular medication has also been shown to upregulate JP2 expression in the heart, as determined by qPCR mediated mRNA analysis. This in tandem with up-regulation of Caveolin 3 and other T-Tubule associated proteins imply that increasing the amount of JPH2 protein available in the heart, specifically the failing heart is beneficial (Wang *et al,* 2014)

5.5: Future Studies

Future work in the area needs to address the levels and functions of JPH1 in disease models (see Chapter 6), and to fully understand the role of calpain cleavage and specific muscle function has on JPH expression. This could involve mutational studies of the postulated PEST or postulated calpain cleavage sequences and subsequent Ca^{2+} imaging studies to assess what function cleaving the junctophilins serves. Murphy *et al,* (2013) suggest that post-stimulatory cleavage of JPH1 *in vitro* creates a "diffusible fragment" of

JPH1, thus disrupting EC coupling and impairing muscle fibre contraction. This would mean repeated cleavage and regeneration of JPH1 in skeletal muscle, and warrants further analysis. This could be achieved by expressing fragments of JPH1 and incubating with and without various calpains followed by SDS page to determine a) If calpain cleavage is at play and b) to determine where on the JPH proteins these proteases actually cut.

Another area worth investigating the role of JPH1 in smooth muscle, and whether it is processed the same way as in skeletal muscle. Preliminary data from the current project indicate that JPH1 and 2 are not cleaved in smooth muscle embryonic cell line in the same way as they are in muscle cells (Appenidix II, A7r5 data Figures 8.2.d and e). This indicates that a high degree of cleavage of JPH1 and 2 could be skeletal muscle specific. The role of JPHs in smooth muscle, unlike its role in skeletal or cardiac tissue has not been investigated, and could be very easily studied using excised vascular tissue and cell line models. Such analyses could include examination of JPH expression patterns in smooth muscle (western blot or mRNA analysis), and whether or not JPHs respond to common antihypertensive drugs. A simple study would be the comparison of male and female hormones and the effect they have, if any, on JPH expression in vascular tissues, as estrogen is reported to have protective effects on damaged vascular tissues (Brouchet *et al,* 2001).

The phosphorylation of JPH1 by an endogenous kinase, as discovered by Guo *et al* in 1994 also warrants further investigation, as this could have huge implications on the signalling state of the protein. This could be achieved using 1) bioinformatic approaches to identify potential consensus phosphorylation motifs followed by either bacterial expression of

clones of this region of JPH1 and kinase assays or 2) tryptic digestion of the isolated JPH1 followed by phosphopeptide mapping or mass spectrometry. This could provide crucial data on how JPH1 interacts with and or regulates other proteins such as RyR1.

Chapter 6: Junctophilin 1 and 2 abundance in models of disease

6.1. :Introduction

Having established that mAb VF1c detects JPH1, experiments were undertaken to analyse JPH1 and JPH2 levels in various disease states such as sarcopenia, chronic intermittent hypoxia (CIH) and Duchenne muscular dystrophy (DMD). These disease models were chosen as they have been shown or are suspected to have EC coupling irregularities, and thus an investigation of JPH expression is fitting. Sarcopenia, DMD and CIH share some striking similarities in terms of muscle-specific pathologies, namely altered Ca^{2+} homeostasis and the potential for drastic muscular remodelling (e.g. fibre type switching, fatty tissue infiltration). Because changes in Ca^{2+} handling or fibre type are known to have repercussions for EC coupling proteins, it was prudent to investigate the effects of these pathological states on JPH1 and JPH2 abundance in various skeletal muscle groups. To test this hypothesis, Western blot experiments were undertaken to clarify if any such differences in EC coupling proteins exist in these disease states.

Duchenne muscular dystrophy is an X-linked recessive condition that affects approximately 1 in 4000 male births per year (Dooley *et al*, 2010). It is characterised by delayed motor milestones, Gowers sign (using the hands to walk to a standing position from a seated position) and progressive muscle atrophy. This atrophy begins in the lower limb muscles and progresses to the upper limbs, trunk and diaphragm, which is usually the worst affected. Diaphragm atrophy leads to loss of life in the second decade, usually via respiratory failure. DMD is caused by a premature stop codon in the dystrophin gene, causing loss of

174

production or truncated forms of the dystrophin protein (Kunkel *et al,* 1986; Hoffman *et al,* 1987; Bonilla *et al,* 1988). Dystrophin forms an important link between a complex of dystroglycans and sarcoglycans (which mediate contact with the extracellular matrix via laminin) and the actin cytoskeleton of cells (see Fig 6.1.1a). It functions almost as a force transducer/ shock absorber for the membrane, while also acting as a massive hub for protein-protein interactions (Davies and Novak, 2006). These interactions are severely perturbed in muscles which lack the dystrophin protein, they undergo recurrent degeneration-regeneration cycles, as well as immune cell and fatty tissue infiltration, often causing the pseudohyertrophy evident in DMD patient calf muscles (an overview of skeletal muscle effects can be seen in Fig 6.1.1.b) (Alderton *et al,* 2000; Jørgensen *et* al, 2009). As well as skeletal muscle pathologies, smooth and cardiac muscle are affected, and there are mild cognitive effects. Because of the massive complex formation at the membrane, the absence of dystrophin causes several irregularities in muscle cells including impaired metabolism, structural weakness, decreased membrane integrity, fibrosis and increased Ca^{2+} handling abnormalities (Ohlendieck *et al,* 2012). Ca^{2+} handling is affected in several different ways in both DMD patients and in a naturally occurring model, the *mdx* mouse. Raised intracellular calcium levels have been found in both DMD and *mdx* muscle fibres by Lopez *et al* (1987). Aberrations in RyR receptor signalling and expression have been shown in dystrophic myotubes, as well as altered Ca^{2+} sequestering into the SR via SERCA pumps (Schneider *et al,* 2013, Altamirano *et al,* 2012). Zhao *et al* found the dystrophic *mdx* fibres had increased Orai expression compared to WT samples, which as part of the store operated calcium entry (SOCE) pathway in muscle cells caused an increase in cytosolic calcium levels. (Zhao *et al,* 2012).The Orai calcium channels are recruited and opened in concert with STIM1 proteins,

which when overexpressed in mouse myotubes causes a *mdx*-like phenotype (Goonasekara *et al*, 2014). As JPHs have been linked with RyR regulation and SOCE via STIM and Orai mechanisms, it was prudent to examine the abundance of JPH1 and JPH2 in *mdx* tissue. Disruption of the dystrophin complex also affects the interaction of CAV3 with the plasma membrane. CAV3 has been shown to interact with JPH2, and is over-expressed in dystrophic myotubes (Minetti *et al,* 1998; Minamisawa *et al,* 2004). Samples were obtained from the *mdx* mouse, a naturally occurring mutant which lacks dystrophin protein (although it does express utrophin, a similar protein which compensates to a small degree) (Tan, Lansman, 2014). The *mdx* mouse is the most widely characterised model of DMD, even though they have distinct differences to the human pathology, namely longer life and less severe disease progression (Partridge, 2013).

Irregularities in Ca^{2+} handling and spark disruption have been described in mouse *mdx* tissue before. Such irregularities include an elevated resting Ca^{2+} concentration in *mdx* fibres from the EDL muscle as well as increased sensitivity to endurance exercise and osmotic shock in comparison to WT muscle fibres (Freyesse *et al,* 2004;Wang *et al* 2005). It has been suggested that these Ca^{2+} handling abnormalities are caused by several mechanisms, including: i) increased SOCE and ii) increased Ca^{2+} sparks‚ caused by a disruption in DHPR-RyR coupling. Ca^{2+} spark frequency is also permanently increased after strenuous exercise or osmotic shock in *mdx* fibres but not WT samples (Wang *et al,* 2005). Bellinger *et al* (2009) found impaired forces in *mdx* muscle compared to WT after eccentric contractions (Wang *et al,* 2005; Bellinger *et al,* 2009) and as this form of exercise is known to cause deleterious effects on JPHs, analysis of these proteins in *mdx* muscle is warranted (Corona *et al,* 2010).

To this end, the relative levels of JPH1 and JPH2 proteins in vastus lateralis, diaphragm, gastrocnemius and soleus muscles from wildtype and *mdx* mice were analysed via western blot, using pAb JP2 and mAb VF1c antibodies. Results are described in Section 6.3.b.
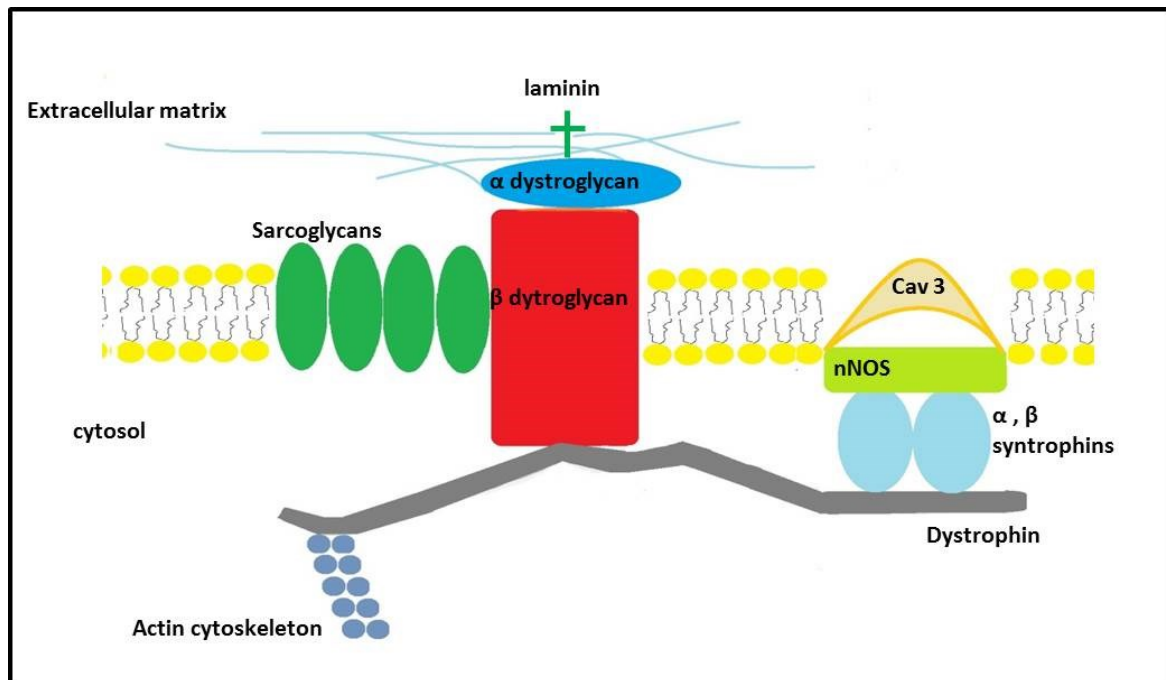
Figure 6.1.a: A diagram of the dystrophin associated proteins in complex at the cell membrane of skeletal muscle cells. Dystrophin interacts with sarcoglycans and dystroglycans which together maintain the link between the extracellular matrix and the cytoskeleton. This diagram also shows the dystrophin can also act as a hub as it associates with CAV3, nNOS (neuronal nitric oxide synthase) and syntrophins. Image adapted from (Davies and Novak, 2006).
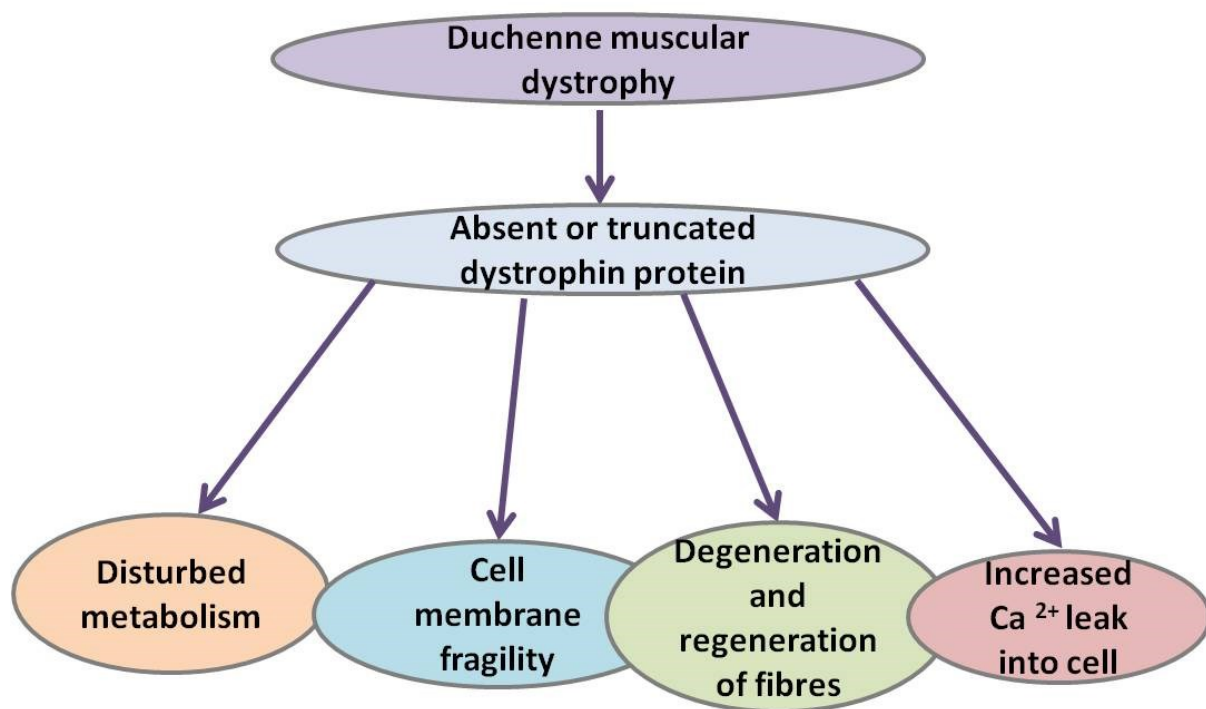
Figure 6.1.b: Overview of muscular effects caused by lack of Dystrophin expression.

Sarcopenia is a disease of aging, whereby muscle mass and strength decrease approximately 4-8 % every decade after the fourth decade of life in humans. This is associated with a reduced force of muscle, which in turn hampers physical activity and well-being (Mitchell *et al,* 2012). It is characterised by decreased muscle strength, increased type I to type II fibre type ratio and a decrease in fibre type cross-sectional area (Lexell *et al,* 1988; Evans and Lexell, 1995). Due to the increased length of human life, sarcopenia represents a major factor in the health and well-being of elderly people, as falls due to muscle weakness can be a major cause of loss of independence and morbidity. In addition to frailty and slow walking speed increasing the risk of falls, sarcopenia also affects the internal muscles. These muscles are particularly important in maintaining structural integrity of the body, especially in women. Studies have found that an increased risk of urinary incontinence, vaginal prolapse

178

and thus increased care costs, possible surgeries and a concomitant increase in morbidity are associated with weakening of skeletal muscles with age (Morris *et al,* 2012; Stav *et al,* 2012). By the year 2050, it is estimated that the global population of over-60's will number 2 billion people, thus investigations need to be performed into possible treatments and causes of sarcopenia now (Stav *et al,* 2012). An overview of the effects of sarcopenia on skeletal muscle can be seen in Fig 6.1.c.

So far, although dietary and hormone-replacement based therapies have been investigated with mixed results, a resistance exercise regimen has been suggested as the best treatment option (Cruz-Jentoft *et al,* 2014). As well as (or as a feature of) increased weakness and decreased muscle mass, aging muscle has several other molecular pathologies including motor neuron loss, decreased growth hormone signalling, decreased reactive oxygen species (ROS) handling capabilites and dysregulation of Ca^{2+} homeostasis (Mitchell, *et al,* 2012). A decrease in satellite cell function and number has also been implicated in the pathogenesis of sarcopenia, and may be related to altered IL-6 signalling (McKay *et al,* 2013; Tierney *et al,* 2014). The decrease in muscle mass may be due to increased or dysregulated proteolyic mechanisms, as both caspase (in EDL but not soleus) and calpain activity have been shown to be increased in aged rodent muscle compared to their young counterparts (Rice and Blough, 2006; Brule and Dargelos, 2010). Calcium ion homeostasis has also been shown to be dysregulated in aged muscle, and calcium release units (CRUs) are decreased in both fast and slow fibre types, and EC–uncoupling has been suggested as a cause (Delbono *et al* 1995; Boncompagani *et al,* 2006). Interestingly, Ryan and Ohlendieck (2004) found that JSR90 protein levels were elevated in aged human VL muscle compared to younger samples (Ryan

and Ohlendieck, 2004). As we now know that JSR90 is in fact JPH1, further investigation of the role of this protein in sarcopenia were undertaken.
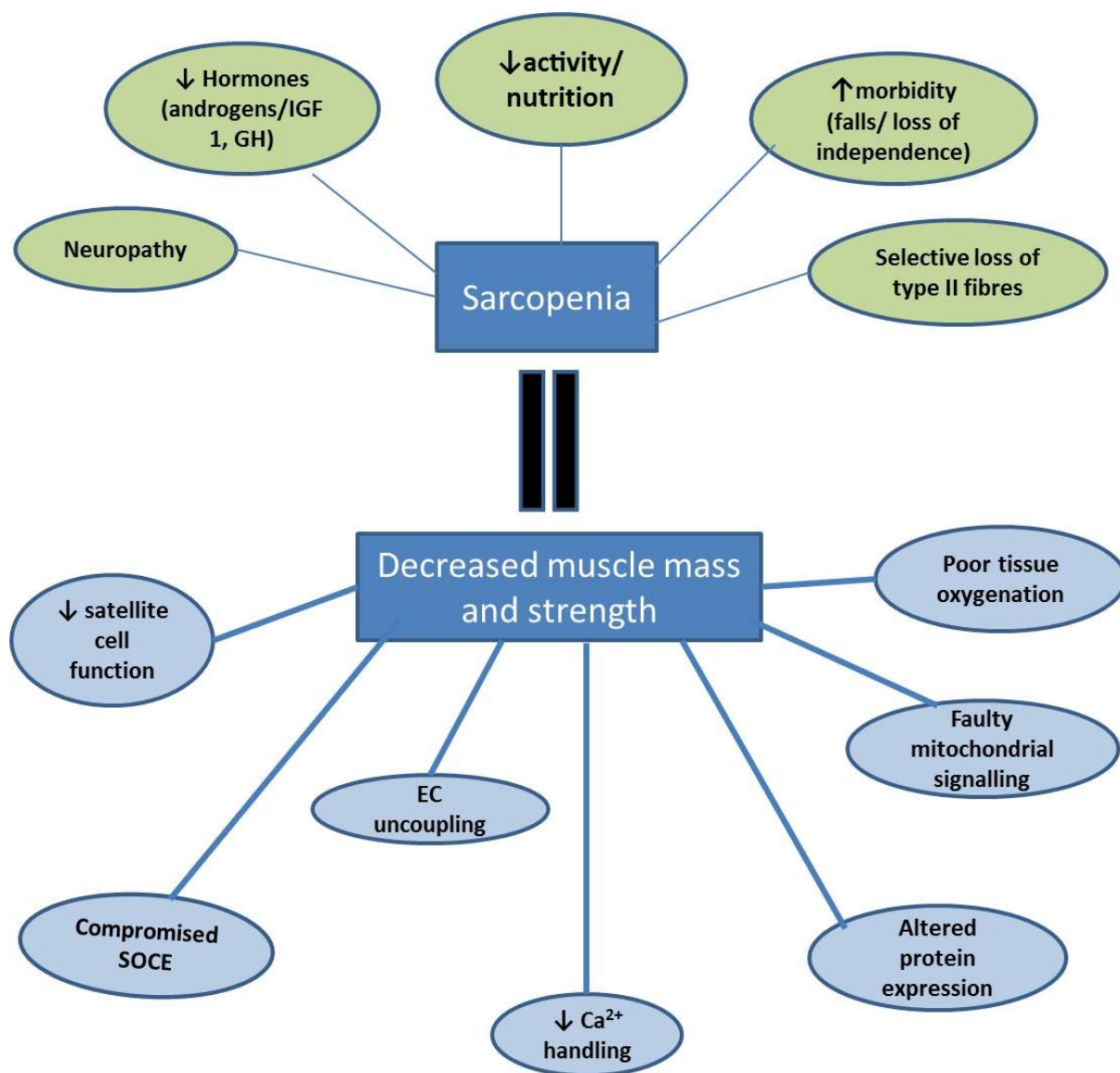
Figure 6.1.c.: diagram of factors involved in sarcopenia .

Chronic Intermittent Hypoxia (CIH) is a feature of diseases such as sleep apnoea and chronic obstructive pulmonary disorder (COPD), and comprises weakness in the primary and secondary muscles used in respiration, leading to apneustic periods. This causes

fluctuations in blood oxygen levels, and has wide ranging deleterious effects. While a substantial body of work has been done on the loss of function and fibrosis of respiratory muscles, little has shown the effect of CIH on peripheral muscles. A widely used rat model of intermittent hypoxia uses hypoxic chambers and alternating room and hypoxic air to replicate the apnoea seen in the human form of this disease, generating hypoxic animals with similar hallmarks to human hypoxic disease seen in COPD and sleep apnoea. CIH has well-documented effects on muscles of the upper airways, especially the diaphragm where remodelling occurs after only one week of CIH treatment in rats (Shortt *et al,* 2013). The effects of CIH are not limited to respiratory muscles. Chien *et al* (2010) showed that newly-diagnosed obstructive sleep apnoea (OSA) patients had decreased functional performance in knee extensor muscle (to assess quadriceps function) compared to controls, while Sauleda *et al* (2003) showed that VL samples of OSA patients had altered cytochrome C oxidase activity and upregulated phophofructokinase activity, as well as higher protein concentrations and increased type II fibre diameter compared to healthy age matched controls (Chien *et al,* 2010: Sauleda *et al,* 2003). However, no thorough analysis of the effects of CIH on peripheral muscles and EC coupling protein function or levels therein has been performed. To rectify this, and to complement mRNA based studies undertaken in the O'Halloran laboratory, EDL and soleus samples from rats exposed to CIH for 2 weeks and sham controls were analysed for JPH1 and JPH2 protein expression via Western blotting, section 6.3.c.

6.2: Aims:

The aims of this chapter were to estimate JPH1 and JPH2 abundance in 8 month old *mdx* mouse; in aged and exercised mouse tissue; and in a 2 week model of intermittent hypoxia in rat muscle. These experiments were performed to fully understand the roles of JPH1 and JPH2 in models of disease. This also verified that mAb VF1c interacts with the JPH1 protein.

6.3: Results:

6.3.a: JPH1 and 2 in 8 month old *mdx* and BL10 (WT)mouse strains

Four muscle types (vastus lateralis, diaphragm, gastrocnemius and soleus) were excised from 8 month old WT and *mdx* mice, homogenised and subjected to western blotting analysis as described in section 3.3 and 3.5. Results are shown in the figures below, and the accompanying bar graphs display total abundance and the percentage of cleaved or uncleaved JPH protein in each muscle. In vastus lateralis samples probed with mAb VF1c (against JPH1, see Chapter 5) a major band which migrated at 85kDa and a minor band with an apparent molecular weight of 65 kDa were detected (see Fig.6.1.3.a.i). When normalised to a β-tubulin loading control and expressed as a percentage of WT samples, no significant change in the level of JPH1 protein was detected. Similar results were seen when comparing JPH2 expression as detected by Western blot. No significant changes were found when

comparing WT to *mdx* samples. (n= 3 *mdx*, 5 WT: 2 technical replicates, statistical analysis was performed using Students' Unpaired T-test (two tailed). All molecular weights were calculated as shown in Appendix I, figure 8.1.a.)

In diaphragm muscle, no significant differences were found in the abundance of either JPH1 or JPH2;(Fig. 6.3.a.ii); however mAb VF1c detected bands of an apparent molecular weight 90, 70, 50 and 35 kDa, indicating that may be increased cleavage of JPH1 in this tissue (p= 0.7, 0.5, 1, Students' Unpaired T Test of WT vs *mdx* for the 90 kDa, 70 kDa and 50 kDa bands). JPH2 in the diaphragm migrates as two major bands, detected at 105 and 85 kDa (left panel, demarcated by arrows) slightly smaller than JPH2 detected in VL or GC, but this change in molecular weight was not statistically significant. The level of 100 kDa form of JPH2 detected via in *mdx* diaphragm was slightly increased compared to WT samples, but again, this was not statistically significant (p = 0.4, 0.9 Students' Unpaired T test of WT vs *mdx* 105 and 85 kDa bands). High variability between samples could be a factor.

In soleus muscle, JPH1 abundance was detected by mAb VF1c at 90 kDa, 75 kDa and 50 kDa, and no change in abundance is detectable in *mdx* tissue compared to WT controls (Fig. 6.1.3.a.iv, right panel.). This contrasts with JPH2 protein, which appears increased in comparison to WT; however statistical significance was not reached (p= 0.1, 0.5, Students' Unpaired T-test of WT vs *mdx* 110 kDa and 90 kDa bands). A trend towards what is likely to be greater cleavage of JPH1 in *mdx* soleus can be seen (84 % of total JPH1 was found at 85 kDa in soleus compared to 94% in WT), however JPH2 appears preserved in this muscle,

with 57% of *mdx* total JPH2 being detected at the full length of 100 kDa (Murphy *et al,* 2013). It is possible that higher numbers of experiments could provide more significant data.

In gastrocnemius muscles, a decrease in JPH1 protein is again observed in *mdx* tissue compared to WT, but this does not reach significance (p= 0.1, See Fig. 6.3.b.iii)). However, a notable difference exists in JPH1 cleavage in this muscle, as only one band was detected, of 70 kDa apparent molecular weight. Although this is much lower than the 90 kDa form detected in the diaphragm or 85 kDa in the soleus samples, comparison of molecular weights via Students T-test shows no significant difference. JPH2 was detected as two major bands migrating at 110 and 90 kDa. When WT and *mdx* levels of both forms were compared, a significant decrease was found in *mdx* tissue (p=0.05 (110 kDa WT vs *mdx*) and p = 0.04 (90 kDa WT vs *mdx*)). This may reflect the pseudohypertrophy seen in these muscles in *mdx* mice and DMD patients. Interestingly, a difference in cleavage of JPH2 was seen in gastrocnemius muscle between *mdx* and WT muscle. While JPH2 appeared significantly less abundant (total protein levels) in *mdx* tissue, there was more "full length" JPH2 in *mdx* muscle compared to WT samples. This is very interesting, and may imply that the role of calpain cleavage of JPH2 seen in younger *mdx* mice is less prominent in older mice. It could also be indicative of the "steady state" reached in dystrophic mouse models, where the degeneration and regeneration cycles are slower and less destructive than they would be in younger mice.
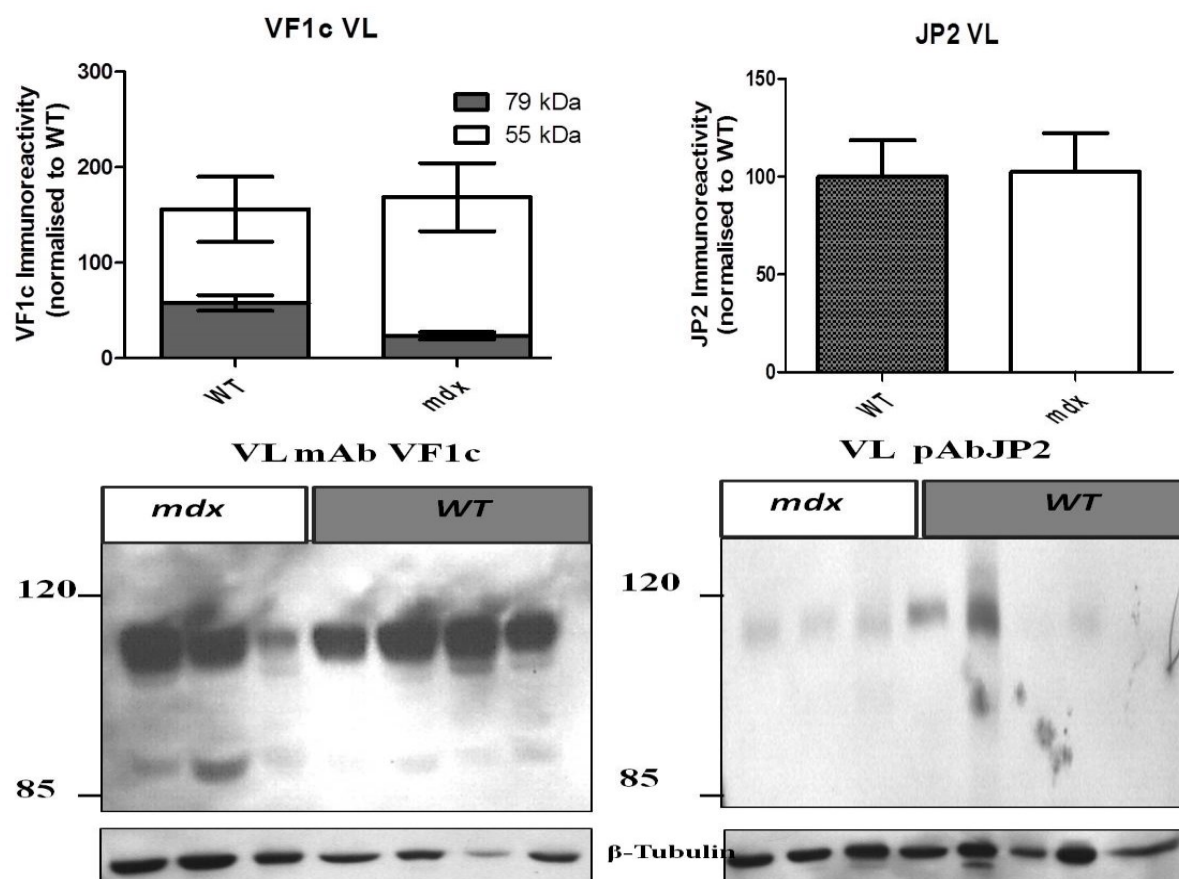
Figure 6.3.a.i: VL muscles of *mdx* and WT type mice (50μg protein per lane) were analysed via western blot for JPH1 and JPH2 expression using mAb VF1c and pAb JP2 antibodies (*mdx* n =3, WT n = 4, normalised to β-Tubulin expression, two technical replicates). No significant differences in either JPH1 or JPH2 abundance were found in *mdx* samples (*mdx* n = 3, WT n = 4, 3 technical replicates).
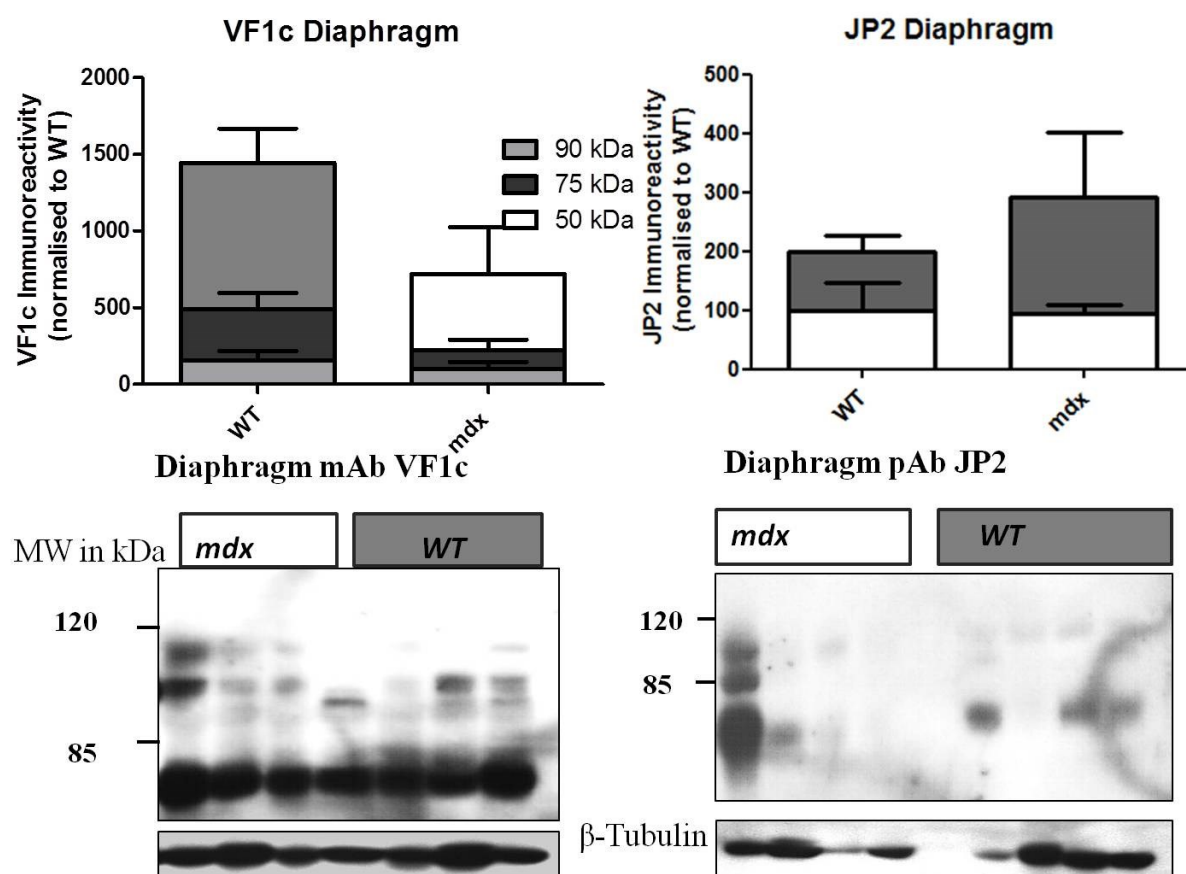
Figure 6.3.a.ii: analysis of JPH1 and JPH2 abundance in WT and *mdx* mouse diaphragm (40 µg of protein per lane). No significant differences were seen in either JPH1 (detected using mAbVF1c) or JPH2 expression in *mdx* diaphragm compared to WT (*mdx* n = 3, WT n = 4, 3 technical replicates).
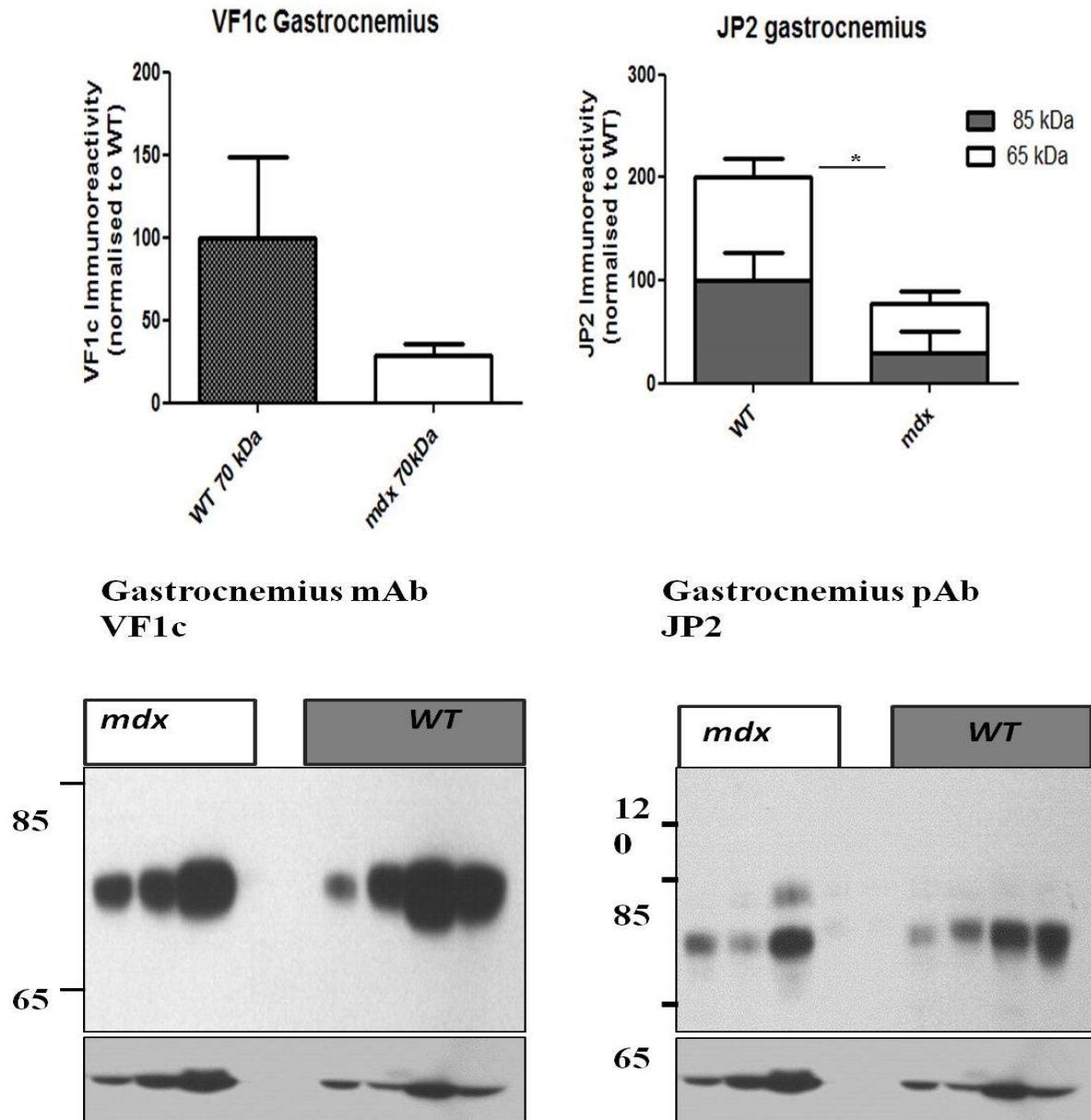
Figure 6.3.a.iii: Analysis of JPH1 and 2 in gastrocnemius muscle of WT and *mdx* mice (50µg of protein per lane). No significant change was observed in JPH1 levels, but there was a significant decrease in 85 kDa JPH2 protein (as detected by pAb JP2) in *mdx* samples compared to WT (p= 0.05) (*mdx* n = 3, WT n = 4, 3 technical replicates).
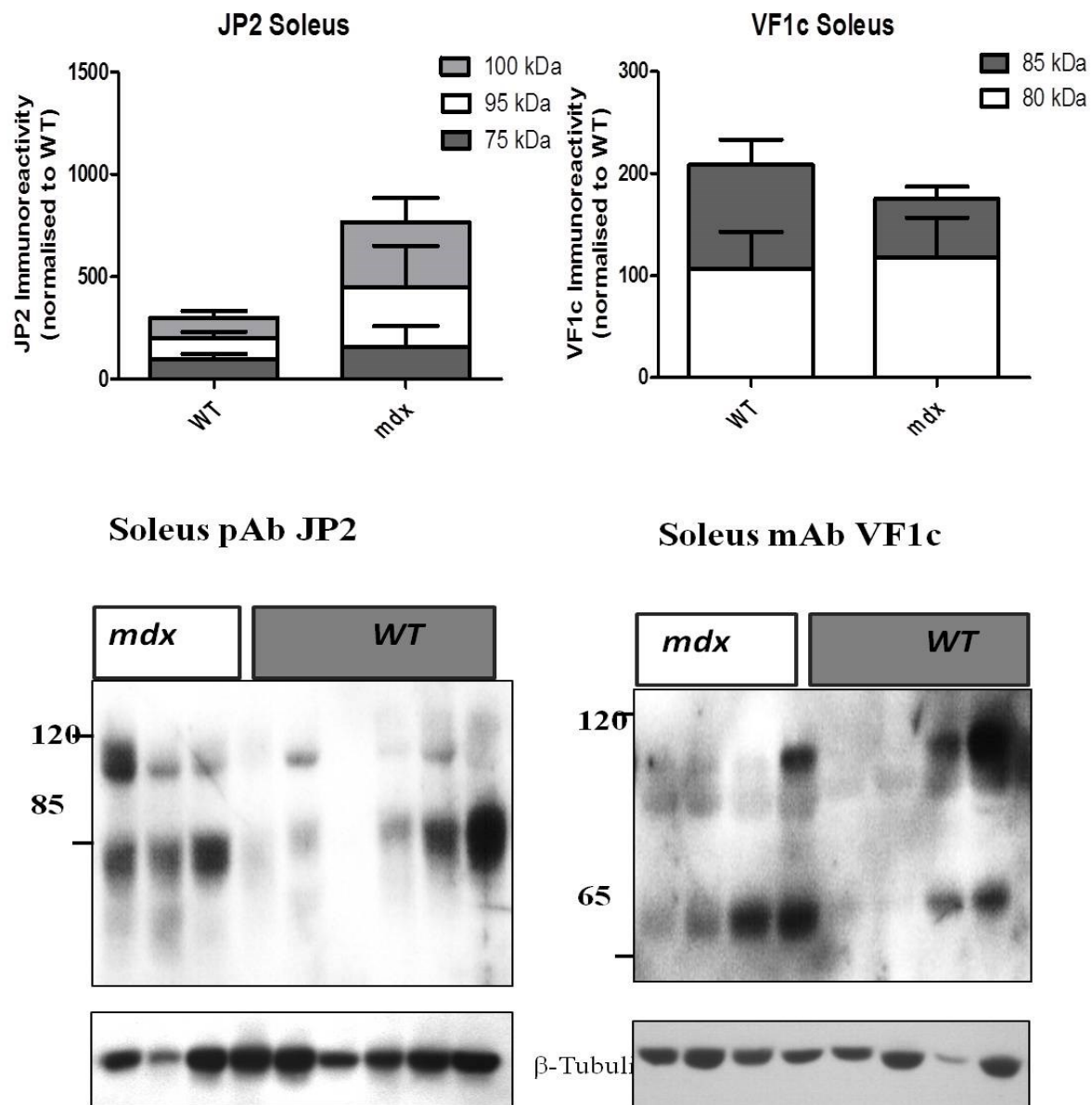
Figure 6.3.a.iv: analysis of JPH1 and 2 expression in *mdx* and WT soleus (30 µg of protein per lane). No significant differences were found between control and *mdx* samples in JPH1 or JPH2.

6.3.b: JPH1 and JPH2 in sarcopenia: effect of exercise.

The effect of sarcopenia on EC coupling proteins has been touched on before, but few studies have looked at JPH expression in aged muscle (Weisleder and Ma, 2007). Thus quadriceps muscle (which contains vastus lateralis muscle) and soleus muscle of four groups of mice were analysed. The mice were housed and maintained for 12 months (adult) or 24 months (aged) in the laboratory of Dr. Brian McDonagh in the University of Liverpool. The McDonagh group used samples of the muscles listed for proteomic analyses, while I performed western blotting of these using the mAb VF1c, pAb JP1 and pAb JP2. The adult and aged groups were further split into exercised versus non-exercised controls, (using an *in vivo* isometric regimen prior to snap freezing) to assess any effect this had on the proteins in question.

In quadriceps muscle, two bands were detected using the mAb VF1c, of 75 and 60 kDa apparent molecular weight, in adult, aged exercised adult and exercised aged muscles. A lower band at 50 kDa was seen in some samples. No difference in JPH1 total protein abundance (measured as cumulative total of bands), however exercised aged quad had signidicantly less total JPH1 than its rested counterpart was found between exercised adult versus adult(p = 0.0004). Figure 6.3.b.i also shows the percentages of JPH1 fragments in the bar chart on the right hand side. It can be seen that 50% more full length (90 kDa apparent MW) protein is found in the un-exercised samples, while those samples subjected to exercise protocol have increased JPH1 cleavage, as shown by detection of JPH1 a the lower molecular weights (adult versus exercised adult, 75kDa p= 0.031: Aged vs exercised aged samples 75

kDa p =0.0001, Students' T-Test, 2 tailed). This hsows that exercised samples underwent significant cleavage of JPH1 protein.

.
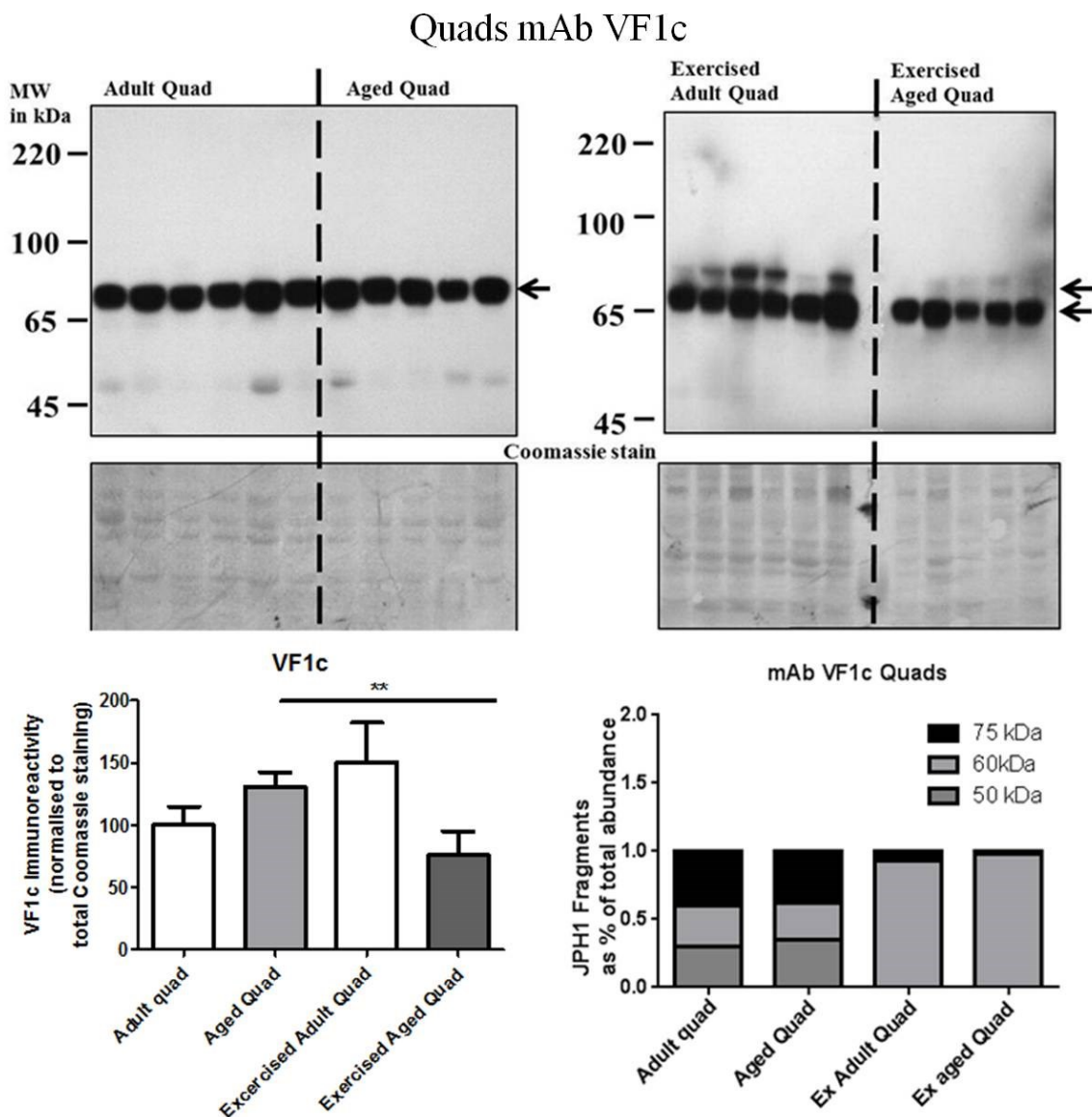
Figure 6.3.b.i: Mouse quadriceps from adult (12 mth) and aged (24 mth) animals (exercised and non-exercised) were homogenised and assayed for JPH1 abundance via

western blot using the mAb VF1c. Exercised adult and aged quadriceps show a shift in molecular weight from 90 kDa in unexercised samples to two bands at 90 and 80 kDa in exercised adult and aged quadriceps. All samples to the right of the dashed lines are adult, while all samples falling on the left hand side of the dashed line are from aged animals. Blots containing exercised samples are on the left hand side (adult samples n = 6, aged samples, n =
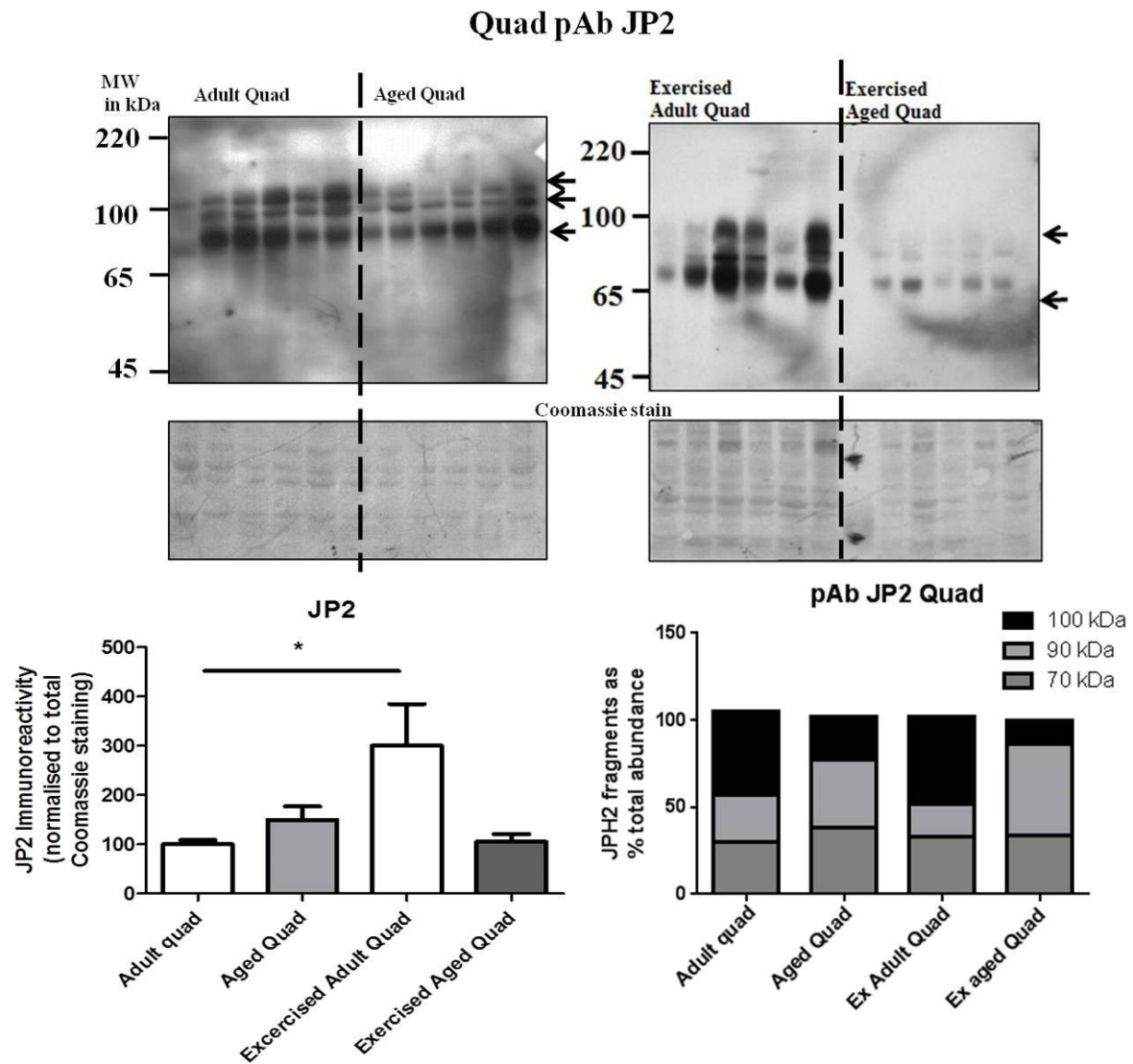
5, 2-3 technical replicates)

Figure 6.3.b.ii: Mouse quadriceps from adult, aged, adult excercised and aged exercised animals subjected to western blot and immunodectection of JPH2 protein using pAb JP2. In all samples JPH2 was detected as three bands, at 100, 90 and 70 kDa. Total abundance of JPH2 protein was significantly increased in exercised adult quad compared to its unexercised controls (p=0.04). Differences can also bee seen in the percentage of cleaved to full length protein. Both aged samples have less full length (100kDa) JPH2 than either adult or exercised adult.

In the quadriceps muscles, proteins of 100, 90 and 70 kDa were detected in the adult and aged tissue (upper panel, demarcated by arrows, figure 6.3.b.ii). Total JPH2 protein abundance was significantly increased in exercised adult compared to adult quadriceps muscle (p = 0.04,* symbol in Figure 6.3.b.ii). Surprisingly, despite a visible decrease in intensity in aged exercised quadriceps compared to unexercised aged controls, this difference was not significant (Figure 6.3.b.ii) when normalised to total protein for the corresponding lanes, highlighting the importance of controls. Looking at the percentage cleavage pattern for this protein, (right hand side of graph) it is clear that unexercised adult samples have higher percantages of full length JPH2 than either of the aged samples (Adult versus aged samples had a p value of 0.034) while it is interesting that a significant increase in JPH2 at 100 kDa was seen in exercised adult compared to its rested counterpart (Adult versus exercised adult: p= 0.031). This implies that exercise might increase or enhance the detection of JPH2 by western blot, perhaps by increasing solubility.

Using pAb JP1, greater abundance of JPH1 protein was detected in adult muscle compared to aged muscle, (p= 0.02). As pAb interacts with the C-terminal region JPH1 protein, it is likely that the bands detected at 75 kDa are "full length" JPH1 (For a comparison

of VF1c and JP1antibodies, please refer to figure 8.3.f). Decreased total abundance was seen in exercised aged samples compared to adult excersied samples, but this was not found to be significant using this antibody.
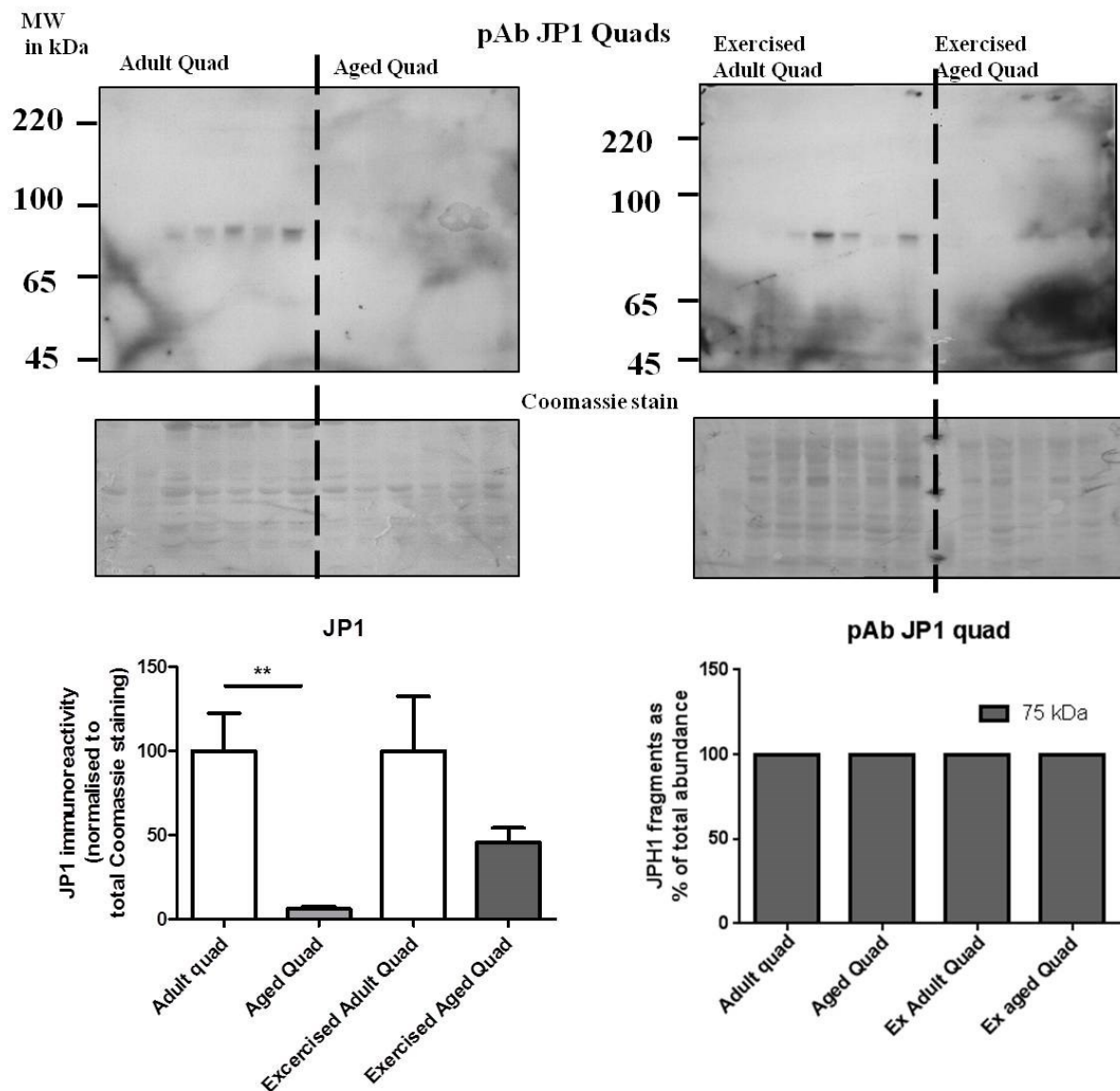
Figure 6.3.b.iii: Adult, aged, exercised adult and exercised aged mouse soleus muscles were analysed for JPH1 total abundance via western blot. Using the mAb VF1c,

total JPH1 abundance was determined in each tissue, normalised to total protein content via Coomassie staining. Aged soleus has significantly increased JPH1 total abundance compared to adult counterparts (Students'T Test, p=0.0) No shift in molecular weight of JPH1 was detected in soleus muscle samples of exercised versus non exercised controls.

In soleus muscles samples, there is no detectable difference in JPH1 abundance as detected by pAb JP1 between aged and adult JPH1 levels, and no significant changes were found when aged exercised samples were compared with adult exercised or adult (unexercised) JPH1abundance levels. However, exercised soleus samples all showed an increase in a probable cleavage event (two bands visible at 90 and 55 kDa) while unexercised soleus muscle displays JPH1 protein at 90 kDa.These comparisons did not reach significance however. A diagram of cleavage can be seen in figure 8.3.f.

In the soleus, pAb JP2 detects proteins at 100, 75 and 60 kDa, which are lower molecular weights than those found in quad muscles, although comparisons using Students' T-tests show that these differences in apparent molecular weight are non-significant. A significant decrease in JPH2 abundance was found in aged samples compared to adult samples (p=0.050, Students' T-Test). No other significant differences in abundance were found, however some interesting changes in molecular weight are visible. There is increased 100 kDa JPH2 detected in exercised adult samples compared to rested adult samples (p=0.035), implying a direct effect of exercise. Aged soleus samples displayed the lowest amount of full length JPH2.

In the soleus muscles, the mAb VF1c detects a doublet with a molecular weight of 65 kDa, as compared with molecular weight markers (Figure 6.3.b.iv). A significant increase in total

JPH1 protein is found in aged soleus compared to adult samples (p= 0.02, Students' unpaired T-test), and this is paralleled by a similar but non-significant increase in JPH1 abundance in exercised aged soleus compared to exercised adult. This echoes the increase in total abundance detected in aged quad samples versus adult controls, and shows that a global increase in JPH1 abundance is occurring in limb muscles with aging. Cross-comparison of muscles found that aged soleus has significantly higher amounts of JPH1 protein than aged quad, when normalised to total protein staining (p= 0.04). This could be indicative of a compensatory mechanism in slow, gravity bearing muscles.
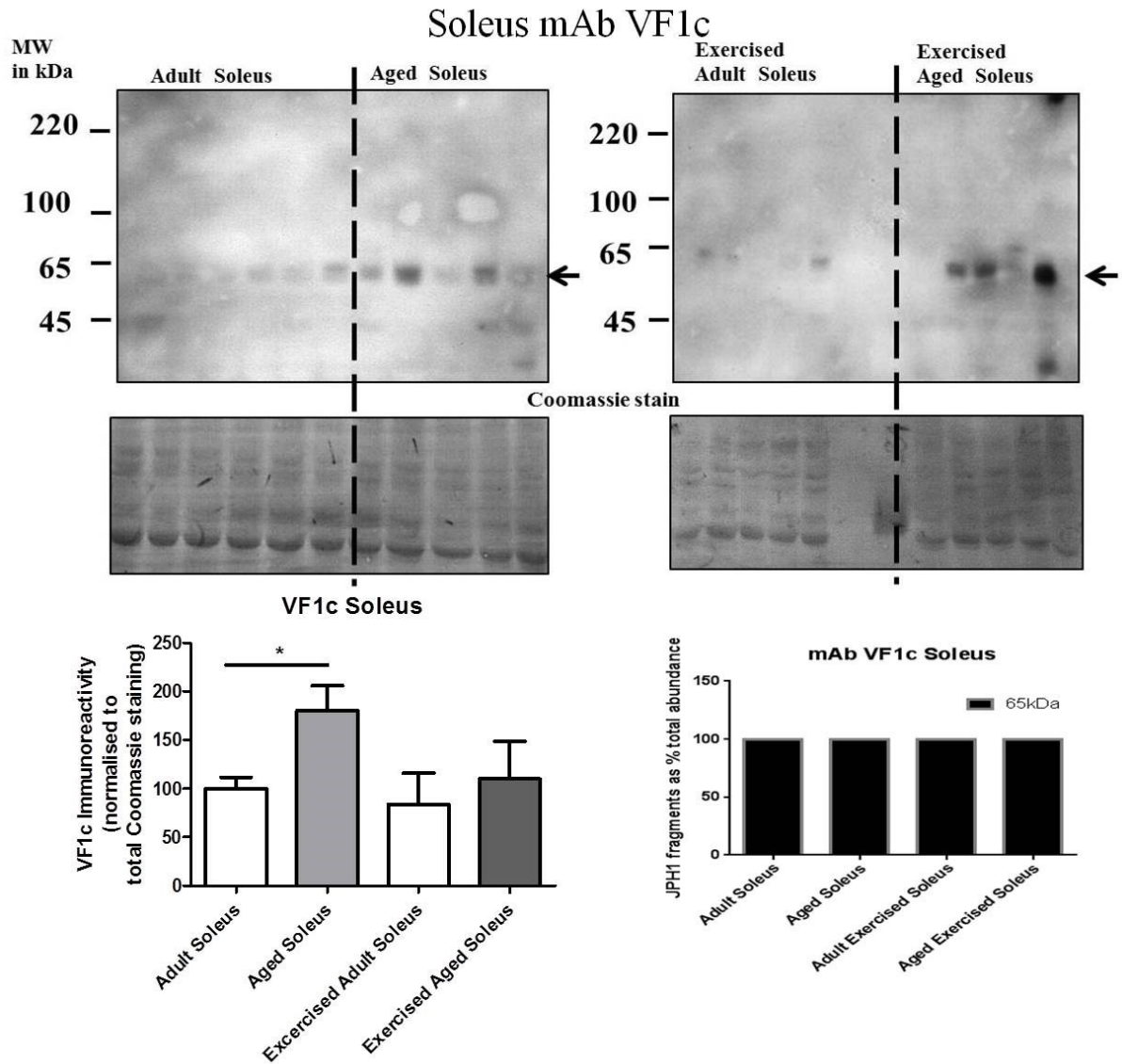
Figure 6.3.b.iv: Soleus from adult, aged, adult exercised and aged exercised samples were analysed for JPH1 protein content using the VF1c mAb. One main band(has doublet appearance in some samples) is detected in all samples at 65 kDa. The total abundance of this protein was compared among the smples tested, and aged soleus had higher amount of total JPH1 abundance (p=0.02)
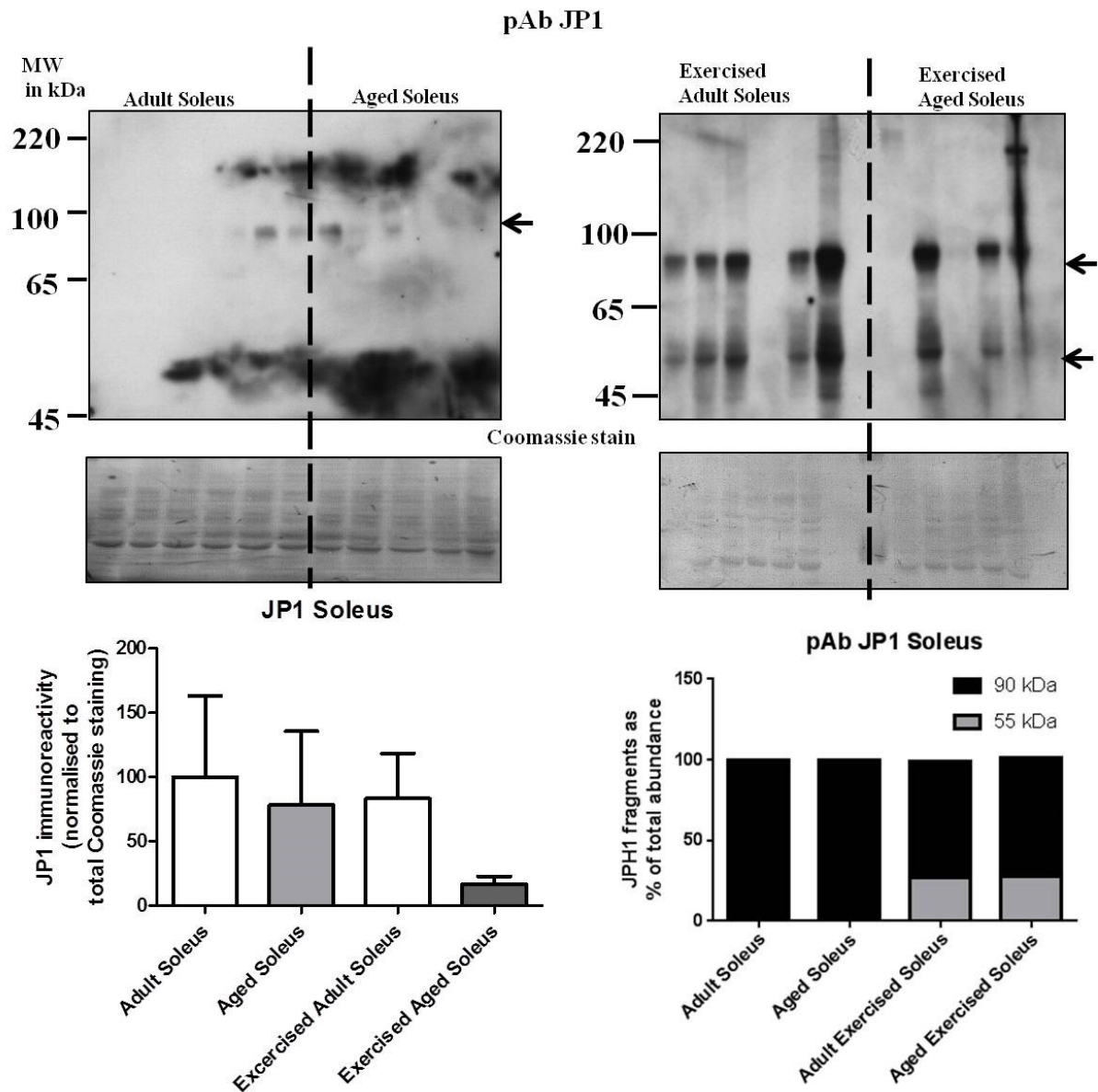
Figure 6.3.b. iv: Soleus muscle from Adult, aged, adult exerdcised and aged exercised animals subjected to western blotting and immunodetection using pAb JP1. The pAb JP1 antibody detected only one band, at 65 kDa (n=5 and 6 for each group, 2 technical replicates, compared using Students T-test). Increased protein cleavage was seen in exercised samples compared to rested controls.
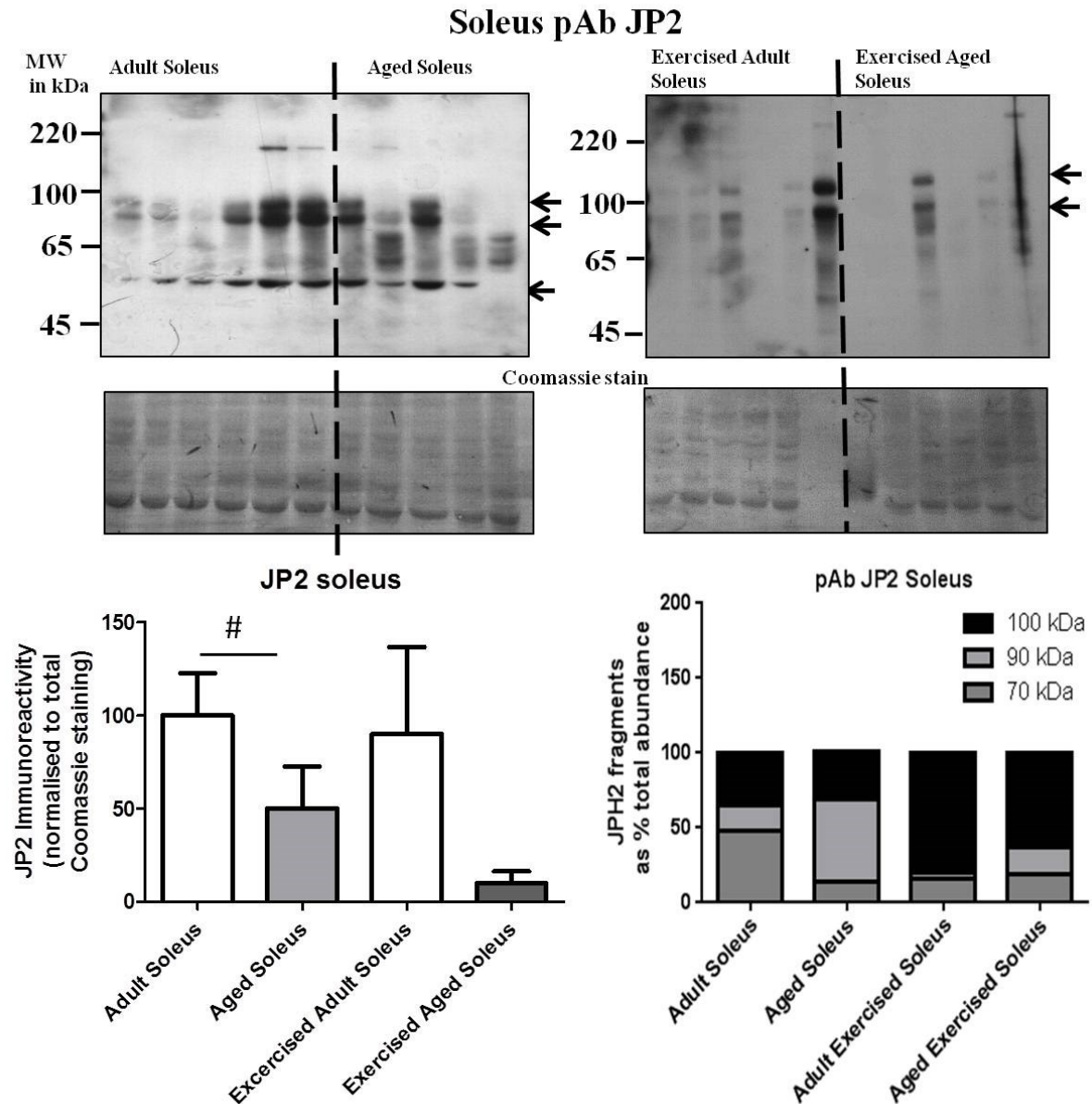
Figure 6.1.3.b.vi: Soleus muscles from adult, aged, adult exercised and aged exercised mice were analysed for JPH2 expression via Western blot. Aged soleus had less abundant JPH2 than adult soleus muscle, (#, $p < 0.05$) while the highest amount of 100kDa JPH2 (full; length) was found in adult exercised soleus. Aged soleus had the lowest amount of full length JPH2. There is a significant increase in 90kDa JPH2 in exercised versus adult muscle ($p = 0.035$, Students' T Test)

6.3.c: JPH1 and 2 expression in the 2 week CIH rat

Male Wistar rats underwent two weeks of chronic intermittent hypoxia (CIH) or sham treatment as described in section 3.2 and by Shortt *et al* (Shortt *et al,* 2013). Extensor digitorum longus (EDL) and soleus muscles were analysed for JPH1 and 2abundance. In EDL muscle, CIH animals display an apparent decrease in JPH1 protein levels (detected using VF1c and JP1 antibodies) compared to Sham treated controls, but this was not significantly different (Student's T-test, p= 0.4528 and 0.1259 for CIH vs Sham animals in mAb VF1c and pAb JP1 immunoreactivity respectively, normalised to total protein via Coomassie staining, Figure 6.3.c.i and Fig 6.3.c.ii). In both pAb JP1 and mAb VF1c blots, bands were detected at 70 kDa, reconfirming that the mAb VF1c interacts with the JPH1 protein. No difference was found in molecular weight of JPH1 between CIH and sham animals. In EDL muscle, JPH2 protein was detected as two bands with apparent molecular weights of 95 and 76 kDa. Despite an apparent decrease in protein levels of both 90 and 76 kDa bands in CIH treated animals compared to controls, this difference was also non-significant (p= 0.2789 and 0.1258, for CIH vs Sham 90 and 70 kDa respectively, Student's T-test) (Figure 6.3.c.ii).

In the soleus muscle, JP1 and VF1c antibodies both detected bands at 73 kDa. When comparing CIH and Sham treated samples, an increase was again seen in Sham tissue but this did not reach statistical significance (p= 0.6154 (mAb VF1c) and p = 0.8033 (JP1 antibody)). In the case of JPH2 abundance (Figure 6.3.c.iii.), two bands were again detected, this time at 100 and 76 kDa, a slightly higher molecular weight than that seen with JPH2 in EDL muscle.

No changes were seen in abundance for either band when CIH and Sham muscles were compared (p= 0.6371 and 0.2208 for 100 and 76 kDa bands respectively).

When comparing the JPH1 expression of EDL to soleus muscles with and without CIH treatment, both muscle types showed similar levels of JPH1 protein, both of which were non-significantly decreased compared to their Sham counterparts. In contrast, full length JPH2 displayed a downward trend in CIH treated EDL compared to IH treated soleus but this was just below the threshold for significance (p = 0.054). However, when comparing levels of 76 kDa JPH2 in CIH EDL and soleus muscle, soleus muscle showed a significant increase compared to EDL (p = 0.01), (Figure 6.3.c.iii). No differences were found between Sham and CIH EDL and soleus at either molecular weight.
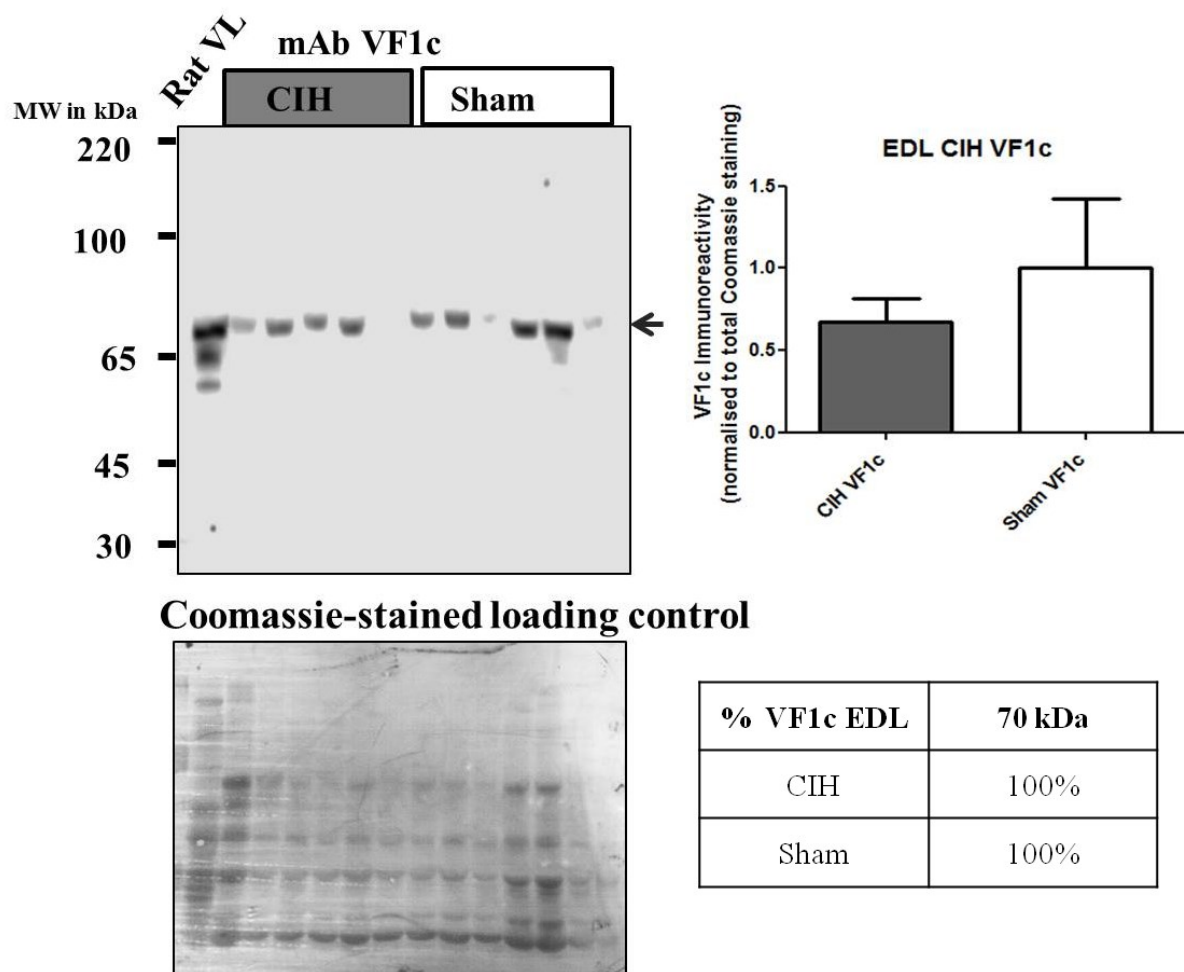
Figure 6.3.c.i: CIH and sham rat EDL muscle analysed using mAb VF1c (30μg/well). Although variation existed between the sham and CIH group, this difference was not significant. The bands detected match closely with those detected using pAb JP1, confirming the interaction of mAb VF1c with this protein.

EDL pAb JP2

% EDL JPH2	95 kDa	76 kDa
IH	58%	42%
Sham	46%	54%
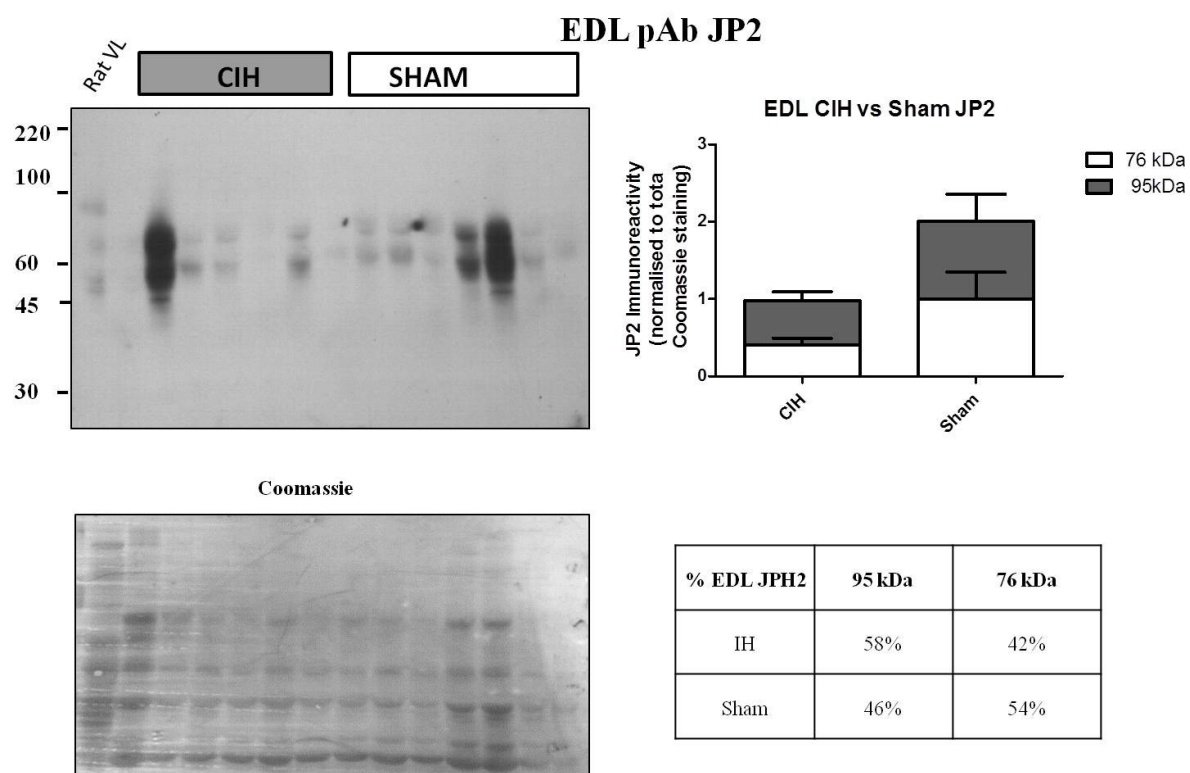
Figure 6.3.c.i: EDL muscle from Sham and CIH treated rat was analysed for JPH1 and JPH2 expression (30μg protein per lane). mAb VF1c and pAb JP1 antibodies both detect a band at 70 kDa, and despite a trend towards increased JPH1 in tissue from sham-treated rats, this was non-significant. Similar results are seen in JP2 blots, where two bands at 95 and 76 kDa were detected.
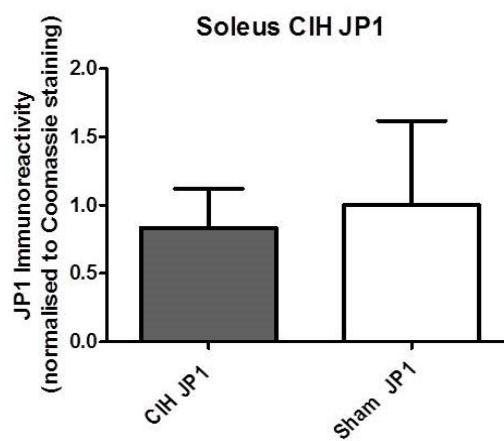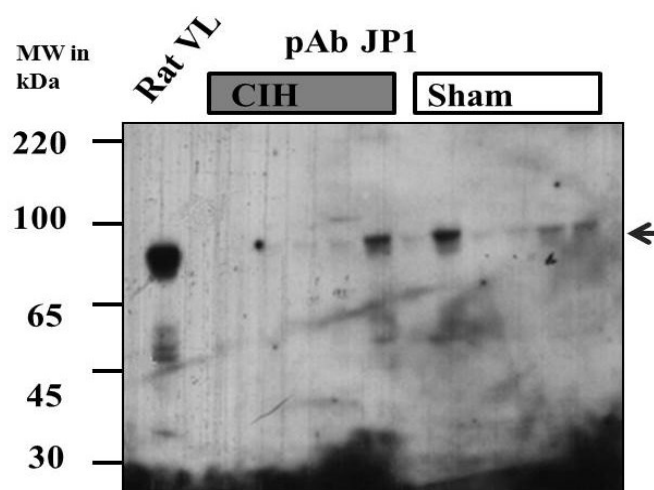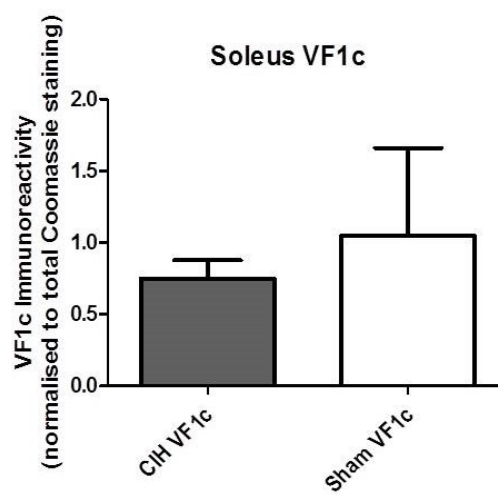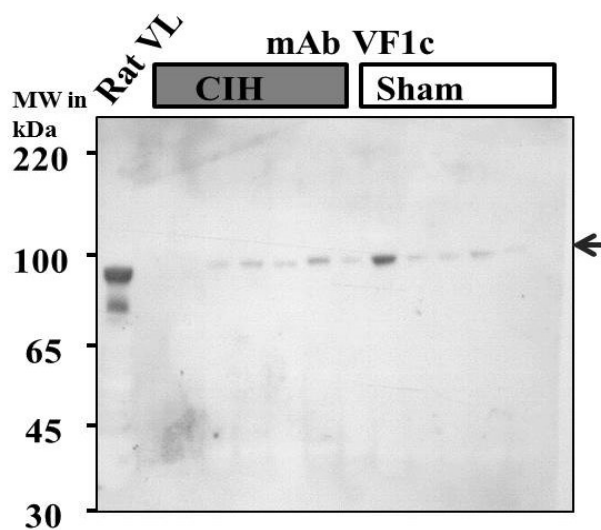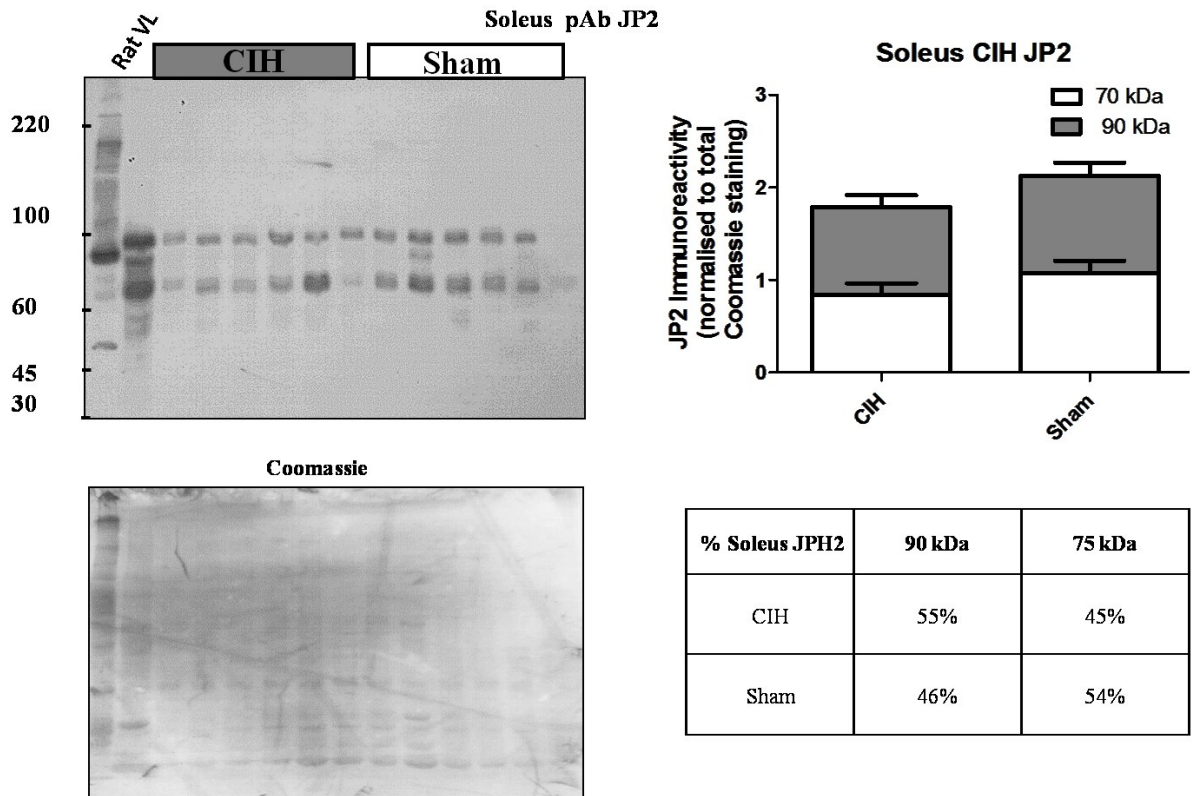
Figure 6.3.c.ii: Sham and CIH treated rat soleus were analysed via western blot for JPH1 and JPH2 expression (30µg protein/lane). In soleus, one band was detected in both JP1 and VF1c blots at 70 kDa, while in JP2 exposed blots, two bands were detected at 100 kDa and 76 kDa, slightly higher than those found in EDL. No significant changes were found in either JPH1 or JPH2 when Sham treated animals were compared to CIH samples.
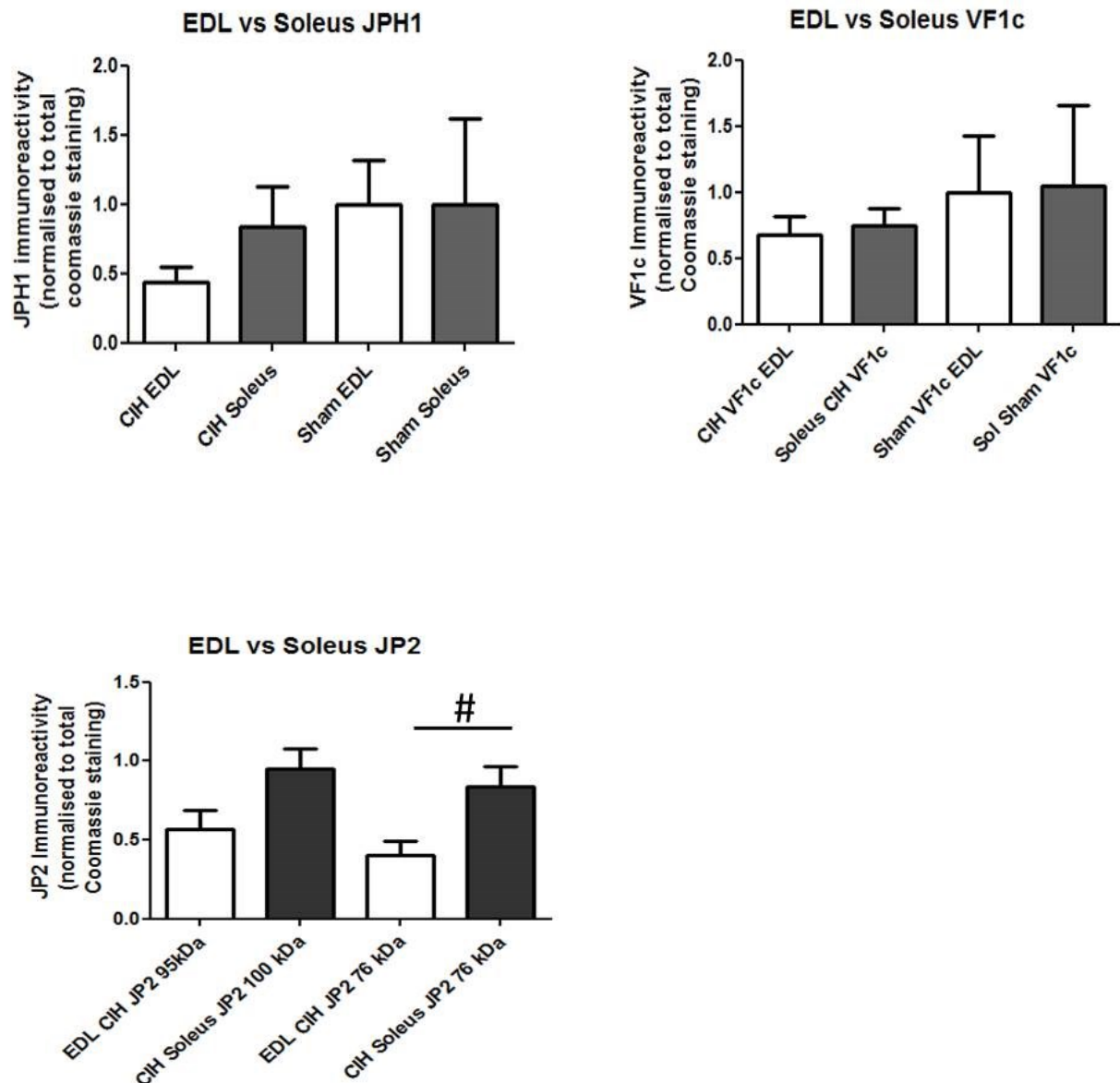
Figure 6.3.c.iii: Graphs showing comparison of JPH1 (mAb VF1c and pAb JP1) and JPH2 (pAb JP2) abundance in EDL and soleus muscle from CIH and Sham–treated rats (30μg protein/lane). A significant increase in 76 kDa JPH2 protein is observed in CIH treated soleus compared to EDL muscle (p>0.05, #). No differences were seen in JPH1 abundance when CIH and sham EDL and soleus were compared.

6.4: Discussion

6.4.a: JPH1 and JPH2 abundance in *mdx* and WT mouse muscle.

Although no significant changes in JPH1 or JPH2 were seen in VL, soleus or diaphragm at 8 months of age, JPH2 protein levels were significantly decreased in *mdx* gastrocnemius compared to WT controls. This could be because of the increased psuedohypertrophy and necrotic tissue found in what is a comparatively large muscle, or perhaps another facet of the disease. Such inputs could include increased reactive oxygen species generation influencing JPH2 synthesis or dysregulated Ca^{2+} causing this decrease. Either way, it is interesting that while JPH2 is affected, uncleaved JPH1 levels are unchanged at this age, and further highlights the muscle specific regulation of each JPH protein. Taken together the results of this study show non-significant changes in diaphragm, VL and soleus, which is surprising as diaphragm is often the worst affected muscle in this disease (respiratory failure is very often a cause of death in DMD patients), as well as in this model. The decreased JPH2 expression in gastrocnemius muscle could be related to increased store operated Ca^{2+} entry, found to be elevated in *mdx* fibres, perhaps as a compensatory mechanism for leaky SR (Wang *et al,* 2005). As JPH2 has been suggested to interact in some way with the SR Ca $^{2+}$ sensor STIM1 and its associated store operated channel, Orai it is plausible that an increase in Ca^{2+} entry could affect either cleavage or expression of JPH2 (Woo *et al,* 2012). These results are in contrast to previous studies by Murphy *et al* (2013), who found that increased JPH2 expression in TA muscles of 2.5 month old *mdx* mice. They

also noted that increased proteolysis of both JPH1 and JPH2 (from 90 to 75 kDa) were found in *mdx* muscles compared to WT controls, with markedly increased proteolytic cleavage of JPH1 in 7 month old diaphragm compared to WT, but unfortunately do not comment on abundance of total protein of either JPH1 or JPH2 in this tissue. The amounts of proteolytic cleavage of JPH1 and 2 were also analysed in these studies, and no significant differences in proteolytic cleavage were found (as measured by Students' T-Test). It may be possible that by 8 months of age in the *mdx* mouse, a steady state of JPH expression has been reached, and that disease pathology is not as marked as it would be in their human counterparts, who display necrosis and psuedohypertrophy (infiltration of fibrotic, non-contractile tissue in to muscle) in the lower limb muscles before others are affected. A temporal gene expression analysis of *mdx* mouse muscle tissue from animals ranging from 2 weeks to 1 year in age found that in the diaphragm, but not in hindlimb muscle, RyR1 levels were altered compared to control mice, and that the *mdx* mouse had different alterations in comparison to biopsies from DMD patients (Rouger *et al,* 2002). Carberry *et al* noted that in proteomic analysis of muscles from *mdx* mice that different proteins (such as parvalbumin, a calcium binding protein in the cytosol of fast muscles which was increased in flexor digitorum brevis (FDB) and interosseus muscles but not in EDL or soleus) are differentially regulated, which further corroborates the hypothesis that different muscles regulate their protein content and modification based on activity and disease progression (Carberry *et al,* 2013).

It should be noted that the *mdx* mouse is not a perfect model of Duchenne muscular dystrophy, as the mice live longer and are protected in part by a natural overexpression of a compensatory protein, utrophin. It has been suggested by Capote *et al* that knock-out of the

utrophin protein in the *mdx* model generates a more faithful representation of the human disease.(Larcher *et al,* 2014, Capote *et al,* 2010), or the use of Transcription-Activator Like Effector Nucleases (TALEN) generated *mdx* rats could provide a better model for this disease.

6.4.b: JPH1 and 2 in exercised and unexercised adult and aged mice

As shown in section 6.1.3.a, JPH1 protein is increased in aged soleus muscle but not in quadriceps muscle in aged compared to adult controls. It is possible that this increase is a compensatory response to EC uncoupling, a documented process in aged skeletal muscle, or as a regulatory response to hypernitrosylated and leaky RyRs found in aged skeletal muscle (Boncompagani *et al,* 2006; Andersson *et al,* 2011). Increased JPH1 is also likely tied to the described decrease in DHPR α1S subunits in aged muscle. As this subunit of DHPR is known to interact with both JPH1 and JPH2, compensatory efforts to overcome DHPR decrease via JPH1 upregulation are plausible (O'Connell *et al,* 2008; Golini *et al,* 2011). Other EC coupling proteins including RyR1 and interestingly, RyR2 are altered in aged skeletal muscle. Gheorge *et al* (2014) performed proteomic analysis of aged and adult human muscle, and found that Ca^{2+} homoestasis and lipid metabolism protein expression levels were altered before those involved in mitochondria and apoptosis signalling, which may imply that Ca^{2+} homeostasis dysregulation occurs before ROS-mediated perturbations, and may explain why progressive aging and defective ROS signalling lead to leaky RyR1 channels in aged skeletal muscle. They also found that RyR2 and JPH2 were upregulated in aged VL muscles compared to adult controls. Increased expression of RyR1 was also found in the gastrocnemius muscles of aged mice compared to adult controls. This implies that the

alteration seen in Ca^{2+} levels in aged tissue may represent a larger reliance on calcium induced calcium release, which given the decreased L-type calcium current influx (due to decreased DHPR subunit expression) makes sense. It may also explain why JPH levels have to change in ageing muscle, as a shift from RyR1 to RyR2 expression in aged tissue would necessitate the concomitant increase or decrease in regulatory proteins (Gheorghe *et al,* 2014; Hwang *et al,* 2013). This indicates that exercise may have a solubilising effect on the muscle, perhaps allowing increased release of JPH1 from membranes and thus increasing detection of said protein. Detection using the pAb JP1 was very difficult, and persistant background may have obscured some results using this antibody, similar to that seen in A7r5 experiments.

The change in JPH2 levels could be due to alterations in PM-ER interaction sites, and implies that JPH1 and JPH2 are separately regulated within muscle types, or could be linked to RyR isoform expression in this muscle. A three-fold increase in JPH2 in exercised versus unexercised adult quad muscle along with the shift in molecular weight could imply that strenuous exercise might have a solubilising effect on JPH2, thus making the protein more detectable by freeing it from the SR membrane. This is akin to what occurs after exercise in JPH1 protein, as suggested by Murphy *et al* (2013) , who stated that after exercise JPH1 was cleaved by calpains into a 75 kDa soluble fraction and a 15 kDa C-terminal segment which stays embedded in the SR membrane (Murphy *et al,* 2013). After bouts of exercise, and in some aged samples both JPH1 and JPH2 exhibited altered molecular weights, indicating that increased calpain cleavage (or cleavage by another proteolytic enzyme) of these proteins could indeed be a factor in aging. This is prominent in JPH2 molecular weights seen in soleus, where adult muscle which was subjected to the exercise protocol had significantly

increased cleavage of JPH2 (p=0.035) compared to its rested counterpart. This corroborates previous studies where increased cleavage of JPH2 was found in skeletal muscle after exercise. Alterations in proteolytic activity and calpain cleavage activity have been shown to occur in aged muscle samples and to display fibre type specificity (Dargelos *et al*, 2007). A comparison of 3, 6, 30 and 36 month old rat EDL and soleus muscle found that caspase cleavage increased dramatically in aged soleus compared to younger counterparts, but that this did not occur to the same extent in EDL muscle (Rice and Blough, 2006). Brule and Dargelos (2010) also found that RyR1 cleavage by calpains (μ- and m subtypes) was significantly increased in aged rat muscle, and likely contributed to Ca^{2+} handling irregularities therein (Brule and Dargelos, 2010). Taken together, the results described in Section 6.1.3.b imply that JPHs are differentially regulated in aging and after exercise, and are likely effected by the altered intracellular calcium levels, increased proteolytic activity and changes in EC coupling protein expression which occur in aging. Further analysis will have to be performed to fully elucidate the exact effects up or down regulation (as well as the change in molecular weight) of JPHs have in aged and exercised muscle.

6.4.c: JPH1 and JPH2 in CIH and sham treated rat EDL and Soleus Muscles

As a foundation for the study of EC coupling protein in a model of intermittent hypoxia, these results provide some interesting results; namely that JPH1 is not changed in rat EDL or soleus muscles after two weeks of CIH treatment compared to sham controls. JPH2 is unchanged in EDL and soleus compared to SHAM muscles, however 76 kDa JPH2

protein is more abundant in CIH treated soleus compared to EDL muscle. This is very interesting, as it is vastly different from previous results in other animal models which show that soleus typically has a decreased amount of both JPH1 and JPH2 compared to EDL muscle, although soleus muscle do tend to show higher rates of suspected JPH proteolytic cleavage (see Chapter 5). Perhaps this slight increase may make the muscle more efficient, or perhaps it is indicative of increased calcium ion dysregulation. Intermittent hypoxia training is utilised by athletes to improve performance, (a "Live high, train low" hypothesis) but several studies have questioned its efficacy (Katayama *et al*, 2003). Vogt *et al* (2001) found altered levels of VEGF, HIF1α and myoglobin mRNA in muscle biopsies of endurance athletes trained at simulated hypoxia compared to normoxic controls. However Nordsborg *et al* (2012) and Siebenmann *et al* (2012) found no difference in endurance performance or VO_2 max in hypoxic-trained endurance cyclists compared to normoxic controls. So far, little work has been performed on EC coupling proteins in hypoxia treated skeletal muscle, although some work on cardiac muscle has shown increased activity and expression of RyR2, CASQ2 and SERCA2 in rat hearts after two weeks of CIH exposure facilitating an improvement in Ca^{2+} handling (Li *et al*, 2009). In isolated cardiomyocytes from neonatal rats, four days of CIH caused an increase in Ca^{2+} extrusion from the cell and a small increase in ROS generation along with an increase in SERCA2 and RyR2 expression and activity (Chen *et al*, 2014). This implies that CIH can cause changes to both Ca^{2+} handling and EC coupling protein level, and this deserves to be investigated further in skeletal muscle. Sun *et al* (2013) also found that pO_2 levels of skeletal muscle were linked to RyR1 S-nitrosylation, where low pO_2 levels were shown to correspond to lower levels of cysteine oxidation on the RyR1 monomers. An increase in S-oxidation (at higher pO_2 levels) of RyR1 was also found to

increase RyR1 activity (Sun *et al,* 2013). Hence, Ca^{2+} release via RyR1 in skeletal muscle can be shaped by the pO_2 concentration, and implies that hypoxia may have an effect on EC coupling proteins via post translational modification, expression changes and alterations in activity levels. It is likely that an increase in the exposure time of CIH or the analysis of other muscles could provide more data on the subject of JPH regulation in CIH treatment.

It is interesting that in CIH tissue and *mdx* muscle (both of which are reported to undergo increased ROS activity) both showed non-significant changes in JPH1 expression, even though it is known that oxidation status can affect the interaction of RyR1 with JPH1 (Phimister *et al,* 2010). This contrasts with aged muscle, where increased ROS activity are cited as a pathological pathway in sarcopenia, and implies that perhaps that cumulative effects of calcium dysregulation combined with overactive ROS lead to a sharper change in regulation of JPHs, and that these events could occur at different times or feed into the worsening of disease (Gheorghe *et al* 2014).

6.5: Future studies

It would be beneficial to include intercostal muscle into further analysis of EC proteins in further analysis of DMD/*mdx* model muscle samples as DMD causes kyphoscoliosis (an abnormal curve of the spine), in part due to intercostals muscle weakness. As it is known that these muscles have specialized Ca^{2+} handling mechanisms it is likely that JPHs or RyRs could be altered. Further analysis could include the use of different *mdx*

models such as the *mdx* rat, which is reported to be more in-keeping with the human form of the disease (Larcher *et al,* 2014). It would also be relevant to analyse the effects of DMD on cardiac muscle JPH2 and RyR2 levels, as cardiomyopathy is a significant pathology in this disease and there is evidence of enhanced post-translational modifications of RyR2 in DMD models (Kyrychenko *et al,* 2013)

Further analysis of EC coupling proteins in CIH models is required to fully elucidate the effect this treatment has on protein levels, activities and post-translational modifications. This would require the use of a standardized model of CIH, as many different lab groups use different levels and timeframes of hypoxia treatment. The effect of exercise training under CIH conditions on skeletal muscle should also be clarified, perhaps with a large scale proteomics based study to identify any proteins which are differentially expressed to those normally found in trained muscle. It is also possible that as shown in the differing levels of the 76 kDa fragment of JPH2 in EDL and soleus muscles in response to IH, muscle specific responses to hypoxia could be worth studying, as it may explain some deleterious effects seen in obstructive sleep apnoea and COPD patients.

In sarcopenia research, investigations into the field of EC coupling proteins could be expanded by characterising the effect of increased JPH1 in the soleus of aged muscles and clarifying whether this is a compensatory response or an effect of the disease. This could be accomplished via single fibre studies of aged versus adult studies combined with Ca^{2+} imaging studies to assess any effect this upregulation has on RyR gating. Comparison of effects across muscle fibre types would be useful here also. Another method would be to use

inducible knock-out of JPH1 or JPH2 in aged animals (such as that demonstrated by Hirata et al, 2006) which could be very interesting. Further analysis of the postulated JPH cleavage after exercise could be performed in two ways; using a muscle cell line or isolated myocytes and either using molecular techniques to delete potential proteolytic cleavage sites within junctophilins, thereby inhibiting calpain mediated cleavage and assessing the effect on RyR gating and Ca^{2+} homeostasis; or by incubating cells under contraction-inducing conditions with and without specific calpain inhibitors. Either way, although some work has shown that JPHs are cleaved by calpains in muscle cells after contractions (Corona *et al,* 2010; Murphy *et al*, 2013) there is plenty of scope for further analysis.

Chapter 7: Discussion

7.1: Introduction

The results outlined in chapters 4, 5 and 6 together illustrate interesting aspects of SR channel function, especially in regard to type 1 ryanodine receptors. Over all, a potential novel interaction between RyR1 and GRB2 has been found in rat muscle using pull-down of the RyR complex followed by western blotting. It has also been confirmed that mAb VF1c, originally generated against the junctional sarcoplasmic reticulum protein of 90 kDa, actually interacts with the junctophilin 1 protein. JPH1 has been shown to be differentially regulated in different skeletal muscles, and to be expressed (although as a minor subtype) in smooth muscle. Characterisation of JPH1 and JPH2 expression in disease models has shown increased abundance of JPH1 in aged soleus, but not quadriceps of male mice, and that exercise has an effect on the molecular weight of the protein (as determined by SDS-PAGE). It was also found that there are no differences in abundance of JPH1 or JPH2 in limb muscles from 8 month *mdx* versus wild type mice, with the exception of decreased levels of an 85kDa form of the JPH2 protein in *mdx* GC muscle. No difference was seen in rats which underwent 2 weeks of chronic intermittent hypoxia. The implications of these results will be discussed below.

7.2: GRB2-RyR1 interaction

In chapter 4, it was found that peptide analogs of the proline rich region are difficult to use experimentally, but that the proline rich region of RyR1 may interact with the GRB2 adapter protein. As this protein is especially important in cell signalling, specifically via the MAP-kinase pathway, an interaction with RyR1 could give badly needed clues as to its regulation or wider effects on muscle cells, as have been seen in hippocampal neurons (Aronson *et al,* 1997; Huddleston *et al,* 2008).

It is important to note that much further work remains to be done to characterise this interaction. It must be clarified whether or not this protein interacts with ion channels related to RyR1, such as RyR2 or RyR3, or even InsP$_3$ Receptors. This could give clues as to the function and site of this interaction.

The GRB2-RyR1 interaction must be validated: the use of molecular and genomic strategies, such as CRISPR/CAS-9 or other molecular tool could be used to mutate the proline rich region of RyR1, or indeed one of the SH3 domains located on GRB2, to determine the effect this would have on this interaction. This could also allow for functional work, to determine what effect inhibiting this interaction would have on the health of the cell, Ca^{2+} release and abundance of SR related proteins.

Postulated functions for the GRB2-RyR1 interaction include a myriad of possibilities. GRB2 is a linker protein, and is likely facilitating the interaction of RyR1 with other proteins, probably proteins close to the cell membrane or in the cytosol, due to the location of the

candidate binding site. It is possible that the interaction of GRB2 and RyR1 is linking a protein already known to interact with RyR1, but the interaction domain is unclear. However, it is also possible that GRB2 is bringing regulatory effectors to the surface of RyR1, and that these interactions could be fleeting, such as that seen between Bin 1 and actin and myosin in sarcomere assembly (Fernando *et al,* 2009). Various cellular conditions such as alterations in pH or nearby ionic composition which could encourage such an interaction could be analysed to see if they promote or hinder the GRB2-RyR1 interaction, and for this a human muscle-derived cell line that expresses both proteins would be advantageous. It also remains to be seen whether GRB2 interacts with RyR1 (or the RyR1 associated complex) in other cell and muscle types. The experiments outlined in chapter 4 were performed using mixed muscle from rat hindlimb, which contains muscles with a high proportion of type II (fast) fibres (Kohn and Myburgh, 2007). This interaction could very well be specific to conditions favoured in fast type muscles (such as gene regulation etc), and this could be checked by performing pull down experiments using fast and slow muscles (e.g. EDL and Soleus) or indeed cell lines from the respective muscle types, although these would have to be from the same species. It could also be confirmed that this interaction occurs in human muscle using easily accessible VL biopsies, or banked tissue and co-localization and immunoprecipitation studies. A caveat here is that reliable antibodies which detect RyR1 consistently and sensitively are a necessity.

It is interesting that the interaction of RyR1 with PLCγ1 and PTN were not confirmed in this instance, and highlights the need to experimentally validate *in silico* data. However it would be ideal to validate such interactions under a wider range of conditions, to

fully test whether these proteins do in fact interact under certain circumstances these experiments could be improved by chemically cross-linking proteins pulled out of solution in complex with RyR, thus preserving and aiding visualisation of any such interaction, or by examining the RyR complex and its putative interactions under a wider range of conditions, such as altered ionic strength, high and low Ca^{2+} concentration, or under varying pH conditions, all of which could contribute to the interactions of proteins with this complex. It is necessary to study putative interactions of the RyR channel under open and closed conditions, as suggested by Phimister *et al*, who noted that JP1 is more likely to interact with RyR1 when it is in the open conformation (Phimister *et al.*, 2007).

The interaction of GRB2 with RyR1 protein complex provides very interesting avenue for research, and scope for the role of RyR1 in signalling events other than Ca^{2+} release. Indeed, purely because of its size, the RyR1 complex may indeed act as massive hubs for protein interactions that may or may not be related to the function of the protein, and is reported to have other roles such as glutathione transport (Banhegyi *et al*, 2003). Due to the many roles of GRB2 in signalling pathways (e.g. insulin receptor signalling, fibroblast growth receptor signalling, activation of the MAP kinase pathway etc), this is a possibility, although unlikely. It would be tempting to speculate that the GRB2-RyR1 complex interaction could be involved in the insulin receptor pathway, which might facilitate easy coordination of insulin-based signalling and RyR1 (and therefore muscle contraction) activity. It is also entirely possible that the GRB2 protein is not the only SH3-domain containing adapter protein to potentially interact with the proline rich region of RyR1, and it

is also feasible that GRB2 could form dimers to block activity, as seen with the fibroblast growth factor receptor (Lin *et al,* 2012).

Altogether, the interaction of GRB2 with the RyR1 complex opens up a new avenue for RyR research, and demonstrates that a huge amount of work remains to be done on RyR interaction partners and their roles in calcium signalling. It may also provide clues as to the role of RyRs in non-muscle tissue.

7.3: Characterisation of mAb VF1c.

Chapter 5 shows the results of the mAb VF1c characterisation experiments, where, building on previous work performed in this laboratory, mAb VF1c was shown to interact with the junctophilin 1 protein. This allows the alignment of previous research using this antibody, meaning that it is now known that JPH1 is phosphorylated by an endogenous kinase, is non-glycosylated and is increased in abundance after chronic low frequency stimulation (Campbell *et al,* 1987; Guo *et al,* 1994; Froemming *et al,* 1999; Froemming *et al,* 2000). This was elaborated further by showing that JPH1 protein abundance was increased in fast type muscle fibres (such as those found in EDL and VL muscles), as detected by western blotting. It was also shown, in collaboration with the Sorrentino group that mAb VF1c binds to a region between amino acids 369-460 of JPH1, although attempts to narrow this further were hampered by rogue secondary antibody binding to peptide arrays. It is possible that the mAb VF1c binds to a conformational epitope on this protein.

The implications of these results are far-ranging. The amalgamation of old and new knowledge on JPH1 function can add to the field, although regrettably we do not yet know which kinase is involved in phosphorylating it, or the effect this has on the protein and its binding partners.

Uncovering the binding region for mAb VF1c allows the drawing of some interesting conclusions: for instance in western blots of rabbit muscle, the JPH1 protein as detected with mAb VF1c can be seen as two bands at 90 and 80 kDa. As neither of these bands are visible in secondary only controls, a logical conclusion is that the JPH1 protein is in some way cleaved within the region of 369-460, or that shorter splice variants of JPH1 exist in skeletal muscle. This provides an interesting starting point for why and how is JPH1 cleaved. Although Murphy et al suggested that JPH1 and JPH2 are subject to calpain cleavage via µ-calpain, it remains to be fully investigated (Murphy et al, 2013). It is tempting to think that cleavage of JPH1 or 2 may be linked to activity and or regulation in some way, and thus alterations in calpains acting upon these proteins could have very serious ramifications for muscular disorders, or that variances in molecular weight of these proteins could exert differing effects on their interaction partners as seen with the 45 kDa junctional Sarcoplasmic reticulum protein, JSRP1/ JSRP 45 (Yasuda et al, 2013). If the action of proteolytic enzymes on the JPH protein is also relevant to those expressed in neuronal tissue, these ramifications could be necessary to understand diseases of these tissues as well, such as Huntingtons like disease 2(HLD2)(Nishi et al., 2002)(Margolis, 2003). JPH1 has also been implicated in Charcot-Marie-Tooth disease, a peripheral neuropathy of varying severity caused by mutations in the GDAP1 (ganglioside induced differentiation associated protein 1) gene (Pla-

Martin *et al.,* 2014). Thus the investigation of proteins which act upon JPH1 and 2 are necessary.

The characterisation of mAb VF1c also confirmed previous reports of increased abundance of JSR-90 (JPH1) in type II muscle fibres (Froemming *et al* 2000). JSR-90 was found to be decreased in rabbit tibialis anterior, a predominantly fast muscle, after chronic low frequency stimulation, and this was paralleled in the work presented here via Western blotting of several muscle types (Froemming *et al,* 2000). The soleus muscle types in both rabbit and rat both displayed lower abundance of JPH1 and JPH2 compared to faster muscles such as EDL, and may represent a matched expression level to that found for RyR1 in fast and slow muscle types (Froemming *et al ,*2000; Salanova *et al,* 2008). It is also possible that this differential of JPH1 and JPH2 expression in skeletal muscle is a reflection of the varying embryonic origins of the muscle groups. This could definitely be the case for the intercostal and diaphragm muscles, which arise from a separate somite to the limb buds in embryonic differentiation, and require slightly altered levels of muscle differentiation factors MyoD and Myf-5 (Kablar *et al,*1997).

Chapter 5 also demonstrates the need for carefully controlled data, particularly when examining cell culture samples by Western blot. The expression of JPH1 and JPH2 protein were demonstrated in A7r5 and C2C12 cell lines. The C2C12 mouse myoblast cell line must be used at as low a passage number as possible, and unfortunately did not provide a clear timeline of JPH expression during myotube differentiation. It is also difficult to transfect these cells once they have been differentiated. Interesting results were obtained using the

A7r5 cell line, where both JPH1 and JPH2 (the major isoform in smooth muscle) are expressed. It is noteworthy that JPH1 is expressed in this cell line, and may hint that these proteins have distinct roles in smooth muscle, which has already been shown in skeletal and cardiac muscle (Beavers *et al.,* 2013; Jayasinghe *et al.,* 2014). It has been shown that application of cholesterol oxidation products, also known as oxysterols, onto A7r5 cell had no effect on JPH1 abundance (Hammoud *et al,* 2012), but it would be interesting to analyse JPH2 under the same conditions, especially as JPH2 alterations have been noted in hypertensive states, as well as hypertrophic cariomyopathy (Cai *et al,* 2015:Guo *et al,* 2015). It was also seen that JPH1 and JPH2 in A7r5 cells do not undergo the same cleavage events as they do in skeletal muscle (both proteins were detected at approx. 90 kDa in A7r5 lysates), despite expressing the same calpain cleavage proteins (μ and M-calpain, also known as calpains I and II, respectively) reported to act on JPH1 and JPH2 (Ariyoshi *et al,*2007; Kar *et al,*2007; Murphy *et al,* 2012).

Another important point when examining these data is the issue of molecular weight. Calpain cleavage aside, full length JPH1 is detected in some tissues at a molecular weight of 90 kDa, despite having a predicted molecular weight of 72 kDa. Given that we know JPH1 is not glycosylated (Froemming *et al,* 1999) and that even though JPH1 is phosphorylated by an as yet unkown kinase, this does not account for the almost 20 kDa upward shift in molecular weight as seen in SDS PAGE and western blots of this protein. A possibility is that JPH structure is affecting its apparent molecular weight. All junctophilins posess membrane binding regions (MORN motifs), a middle α-helical region and a C-terminal membrane spanning domain. These attributes have been shown in other proteins to affect the relative

mobility in SDS PAGE gels. Rath *et al* state that in CFTR (Cystic Fibrosis transmembrane conductance regulator channels, chloride channels associated with cystic fibrosis) mutants with added helical turns, relative mobility could be slowed in the same gel by up to thirty percent, and they postulate that this is due to the uneven SDS binding of these helices and membrane spanning regions, which in some cases have been shown to bind twice the amount of SDS as other non-helical soluble proteins. Abberant SDS binding was also shown to encourage the partial refolding of proteins, which if it occurred in any of the data shown here could explain unusual binding patterns seen with some antibodies, particularly pAb JP1. It was also shown that proten-lipid interactions could be a factor in altering relative mobility in gels, and as all junctophilin proteins contain lipid binding motifs, and have been shown to change shape depending on the compositiionof the lipids they interact with, this could account for some of the disparites in measured molecular weights (Rath *et al.,* 2009: Bennet *et al.,* 2013). Transmembrane regions have also been shown to be responsible for detergent resistant dimerization, as occurs in the glycoporin A protein, and if the C terminal region of JPHs are cleaved off and free, it is possible that they dimerize and could account for 30 kDa bands seen in some gels (Furthmyer and Marchesi, 1976: Li *et al.,* 2012). It has been suggested by Rath *et al* that when analysing proteins with potentially troublesome regions such as α-helices and TM domains that specialised molecular weight markers be used, perhaps as specific set of helical proteins could be bacterially expressed (Rath *et a.l,* 2013).

This chapter also demonstrated that JPH1 and 2 are expressed in A7r5 rat aortic cell line, and that they can be of (limited) use in studying calpain cleavage of said proteins. DMSO (in A7r5s) and N-ter peptides, both membrane disrupting compounds had

upregulatory effects on JPH1 and 2 expression. This is probably due to either a change in lipid composition around/ near JPHs proteins, which may have affected either transcriopption or nmay have solubilised or "freed" the protein from the membranes, allowing it to be more easily detected via western blot. Interestingly, BAPTA-AM and A23187 had opposing effects depending on the timescale, and may hint at time and calcium based regulation of JPH1 and 2 expression in smooth muscle. A contraction study would be an excellent follow up to these data. An *in silico* analysis showed that the most likely calpain cleavage sites on JPH1 in the N terminal portion at approximately 150-160 aa and in the C terminal region, at approximately 600-610, in rabbit, rat, mouse and human JPH1 and 2. This corroborates Guo *et al*, who found that the primary calpain cleavage site is found at the C-terminal end of JPH2. JPH proteins are necessary for T-tubule arrangement and calcium release, and increased cleavage of both JPH1 and 2 have been implicated in skeletal muscle myopathy, aging and cardiopathies. (Murphy *et al.,* 2013: Wu *et al.,* 2014, Guo *et al.,* 2015). Thus the *in silico* analysis presented here will provide a frim basis for future inhibitory work using compound such as ALL-N or via mutagenesis of suspected cleavage sites, similar to the experiemtns performed in Gou *et al* (2015).

Taken together, these data imply that the regulation of JPH1 and JPH2 protein levels is muscle specific, and that JPH1 is cleaved between the amino acids 369 and 460. This provides a new reliable antibody to aid the study of JPH1 protein, and may yet yield valuable clues as to if and why it is cleaved in skeletal muscle cells, but not in smooth muscle. Further study will clarify the role this protein has in maintenance of health and its role in disease.

7.4: JPH1 and JPH2 in disease models.

Experiments were performed to analyse the abundance of JPH1 and JPH2 in rodent models of aging, chronic intermittent hypoxia (CIH) and Duchenne muscular dystrophy (DMD). While no differences were found in JPH1 or JPH2 protein abundance in CIH compared to controls, a decrease in the abundance of the 85 kDa form of JPH2 was found in *mdx* compared to wild type GC muscle. Similarly in CIH EDL and soleus muscles, no change in JPH1 abundance was found, whereas a small non-significant decrease in JPH2 was found in CIH EDL compared to sham animals. In the study of aged and exercised mouse soleus and quadriceps, some intriguing results were obtained. Firstly, when aged soleus and aged quadriceps were compared, an increase in JPH1 abundance (detected with mAb VF1c) was found in aged soleus compared to aged quadriceps and adult soleus samples. Detection of JPH1 abundance using pAb JP1 found decreased abundance in aged quads compared to adult quadriceps, and that that abundance of JPH1 was increased in exercised aged quadriceps compared to aged quadriceps. Interestingly, a decrease in JPH1 abundance in exercised aged soleus was detected compared to exercised aged quadriceps. JPH2 abundance was found to be lower in aged soleus compared to aged quadriceps, contrasting the increase found in JPH1 levels. Following on from this, JPH2 abundance was also decreased in exercised aged soleus compared to exercised and aged quadriceps samples. This was different to the results found with adult exercised samples, where JPH2 abundance was higher in exercised adult quadriceps compared to adult quadriceps. It is possible that exercising the muscle may have caused increased liberation of JPH2 from the SR membrane, thus increasing detection.

In CIH tissue compared to control tissue, it is noteworthy that there was no change in JPH1 abundance as detected by western blotting. As these samples were collected after two weeks of CIH treatment, it is entirely possible that the effects seen in limb muscles from this treatment occur after a longer period of time. Either way, it is a poorly-explored avenue of research, as plenty of work exists on the whole-body or diaphragmatic effects of CIH, but very little on the molecular effects in limb muscle. It has been shown that alterations in RyR function and modification (e.g. oxidation of Cys residues) occur in hypoxic tissue, and it follows that interacting proteins would incur similar effects (Sun *et al,* 2013). In this instance, a change in the oxidation status of the cysteine residues on RyR1 can affect the interaction of RyR1 with JPH1 (Phimister *et al* 2007). In the case of JPH1, it is likely that it would be affected by any form of hypoxia as this has been shown to have an effect on metabolism of the cell and thus of redox potential at the SR membrane. As increasing hypoxic status also increases inflammatory effects in muscle cells, raised levels of membrane alterations and increased reactive oxygen species could certainly have an effect on JPH1 abundance and the status of the protein (Phimister *et al,* 2007).

Ideally, one would perform a long term study of in limb, smooth and respiratory muscles under hypoxic conditions and examine a range of EC coupling related proteins. This would allow the pinpointing of when CIH-mediated limb dysfunction arises, and if any EC coupling proteins are involved.

The comparison of *mdx* mouse with wild type showed no difference in JPH1 abundance in animals of 8 months of age. This contrasts to previous results obtained by Murphy *et al,*

although the mice sampled in their study were of a different age group (Murphy *et al,* 2012). It is possible that by 8 months, the degeneration and regeneration seen in *mdx* muscle has reached a steady state, a stark contrast to the progression of the disease seen in the human disease Duchenne muscular dystrophy. An exception to this is the decrease seen in abundance of the 85 kDa form of JPH2 in *mdx* gastrocnemius muscle compared to wild type controls, and this could be a parallel of the pseudohypertrophic effect seen in DMD calf muscle, but confirmation of this would need further experimentation. Alterations in skeletal muscle hypertrophy have been linked to a mutation in JPH2, and this could add to the pathology of the disease (Woo *et al,* 2010). As dystrophin is absent in DMD and in the *mdx* mouse, and as the dystrophin protein is in complex with CAV3, a protein known to interact with JPH2, the decrease in JPH2 abundance could be linked to this (Woo *et al,* 2010). It is very possible that the decrease in JPH2 has an implication for (or is because of) the structural defects seen in *mdx* muscle. Future studies could include the analysis of JPH1 and JPH2 abundance and monitoring of their molecular weight in an animal model of DMD, or preferably in DMD patient biopsies. The investigation of the effects of decreased JPH2 abundance on calcium signalling could also be further elucidated, perhaps in single fibre studies using calcium imaging.

Further work must also be performed on JPH expression in aged and exercised skeletal muscle. Considering that the population of those over 60 years of age is going to increase in the coming decades, sarcopenia is and will become a significant burden to patients and healthcare systems alike (Cruz-Jentoft *et al.,* 2010; Cruz-Jentoft *et al.,* 2014). The increases found in JPH expression in aged soleus compared to quadriceps muscles indicate

that use- or perhaps pathway-dependent factors are at play in aged muscle. It is also quite likely that the increase in soleus JPH1 levels is a compensatory measure to attempt to alleviate EC uncoupling, found to be increased in aged muscle (Boncompagnani *et al.,* 2006). It is also possible that defective or ablated T-tubule or altered SR geometry could be part of the reason for the changes in JPH abundance. In the soleus, a predominantly type I muscle with many mitochondria, it is feasible that the increased ROS-mediated signalling associated with aging could result in a requirement for higher abundance of JPH1 to help regulate RyR1 and minimise aberrant Ca^{2+} release, as increased reactive oxygen species in muscle have been shown to have an effect on RyR1 (Sun *et al.,* 2013). The increase in JPH1 may also give clues as to the regulation of junctophilins in muscle tissue, but this would require further study to fully elucidate the mechanism involved. The increased JPH1 abundance in soleus compared to quadriceps muscle may also be due to the bigger role this muscle has in anti-gravity functions, which may be even more relevant in bipedal humans.   The exercised samples showed interesting results, whereby the JPH2 abundance was found to be increased in exercised quadriceps compared to unexercised adult controls. This may be due to a solubilising effect of exercise on the JPH proteins (Murphy *et al.,* 2013). The decrease in JPH2 abundance in exercised quadriceps could also be due structural rearrangements in sarcopenic muscle. Taken together, these results have interesting implications for the field of aging research. Although further work is necessary, the alterations in JPH2 and JPH1 are of interest. The differential regulation of JPH1 and JPH2 during aging could not only be linked to RyR mediated calcium release, but also to interacting proteins such as STIM and Orai, TRPC3 and CAV3. It is possible that as Ca^{2+} dysregulation progresses, the compensatory drive to maintain intact RyR1 signalling is increased, while the need for accessory Ca^{2+}

influx (such as SOCE channel and sensor Orai and STIM) decreases. Ideally, several groups of aged animals could be treated with superoxide dismutase inhibitors, an exercise regime and controls the pathways affecting sarcopenia and thus JPH regulation could be disentangled. If there was also a pharmacological, molecular or physiological method of altering JPH expression in muscles susceptible to sarcopenia this could alleviate some portion of the aberrant Ca^{2+} signalling in this disease. Exercise would be an excellent method of doing this. Previous work has shown that after acute bouts of eccentric (lengthening contractions), JPH1 expression was decreased; however there are no data commenting on JPH1 or JPH2 expression after chronic training programs. It would be worth investigating as this could lead to a rationally designed exercise regime specifically created to stave off the adverse effects of sarcopenia on skeletal muscles. In designing such an exercise regime it would be important to consider the muscle specific differences and to encourage exercise of trunk and core muscles. This could greatly improve not only the devastating and often expensive effects of sarcopenia, but also ward off the often-overlooked complications of this disease.

7.5: Conclusions:

RyR1 is a rapidly expanding hub of protein-protein interactions necessary to regulate the movement of Ca^{2+} in a wide variety of cell types. In the work presented here, RyR1 has been shown to form a complex with GRB2, an adapter protein crucial to many signalling pathways. It is likely that one of the SH3 domains on the GRB2 protein interacts with the proline rich region in RyR1. GRB2 may bring the RyR complex into close approximation with a number of other protein networks, such as those involved in MAPK signalling or the dyrophin-dystroglycan complexes. GRB2 is likely to exert different roles and may bring RyR into conmtact with different intracellular pathways in non-muscle tissues, such as in B-cells. Further analysis is necessary to characterise other potential interactors of this complex, and to assess any effect they have on RyR1 gating or regulation.

This work also demonstrated that another interactor of RyR1, junctophilin 1, can be detected using the mAb VF1c. It was shown that this antibody binds to a region located between amino acids 369-450, and that this may be a conformational epitope. This allows the cohesion of previous data using the mAb VF1c, and thus provides novel information about the JPH1 protein, namely that this protein is phosphorylated by an endogenous kinase and is non-glycosylated. It was also found that both JPH1 and JPH2 are differentially expressed in skeletal muscle of rabbit limb and trunk, and that this difference in abundance may depend on muscle developmental origin or may be use-dependent. This has massive implications for the study of EC coupling in many muscle types, and potentially on the selection of muscle types best suited for the future of JPH-based research. Calpain cleavage

studies confirmed the action of calpains on JPH1 and 2, and *in silico* studies suggested the amino acids likely to be cleaved by calpains I or II. It was seen that memebrane disrupting compounds such as DMSO and N-ter peptide siRNA transfection system may cause upregulation of JPH1 and 2 proteins.

The effects of sarcopenia on soleus and quadriceps muscle were found to be different, and to have opposing effects on JPH1 and JPH2 expression. Aged soleus showed increased JPH1 abundance compared to aged quadriceps, and this is likely to compensate for increased EC uncoupling found in skeletal muscle. In contrast, JPH2 decreased in aged soleus compared to aged quadriceps, in exercised and non exercised samples, while JPH2 abundance was increased in exercised adult quadriceps compared to non-exercised adult quadriceps. Taken together, these results imply that alterations in muscle structure and EC coupling proteins are implicated in the pathology of sarcopenia, and that exercise may have a solubilising effect on JPH proteins. Further analysis is needed to ascertain the exact effect these changes in JPH1 and JPH2 have on Ca^{2+} release in the muscle cell.

8.1: Appendices

	Dist travelled (mm)	Rf	Rf-c	Rf/x	MW
"100 kDa" band					
A549	8	0.145	-4.533	5.17	147.51
JEG 3	8	0.145	-4.533	5.17	147.51
A7r5	8	0.145	-4.533	5.17	147.51
ShSy 5y	8	0.145	-4.533	5.17	147.51
JURKAT	-				
U937	8	0.145	-4.533	5.17	147.51
HL-60	-				
C2C12	8	0.145	-4.533	5.17	147.51
"75 kDa band"					
A549	16.5	0.3	-4.378	4.99	98.3
JEG 3	16.5	0.3	-4.378	4.99	98.3
A7r5	16.5	0.3	-4.378	4.99	98.3
ShSy 5y	16.5	0.3	-4.378	4.99	98.3
JURKAT	-				
U937	14	0.254545	-4.4234545	5.04	110.77
HL-60	16.5	0.3	-4.378	4.99	98.3
C2C12	16.5	0.3	-4.378	4.99	98.3

Figure 8.1.b: MW calculation of cell culture screen: SH3B blot. Bands have apparent molecular weight of 147 kDa and 98 kDa, except for U937 cells, which have bands at 147 and 110 kDa.

A549 homogenate	"150 kDa" protein	average kDa	"75 kDa" protein	Average kDa	
Cell screen	147.51	143.23	98.3	90.27	
Peptide Optimisation	132.8		83.27		
Hydroxyapatite	149.37		89.234		

Table 8.1.a: average of molecular weights of proteins detected using SH3B peptide calculated from cell culture screen, peptide optimisation and hydroxyapatite experiments.

KALRN_HUMAN (O60229-4) Isoform 4 of Kalirin OS=Homo sapiens GN=KALRN Chain:1-1289, pI:5.97, Mw:144486	**M3K9_HUMAN (P80192-4)** Isoform 2 of Mitogen-activated protein kinase kina… Chain:1-1118, pI:5.56, Mw:123374	**RPGF1_HUMAN (Q13905)** Rap guanine nucleotide exchange factor 1. Chain:1-1077, pI:5.64, Mw:120548
KALRN_HUMAN (O60229-6) Isoform 6 of Kalirin OS=Homo sapiens GN=KALRN Chain:1-1257, pI:5.94, Mw:141165	**M3K9_HUMAN (P80192)** Mitogen-activated protein kinase kinase kinase 9. Chain:1-1104, pI:5.64, Mw:121895	**S3TC1_HUMAN (Q8TE82)** SH3 domain and tetratricopeptide repeat-containing prote… Chain:1-1336, pI:5.85, Mw:146962
SASH1_HUMAN (O94885) SAM and SH3 domain-containing protein 1. Chain:1-1247, pI:5.78, 136654	**ASPP2_HUMAN (Q13625-3)** Isoform 3 of Apoptosis-stimulating of p53 protein 2 OS=Ho… Chain:1-1134, pI:5.89, 126324	**S3TC2_HUMAN (Q8TF17-5)** Isoform 5 of SH3 domain and tetratricopeptide repeat-cont… Chain:1-1281, pI:5.94, 144777
PLCG1_HUMAN (P19174-2) Isoform 2 of 1-phosphatidylinositol 4,5-bisphosphate phos… Chain:1-1291, pI:5.72, Mw:148661	**ASPP2_HUMAN (Q13625)** Apoptosis-stimulating of p53 protein 2. Chain:1-1128, pI:5.78, Mw:125617	**S3TC2_HUMAN (Q8TF17)** SH3 domain and tetratricopeptide repeat-containing prote… Chain:1-1288, pI:5.94, Mw:144023
PLCG1_HUMAN (P19174) 1-phosphatidylinositol 4,5-bisphosphate phosphodiesterase… Chain:2-1290, pI:5.72, Mw:148402		**SHAN2_HUMAN (Q9UPX8-4)** Isoform 4 of SH3 and multiple ankyrin repeat domains prot… Chain:1-1254, pI:5.45, Mw:134932

Table 8.1.c: TagIdent (expasy.org) search using parameters defined by experimental

results from section 4.3.a-g. TagIdent was searched using molecular weight of 146 kDa (+/-20%) and a pI of 4-5, with a keyword of "SH3", and limited to *homo sapiens*. Of the proteins returned by the search, PLCγ1 is a protein suggested by data from Wu *et al* (2007).

Triadin	Dist. Travelled (mm)	dist. travelled / gel length	$R_f - c$	R_f / x	MW (kDa)
	2.5	0.053763	-4.80192	5.289619	194
Brain	25.5	0.548387	-4.30729	4.74476	55.46
	40.2	0.864516	-3.99116	4.396523	24.54
		0	-4.85568	5.348843	
Muscle	3	0.064516	-4.79116	5.277775	189.234
	11.5	0.247312	-4.60837	5.076413	119.23
	40.2	0.864516	-3.99116	4.396523	24.918
Post sol mus	10	0.215054	-4.64063	5.111948	129.404
Flow through	8	0.172043	-4.68364	5.159327	144.32

GRB 2	Distance travelled(mm)	Dist. Travelled / gel length	$R_f - c$	R_f / x	MW (kDa)
Muscle Hom	34	0.73913	-4.65487	4.59604	38.904
Post sol Muscle	5	0.108696	-5.2853	5.218507	162.181
	6.5	0.141304	-5.2527	5.186311	151.356
	12	0.26087	-5.13313	5.068257	114.18
FKBP12 Mus	34	0.73913	-4.65487	4.59604	38.904
Mouse secondary band	36	0.782609	-4.61139	4.553111	35.481

PLC γ 1	Dist. Travelled (mm)	dist. travelled / gel length	Rf – c	Rf / x	MW (kDa)
Brain	4	0.086022	-4.77078	5.255319	180
	5.75	0.123656	-4.73314	5.213862	163.62
Muscle	3	0.064516	-4.79228	5.279008	190.111
	4.5	0.096774	-4.76003	5.243474	175.175
Mus PO	1.5	0.032258	-4.82454	5.314543	206.062

H300	Dist. Travelled (mm)	dist. travelled / gel length	Rf – c	Rf / x	MW (kDa)
Muscle Hom	14.5	0.318681	-6.32442	5.225929	168.239
	14	0.307692	-6.33541	5.235009	171.794
FKBP12 Mus	5.5	0.120879	-6.52222	5.389374	245.117
	7.5	0.164835	-6.47826	5.353053	225.45
	21.25	0.467033	-6.17607	5.103344	126.865

PTN	Dist. Travelled (mm)	dist. travelled / gel length	Rf – c	Rf / x	MW (kDa)
	10.8	0.20377358	-3.57863	5.069594	117
	15.8	0.29811321	-3.48429	4.93595	86.287

Figure 8.1.d: Rf calculations for FKBP12 pull down experiments. Apparent molecular weights were calculated using the same method as described in Fig8.1.a.
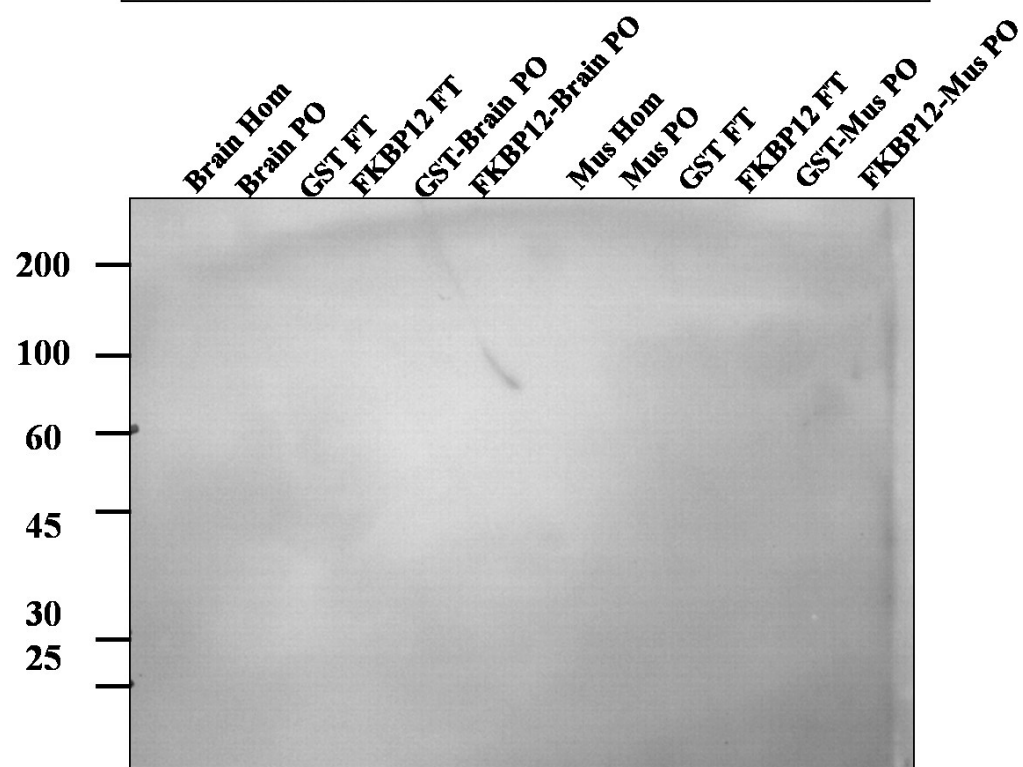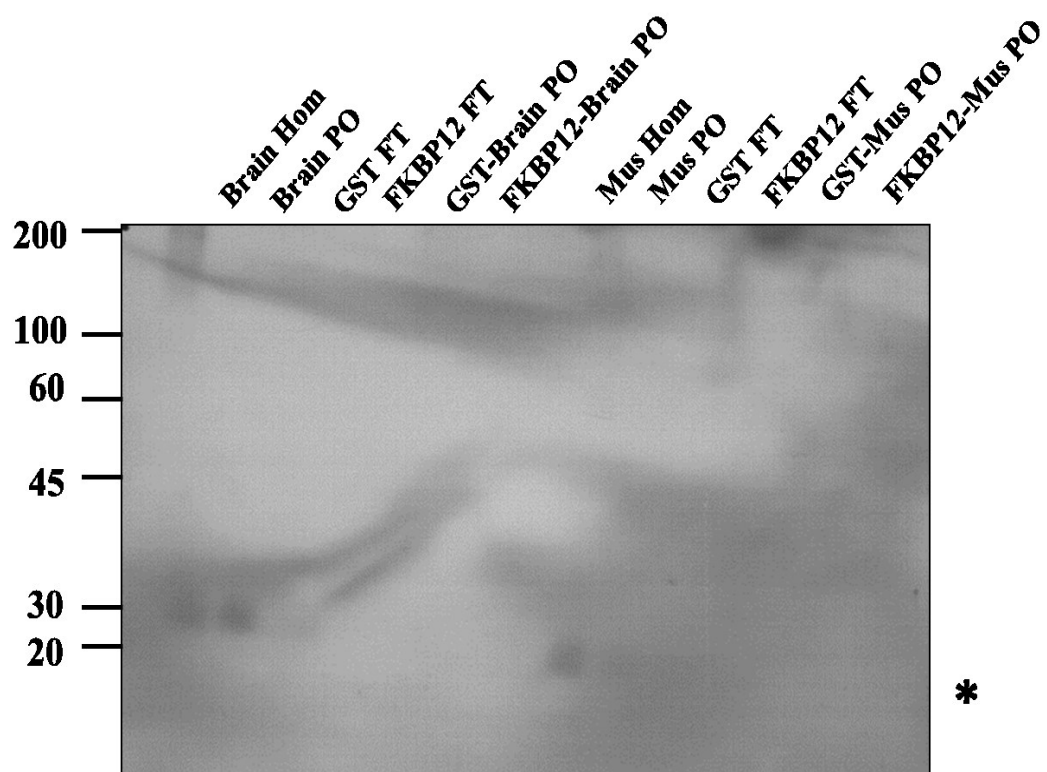
Figure 8.1.e: FKBP 12 pull down of rat Brain and muscle, probed with anti- mouse or anti-Rabbit secondary antibody only. Brain and muscle homogenate, post solubilisation (PO), GST control flowthrough (GST FT), FKBP12 FT, GST-post solubilised (brain/muscle gst beads plus post solubilisation material), FKBP 12 –PO (brain/muscle incubated post solubilisation sample with FKBP 12 beads) samples were run on 10% SDS PAGE gels followed by wet transfer as described in materials and methods.

Blots were probed with 1:1000 anti mouse or anti rabbit secondary and exposed to film. The anti- mouse blot (A) shows a background band at 30 kDa, marked with an asterisk. No background bands were seen with the anti-rabbit only control.
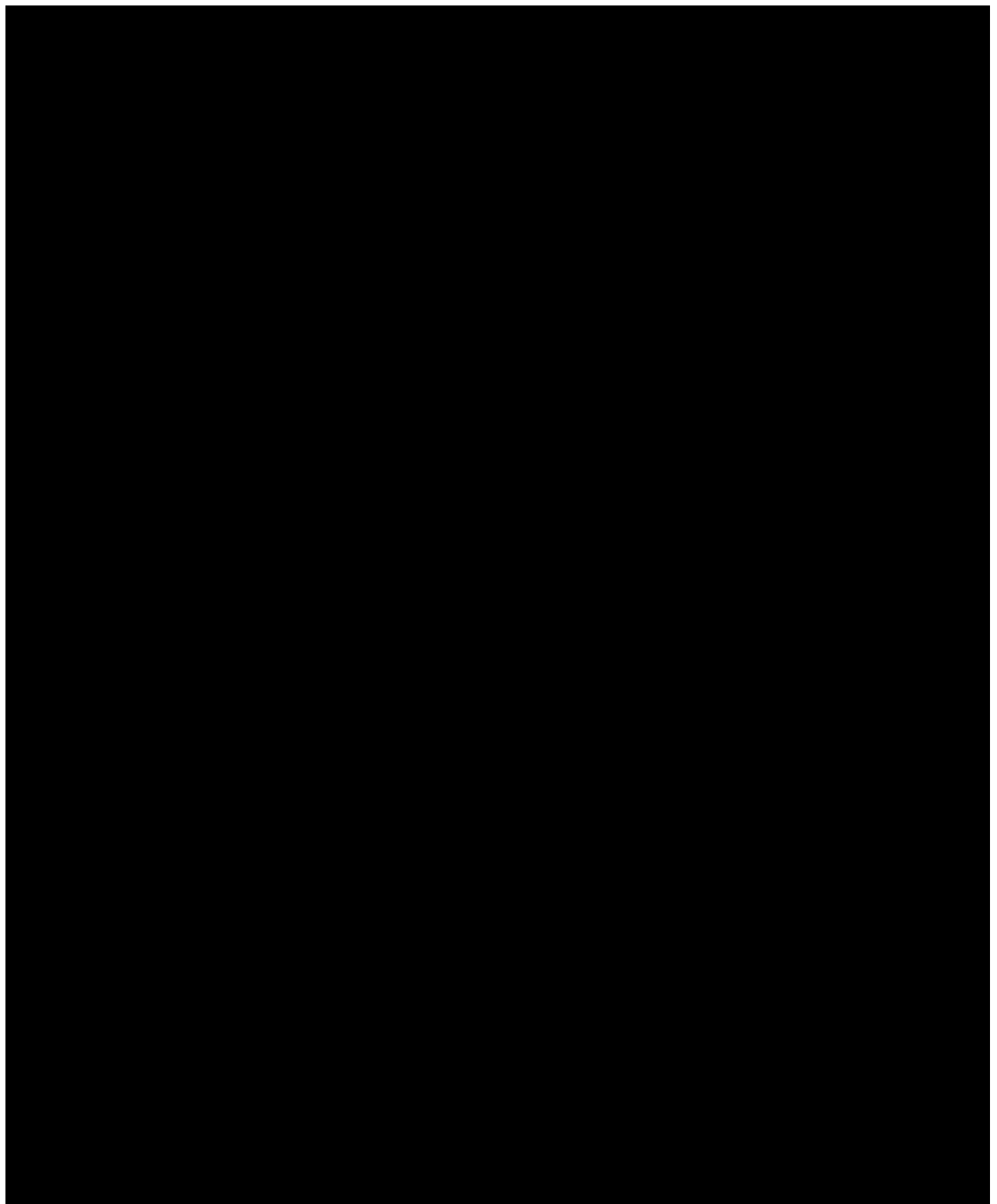
Figure 8.1.f: OPHID search using "RyR1" as input method returns 38 known or predicted interactors. Notable described interactors (e.g. PLCγ1, GRB2 and NCK) are

described in Wu *et al* (2007). Some descrepancies exist, e.g., absence of Junctophilin, a known RyR1 interaction partner. The experiments in section 4.4 describe tests to validate some of these interactions.
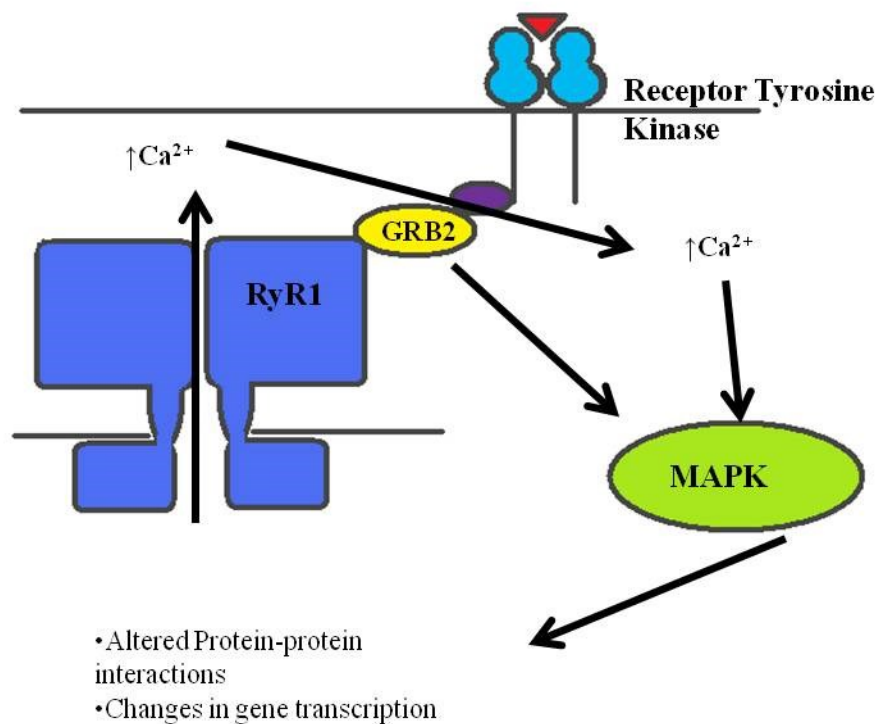
Figure 8.1.g: Diagram of hypothetical role for GRB2-RyR1 interaction. GRB2 may facilitate the interaction of RyR1 with receptor Tyrosine kinases, such as Insulin receptors, which may allow linking of intracellular calium ion concentrations with extracellular signalling eents, allowing a concerted mitogenic response via the MAPK pathway.
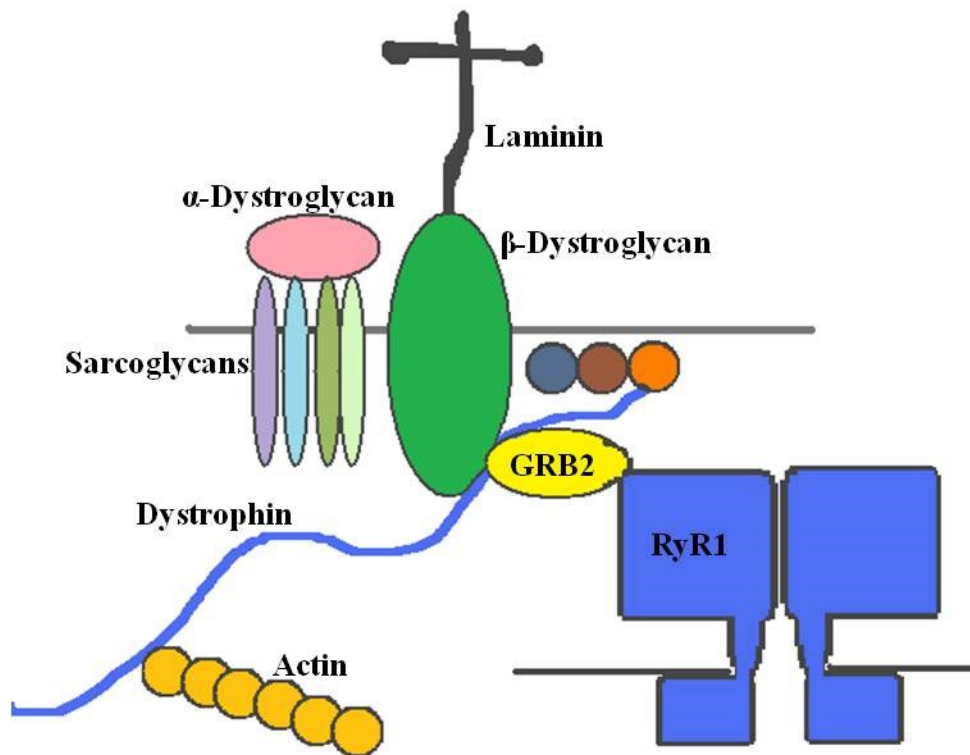
Figure 8.1.h: another possible role for GRB2-RyR1 complex. GRB2 has been shown to interact with the dystrophin complex in muscle cells, and it is feasible that it may act as an anchor to tether this complex to RyR rich areas. Junctophilin 1, which interacts with RyR1, has also been shown to associate with CAV3, which is part of the dystrophin complex in skeletal muscle. Anchoring large protein complexes could be purely structural or have implications for signalling, especially in muscle afflicted Duchenne muscular dystrophy.

8.2: Appendix II
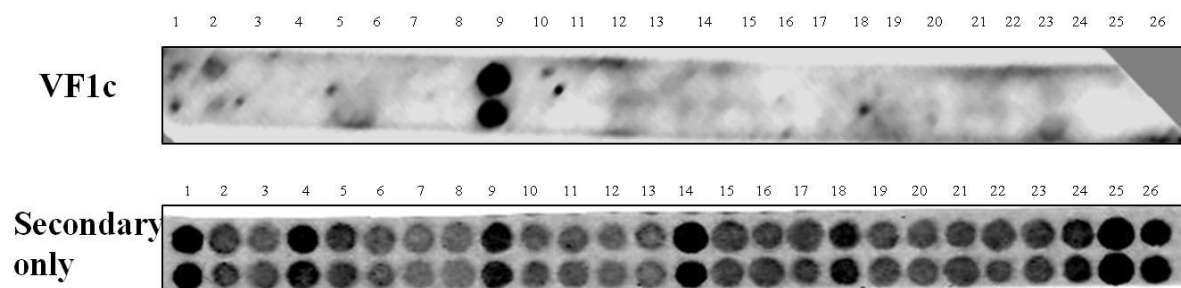
Peptide Array Data

Figure 8.2.a: Peptide array of amino acid fragments from JPH1 probed with VF1c and with secondary antibody only. VF1c interacts with spot 9, which contains the sequence QAALAARQECDIARAVAR. This result is confounded by the secondary only control which displays strong interaction with spots 1, 4, 9, 14, 18, 24, 25 and 26. It is possible that VF1c antibody binds a conformational epitope, and that this region of JPH1 resembles an antibody binding protein.

Spot no.	Peptide Sequence	Interacts with VF1c antibody	Interacts with Secondary alone
1	MARTKVEIANSRTAHARA		√
2	TKVEIANSRTAHARAKAD		√
3	EIANSRTAHARAKADAAD		√
4	NSRTAHARAKADAADQAA		√
5	TAHARAKADAADQAALAA		√
6	ARAKADAADQAALAARQE		√
7	KADAADQAALAARQECDI		√
8	AADQAALAARQECDIARA		√
9	QAALAARQECDIARAVAR	√	√
10	LAARQECDIARAVARELS		√
11	RQECDIARAVARELSPDF		√
12	CDIARAVARELSPDFYQP		√
13	ARAVARELSPDFYQPGPD		√
14	VARELSPDFYQPGPDYIK		√
15	ELSPDFYQPGPDYIKQRL		√
16	PDFYQPGPDYIKQRLQEG		√
17	YQPGPDYIKQRLQEGVDA		√
18	GPDYIIKQRLQEGVDAKEN		√
19	YIKQRLQEGVDAKENPEE		√
20	QRLQEGVDAKENPEEKVP		√
21	QEGVDAKENPEEKVPAKP		√
22	VDAKENPEEKVPAKPPTP		√
23	KENPEEKVPAKPPTPKES		√
24	PEEKVPAKPPTPKESPHF		√
25	KVPAKPPTPKESPHFYRK		√
26	PAKPPTPKESPHFYRKGT		√

Table 8.2.a: Amino acids from JPH1 (VF1c interacting region 369-460) synthesised via fmoc chemistry and probed with VF1c antibody. Coloured bars indicate the spots that VF1c interacted with. Blue bars indicate strong interaction, green indicate medium interactions with the secondary alone while red bars denote interaction with the VF1c antibody. the VF1c antibody detects a spot corresponding to 393-410. It is possible that VF1c binds to the JPH1 protein in a conformational manner.

Rabbit pAb JP1, JP2 and VF1c screen : Coomassie loading controls and secondary antibody controls

Coomassie stain: VF1c blot

Coomassie stain: JPH2 blot
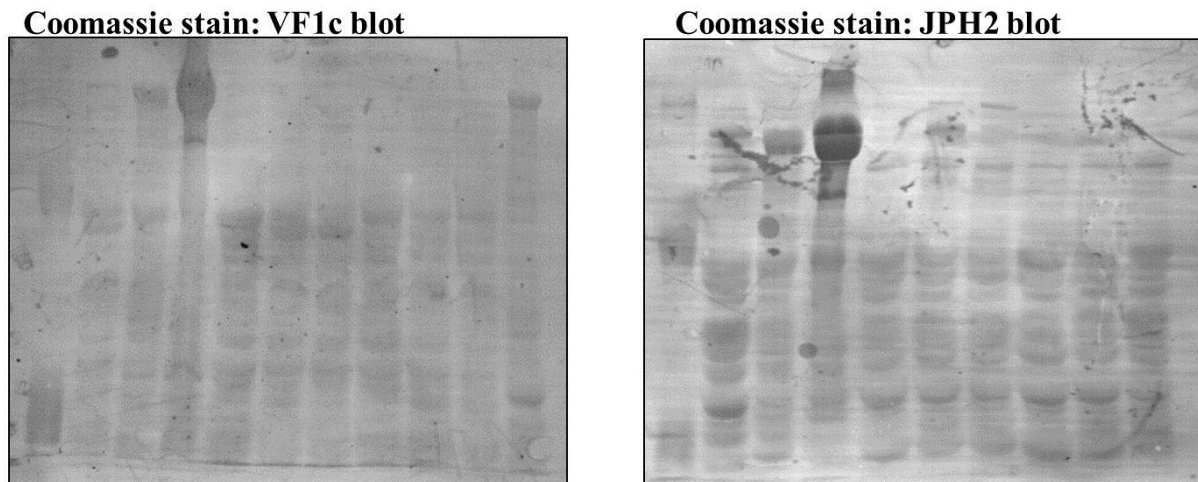
Figure 8.2.b: Post antibody detection via ECl and Film, rabbit tissue blots were stained with Coomassie for densitometric analysis. Signals obtained from each antibody were normalised to total protein per lane.

Muscle	Lat Dorsi	Diaph	Intercostal	EDL	Soleus	GC	VL	SH	SM
VF1c mAb MW	55.02	43.65	77.85	60	56.63	56.63	56.63	56.63	56.63
	46.25		60	49	47.61	46.25	46.25	46.25	46.25
JP2 pAb MW	102	61.49	139.84	106.34	102.26	98.34	94.56	98.34	98.34
	80.87		74.78	74.78	74.78	74.78	74.78	74.78	74.78
	54.68		61.46	59.13	59.13	59.13	59.138	59.13	59.13

Table 8.2.b: Calculated molecular weight of JPH1 and JPH2 in various rabbit skeletal muscle.
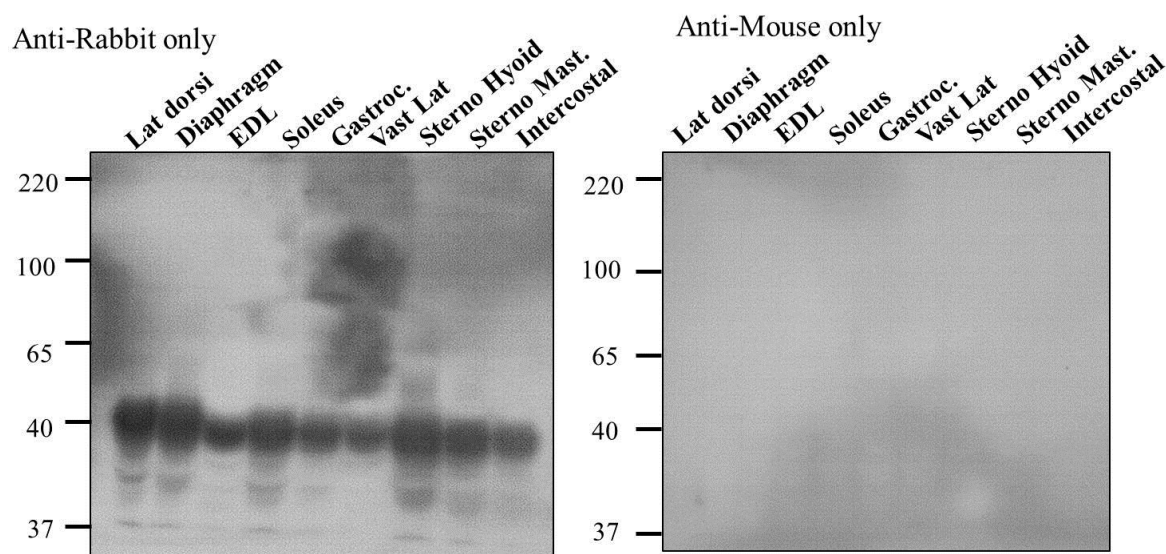
Figure 8.2.c: Rabbit muscle secondary only blots. Fresh rabbit tissue blots were probed with anti-rabbit or anti mouse secondary antibodies only. Anti-Rabbit blots contain a background band at 45kDa which was then excluded from analysis of JPH1 and 2. The VF1c antibody was detected using the anti-mouse secondary, thus no extraneous bands were seen. Alternatives to using the anti-rabbit secondary are tagging the primary JPH1 and 2 antibodies with fluorescent probes or HRP enzyme and detecting them directly, without the use of a secondary.

A7r5 Calpain Cleavage Study
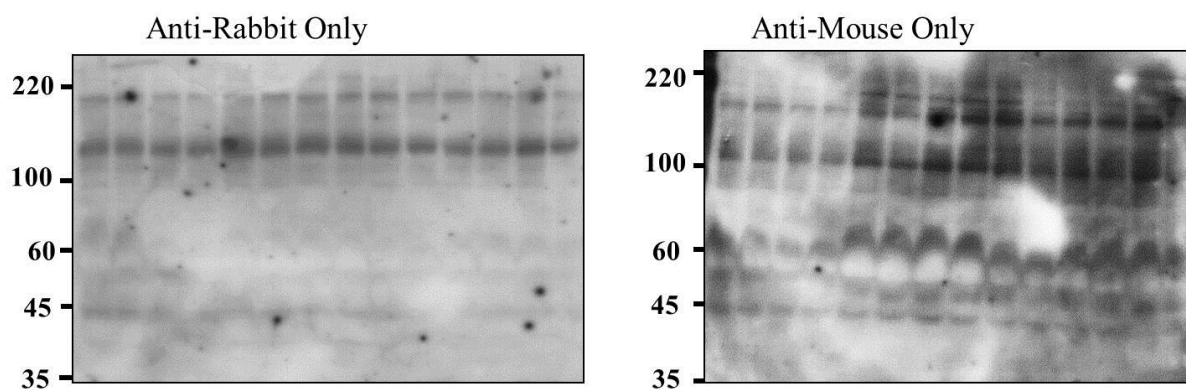
Figure 8.2.f:A7r5 secondary only controls. A7r5 cells were incubated with media only, 0.1% DMSO, ALL-N, A23187 and BAPTA-AM**.** Western blotting was performed and blots were incubated with anti-mouse and anti-rabbit secondary antibodies only. Background bands can be seen at 220 and 100 kDa in the left hand panel, and at 60 50 and 45 kDa in the right hand panel.

Figure 8.2.g: Clustal Ω alignment of protein sequences from JPH1 and JPH2 from human, rabbit, rat and mouse.

N-15

pAb to N-terminal of JPH1
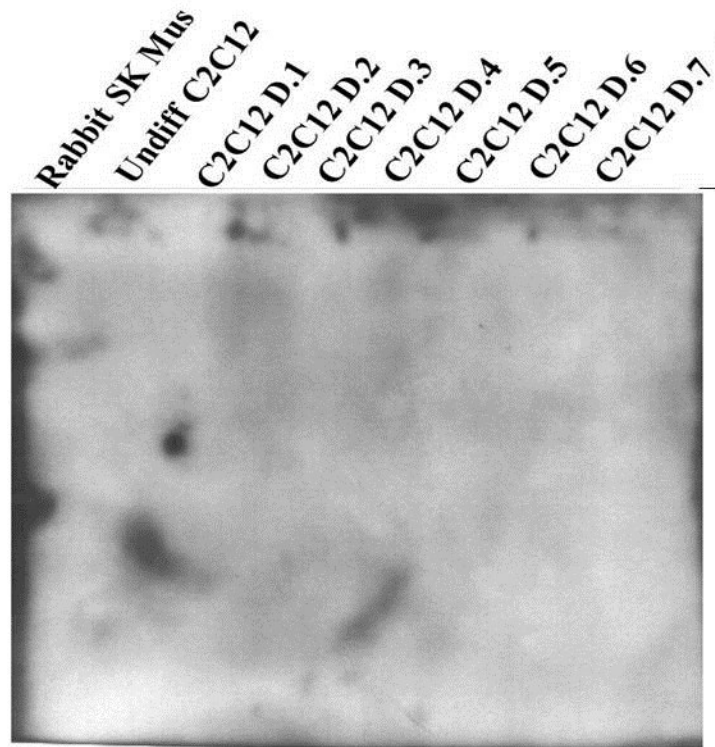
Figure 8.2.h: antibody to N-terminal end of JPH1 was used to probe C2C12 cells. The only available antibody to JPH1 (Santa Cruz biotechnology) was purchased and used to probe C2C12 differentiation samples. Despite multiple attempts and trials with many secondary antibody concentrations, different muscle tissue and buffer controls, this antibody was determined to be completely ineffectual, thus the lab wsa refunded by the SCBT. This is unfortunate an N-terminal targeting antibody would have provided for a clear and concise study of JPH1 via western blot or other methods such as ELISA or immunohistological study.

8.3: Appendix III
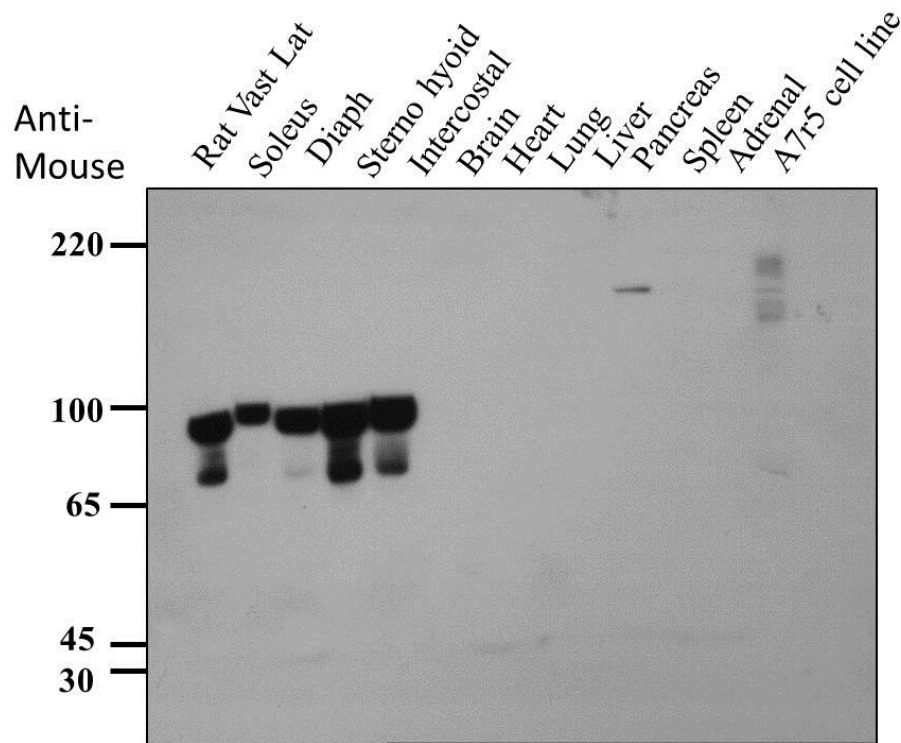
Figure 8.3.a: Western blot of rat muscle and organ tissue probed with anti-mouse secondary antibody only. Two bands are seen in rat muscle samples (VL, soleus, diaphragm, sternohyoid and intercostals). A band at 220 kDa can be seen in pancreas sample and in A7r5 cell lysates.

Anti Mouse ctrl		l = 57			
mw	dist trav		Log MW	rf	
220000	5.5		5.342423	0.096491	
100000	25		5	0.438596	
65000	35.5		4.812913	0.622807	
45000	53.5		4.653213	0.938596	
30000	57		4.477121	1	
	Dist Trav	Rf	rf-c	rf/x	MW
Muscle samples	7.5	0.131579	-5.84382	5.299557	199.322
	10	0.175439	-5.79996	5.259782	181.779
	25	0.438596	-5.5368	5.021133	104.986
	32.5	0.570175	-5.40522	4.901809	79.764

Table 8.3.a: R_f of proteins analysed from rat muscle as detected with anti mouse secondary antibodies. Blots probed with other antibodies raised in mouse were then carefully analysed to ensure no rogue secondary antibody was detected as a valid interaction.
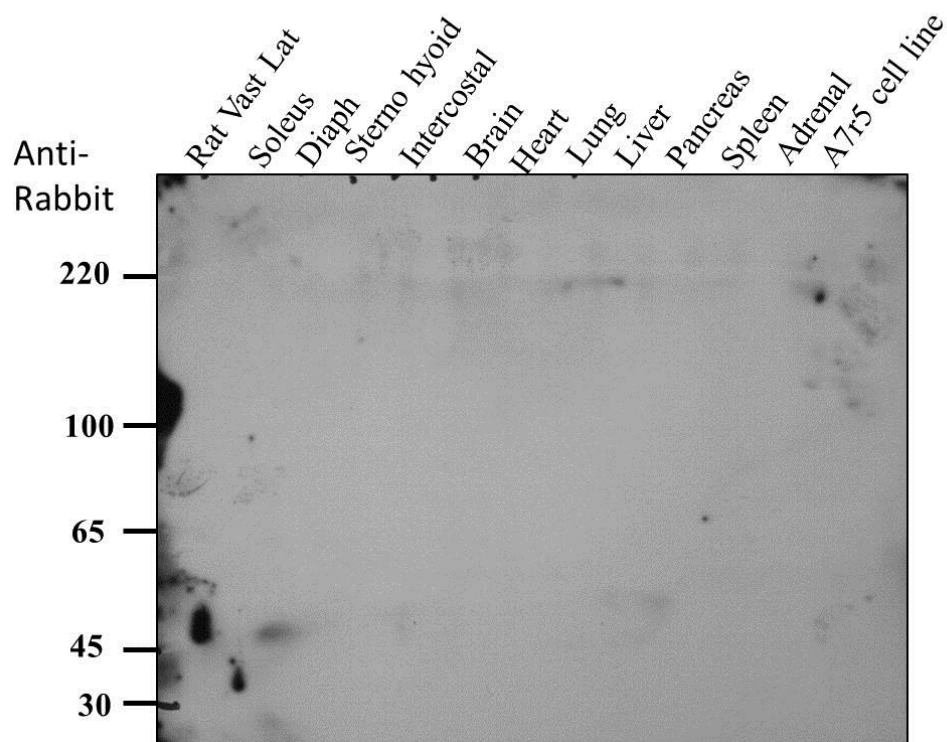
Figure 8.3.b: Rat muscle and organ samples probed with anti-rabbit antibody. Western blot of rat muscle (VL, soleus, diaphragm, sternohyoid and intercostals) and organs (brain, heart, lung, liver, pancreas, spleen, adrenal gland) and A7r5 cell line were incubated with anti-rabbit secondary only. No bands were detected.

Anti Rabbit only

Brain Heart Lung Liver Pancreas Spleen Diaphragm Intercostal Vast Lat EDL Gastroc Sol

220
100
60
45
30
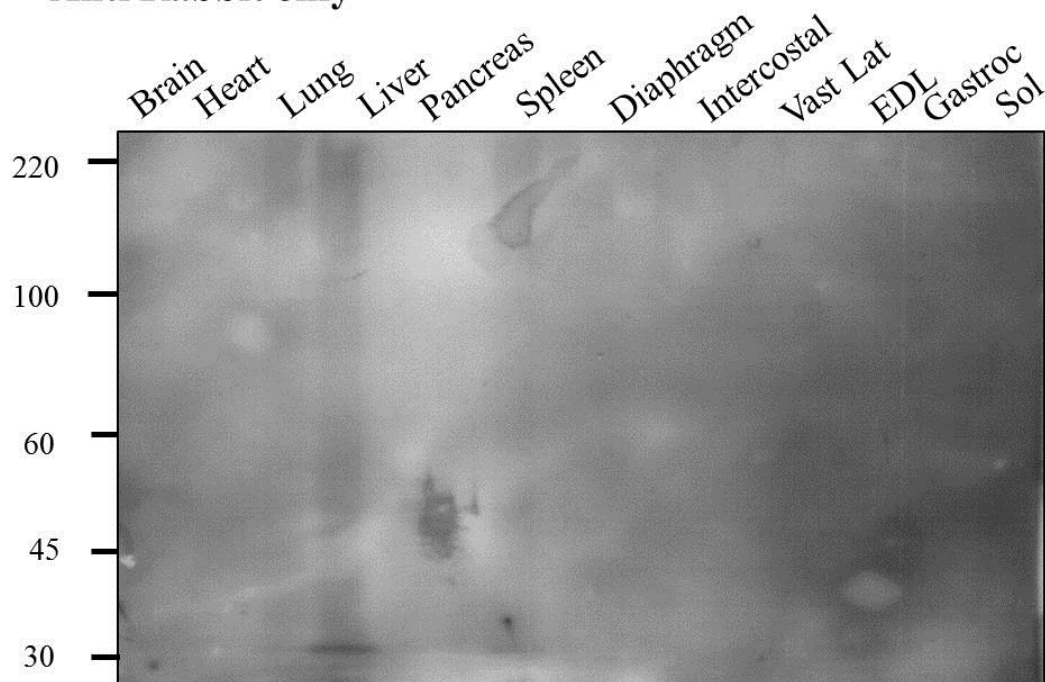
Figure 8.3.c: Anti-rabbit secondary control of Mouse organ and muscle tissue. Mouse organ tissue (brain, heart, lung, liver, pancreas, spleen) and muscle samples (diaphragm, intercostals, Vast lateralis, EDL, Gastrocnemuis, soleus) were analysed by western blot and incubated with anti-rabbit secondary antibody. Some bands were detected in lung, liver and spleen samples. No bands were detected in muscle samples.
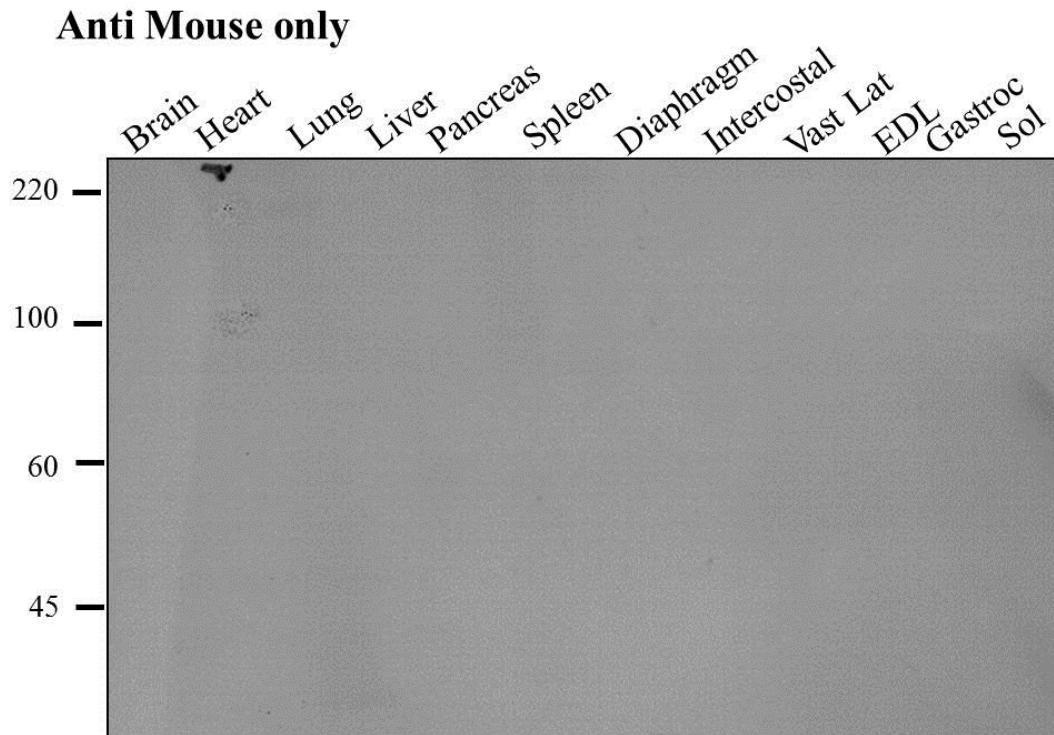
Anti Mouse only

Figure 8.3.d: Anti-Mouse secondary control western blot of mouse organ and muscle. Organ tissue (brain, heart, lung, liver, pancreas, spleen) and muscle samples (diaphragm, intercostals, vastus lateralis, EDL, gastrocnemius, soleus) were subjected to SDS-PAGE and western blot procedures and probed with anti mouse secondary antibodies. No bands were detected in any of the samples analysed.
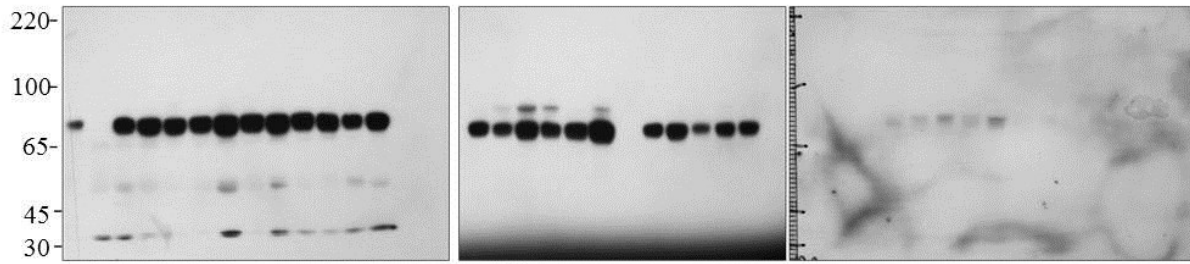
Figure 8.3.e: Quadriceps from adult and aged exercised and unexercised mouse probed with mAb VF1c and pAb JP1 antibodies. Blots were aligned visually using the molecular weight markers. A and C are the sme blot probed first with pAb JP1, stripped and reprobed with mAb VF1c. Blot B is exercised adult and aged samples.When lined up, it can be seen the two antibodies detect the same protein at different molecular weights. pAb JP1 detects full length JPH1, seen here at 75 kDa, and occasionally as a doublet. There is much more background detected with this antibody and it required long exposure. mAb VF1c detects several bands, at 75 kDa (full length), 65 kDa and much lower at 50 kDa(cleaved JPH1) The JP1 and VF1c bands line up at an apparent MW of 75 kDa in A and C, while the exercised samples in B shoe=w two main bands. Given that we know the binding locations of these anitbodies (Cterminal for JP1 and mid-region for VF1c) we can say that a cleavage effect is occurring due to exercise, which cleaved the JPH1 protein in the somewhere along the middle to C terminal portion.
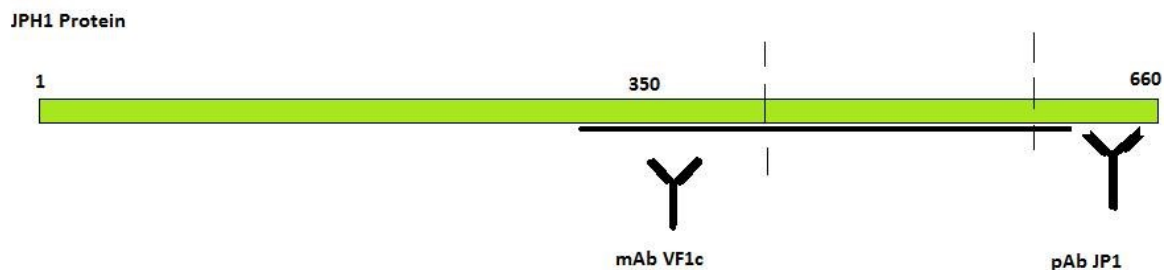
Figure 8.3.f: Diagram of possible cleavage of JPH1 protein (dashed lines). mAb VF1c and pAb JP1 binding regions are shown as well. Cleavage in the region of the dashed lines would account for the staining pattern seen using these antibodies, and is corroborated by the

calpain cleavage studies in chapter 5. If the caleage domains are conserved between JPH1 and 2 we can assume that the main calpain cleavage in JPH1 is also C terminal, as described for JPH2 in (Guo *et al,* 2015). This is supported by the experimental data shown in chapters 5 and 6.

References

Aigner, S., & Pette, D. (1992). Fast-to-slow transition in myosin heavy chain expression of rabbit muscle fibres induced by chronic low-frequency stimulation. *Symposia of the Society for Experimental Biology*, *46*, 311–7.

Almers, W., Stanfield, P. R., & Stühmer, W. (1983). Lateral distribution of sodium and potassium channels in frog skeletal muscle: measurements with a patch-clamp technique. *The Journal of Physiology*, *336*, 261–84

Andersson, D. C., Betzenhauser, M. J., Reiken, S., Umanskaya, A., Shiomi, T., & Marks, A. R. (2012). Stress-induced increase in skeletal muscle force requires protein kinase A phosphorylation of the ryanodine receptor. *The Journal of Physiology*, *590*(Pt 24), 6381–7.

Andersson, D. C., Betzenhauser, M. J., Reiken, S., Meli, A. C., Umanskaya, A., Xie, W., Shiomi, T. Zalk, R. Lacampagne, A.,Marks, A. R. (2011). Ryanodine receptor oxidation causes intracellular calcium leak and muscle weakness in aging. Cell Metabolism, 14(2), 196–207.

Altamirano, F., López, J. R., Henríquez, C., Molinski, T., Allen, P. D., & Jaimovich, E. (2012). Increased resting intracellular calcium modulates NF-κB-dependent inducible nitric-oxide synthase gene expression in dystrophic mdx skeletal myotubes. *The Journal of Biological Chemistry*, *287*(25), 20876–87.

Anderson, A. A., Treves, S., Biral, D., Betto, R., Sandonà, D., Ronjat, M., & Zorzato, F. (2003). The novel skeletal muscle sarcoplasmic reticulum JP-45 protein. Molecular cloning, tissue distribution, developmental expression, and interaction with alpha 1.1 subunit of the voltage-gated calcium channel. *The Journal of Biological Chemistry*, *278*(41), 39987–92.

Avila, G., O'Connell, K. M., Groom, L. A., & Dirksen, R. T. (2001). Ca2+ release through ryanodine receptors regulates skeletal muscle L-type Ca2+ channel expression. The Journal of Biological Chemistry, 276(21), 17732–8

Aronson, D., Violan, M. A., Dufresne, S. D., Zangen, D., Fielding, R. A., & Goodyear, L. J. (1997). Exercise stimulates the mitogen-activated protein kinase pathway in human skeletal muscle. *The Journal of Clinical Investigation*, *99*(6), 1251–7.

Bagnato, P., Barone, V., Giacomello, E., Rossi, D., & Sorrentino, V. (2003). Binding of an ankyrin-1 isoform to obscurin suggests a molecular link between the sarcoplasmic reticulum and myofibrils in striated muscles. *The Journal of Cell Biology*, *160*(2), 245–53

Bánhegyi, G., Csala, M., Nagy, G., Sorrentino, V., Fulceri, R., & Benedetti, A. (2003). Evidence for the transport of glutathione through ryanodine receptor channel type 1. *The Biochemical Journal*, *376*(Pt 3), 807–12.

Bannister, R. A. (2013). Dantrolene-induced inhibition of skeletal L-type Ca^{2+} current requires RyR1 expression. *BioMed Research International*, *2013*, 390493.

Baylor, S. M., & Hollingworth, S. (2003). Sarcoplasmic reticulum calcium release compared in slow-twitch and fast-twitch fibres of mouse muscle. *The Journal of Physiology*, *551*(Pt 1), 125–38.

Beard, N. A., Wei, L., & Dulhunty, A. F. (2009). Ca^{2+}) signaling in striated muscle: the elusive roles of triadin, junctin, and calsequestrin. *European Biophysics Journal : EBJ*, *39*(1), 27–36.

Beavers, D. L., Wang, W., Ather, S., Voigt, N., Garbino, A., Dixit, S. S., … Wehrens, X. H. T. (2013). Mutation E169K in junctophilin-2 causes atrial fibrillation due to impaired RyR2 stabilization. *Journal of the American College of Cardiology*, *62*(21), 2010–9.

Bellinger, A. M., Reiken, S., Carlson, C., Mongillo, M., Liu, X., Rothman, L., … Marks, A. R. (2009). Hypernitrosylated ryanodine receptor calcium release channels are leaky in dystrophic muscle. *Nature Medicine*, *15*(3), 325–30.

Berridge, M. J., Lipp, P., & Bootman, M. D. (2000). The versatility and universality of calcium signalling. *Nature Reviews. Molecular Cell Biology*, *1*(1), 11–21.

Berridge, M. J. (2004). Calcium signal transduction and cellular control mechanisms. *Biochimica et Biophysica Acta*, *1742*(1-3), 3–7.

Benacquista, B. L., Sharma, M. R., Samsó, M., Zorzato, F., Treves, S., & Wagenknecht, T. (2000). Amino acid residues 4425-4621 localized on the three-dimensional structure of the skeletal muscle ryanodine receptor. *Biophysical Journal*, *78*(3), 1349–58.

Boncompagni, S., d'Amelio, L., Fulle, S., Fano, G., & Protasi, F. (2006). Progressive Disorganization of the Excitation-Contraction Coupling Apparatus in Aging Human Skeletal Muscle as Revealed by Electron Microscopy: A Possible Role in the Decline of Muscle Performance. *The Journals of Gerontology Series A: Biological Sciences and Medical Sciences*, *61*(10), 995–1008.

Boncompagni, S., Loy, R. E., Dirksen, R. T., & Franzini-Armstrong, C. (2010). The I4895T mutation in the type 1 ryanodine receptor induces fiber-type specific alterations in skeletal muscle that mimic premature aging. *Aging Cell*, *9*(6), 958–70.

Bradford, M. (1976) A Rapid and Sensitive method for the Quantitation of Microgram Quantities of Protein Utilizing the method of Protein-Dye Binding. *Analytical Biochemistry*, 72, 248-254.

Brini, M., & Carafoli, E. (2011). The plasma membrane Ca^2+ ATPase and the plasma membrane sodium calcium exchanger cooperate in the regulation of cell calcium. *Cold Spring Harbor Perspectives in Biology*, *3*(2), a004168–.

Brulé, C., Dargelos, E., Diallo, R., Listrat, a, Béchet, D., Cottin, P., & Poussard, S. (2010). Proteomic study of calpain interacting proteins during skeletal muscle aging. *Biochimie*, *92*(12), 1923–33.

Brown, K.R., and Jurisica, I. (2005) Online Predicted Human Interaction Database. Bioinformatics, 21(9):2076-82

Brouchet, L., Krust, A., Dupont, S., Chambon, P., Bayard, F., & Arnal, J. F. (2001). Estradiol Accelerates Reendothelialization in Mouse Carotid Artery Through Estrogen Receptor-but Not Estrogen Receptor- . *Circulation*, *103*(3), 423–428.

Buck, E. D., Nguyen, H. T., Pessah, I. N., & Allen, P. D. (1997). Dyspedic mouse skeletal muscle expresses major elements of the triadic junction but lacks detectable ryanodine receptor protein and function. *The Journal of Biological Chemistry*, *272*(11), 7360–7.

Bultynck, G., De Smet, P., Rossi, D., Callewaert, G., Missiaen, L., Sorrentino, V., … Parys, J. B. (2001). Characterization and mapping of the 12 kDa FK506-binding protein (FKBP12)-binding site on different isoforms of the ryanodine receptor and of the inositol 1,4,5-trisphosphate receptor. *The Biochemical Journal*, *354*(Pt 2), 413–22.

Caldwell, T. A., Sumner, I., & Wright, N. T. (2015). Mechanical dissociation of the M-band titin/obscurin complex is directionally dependent. *FEBS Letters*, *589*(15), 1735–9.

Campbell, K. P., Knudson, C. M., Imagawa, T., Leung, A. T., Sutko, J. L., Kahl, S. D., … Madson, L. (1987). Identification and characterization of the high affinity [3H]ryanodine receptor of the junctional sarcoplasmic reticulum Ca2+ release channel. *The Journal of Biological Chemistry*, *262*(14), 6460–3.

Canato, M., Capitanio, P., Reggiani, C., & Cancellara, L. (2014). The disorders of the calcium release unit of skeletal muscles: what have we learned from mouse models? *Journal of Muscle Research and Cell Motility*. doi:10.1007/s10974-014-9396-7

Calderón, J. C., Bolaños, P., & Caputo, C. (2014). The excitation–contraction coupling mechanism in skeletal muscle. *Biophysical Reviews*, *6*(1), 133–160.

Camerino, G. M., Pierno, S., Liantonio, A., De Bellis, M., Cannone, M., Sblendorio, V., … Desaphy, J.-F. (2013). Effects of pleiotrophin overexpression on mouse skeletal muscles in normal loading and in actual and simulated microgravity. *PloS One*, *8*(8), e72028.

Capote, J., DiFranco, M., & Vergara, J. L. (2010). Excitation-contraction coupling alterations in mdx and utrophin/dystrophin double knockout mice: a comparative study. *American Journal of Physiology. Cell Physiology*, *298*(5), C1077–86.

Carberry, S., Brinkmeier, H., Zhang, Y., Winkler, C. K., & Ohlendieck, K. (2013). Comparative proteomic profiling of soleus, extensor digitorum longus, flexor digitorum brevis and interosseus muscles from the mdx mouse model of Duchenne muscular dystrophy. *International Journal of Molecular Medicine*, *32*(3), 544–556.

Carmody, M., Mackrill, J. J., Sorrentino, V., & O'Neill, C. (2001). FKBP12 associates tightly with the skeletal muscle type 1 ryanodine receptor, but not with other intracellular calcium release channels. *FEBS Letters*, *505*(1), 97–102.

Castets, P., Lescure, A., Guicheney, P., & Allamand, V. (2012). Selenoprotein N in skeletal muscle: from diseases to function. *Journal of Molecular Medicine (Berlin, Germany)*, *90*(10), 1095–107.

Chen, S. R., Vaughan, D. M., Airey, J. A., Coronado, R., & MacLennan, D. H. (1993). Functional expression of cDNA encoding the Ca2+ release channel (ryanodine receptor) of rabbit skeletal muscle sarcoplasmic reticulum in COS-1 cells. *Biochemistry*, *32*(14), 3743–53.

Cheng, H., & Lederer, W. J. (2008). Calcium sparks. *Physiological Reviews*, *88*(4), 1491–545.

Chien, M.-Y., Wu, Y.-T., Lee, P.-L., Chang, Y.-J., & Yang, P.-C. (2010). Inspiratory muscle dysfunction in patients with severe obstructive sleep apnoea. *The European Respiratory Journal*, *35*(2), 373–80.

Chopra, N., Yang, T., Asghari, P., Moore, E. D., Huke, S., Akin, B., … Knollmann, B. C. (2009). Ablation of triadin causes loss of cardiac Ca2+ release units, impaired excitation-contraction coupling, and cardiac arrhythmias. *Proceedings of the National Academy of Sciences of the United States of America*, *106*(18), 7636–41.

Choudhary, K.R., Zheng, L., Mackrill., J.J. (2010). Analysis of Spatial Distribution in Cells using Boundary Distance plots. *The Annals of Applied Statistics*. Vol. 4, No. 3, 1365–1382

Conti, A., Gorza, L., & Sorrentino, V. (1996). Differential distribution of ryanodine receptor type 3 (RyR3) gene product in mammalian skeletal muscles. *The Biochemical Journal*, *316 (Pt 1*, 19–23.

Cooke, R. (2004). The sliding filament model: 1972-2004. *The Journal of General Physiology*, *123*(6), 643–56.

Cornea, R. L., Nitu, F., Gruber, S., Kohler, K., Satzer, M., Thomas, D. D., & Fruen, B. R. (2009). FRET-based mapping of calmodulin bound to the RyR1 Ca2+ release channel. *Proceedings of the National Academy of Sciences of the United States of America*, *106*(15), 6128–33.

Corona, B. T., Balog, E. M., Doyle, J. A., Rupp, J. C., Luke, R. C., & Ingalls, C. P. (2010). Junctophilin damage contributes to early strength deficits and EC coupling failure after eccentric contractions. *American Journal of Physiology. Cell Physiology*, *298*(2), C365–76.

Cummings, L. J., Snyder, M. A., & Brisack, K. (2009). Protein chromatography on hydroxyapatite columns. *Methods in Enzymology*, *463*, 387–404.

Crabtree, G. R. (1999). Generic signals and specific outcomes: signaling through Ca2+, calcineurin, and NF-AT. *Cell*, *96*(5), 611–4.

Craig, R., & Woodhead, J. L. (2006). Structure and function of myosin filaments. *Current Opinion in Structural Biology*, *16*(2), 204–12.

Cruz-Jentoft, A. J., Landi, F., Schneider, S. M., Zuniga, C., Arai, H., Boirie, Y., … Cederholm, T. (2014). Prevalence of and interventions for sarcopenia in ageing adults: a systematic review. Report of the International Sarcopenia Initiative (EWGSOP and IWGS). *Age and Ageing*, *43*(6), 748–59.

Davies, K. E., & Nowak, K. J. (2006). Molecular mechanisms of muscular dystrophies: old and new players. *Nature Reviews. Molecular Cell Biology*, *7*(10), 762–73.

Davis, F. M., Parsonage, M. T., Cabot, P. J., Parat, M.-O., Thompson, E. W., Roberts-Thomson, S. J., & Monteith, G. R. (2013). Assessment of gene expression of intracellular calcium channels, pumps and exchangers with epidermal growth factor-induced epithelial-mesenchymal transition in a breast cancer cell line. *Cancer Cell International*, *13*(1), 76.

Dargelos, E., Brulé, C., Combaret, L., Hadj-Sassi, A., Dulong, S., Poussard, S., & Cottin, P. (2007). Involvement of the calcium-dependent proteolytic system in skeletal muscle aging. *Experimental Gerontology*, *42*(11), 1088–98.

Denborough, M.A., Forster, J.F.A., Lovell, R.R.H., Maplestone, P.A., Villiers, J.D. (1962). Anaesthetic deaths in a family. *BJA: British Journal of Anaesthesia*, *34*(6), 395–396.

Delbono, O., O'Rourke, K. S., & Ettinger, W. H. (1995). Excitation-calcium release uncoupling in aged single human skeletal muscle fibers. *The Journal of Membrane Biology*, *148*(3).

De Ménorval, M.-A., Mir, L. M., Fernández, M. L., & Reigada, R. (2012). Effects of dimethyl sulfoxide in cholesterol-containing lipid membranes: a comparative study of experiments in silico and with cells. *PloS One*, *7*(7), e41733. doi:10.1371/journal.pone.0041733

Dooley, J., Gordon, K. E., Dodds, L., & MacSween, J. (2010). Duchenne muscular dystrophy: a 30-year population-based incidence study. *Clinical Pediatrics*, *49*(2), 177–9.

Du, G. G. (2000). Mutation of Divergent Region 1 Alters Caffeine and Ca2+ Sensitivity of the Skeletal Muscle Ca2+ Release Channel (Ryanodine Receptor). *Journal of Biological Chemistry*, *275*(16), 11778–11783.

Dulhunty, A., Wei, L., & Beard, N. (2009). Junctin - the quiet achiever. *The Journal of Physiology*, *587*(Pt 13), 3135–7.

Efremov, R. G., Leitner, A., Aebersold, R., & Raunser, S. (2014). Architecture and conformational switch mechanism of the ryanodine receptor. *Nature*, *517*(7532), 39–43.

English, K.K., Sorrentino, V., Aiello, A.C., Kiely, M., Kiely, P.A., Mcdonagh, B., Mackrill, J.J. (2014) Closing a small gap in our understanding of excitation-contraction coupling: JSR90/JFP90 is Junctophilin 1. Calcium Signaling VOL.1 NO.1 2373-1168

Epstein, N. D., & Davis, J. S. (2003). Sensing stretch is fundamental. *Cell*, *112*(2), 147–50.

Evans, W. J., & Lexell, J. (1995). Human Aging, Muscle Mass, and Fiber Type Composition. *The Journals of Gerontology Series A: Biological Sciences and Medical Sciences*, *50A*(Special), 11–16.

Flucher, B. E., Obermair, G. J., Tuluc, P., Schredelseker, J., Kern, G., & Grabner, M. (2005). The role of auxiliary dihydropyridine receptor subunits in muscle. *Journal of Muscle Research and Cell Motility*, *26*(1), 1–6.

Feng, W., Tu, J., Yang, T., Vernon, P. S., Allen, P. D., Worley, P. F., & Pessah, I. N. (2002). Homer regulates gain of ryanodine receptor type 1 channel complex. *The Journal of Biological Chemistry*, *277*(47), 44722–30

Feng, W., Tu, J., Pouliquin, P., Cabrales, E., Shen, X., Dulhunty, A., … Pessah, I. N. (2008). Dynamic regulation of ryanodine receptor type 1 (RyR1) channel activity by Homer 1. *Cell Calcium*, *43*(3), 307–14.

Ferreiro, A., Quijano-Roy, S., Pichereau, C., Moghadaszadeh, B., Goemans, N., Bönnemann, C., … Guicheney, P. (2002). Mutations of the selenoprotein N gene, which is implicated in rigid spine muscular dystrophy, cause the classical phenotype of multiminicore disease: reassessing the nosology of early-onset myopathies. *American Journal of Human Genetics*, *71*(4), 739–49.

Fernando, P., Sandoz, J. S., Ding, W., de Repentigny, Y., Brunette, S., Kelly, J. F., … Megeney, L. A. (2009). Bin1 SRC homology 3 domain acts as a scaffold for myofiber sarcomere assembly. *The Journal of Biological Chemistry*, *284*(40), 27674–86.

Fill, M., & Copello, J. A. (2002). Ryanodine receptor calcium release channels. *Physiological Reviews*, *82*(4), 893–922.

Franzini-Armstrong, C., Pincon-Raymond, M., & Rieger, F. (1991). Muscle fibers from dysgenic mouse in vivo lack a surface component of peripheral couplings. *Developmental Biology*, *146*(2), 364–76.

Franzini-Armstrong, C. (2009). Architecture and regulation of the Ca2+ delivery system in muscle cells. *Applied Physiology, Nutrition, and Metabolism = Physiologie Appliquée, Nutrition et Métabolisme*, *34*(3), 323–7.

Fraysse, B., Liantonio, A., Cetrone, M., Burdi, R., Pierno, S., Frigeri, A. Camerino, C., De Luca, A. (2004). The alteration of calcium homeostasis in adult dystrophic mdx muscle fibers is worsened by a chronic exercise in vivo. *Neurobiology of Disease*, *17*(2), 144–54.

Froemming, G. R., Murray, B. E., Harmon, S., Pette, D., & Y, K. O. (2000). Comparative analysis of the isoform expression pattern of Ca -regulatory membrane proteins in fast-twitch , slow-twitch , cardiac , neonatal and chronic low-frequency stimulated muscle fibres. *Biochemica et Biophysica Acta 1466 (2000)* 151-168.

Froemming, G. R., Pette, D., & Ohlendieck, K. (1999). The 90-kDa junctional sarcoplasmic reticulum protein forms an integral part of a supramolecular triad complex in skeletal muscle. *Biochemical and Biophysical Research Communications*, *261*(3), 603–9.

Fukami, K., Inanobe, S., Kanemaru, K., & Nakamura, Y. (2010). Phospholipase C is a key enzyme regulating intracellular calcium and modulating the phosphoinositide balance. *Progress in Lipid Research*, *49*(4), 429–37.

Furthmayr, H., & Marchesi, V. T. (1976). Subunit structure of human erythrocyte glycophorin A. *Biochemistry*, *15*(5), 1137–1144.

Gaburjakova, M., Gaburjakova, J., Reiken, S., Huang, F., Marx, S. O., Rosemblit, N., & Marks, A. R. (2001). FKBP12 binding modulates ryanodine receptor channel gating. *The Journal of Biological Chemistry*, *276*(20), 16931–5.

Garbino, A., van Oort, R. J., Dixit, S. S., Landstrom, A. P., Ackerman, M. J., & Wehrens, X. H. T. (2009). Molecular evolution of the junctophilin gene family. *Physiological Genomics*, *37*(3), 175–86.

Galbiati, F., Engelman, J. A., Volonte, D., Zhang, X. L., Minetti, C., Li, M., … Lisanti, M. P. (2001). Caveolin-3 null mice show a loss of caveolae, changes in the microdomain

distribution of the dystrophin-glycoprotein complex, and t-tubule abnormalities. *The Journal of Biological Chemistry*, *276*(24), 21425–33.

Gaburjakova, M., Gaburjakova, J., Reiken, S., Huang, F., Marx, S. O., Rosemblit, N., & Marks, A. R. (2001). FKBP12 binding modulates ryanodine receptor channel gating. *The Journal of Biological Chemistry*, *276*(20), 16931–5.

Gehlert, S., Bungartz, G., Willkomm, L., Korkmaz, Y., Pfannkuche, K., Schiffer, T., … Suhr, F. (2012). Intense resistance exercise induces early and transient increases in ryanodine receptor 1 phosphorylation in human skeletal muscle. *PloS One, 7*(11), e49326.

Girard, T., Cavagna, D., Padovan, E., Spagnoli, G., Urwyler, A., Zorzato, F., & Treves, S. (2001). B-lymphocytes from Malignant Hyperthermia-susceptible Patients Have an Increased Sensitivity to Skeletal Muscle Ryanodine Receptor Activators. *J. Biol. Chem.*, *276*(51), 48077–48082.

Golini, L., Chouabe, C., Berthier, C., Cusimano, V., Fornaro, M., Bonvallet, R., … Sorrentino, V. (2011). Junctophilin 1 and 2 interact with the L-type Ca2+ channel dihydropyridine receptors (DHPRs) in skeletal muscle. *The Journal of Biological Chemistry*, *286*(51), 43717–43725.

Goonasekera, S. A., Beard, N. A., Groom, L., Kimura, T., Lyfenko, A. D., Rosenfeld, A., … Dirksen, R. T. (2007). Triadin binding to the C-terminal luminal loop of the ryanodine receptor is important for skeletal muscle excitation contraction coupling. *The Journal of General Physiology*, *130*(4), 365–78.

Goonasekera, S. A., Davis, J., Kwong, J. Q., Accornero, F., Wei-LaPierre, L., Sargent, M. A., Dirksen, R. T., Molkentin, J. D. (2014). Enhanced Ca^{2+} influx from STIM1-Orai1 induces muscle pathology in mouse models of muscular dystrophy. *Human Molecular Genetics*, *23*(14), 3706–15.

Gordon, A. M., Huxley, A. F., & Julian, F. J. (1966). The variation in isometric tension with sarcomere length in vertebrate muscle fibres. *The Journal of Physiology*, *184*(1), 170–92.

Gheorghe, M., Snoeck, M., Emmerich, M., Bäck, T., Goeman, J. J., & Raz, V. (2014). Major aging-associated RNA expressions change at two distinct age-positions. *BMC Genomics*, *15*, 132.

Guo, A., Hall, D., Zhang, C., Peng, T., Miller, J. D., Kutschke, W., … Song, L.-S. (2015). Molecular determinants of calpain-dependent cleavage of junctophilin-2 in cardiomyocytes. *The Journal of Biological Chemistry*.

Guo, W., Jorgensen, A. O., & Campbell, K. P. (1994). Characterization and ultrastructural localization of a novel 90-kDa protein unique to skeletal muscle junctional sarcoplasmic reticulum. *The Journal of Biological Chemistry*, *269*(45), 28359–65.

Guo, A., Zhang, X., Iyer, V. R., Chen, B., Zhang, C., Kutschke, W. J., … Song, L.-S. (2014). Overexpression of junctophilin-2 does not enhance baseline function but attenuates heart failure development after cardiac stress. *Proceedings of the National Academy of Sciences of the United States of America*, *111*(33), 12240–5.

Gundersen, K. (2011). Excitation-transcription coupling in skeletal muscle: the molecular pathways of exercise. *Biological Reviews of the Cambridge Philosophical Society*, *86*(3), 564–600

Guo, A., Hall, D., Zhang, C., Peng, T., Miller, J. D., Kutschke, W., … Song, L.-S. (2015). Molecular determinants of calpain-dependent cleavage of junctophilin-2 in cardiomyocytes. *The Journal of Biological Chemistry*.

Guo, A., Zhang, X., Iyer, V. R., Chen, B., Zhang, C., Kutschke, W. J., … Song, L.-S. (2014). Overexpression of junctophilin-2 does not enhance baseline function but attenuates heart failure development after cardiac stress. *Proceedings of the National Academy of Sciences of the United States of America*, *111*(33), 12240–5.

Guse, A. H., Tsygankov, A. Y., Weber, K., & Mayr, G. W. (2001). Transient tyrosine phosphorylation of human ryanodine receptor upon T cell stimulation. *The Journal of Biological Chemistry*, *276*(37), 34722–7.

Hammoud, Y., Rice, T., & Mackrill, J. J. (2013). Oxysterols modulate calcium signalling in the A7r5 aortic smooth muscle cell-line. *Biochimie*, *95*(3), 568–77.

He, L.-L., Zhang, Y., Chen, Y.-H., Yamada, Y., & Yang, J. (2007). Functional modularity of the beta-subunit of voltage-gated Ca2+ channels. *Biophysical Journal*, *93*(3), 834–45.

Hirata, Y., Brotto, M., Weisleder, N., Chu, Y., Lin, P., Zhao, X., … Pan, Z. (2006). Uncoupling store-operated Ca2+ entry and altered Ca2+ release from sarcoplasmic reticulum through silencing of junctophilin genes. *Biophysical Journal*, *90*(12), 4418–27.

Hirata, H., Watanabe, T., Hatakeyama, J., Sprague, S. M., Saint-Amant, L., Nagashima, A., … Kuwada, J. Y. (2007). Zebrafish relatively relaxed mutants have a ryanodine receptor defect, show slow swimming and provide a model of multi-minicore disease. *Development (Cambridge, England)*, *134*(15), 2771–81.

Holmberg, A., Blomstergren, A., Nord, O., Lukacs, M., Lundeberg, J., & Uhlén, M. (2005). The biotin-streptavidin interaction can be reversibly broken using water at elevated temperatures. *Electrophoresis*, *26*(3), 501–10.

Høydal, M. A., Stølen, T. O., Johnsen, A. B., Alvez, M., Catalucci, D., Condorelli, G., … Wisløff, U. (2014). Reduced aerobic capacity causes leaky ryanodine receptors that trigger arrhythmia in a rat strain artificially selected and bred for low aerobic running capacity. *Acta Physiologica (Oxford, England)*, *210*(4), 854–64.

Hosoi, E., Nishizaki, C., Gallagher, K. L., Wyre, H. W., Matsuo, Y., & Sei, Y. (2001). Expression of the ryanodine receptor isoforms in immune cells. *Journal of Immunology (Baltimore, Md. : 1950)*, *167*(9), 4887–94.

Hou, Y., Morrison, C. J., & Cramer, S. M. (2011). Classification of protein binding in hydroxyapatite chromatography: synergistic interactions on the molecular scale. *Analytical Chemistry*, *83*(10), 3709–16.

Hu, L.-Y. R., Ackermann, M. A., & Kontrogianni-Konstantopoulos, A. (2015). The sarcomeric M-region: a molecular command center for diverse cellular processes. *BioMed Research International*, *2015*, 714197.

Huang, X., Fruen, B., Farrington, D. T., Wagenknecht, T., & Liu, Z. (2012). Calmodulin-binding locations on the skeletal and cardiac ryanodine receptors. *The Journal of Biological Chemistry*, *287*(36), 30328–35.

Huddleston, A. T., Tang, W., Takeshima, H., Hamilton, S. L., & Klann, E. (2008). Superoxide-induced potentiation in the hippocampus requires activation of ryanodine receptor type 3 and ERK. *Journal of Neurophysiology*, *99*(3), 1565–71.

Huxley, A.F., Niedergerke, R. (1954) Structural Changes in Muscle during Contraction: Interference Microscopy of living muscle fibres. *Nature, 173*(4412), 973–976.

Huxley H., & Hanson J. (1954). Changes in the Cross-Striations of Muscle during Contraction and Stretch and their Structural Interpretation. *Nature*, *173*(4412), 973–976.

Huxley, A. F., & Simmons, R. M. (1971). Proposed Mechanism of Force Generation in Striated Muscle. *Nature*, *233*(5321), 533–538.

Huxley, A. F. (1975). The origin of force in skeletal muscle. *Ciba Foundation Symposium*, (31), 271–90

Hwang, C. Y., Kim, K., Choi, J. Y., Bahn, Y. J., Lee, S.-M., Kim, Y. K., … Kwon, K.-S. (2013). Quantitative proteome analysis of age-related changes in mouse gastrocnemius muscle using mTRAQ. *Proteomics*.

Ito, K., Komazaki, S., Sasamoto, K., Yoshida, M., Nishi, M., Kitamura, K., & Takeshima, H. (2001). Deficiency of triad junction and contraction in mutant skeletal muscle lacking junctophilin type 1. *The Journal of Cell Biology*, *154*(5), 1059–67.

Jang, I. K., Cronshaw, D. G., Xie, L., Fang, G., Zhang, J., Oh, H., … Zou, Y. (2011). Growth-factor receptor-bound protein-2 (Grb2) signaling in B cells controls lymphoid follicle organization and germinal center reaction. *Proceedings of the National Academy of Sciences of the United States of America*, *108*(19), 7926–31.

Jayasinghe, I. D., Baddeley, D., Kong, C. H. T., Wehrens, X. H. T., Cannell, M. B., & Soeller, C. (2012). Nanoscale organization of junctophilin-2 and ryanodine receptors within peripheral couplings of rat ventricular cardiomyocytes. *Biophysical Journal*, *102*(5), L19–21.

Jayasinghe, I. D., Munro, M., Baddeley, D., Launikonis, B. S., & Soeller, C. (2014). Observation of the molecular organization of calcium release sites in fast- and slow-twitch skeletal muscle with nanoscale imaging. *Journal of the Royal Society, Interface / the Royal Society*, *11*(99), 20140570–.

Jia, C. Y. H., Nie, J., Wu, C., Li, C., & Li, S. S.-C. (2005). Novel Src homology 3 domain-binding motifs identified from proteomic screen of a Pro-rich region. *Molecular & Cellular Proteomics : MCP*, *4*(8), 1155–66.

Jóna, I., Szegedi, C., Sárközi, S., Szentesi, P., Csernoch, L., & Kovács, L. (2001). Altered inhibition of the rat skeletal ryanodine receptor/calcium release channel by magnesium in the presence of ATP. *Pflügers Archiv : European Journal of Physiology*, *441*(6), 729–38.

Jørgensen, L.H., Larochelle, N., Orlopp, K., Dunant,P., Dudley, R.W., Stucka, R., Thirion,C., Walter, M.C., Laval, S.H., Lochmüller, H. (2009) Effecient and fast functional screening of microdystrophin constructs in vivo and in vitro for therapy of Duchenne Muscular Dystrophy. Hum. Gene Ther., Jun: 20(6):641-650

Jurynec, M. J., Xia, R., Mackrill, J. J., Gunther, D., Crawford, T., Flanigan, K. M., … Grunwald, D. J. (2008). Selenoprotein N is required for ryanodine receptor calcium release channel activity in human and zebrafish muscle. *Proceedings of the National Academy of Sciences of the United States of America*, *105*(34), 12485–90.

Jungbluth, H. (2007). Central core disease. *Orphanet Journal of Rare Diseases*, *2*(1), 25.

Jungbluth, H. (2007). Multi-minicore Disease. *Orphanet Journal of Rare Diseases*, *2*(1), 31.

Kablar, B., Krastel, K., Ying, C., Asakura, A., Tapscott, S., & Rudnicki, M. (1997). MyoD and Myf-5 differentially regulate the development of limb versus trunk skeletal muscle. Development, 124(23), 4729–4738.

Kalhovde, J. M., Jerkovic, R., Sefland, I., Cordonnier, C., Calabria, E., Schiaffino, S., & Lømo, T. (2005). "Fast" and "slow" muscle fibres in hindlimb muscles of adult rats regenerate from intrinsically different satellite cells. The Journal of Physiology, 562(Pt 3), 847–57.

Kang, H., Freund, C., Duke-Cohan, J. S., Musacchio, A., Wagner, G., & Rudd, C. E. (2000). SH3 domain recognition of a proline-independent tyrosine-based RKxxYxxY motif in immune cell adaptor SKAP55. *The EMBO Journal*, *19*(12), 2889–99.

Katayama, K., Matsuo, H., Ishida, K., Mori, S., & Miyamura, M. (2003). Intermittent hypoxia improves endurance performance and submaximal exercise efficiency. *High Altitude Medicine & Biology*, *4*(3), 291–304.

Katusic, Z. S., Shepherd, J. T., & Vanhoutte, P. M. (1988). Endothelium-dependent contractions to calcium ionophore A23187, arachidonic acid, and acetylcholine in canine basilar arteries. *Stroke*, *19*(4), 476–479.

Kim, J. H., Chang, T. M., Graham, A. N., Choo, K. H. A., Kalitsis, P., & Hudson, D. F. (2010). Streptavidin-Binding Peptide (SBP)-tagged SMC2 allows single-step affinity fluorescence, blotting or purification of the condensin complex. *BMC Biochemistry*, *11*, 50.

Kobayashi, T., Morone, N., Kashiyama, T., Oyamada, H., Kurebayashi, N., & Murayama, T. (2008). Engineering a novel multifunctional green fluorescent protein tag for a wide variety of protein research. *PloS One*, *3*(12), e3822

Kohn, T. A., & Myburgh, K. H. (2007). Regional specialization of rat quadriceps myosin heavy chain isoforms occurring in distal to proximal parts of middle and deep regions is not mirrored by citrate synthase activity. *Journal of Anatomy*, *210*(1), 8–18.

Kong, H., Wang, R., Chen, W., Zhang, L., Chen, K., Shimoni, Y., … Chen, S. R. W. (2007). Skeletal and cardiac ryanodine receptors exhibit different responses to Ca2+ overload and luminal ca2+. *Biophysical Journal*, *92*(8), 2757–70.

Koutsioumpa, M., Drosou, G., Mikelis, C., Theochari, K., Vourtsis, D., Katsoris, P., Giannopoulou, E., Courty, J.,Petrou, C.,Magafa, V.,Cordopatis, P., Papadimitriou, E. (2012). Pleiotrophin expression and role in physiological angiogenesis in vivo: potential involvement of nucleolin. Vascular Cell, 4(1), 4.

Kontrogianni-Konstantopoulos, A., Jones, E. M., Van Rossum, D. B., & Bloch, R. J. (2003). Obscurin is a ligand for small ankyrin 1 in skeletal muscle. *Molecular Biology of the Cell*, *14*(3), 1138–48. doi:10.1091/mbc.E02-07-0411

Kozian, D., Proulle, V., Nitsche, A., Galitzine, M., Martinez, M.-C., Schumann, B., … Kerbiriou-Nabias, D. (2005). Identification of genes involved in Ca2+ ionophore A23187-mediated apoptosis and demonstration of a high susceptibility for transcriptional repression of cell cycle genes in B lymphoblasts from a patient with Scott syndrome. *BMC Genomics*, *6*(1), 146.

Kyrychenko, S., Poláková, E., Kang, C., Pocsai, K., Ullrich, N. D., Niggli, E., & Shirokova, N. (2013). Hierarchical accumulation of RyR post-translational modifications drives disease progression in dystrophic cardiomyopathy. *Cardiovascular Research*, *97*(4), 666–75.

Larson, S. M., & Davidson, a R. (2000). The identification of conserved interactions within the SH3 domain by alignment of sequences and structures. *Protein Science : A Publication of the Protein Society*, *9*(11), 2170–80.

Larcher, T., Lafoux, A., Tesson, L., Remy, S., Thepenier, V.,François, V., Le Guiner, C.,Goubin, H.,Dutilleul, M.,Guigand, L.,Toumaniantz, G.,De Cian, A.,Boix, C.,Renaud, J.,Cherel, Y.,Giovannangeli, C.,Concordet, J.,Anegon, I., Huchet, C. (2014). Characterization of Dystrophin Deficient Rats: A New Model for Duchenne Muscular Dystrophy. PloS One, 9(10), e110371.

Landstrom, A. P., Weisleder, N., Batalden, K. B., Bos, J. M., Tester, D. J., Ommen, S. R., … Ackerman, M. J. (2007). Mutations in JPH2-encoded junctophilin-2 associated with hypertrophic cardiomyopathy in humans. *Journal of Molecular and Cellular Cardiology*, *42*(6), 1026–35.

Lexell, J., Taylor, C. C., & Sjöström, M. (1988). What is the cause of the ageing atrophy? Total number, size and proportion of different fiber types studied in whole vastus lateralis muscle from 15- to 83-year-old men. *Journal of the Neurological Sciences*, *84*(2-3), 275–94.

Li, H., Ding, X., Lopez, J. R., Takeshima, H., Ma, J., Allen, P. D., & Eltit, J. M. (2010). Impaired Orai1-mediated Resting Ca2+ Entry Reduces the Cytosolic [Ca2+] and Sarcoplasmic Reticulum Ca2+ Loading in Quiescent Junctophilin 1 Knock-out Myotubes. *Journal of Biological Chemistry*, *285*(50), 39171–39179.

Li, X.-Q., Zheng, Y.-M., Rathore, R., Ma, J., Takeshima, H., & Wang, Y.-X. (2009). Genetic evidence for functional role of ryanodine receptor 1 in pulmonary artery smooth muscle cells. *Pflügers Archiv : European Journal of Physiology*, *457*(4), 771–83.

Lin, C.-C., Melo, F. A., Ghosh, R., Suen, K. M., Stagg, L. J., Kirkpatrick, J., … Ladbury, J. E. (2012). Inhibition of basal FGF receptor signaling by dimeric Grb2. *Cell*, *149*(7), 1514–24.

Lieber, R. L., & Ward, S. R. (2011). Skeletal muscle design to meet functional demands. *Philosophical Transactions of the Royal Society of London. Series B, Biological Sciences*, *366*(1570), 1466–76.

Liu, X., Liu, M., Zhang, J., Bai, X., Ramos, F., Van Remmen, H., Richardson, A.,Liu, F.,Dong, L.,Liu, F. (2009). Downregulation of Grb2 contributes to the insulin-sensitizing effect of calorie restriction. American Journal of Physiology. Endocrinology and Metabolism, 296(5), E1067–75.

Lukyanenko, V., Györke, I., Subramanian, S., Smirnov, A., Wiesner, T. F., & Györke, S. (2000). Inhibition of Ca(2+) sparks by ruthenium red in permeabilized rat ventricular myocytes. *Biophysical Journal*, *79*(3), 1273–84.

Luther, P. K. (2000). Three-dimensional structure of a vertebrate muscle Z-band: implications for titin and alpha-actinin binding. *Journal of Structural Biology*, *129*(1), 1–16.

Luther, P. K., Padrón, R., Ritter, S., Craig, R., & Squire, J. M. (2003). Heterogeneity of Z-band structure within a single muscle sarcomere: implications for sarcomere assembly. *Journal of Molecular Biology*, *332*(1), 161–9.

Mackrill, J. J., Challiss, R. A., O'Connell, D. A., Lai, F. A., & Nahorski, S. R. (1997). Differential expression and regulation of ryanodine receptor and myo-inositol 1,4,5-trisphosphate receptor Ca2+ release channels in mammalian tissues and cell lines. *The Biochemical Journal*, *327 (Pt 1*, 251–8.

Mackrill, J. J. (1998). Possible regulation of the skeletal muscle ryanodine receptor by a polyubiquitin binding subunit of the 26S proteasome. *Biochemical and Biophysical Research Communications*, *245*(2), 428–9.

Mackrill, J. J. (1999). Protein-protein interactions in intracellular Ca2+-release channel function. *The Biochemical Journal*, *337 (Pt 3*, 345–61.

Mackrill, J. J., O'Driscoll, S., Lai, F. A., & McCarthy, T. V. (2001). Analysis of type 1 ryanodine receptor-12 kDa FK506-binding protein interaction. *Biochemical and Biophysical Research Communications*, *285*(1), 52–7

Mackrill, J. J. (2010). Ryanodine receptor calcium channels and their partners as drug targets. *Biochemical Pharmacology*, *79*(11), 1535–43

Mackrill, J. J. (2011). Oxysterols and calcium signal transduction. *Chemistry and Physics of Lipids*, *164*(6), 488–95. doi:10.1016/j.chemphyslip.2011.04.001

Mackrill, J. J. (2012). Ryanodine receptor calcium release channels: an evolutionary perspective. *Advances in Experimental Medicine and Biology*, *740*, 159–82. doi:10.1007/978-94-007-2888-2_7

Maignan, S., Guilloteau, J. P., Fromage, N., Arnoux, B., Becquart, J., & Ducruix, A. (1995). Crystal structure of the mammalian Grb2 adaptor. *Science (New York, N.Y.)*, *268*(5208), 291–3.

McKay, B. R., Ogborn, D. I., Baker, J. M., Toth, K. G., Tarnopolsky, M. A., & Parise, G. (2013). Elevated SOCS3 and altered IL-6 signaling is associated with age-related human muscle stem cell dysfunction. *American Journal of Physiology. Cell Physiology*, *304*(8), C717–28.

Maclennan, D. H., & Zvaritch, E. (2010). Mechanistic models for muscle diseases and disorders originating in the sarcoplasmic reticulum. *Biochimica et Biophysica Acta*.

McPherson, P. S., Czernik, A. J., Chilcote, T. J., Onofri, F., Benfenati, F., Greengard, P., … De Camilli, P. (1994). Interaction of Grb2 via its Src homology 3 domains with synaptic proteins including synapsin I. *Proceedings of the National Academy of Sciences of the United States of America*, *91*(14), 6486–90.

Maina, F., Casagranda, F., Audero, E., Simeone, A., Comoglio, P. M., Klein, R., & Ponzetto, C. (1996). Uncoupling of Grb2 from the Met Receptor In Vivo Reveals Complex Roles in Muscle Development. *Cell*, *87*(3), 531–542.

Mayer, B. J. (2001). SH3 domains: complexity in moderation. *Journal of Cell Science*, *114*(Pt 7), 1253–63.

Margolis, R. (2003). Huntington's disease-like 2: a clinical, pathological, and molecular comparison to Huntington's disease. *Clinical Neuroscience Research*, *3*(3), 187–196.

Marín-Aguilera, M., Codony-Servat, J., Kalko, S. G., Fernández, P. L., Bermudo, R., Buxo, E., Mellado, B. (2012). Identification of docetaxel resistance genes in castration-resistant prostate cancer. *Molecular Cancer Therapeutics*, *11*(2), 329–39.

Marx, S. O., Reiken, S., Hisamatsu, Y., Jayaraman, T., Burkhoff, D., Rosemblit, N., & Marks, A. R. (2000). PKA phosphorylation dissociates FKBP12.6 from the calcium release channel (ryanodine receptor): defective regulation in failing hearts. *Cell*, *101*(4), 365–76

McArdle, A., Pattwell, D., Vasilaki, A., Griffiths, R. D., & Jackson, M. J. (2001). Contractile activity-induced oxidative stress: cellular origin and adaptive responses. *Am J Physiol Cell Physiol*, *280*(3), C621–627

McCarthy, T. V, & Mackrill, J. J. (2004). Unravelling calcium-release channel gating: clues from a "hot" disease. *The Biochemical Journal*, *380*(Pt 2), e1–3.

Minetti, C., Sotgia, F., Bruno, C., Scartezzini, P., Broda, P., Bado, M, Bruno, C. Scartezzini, P. Broda, P.Bado, M. Masetti, E. Mazzocco, M. Egeo, A. Donati, M A.Volonte, D. Galbiati, F.Cordone, G. Bricarelli, F DLisanti, M P Zara, F. (1998). Mutations in the caveolin-3 gene cause autosomal dominant limb-girdle muscular dystrophy. Nature Genetics, 18(4), 365–8.

Mitchell, W. K., Williams, J., Atherton, P., Larvin, M., Lund, J., & Narici, M. (2012). Sarcopenia, dynapenia, and the impact of advancing age on human skeletal muscle size and strength; a quantitative review. *Frontiers in Physiology*, *3*, 260.

Minamisawa, S., Oshikawa, J., Takeshima, H., Hoshijima, M., Wang, Y., Chien, K. R., Ishikawa, Y. Matsuoka, R. (2004). Junctophilin type 2 is associated with caveolin-3 and is down-regulated in the hypertrophic and dilated cardiomyopathies. Biochemical and Biophysical Research Communications, 325(3), 852–6.

Monnier, N., Procaccio, V., Stieglitz, P., & Lunardi, J. (1997). Malignant-Hyperthermia Susceptibility Is Associated with a Mutation of the a1-Subunit of the Human Dihydropyridine-Sensitive L-Type Voltage-Dependent Calcium-Channel Receptor in Skeletal Muscle. *The American Journal of Human Genetics*, *60*(6), 1316–1325.

Monnier, N. (2003). A homozygous splicing mutation causing a depletion of skeletal muscle RYR1 is associated with multi-minicore disease congenital myopathy with ophthalmoplegia. *Human Molecular Genetics*, *12*(10), 1171–1178.

Morris, V. C., Murray, M. P., Delancey, J. O. L., & Ashton-Miller, J. A. (2012). A comparison of the effect of age on levator ani and obturator internus muscle cross-sectional areas and volumes in nulliparous women. *Neurourology and Urodynamics*, *31*(4), 481–6.

Murayama, T., & Ogawa, Y. (1997). Characterization of Type 3 Ryanodine Receptor (RyR3) of Sarcoplasmic Reticulum from Rabbit Skeletal Muscles. *Journal of Biological Chemistry*, *272*(38), 24030–24037.

Murphy, R. M., Dutka, T. L., Horvath, D., Bell, J. R., Delbridge, L. M., & Lamb, G. D. (2013). Ca2+-dependent proteolysis of junctophilin-1 and junctophilin-2 in skeletal and cardiac muscle. *The Journal of Physiology*, *591*(Pt 3), 719–29.

Nagaraj, R. Y., Nosek, C. M., Brotto, M. A., Nishi, M., Takeshima, H., Nosek, T. M., & Ma, J. (2000). Increased susceptibility to fatigue of slow- and fast-twitch muscles from mice lacking the MG29 gene. *Physiological Genomics*, *4*(1), 43–9.

Nishi, M., Mizushima, A., Nakagawara, K. i, & Takeshima, H. (2000). Characterization of human junctophilin subtype genes. *Biochemical and Biophysical Research Communications*, *273*(3), 920–7.

Nishi, M., Hashimoto, K., Kuriyama, K., Komazaki, S., Kano, M., Shibata, S., & Takeshima, H. (2002). Motor discoordination in mutant mice lacking junctophilin type 3. *Biochemical and Biophysical Research Communications*, *292*(2), 318–24.

Nordsborg, N. B., Siebenmann, C., Jacobs, R. A., Rasmussen, P., Diaz, V., Robach, P., & Lundby, C. (2012). Four weeks of normobaric "live high-train low" do not alter muscular or systemic capacity for maintaining pH and K^+ homeostasis during intense exercise. *Journal of Applied Physiology (Bethesda, Md. : 1985)*, *112*(12), 2027–36.

Obermann, W. M., Gautel, M., Steiner, F., van der Ven, P. F., Weber, K., & Fürst, D. O. (1996). The structure of the sarcomeric M band: localization of defined domains of myomesin, M-protein, and the 250-kD carboxy-terminal region of titin by immunoelectron microscopy. *The Journal of Cell Biology*, *134*(6), 1441–53.

Oddoux, S., Brocard, J., Schweitzer, A., Szentesi, P., Giannesini, B., Brocard, J., Fauré, J.,Pernet-Gallay, K.,Bendahan, D.,Lunardi, J.,Csernoch, L.,Marty, I. (2009). Triadin

deletion induces impaired skeletal muscle function. The Journal of Biological Chemistry, 284(50), 34918–29.

Ohlendieck, K., Briggs, F. N., Lee, K. F., Wechsler, a W., & Campbell, K. P. (1991). Analysis of excitation-contraction-coupling components in chronically stimulated canine skeletal muscle. *European Journal of Biochemistry / FEBS*, *202*(3), 739–47.

Olojo, R. O., Hernández-Ochoa, E. O., Ikemoto, N., & Schneider, M. F. (2011). Effects of conformational peptide probe DP4 on bidirectional signaling between DHPR and RyR1 calcium channels in voltage-clamped skeletal muscle fibers. *Biophysical Journal*, *100*(10), 2367–77. *1466*, 151–168.

Ondrias, K., Marx, S. O., Gaburjakova M., & Marks, A. R. (1998). FKBP12 Modulates Gating of the Ryanodine Receptor/Calcium Release Channel. *Annals of the New York Academy of Sciences*, *853*(1 CARDIAC SARCO), 149–156.

Oulès, B., Del Prete, D., Greco, B., Zhang, X., Lauritzen, I., Sevalle, J., … Chami, M. (2012). Ryanodine receptor blockade reduces amyloid-β load and memory impairments in Tg2576 mouse model of Alzheimer disease. *The Journal of Neuroscience : The Official Journal of the Society for Neuroscience*, *32*(34), 11820–34.

Park, H., Park, I. Y., Kim, E., Youn, B., Fields, K., Dunker, A. K., & Kang, C. (2004). Comparing skeletal and cardiac calsequestrin structures and their calcium binding: a proposed mechanism for coupled calcium binding and protein polymerization. *The Journal of Biological Chemistry*, *279*(17), 18026–33.

Park, S.-K., & Prolla, T. A. (2005). Gene expression profiling studies of aging in cardiac and skeletal muscles. *Cardiovascular Research*, *66*(2), 205–12.

Parsons, S. A., Wilkins, B. J., Bueno, O. F., & Molkentin, J. D. (2003). Altered Skeletal Muscle Phenotypes in Calcineurin A and A Gene-Targeted Mice. *Molecular and Cellular Biology*, *23*(12), 4331–4343.

Parsons, S. A., Millay, D. P., Wilkins, B. J., Bueno, O. F., Tsika, G. L., Neilson, J. R., … Molkentin, J. D. (2004). Genetic loss of calcineurin blocks mechanical overload-induced skeletal muscle fiber type switching but not hypertrophy. *The Journal of Biological Chemistry*, *279*(25), 26192–200.

Partridge, T. A. (2013). The mdx mouse model as a surrogate for Duchenne muscular dystrophy. The FEBS Journal, 280(17), 4177–86

Paul-Pletzer, K., Yamamoto, T., Bhat, M. B., Ma, J., Ikemoto, N., Jimenez, L. S., Morimoto, H.,Williams, P. G., Parness, J. (2002). Identification of a dantrolene-binding sequence on the skeletal muscle ryanodine receptor. The Journal of Biological Chemistry, 277(38), 34918–23.

Pette, D., & Staron, R. S. (1997). Mammalian skeletal muscle fiber type transitions. *International Review of Cytology*, *170*, 143–223.

Pette, D., & Staron, R. S. (2000). Myosin isoforms, muscle fiber types, and transitions. *Microscopy Research and Technique*, *50*(6), 500–9.

Pette, D., & Staron, R. S. (2001). Transitions of muscle fiber phenotypic profiles. Histochemistry and Cell Biology, 115(5), 359–72.

Phimister, A. J., Lango, J., Lee, E. H., Ernst-Russell, M. A, Takeshima, H., Ma, J., Lee, Eun Allen, P.D., Pessah, I. N. (2007). Conformation-dependent stability of junctophilin 1 (JP1) and ryanodine receptor type 1 (RyR1) channel complex is mediated by their hyper-reactive thiols. *The Journal of Biological Chemistry*, *282*(12), 8667–77.

Pla-Martín, D., Calpena, E., Lupo, V., Márquez, C., Rivas, E., Sivera, R., … Espinós, C. (2014). Junctophilin-1 is a modifier gene of GDAP1-related Charcot-Marie-Tooth disease. *Human Molecular Genetics*, ddu440.

Porta, M., Diaz-Sylvester, P. L., Neumann, J. T., Escobar, A. L., Fleischer, S., & Copello, J. A. (2012). Coupled gating of skeletal muscle ryanodine receptors is modulated by Ca2+, Mg2+, and ATP. *American Journal of Physiology. Cell Physiology*, *303*(6), C682–97.

Pawłowski, K.; Majewska, A.; Szyszko, K.; Dolka, I. Motyl, T. et al. (2011) Gene expression pattern in canine mammary osteosarcoma. *Polish Journal of Veterinary Sciences* vol. 14 (1) p. 11-2

Prosser, B. L., Wright, N. T., Hernãndez-Ochoa, E. O., Varney, K. M., Liu, Y., Olojo, R. O., Zimmer, D. B.,Weber, D. J .,Schneider, M. F. (2008). S100A1 binds to the calmodulin-binding site of ryanodine receptor and modulates skeletal muscle excitation-contraction coupling. *The Journal of Biological Chemistry*, *283*(8), 5046–57

Proctor, B. M., Ren, J., Chen, Z., Schneider, J. G., Coleman, T., Lupu, T. S., Semenkovich, C. F., Muslin, A. J. (2007). Grb2 is required for atherosclerotic lesion formation. *Arteriosclerosis, Thrombosis, and Vascular Biology*, *27*(6), 1361–7.

Protasi, F., Franzini-Armstrong, C., & Allen, P. D. (1998). Role of ryanodine receptors in the assembly of calcium release units in skeletal muscle. *The Journal of Cell Biology*, *140*(4), 831–42

Protasi, F., Takekura, H., Wang, Y., Chen, S. R., Meissner, G., Allen, P. D., & Franzini-Armstrong, C. (2000). RYR1 and RYR3 have different roles in the assembly of calcium release units of skeletal muscle. *Biophysical Journal*, *79*(5), 2494–508.

Protasi, F. (2002). Structural interaction between RYRs and DHPRs in calcium release units of cardiac and skeletal muscle cells. *Frontiers in Bioscience : A Journal and Virtual Library*, *7*, d650–8.

Protasi, F., Paolini, C., Nakai, J., Beam, K. G., Franzini-Armstrong, C., & Allen, P. D. (2002). Multiple regions of RyR1 mediate functional and structural interactions with alpha(1S)-dihydropyridine receptors in skeletal muscle. *Biophysical Journal*, *83*(6), 3230–44.

Protasi, F., Paolini, C., & Dainese, M. (2009). Calsequestrin-1: a new candidate gene for malignant hyperthermia and exertional/environmental heat stroke. *The Journal of Physiology*, *587*(Pt 13), 3095–100.

Rath, A., Cunningham, F., & Deber, C. M. (2013). Acrylamide concentration determines the direction and magnitude of helical membrane protein gel shifts. *Proceedings of the National Academy of Sciences of the United States of America*, *110*(39), 15668–73. doi:10.1073/pnas.1311305110

Rath, A., Davidson, A. R., & Deber, C. M. (2005). The structure of "unstructured" regions in peptides and proteins: role of the polyproline II helix in protein folding and recognition. *Biopolymers*, *80*(2-3), 179–85. doi:10.1002/bip.20227

Rath, A., Glibowicka, M., Nadeau, V. G., Chen, G., & Deber, C. M. (2009). Detergent binding explains anomalous SDS-PAGE migration of membrane proteins. *Proceedings of the National Academy of Sciences of the United States of America*, *106*(6), 1760–5. doi:10.1073/pnas.0813167106

Renganathan, M., Messi, M. L., & Delbono, O. (1997). Dihydropyridine Receptor-Ryanodine Receptor Uncoupling in Aged Skeletal Muscle. *Journal of Membrane Biology*, *157*(3), 247–253. doi:10.1007/s002329900233

Renganathan, M., Messi, M. L., & Delbono, O. (1998). Overexpression of IGF-1 Exclusively in Skeletal Muscle Prevents Age-related Decline in the Number of Dihydropyridine Receptors. *Journal of Biological Chemistry*, *273*(44), 28845–28851.

Ruehr, M. L., Russell, M. A., Ferguson, D. G., Bhat, M., Ma, J., Damron, D. S., … Bond, M. (2003). Targeting of protein kinase A by muscle A kinase-anchoring protein (mAKAP) regulates phosphorylation and function of the skeletal muscle ryanodine receptor. *The Journal of Biological Chemistry*, *278*(27), 24831–6.

Rodney, G. G., Williams, B. Y., Strasburg, G. M., Beckingham, K., & Hamilton, S. L. (2000). Regulation of RYR1 Activity by Ca 2+ and Calmodulin †. *Biochemistry*, *39*(26), 7807–7812.

Robison, P., Hernández-Ochoa, E. O., & Schneider, M. F. (2011). Adherent primary cultures of mouse intercostal muscle fibers for isolated fiber studies. *Journal of Biomedicine & Biotechnology*, *2011*, 393740.

Robison, P., Hernández-Ochoa, E. O., & Schneider, M. F. (2014). Atypical behavior of NFATc1 in cultured intercostal myofibers. *Skeletal Muscle*, *4*(1), 1.

Rossi, D., & Sorrentino, V. (2002). Molecular genetics of ryanodine receptors Ca2+-release channels. *Cell Calcium*, *32*(5-6), 307–319.

Rossi, D., Murayama, T., Manini, I., Franci, D., Ogawa, Y., & Sorrentino, V. (2007). Expression and functional activity of ryanodine receptors (RyRs) during skeletal muscle development. *Cell Calcium*, *41*(6), 573–80

Rossi, D., Barone, V., Giacomello, E., Cusimano, V., & Sorrentino, V. (2008). The sarcoplasmic reticulum: an organized patchwork of specialized domains. *Traffic (Copenhagen, Denmark)*, *9*(7), 1044–9.

Rousseau, E., Smith, J. S., & Meissner, G. (1987). Ryanodine modifies conductance and gating behavior of single Ca2+ release channel. *Am J Physiol Cell Physiol*, *253*(3), C364–368.

Ryan, T., Sharma, P., Ignatchenko, A., Maclennan, D. H., Kislinger, T., & Gramolini, A. O. (2011). Identification of novel ryanodine receptor 1 (RyR1) protein interaction with calcium homeostasis endoplasmic reticulum protein (CHERP). *The Journal of Biological Chemistry*, *1*, 1–18.

Rice, K. M., & Blough, E. R. (2006). Sarcopenia-related apoptosis is regulated differently in fast- and slow-twitch muscles of the aging F344/N x BN rat model. *Mechanisms of Ageing and Development*, *127*(8), 670–9.

Ryan, M., & Ohlendieck, K. (2004). Excitation-Contraction Uncoupling and Sarcopenia, *1*(1). Basic Appl Myol 14(3): 141-154.

Samsó, M., & Wagenknecht, T. (2002). Apocalmodulin and Ca2+-calmodulin bind to neighboring locations on the ryanodine receptor. *The Journal of Biological Chemistry*, *277*(2), 1349–53.

Salanova, M., Schiffl, G., Rittweger, J., Felsenberg, D., & Blottner, D. (2008). Ryanodine receptor type-1 (RyR1) expression and protein S-nitrosylation pattern in human soleus myofibres following bed rest and exercise countermeasure. *Histochemistry and Cell Biology*, *130*(1), 105–18.

Salanova, M., Volpe, P., & Blottner, D. (2013). Homer protein family regulation in skeletal muscle and neuromuscular adaptation. *IUBMB Life*, *65*(9), 769–76.

Sauleda, J. (2003). Skeletal muscle changes in patients with obstructive sleep apnoea syndrome. *Respiratory Medicine*, *97*(7), 804–810

Schneider, J. S., Shanmugam, M., Gonzalez, J. P., Lopez, H., Gordan, R., Fraidenraich, D., & Babu, G. J. (2013). Increased sarcolipin expression and decreased sarco(endo)plasmic reticulum Ca2+ uptake in skeletal muscles of mouse models of Duchenne muscular dystrophy. *Journal of Muscle Research and Cell Motility*, *34*(5-6), 349–56.

Schiaffino, S. (2010). Fibre types in skeletal muscle: a personal account. *Acta Physiologica (Oxford, England)*, *199*(4), 451–63.

Schiaffino, S., & Reggiani, C. (2011). Fiber types in mammalian skeletal muscles. *Physiological Reviews*, *91*(4), 1447–531

Scott, W., Stevens, J., & Binder-Macleod, S. A. (2001). Human Skeletal Muscle Fiber Type Classifications. *Physical Therapy*, *81*(11), 1810–1816.

Seiler, S., Wegener, A. D., Whang, D. D., Hathaway, D. R., & Jones, L. R. (1984). High molecular weight proteins in cardiac and skeletal muscle junctional sarcoplasmic reticulum vesicles bind calmodulin, are phosphorylated, and are degraded by Ca2+-activated protease. *The Journal of Biological Chemistry*, *259*(13), 8550–7.

Shen, X., Franzini-Armstrong, C., Lopez, J. R., Jones, L. R., Kobayashi, Y. M., Wang, Y., Perez, C. F. (2007). Triadins modulate intracellular Ca(2+) homeostasis but are not essential for excitation-contraction coupling in skeletal muscle. *The Journal of Biological Chemistry*, *282*(52), 37864–74.

Sheridan, D. C., Takekura, H., Franzini-Armstrong, C., Beam, K. G., Allen, P. D., & Perez, C. F. (2006). Bidirectional signaling between calcium channels of skeletal muscle requires multiple direct and indirect interactions. *Proceedings of the National Academy of Sciences of the United States of America*, *103*(52), 19760–5.

Shortt, C. M., Fredsted, A., Bradford, A., & O'Halloran, K. D. (2013). Diaphragm muscle remodeling in a rat model of chronic intermittent hypoxia. *The Journal of Histochemistry and Cytochemistry : Official Journal of the Histochemistry Society*, *61*(7), 487–99

Shortt, C. M., Fredsted, A., Chow, H. B., Williams, R., Skelly, J. R., Edge, D., … O'Halloran, K. D. (2014). Reactive oxygen species mediated diaphragm fatigue in a rat model of chronic intermittent hypoxia. *Experimental Physiology*, *99*(4), 688–700.

Sitsapesan, R., McGarry, S. J., & Williams, A. J. (1995). Cyclic ADP-ribose, the ryanodine receptor and Ca2+ release. *Trends in Pharmacological Sciences*, *16*(11), 386–91.

Sievers F, Wilm A, Dineen DG, Gibson TJ, Karplus K, Li W, Lopez R, McWilliam H, Remmert M, Söding J, Thompson JD, Higgins DG (2011). Fast, scalable generation of high-quality protein multiple sequence alignments using Clustal Omega. Molecular Systems Biology 7:539

Siebenmann, C., Robach, P., Jacobs, R. A., Rasmussen, P., Nordsborg, N., Diaz, V., … Lundby, C. (2012). "Live high-train low" using normobaric hypoxia: a double-blinded, placebo-controlled study. *Journal of Applied Physiology (Bethesda, Md. : 1985)*, *112*(1), 106–17.

Squire, J. M. (1997). Architecture and function in the muscle sarcomere. *Current Opinion in Structural Biology*, *7*(2), 247–257.

Stiber, J. A., Zhang, Z.-S., Burch, J., Eu, J. P., Zhang, S., Truskey, G. A., … Rosenberg, P. B. (2008). Mice lacking Homer 1 exhibit a skeletal myopathy characterized by abnormal transient receptor potential channel activity. *Molecular and Cellular Biology*, *28*(8), 2637–47.

Stromer, M. H., Goll, D. E., Young, R. B., Robson, R. M., & Parrish, F. C. (1974). Ultrastructural features of skeletal muscle differentiation and development. *Journal of Animal Science*, *38*(5), 1111–41.

Sudol, M. (1998). From Src Homology domains to other signaling modules: proposal of the "protein recognition code". *Oncogene*, *17*(11 Reviews), 1469–74.

Sun, J., Xu, L., Eu, J. P., Stamler, J. S., & Meissner, G. (2001). Classes of thiols that influence the activity of the skeletal muscle calcium release channel. *The Journal of Biological Chemistry*, *276*(19), 15625–30.

Sun, Q.-A., Wang, B., Miyagi, M., Hess, D. T., & Stamler, J. S. (2013). Oxygen-coupled redox regulation of the skeletal muscle ryanodine receptor/Ca2+ release channel (RyR1): sites and nature of oxidative modification. *The Journal of Biological Chemistry*, *288*(32), 22961–71.

Szegedi, C., Sárközi, S., Herzog, A, Jóna, I., & Varsányi, M. (1999). Calsequestrin: more than "only" a luminal Ca2+ buffer inside the sarcoplasmic reticulum. *The Biochemical Journal*, *337 (Pt 1*, 19–22.

Szentesi, P., Collet, C., Sárközi, S., Szegedi, C., Jona, I., Jacquemond, V., Kovács, L., Csernoch, L. (2001). Effects of dantrolene on steps of excitation-contraction coupling in mammalian skeletal muscle fibers. *The Journal of General Physiology*, *118*(4), 355–75.

Tierney, M. T., Aydogdu, T., Sala, D., Malecova, B., Gatto, S., Puri, P. L., Sacco, A. (2014). STAT3 signaling controls satellite cell expansion and skeletal muscle repair. *Nature Medicine*, *20*(10), 1182–6.

Takekura, H., Takeshima, H., Nishimura, S., Takahashi, M., Tanabe, T., Flockerzi, V., Hofmann, F., Franzini-Armstrong, C. (1995). Co-expression in CHO cells of two muscle proteins involved in excitation-contraction coupling. *Journal of Muscle Research and Cell Motility*, *16*(5), 465–480.

Takekura, H., Nishi, M., Noda, T., Takeshima, H., & Franzini-Armstrong, C. (1995). Abnormal junctions between surface membrane and sarcoplasmic reticulum in skeletal muscle with a mutation targeted to the ryanodine receptor. *Proceedings of the National Academy of Sciences of the United States of America*, *92*(8), 3381–5.

Takeshima, H., Iino, M., Takekura, H., Nishi, M., Kuno, J., Minowa, O., Takano, H Noda, T. (1994). Excitation-contraction uncoupling and muscular degeneration in mice lacking functional skeletal muscle ryanodine-receptor gene. *Nature*, *369*(6481), 556–9.

Takeshima, H., Yamazawa, T., Ikemoto, T., Takekura, H., Nishi, M., Noda, T., & Iino, M. (1995). Ca(2+)-induced Ca2+ release in myocytes from dyspedic mice lacking the type-1 ryanodine receptor. *The EMBO Journal*, *14*(13), 2999–3006.

Takeshima, H., Shimuta, M., Komazaki, S., Ohmi, K., Nishi, M., Iino, M., Miyata, A.,Kangawa, K. (1998). Mitsugumin29, a novel synaptophysin family member from the triad junction in skeletal muscle. *The Biochemical Journal*, *331 (Pt 1*, 317–22.

Takeshima, H., Komazaki, S., Nishi, M., Iino, M., & Kangawa, K. (2000). Junctophilins: a novel family of junctional membrane complex proteins. *Molecular Cell*, *6*(1), 11–22.

Treves, S., Vukcevic, M., Maj, M., Thurnheer, R., Mosca, B., & Zorzato, F. (2009). Minor sarcoplasmic reticulum membrane components that modulate excitation-contraction coupling in striated muscles. *The Journal of Physiology*, *587*(Pt 13), 3071–9.

Treves, S., Chiozzi, P., & Zorzato, F. (1993). Identification of the domain recognized by anti-(ryanodine receptor) antibodies which affect Ca($^{2+}$)-induced Ca^{2+} release. *The Biochemical Journal*, *291 (Pt 3*, 757–63.

Tilgen, N., Zorzato, F., Halliger-Keller, B., Muntoni, F., Sewry, C., Palmucci, L. M.,Schneider, C.,Hauser, E.,Lehmann-Horn, F.,Müller, C.R., Treves, S. (2001). Identification of four novel mutations in the C-terminal membrane spanning domain of the ryanodine receptor 1: association with central core disease and alteration of calcium homeostasis. *Human Molecular Genetics*, *10*(25), 2879–87.

Tiso, N., Stephan, D. A., Nava, A., Bagattin, A., Devaney, J. M., Stanchi, F., … Rampazzo, A. (2001). Identification of mutations in the cardiac ryanodine receptor gene in families affected with arrhythmogenic right ventricular cardiomyopathy type 2 (ARVD2). *Human Molecular Genetics*, *10*(3), 189–94.

Venturi, E., Galfré, E., O'Brien, F., Pitt, S. J., Bellamy, S., Sessions, R. B., & Sitsapesan, R. (2014). FKBP12.6 activates RyR1: investigating the amino acid residues critical for channel modulation. *Biophysical Journal*, *106*(4), 824–33.

Vogt, M., Puntschart, A., Geiser, J., Zuleger, C., Billeter, R., & Hoppeler, H. (2001). Molecular adaptations in human skeletal muscle to endurance training under simulated hypoxic conditions. *J Appl Physiol*, *91*(1), 173–182

Wang, X., Weisleder, N., Collet, C., Zhou, J., Chu, Y., Hirata, Y., Zhao, X.,Pan, Z.,Brotto, M.,Cheng, H Ma, J. (2005). Uncontrolled calcium sparks act as a dystrophic signal for mammalian skeletal muscle. Nature Cell Biology, 7(5), 525–30.

Welinder, C., & Ekblad, L. (2011). Coomassie staining as loading control in Western blot analysis. *Journal of Proteome Research*, *10*(3), 1416–9.

Weisleder, N., & Ma, J. (2008). Altered Ca^{2+} sparks in aging skeletal and cardiac muscle. *Ageing Research Reviews*, *7*(3), 177–88.

Whiteley, G., Collins, R. F., & Kitmitto, A. (2012). Characterization of the molecular architecture of human caveolin-3 and interaction with the skeletal muscle ryanodine receptor. *The Journal of Biological Chemistry*, *287*(48), 40302–16.

Woo, J. S., Cho, C.-H., Lee, K. J., Kim, D. H., Ma, J., & Lee, E. H. (2012). Hypertrophy in skeletal myotubes induced by junctophilin-2 mutant, Y141H, involves an increase in store-operated Ca2+ entry via Orai1. *The Journal of Biological Chemistry*, *287*(18), 14336–48.

Wright, N. T., Prosser, B. L., Varney, K. M., Zimmer, D. B., Schneider, M. F., & Weber, D. J. (2008). S100A1 and calmodulin compete for the same binding site on ryanodine receptor. *The Journal of Biological Chemistry*, *283*(39), 26676–83. doi:10.1074/jbc.M804432200

Wu, S., Ibarra, M. C. A., Malicdan, M. C. V, Murayama, K., Ichihara, Y., Kikuchi, H., … Nishino, I. (2006). Central core disease is due to RYR1 mutations in more than 90% of patients. *Brain : A Journal of Neurology*, *129*(Pt 6), 1470–80. doi:10.1093/brain/awl077

Wu, C., Ma, M. H., Brown, K. R., Geisler, M., Li, L., Tzeng, E., Li, S. S.-C. (2007). Systematic identification of SH3 domain-mediated human protein-protein interactions by peptide array target screening. *Proteomics*, *7*(11), 1775–85.

Xue, H. H., Zhao, D. M., Suda, T., Uchida, C., Oda, T., Chida, K., Zhao, D.M., Ichiyama, A Nakamura, H. (2000). Store depletion by caffeine/ryanodine activates capacitative Ca($^{2+}$) entry in nonexcitable A549 cells. *Journal of Biochemistry*, *128*(2), 329–36.

Yamada, T., Fedotovskaya, O., Cheng, A. J., Cornachione, A. S., Minozzo, F. C., Aulin, C., … Lanner, J. T. (2014). Nitrosative modifications of the Ca2+ release complex and actin underlie arthritis-induced muscle weakness. *Annals of the Rheumatic Diseases*.

Yarov-Yarovoy, V., DeCaen, P. G., Westenbroek, R. E., Pan, C.-Y., Scheuer, T., Baker, D., & Catterall, W. A. (2012). Structural basis for gating charge movement in the voltage sensor of a sodium channel. *Proceedings of the National Academy of Sciences of the United States of America*, *109*(2), E93–102.

Yasuda, T., Delbono, O., Wang, Z.-M., Messi, M. L., Girard, T., Urwyler, A., Treves, S., Zorzato, F. (2013). JP-45/JSRP1 variants affect skeletal muscle excitation-contraction coupling by decreasing the sensitivity of the dihydropyridine receptor. *Human Mutation*, *34*(1), 184–90.

Yeow-Fong, L., Lim, L., & Manser, E. (2005). SNX9 as an adaptor for linking synaptojanin-1 to the Cdc42 effector ACK1. *FEBS Letters*, *579*(22), 5040–8.

Yin, C.-C., D'Cruz, L. G., & Lai, F. A. (2008). Ryanodine receptor arrays: not just a pretty pattern? *Trends in Cell Biology*, *18*(4), 149–56.

Yuchi, Z., Lau, K., & Van Petegem, F. (2012). Disease mutations in the ryanodine receptor central region: crystal structures of a phosphorylation hot spot domain. *Structure (London, England : 1993)*, *20*(7), 1201–11.

Zalk, R., Clarke, O. B., Georges, A. des, Grassucci, R. A., Reiken, S., Mancia, F., … Marks, A. R. (2014). Structure of a mammalian ryanodine receptor. *Nature*.

Zeng, B., Chen, G.-L., Daskoulidou, N., & Xu, S.-Z. (2014). The ryanodine receptor agonist 4-chloro-3-ethylphenol blocks ORAI store-operated channels. *British Journal of Pharmacology*, *171*(5), 1250–9.

Zhang, S., Ren, J., Khan, M. F., Cheng, A. M., Abendschein, D., & Muslin, A. J. (2003). Grb2 is required for the development of neointima in response to vascular injury. *Arteriosclerosis, Thrombosis, and Vascular Biology*, *23*(10), 1788–93.

Zhao, X., Moloughney, J. G., Zhang, S., Komazaki, S., & Weisleder, N. (2012). Orai1 Mediates Exacerbated Ca2+ Entry in Dystrophic Skeletal Muscle. *PLoS ONE*, *7*(11), e49862.

Zhang, H., & Johnson, P. (1992). Differential effects of aluminum ion on smooth muscle calpain I and calpain II activities. *The International Journal of Biochemistry*, *24*(11), 1773–8.

Zimanyi, I., Buck, E., Abramson, J., Mack, M., & Pessah, I. (1992). Ryanodine induces persistent inactivation of the Ca2+ release channel from skeletal muscle sarcoplasmic reticulum. *Mol. Pharmacol.*, *42*(6), 1049–1057.

Zissimopoulos, S., West, D. J., Williams, A. J., & Lai, F. A. (2006). Ryanodine receptor interaction with the SNARE-associated protein snapin. *Journal of Cell Science*, *119*(Pt 11), 2386–97.

Zissimopoulos, S., & Lai, F. a. (2006). Redox regulation of the ryanodine receptor/calcium release channel. *Biochemical Society Transactions*, *34*(Pt 5), 919–21.